

Electrochemical Nitrogen Reduction for Ammonia Synthesis

Elektrochemische Stickstoffreduktion für die Ammoniaksynthese

Von der Fakultät für Maschinenwesen
der Rheinisch-Westfälischen Technischen Hochschule Aachen
zur Erlangung des akademischen Grades
eines Doktors der Ingenieurwissenschaften genehmigte Dissertation

vorgelegt von

Kurt Kugler

Berichter: Univ.-Prof. Dr.-Ing. Matthias Wessling
Univ.-Prof. Dr.-Ing. Detlef Stolten

Tag der mündlichen Prüfung: 02.11.2015

Diese Dissertation ist auf den Internetseiten der Universitätsbibliothek online verfügbar.

Danksagung

Die vorliegende Dissertation konnte nur durch die Hilfe und Unterstützung zahlreicher Personen fertig gestellt werden. Ich möchte mich bei allen Unterstützern und Mitstreitern ganz herzlich bedanken. Mein besonderer Dank gilt:

- Prof. Dr.-Ing. Matthias Wessling für die Möglichkeit meine Dissertation unter seiner Anleitung am Lehrstuhl für Chemische Verfahrenstechnik anfertigen zu können. Das interessante Thema und entgegengebrachte Vertrauen waren immer sehr motivierend. Danke Matthias.
- Meinen Bürokollegen Stefanie, Davide, Robert und Serafin für die stets gute Zusammenarbeit in der ecMR Gruppe. Ohne euch wäre e2chem nicht e2chem.
- John "Johnny" Wong für seine Erfahrung und Unterstützung bei vielen allgemeinen Fragen über den Ablauf einer Promotion und den Forschungsalltag. Danke für deine Ratschläge und Hilfe.
- Youri für die hilfreichen und konstruktiven Diskussionen über diverse Probleme der Elektrochemie und für die Unterstützung bei der Analyse meiner Proben.
- Kalle, Herbert und der mechanischen Werkstatt für die gute Zusammenarbeit beim Planen und Betrieb der Versuchsanlage im Technikum.
- Dr. Khosrow Rahimi und Prof. Wim de Jeu für ihre Hilfe beim Durchführen von XRD Messungen.
- Der Elektronenmikroskopie des DWI für die Hilfe beim Aufnehmen von SEM Bildern und beim Durchführen von EDX Messungen.
- Der Firma Magneto Special Anodes B.V. für die Bereitstellung von diversen Elektrodenmaterialien. Großen Dank an Adriaan, Michel und Vidjay für die hilfreichen Diskussionen und Anregungen während unserer Halbjahrestreffen.
- Meinem langjährigen und stets motivierten Hiwi André für seinen unermüdlichen Einsatz und seine kreativen Ideen wenn es drauf ankam.
- Meinen Abschlussarbeitern Christian, Burkhard, Thomas, Kristof, Elisabeth, Mareike, Sofia, Milan, Martin, Arian, Karolin, Hannah und meiner Hiwine Johanna für die angenehme Zusammenarbeit und ihre motivierte und kreative Mitarbeit. Eure Arbeiten haben wichtige und sehr gute Ergebnisse zu dieser Dissertation beigesteuert. Ihr wart das beste KUKU-TEAM das ich mir wünschen konnte.
- Der Küchenesstruppe Karin, Vera, Johnny, JoLi, Davide und Steffie für die lustigen und niemals langweiligen Mittagspausen.

- Meinem Vater Joachim und meinen Großeltern Agnes und Kurt, die mich während meinem Studium und meiner Promotion fern der Heimat stets unterstützt und motiviert haben.
- Meiner Freundin Bettina, ohne die ich die Zeit in Aachen nicht gemeistert hätte und die mich stets in meinem Handeln bekräftigt hat und immer für mich da war. Gemeinsam sind wir stark.

Allen vielen Dank für die tatkräftige Unterstützung!

Aachen, im Juni 2015

Kurt Kugler

*Für Bettina und meine Eltern
Für meine Großeltern Agnes und Kurt*

Abstract

Ammonia NH₃ is one of the most important chemicals worldwide and quantitatively the second largest heterogeneously catalyzed chemical after H₂SO₄. Around 80% of the produced NH₃ is used as fertilizer precursor to supply the growing world population with sufficient amounts of food. Starting from N₂ and H₂, NH₃ nowadays is typically produced by the Haber process applying an Fe-based catalyst. The worldwide production capacity for NH₃ is about 140 million tonnes per year. Disadvantageously, the Haber process is one of the largest industrial energy consumers and for each ton of NH₃ produced two tonnes of CO₂ are emitted as well. An environmentally more friendly alternative synthesis process is desired, which can help to produce NH₃ in a sustainable and ecological way in the future.

In the present thesis, the electrochemical NH₃ synthesis in an electrochemical membrane reactor (ecMR) was investigated. An ecMR consists of two compartments, the anodic and the cathodic half-cell, which are separated by a cation exchange membrane (CEM). The core of the ecMR is the membrane electrode assembly (MEA) which consists of two electrodes pressed into the CEM. To be environmentally friendly, the needed H⁺ for the NH₃ synthesis were generated by the oxidation of H₂O at the anode. An electrical potential was applied to the ecMR as driving force to create an electrical field, in which the H⁺ migrate through the membrane to the cathode. Nitrogen gas was fed to the cathodic department and was reduced to NH₃ at the cathode. On a large scale application, renewable energy sources such as wind or solar power can drive the process. At the anode a state-of-the-art IrMMO catalyst was applied for the oxidation of H₂O. Based on recently published density functional theory (DFT) calculations Ti, Fe and Ru were chosen as potential cathodic catalysts. Titanium and Fe were commercially available in the form of randomly structured felts and used as received as cathode in the ecMR. Since Ru is an expensive noble metal, a new galvanic coating process of Ru on Ti felts was investigated. The so-prepared Ru electrodes were tested in the ecMR as well as Ti and Fe electrodes. All three catalysts showed a high activity for the electrochemical NH₃ synthesis, while Ru gave the best results with respect to production rate of NH₃ and current efficiency. Parallel to the NH₃ synthesis in gas phase in the ecMR also first experiments with Ti were performed in an one- and two-compartment liquid phase setup. Compared to the results obtained in gas phase, the liquid phase system was less stable and the results were less predictable. To answer the question if an electrochemical NH₃ synthesis process can compete with the state-of-the-art Haber process, a complete synthesis process with N₂ production via air separation, NH₃ synthesis in an ecMR and downstream product separation was modelled and optimized in Aspen+. For the ecMR a new model was developed in Aspen Custom Modeler and implemented in the complete synthesis process in Aspen+.

The results obtained in the present thesis encourage further research of the electrochemical NH₃ synthesis. Particularly new electrocatalysts need to be investigated to further develop and optimize the ecMR to be the technology of choice in the future for the environmentally friendly synthesis of NH₃.

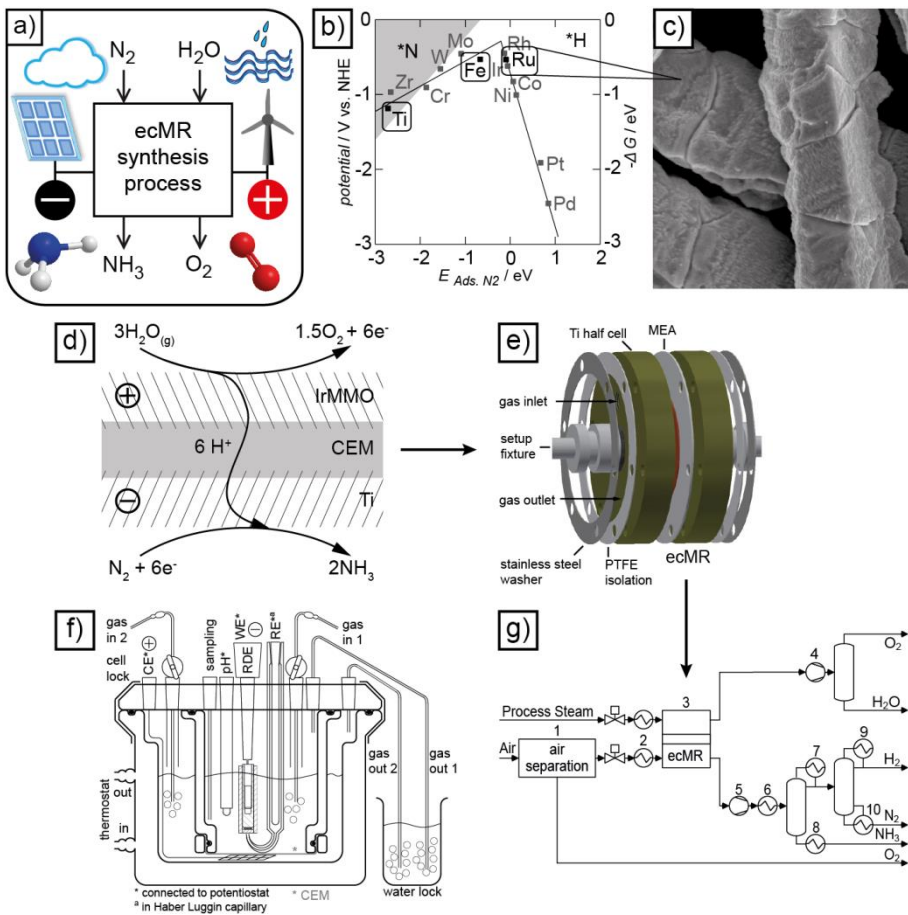
Zusammenfassung

Ammoniak NH_3 ist eine der wichtigsten Chemikalien weltweit und die mengenmäßig zweitgrößte heterogen katalysierte Chemikalie nach H_2SO_4 . Rund 80% des hergestellten NH_3 werden als Düngemittel verwendet um die Weltbevölkerung mit ausreichend Nahrungsmitteln zu versorgen. Ausgehend von N_2 und H_2 wird NH_3 heutzutage nach dem Haber Bosch Verfahren mit einem eisenbasierten Katalysator hergestellt. Die weltweite Produktionskapazität für NH_3 liegt bei 140 Mio. Tonnen jährlich. Nachteilig am Haber Bosch Verfahren ist der hohe Energieverbrauch und der Ausstoß von zwei Tonnen CO_2 pro Tonne produziertem NH_3 . Ein umweltfreundlicheres Alternativverfahren ist erstrebenswert, um NH_3 in Zukunft nachhaltig und umweltverträglich produzieren zu können.

In der vorliegenden Arbeit wurde die elektrochemische Ammoniaksynthese in einem elektrochemischen Membranreaktor (ecMR) untersucht. Ein ecMR besteht aus zwei Hälften, einer anodischen und einer kathodischen Halbzelle, die durch eine Kationenaustauschermembran (CEM) voneinander getrennt werden. Das Herzstück des ecMRs ist die Membranelektrodeneinheit (MEA), die durch EInpressen von zwei Elektroden in die CEM gebildet wird. Die für die Ammoniaksynthese benötigten H^+ wurden umweltfreundlich durch Wasseroxidation an der Anode hergestellt. Ein als Triebkraft an den ecMR angelegtes elektrisches Potential erzeugt ein elektrisches Feld, in dem die H^+ durch die Membran zur Kathode wandern. Stickstoff wurde der kathodischen Halbzelle zugeführt und an der Kathode zu NH_3 reduziert. Großtechnisch können erneuerbare Energiequellen wie Wind- oder Solarenergie genutzt werden um den Prozess anzutreiben. An der Anode wurde ein kommerzieller IrMMO Katalysator für die Wasseroxidation eingesetzt. Basierend auf erst kürzlich veröffentlichten Dichtefunktionaltheorie (DFT) Berechnungen wurden Ti, Fe und Ru als potentielle Katalysatoren für die Kathode ausgewählt. Titan und Fe wurden in Form von unregelmäßigen Geweben käuflich erworben und direkt wie vom Hersteller bezogen als Kathode im ecMR eingesetzt. Da es sich bei Ru um ein teures Edelmetall handelt, wurde ein neuer Prozess untersucht, um Ru auf Titangeweben galvanisch abzuscheiden. Neben Titan- und Eisenelektroden wurden auch die so hergestellten Rutheniumelektroden im ecMR getestet. Alle untersuchten Katalysatoren zeigten eine hohe Aktivität für die Ammoniaksynthese, wobei Ru die besten Resultate für die Produktionsrate und die Stromeffizienz lieferte. Zusätzlich zur Ammoniaksynthese in Gasphase im ecMR wurden auch erste Versuche mit Ti in Flüssigphase in einer ein- und zweigeteilten Glaszelle durchgeführt. Die erzielten Resultate waren im Vergleich zur Gasphase jedoch weniger stabil. Um die Frage zu beantworten, ob die elektrochemische Ammoniaksynthese mit dem Haber Bosch Verfahren konkurrieren kann, wurde ein kompletter Syntheseprozess mit Stickstoffgewinnung durch Luftzerlegung, Ammoniaksynthese in einem ecMR und der nachgeschalteten Produktauf trennung in Aspen+ modelliert und optimiert. Für den ecMR wurde ein neues Modell in Aspen Custom Modeler entwickelt und in den gesamten Syntheseprozess in Aspen+ integriert.

Die in der vorliegenden Arbeit erzielten Resultate regen dazu an, weitere Forschung im Bereich der elektrochemischen Ammoniaksynthese zu betreiben. Insbesondere die Entwicklung von neuen Elektrokatalysatoren kann helfen den ecMR weiter zu optimieren und ihn zur Technologie der Wahl zu machen, um NH_3 in Zukunft umweltfreundlich herstellen zu können.

Graphical abstract



A new synthesis process for NH₃ using an electrochemical membrane reactor (ecMR) was proposed (a). Based on published density functional theory (DFT) calculations, Ti, Fe and Ru were identified as potential cathodic catalysts (b). Ru catalysts were prepared via galvanostatic electroplating on randomly structured Ti felts (c). In gas phase, the oxidation of H₂O and the reduction of N₂ take place at the membrane electrode assembly (MEA) (d), which is the core of the ecMR (e). Catalyst analysis was conducted in a two compartment liquid phase setup (f). A complete synthesis process consisting of an air separation unit, the ecMR and downstream product separation was modelled and optimized in Aspen+ (g).

Symbols and abbreviations

Abbreviation	Unit	Meaning
ACL		active catalyst layer
ACM		Aspen Custom Modeler
ASU		air separation unit
BASF		Badische Anilin- & Soda-Fabrik
BD		back diffusion
BET		Brunauer, Emmett und Teller
c.d.	A m ⁻²	current density
CA		chronoamperometry
C _{corr.}	C = As	corrected charge
C _{He}	C = As	charge measured for He
C _{N₂}	C = As	charge measured for N ₂
CCS		CO ₂ capture and geologic sequestration
CE		counter electrode
CE	%	current efficiency
CE _{corr.}	%	corrected current efficiency
CE _{NH₃}	%	NH ₃ specific current efficiency
CEM		cation exchange membrane
CEM		Controlled Evaporator Mixer unit
Comp		compressor
Cond		condenser
COP		coefficient of performance
cps		counts per second
CV		cyclic voltammetry
CW		heat exchangers using cooling water
D		diffusivity
DC		direct current
DFT		density functional theory
ecMR		electrochemical membrane reactor
ED		electroosmotic drag
EDX		energy-dispersive X-ray spectroscopy
EI		integrated heat exchangers
EIS		electrochemical impedance spectroscopy
E _{spec}	MWh t ⁻¹	specific energy consumption
FeMoCo		iron molybdenum cofactor
GDE		gas diffusion electrode
HER		hydrogen evolution reaction
HX		heat exchangers with external heat or cooling sources
IrMMO		iridium mixed metal oxide
LFM		liquid flow meter
LSV		linear sweep voltammetry

Symbols and abbreviations

Abbreviation	Unit	Meaning
MEA		membrane electrode assembly
MFC		mass flow controller
NHE		normal hydrogen electrode
OCP		open circuit potential
OER		oxygen evolution reaction
P		permeability
PAn		polyaniline
PBI		polybenzimidazole
PEEK		polyether ether ketone
PEM		proton exchange membrane
PEM		polymer electrolyte membrane
PEMFC		polymer electrolyte membrane fuel cell
PI		pressure indication
PIC		pressure indication and control
PPy		polypyrrole
PTFE		polytetrafluoroethylene
RDE		rotating disk electrode
RE		reference electrode
RH	%	relative humidity
S		solubility
SCY		strontia-ceria-ytterbia
SEM		scanning electron microscopy
SPSF		sulfonated polysulfone membrane
SZY		strontia-zirconia-yttria
TC		temperature control
TI		temperature indication
TIC		temperature indication and control
TMFB		Tailor-Made Fuels from Biomass
toe		tonnes of oil equivalent
TPB		triple phase boundary
Turb		turbine
WE		working electrode
XRD		X-ray diffraction

Symbol	Unit	Meaning
α		selectivity of membranes
α		correction factor for effective diffusion coefficient
α	$\text{m}^2 \text{s}^{-1}$	thermal diffusivity
α_A		anodic charge transfer coefficient
α		charge transfer coefficient
α_b		backward charge transfer coefficient
α_c		cathodic charge transfer coefficient

Symbol	Unit	Meaning
α_f		forward charge transfer coefficient
$a_i^{x=0}$		activity of the species i at the electrode surface
$a_i^{x=\infty}$		activity of the species i in the bulk fluid
β	%	current efficiency
β	$m\ s^{-1}$	mass transfer coefficient
β	K^{-1}	thermal expansion coefficient
γ		ratio of H_2 and NH_3 formation rate
δ	μm	thickness of the selective layer of a membrane
ΔE^0	V	difference in anodic and cathodic standard potential
ΔG	$kJ\ mol^{-1}$	Gibbs free energy
$\Delta G(M-H)$	$kJ\ mol^{-1}$	Gibbs free energy of adsorption of hydrogen atoms on the metal surface
$\Delta_R G$	$kJ\ mol^{-1}$	Gibbs free energy for overall reaction
$\Delta_R G^0$	$kJ\ mol^{-1}$	standard Gibbs free energy
$\Delta_R H$	$kJ\ mol^{-1}$	enthalpy of reaction
ΔS	$J\ K^{-1}$	entropy
ΔT_{min}	K	minimum temperature difference
$\Delta U_{Contact}$	V	potential drop due to contact resistance
$\Delta U_{CP, A}$	V	anodic overpotential due to concentration polarization
$\Delta U_{CP, C}$	V	cathodic overpotential due to concentration polarization
$\Delta U_{\Omega, A}$	V	ohmic voltage drop within anode due to ohmic resistance of the anode
$\Delta U_{\Omega, C}$	V	ohmic voltage drop within cathode due to ohmic resistance of the cathode
ϵ		porosity
$\zeta_{i,A/C}$		conversion rate of reactants
η		energy efficiency
η	$Pa\ s$	dynamic viscosity
η_A	V	anodic over potential
η_C	V	cathodic over potential
2Θ	°	scattering angle
κ	$A\ (Vm^2)^{-1}$	membrane conductivity
κ	$S\ m^{-1}$	electrolyte conductivity
λ	nm	wavelength of X-rays
λ	nm	mean free path of gas molecules
λ	$W\ (mK)^{-1}$	thermal conductivity of the reactor wall
λ_f	$W\ (mK)^{-1}$	thermal conductivity of the fluid within the flow channel
ν	$m^2\ s^{-1}$	kinematic viscosity
v_e		number of transferred electrons
$v_{e,A}$		number of transferred electrons anode
$v_{e,C}$		number of transferred electrons cathode
v_i		stoichiometric coefficient

Symbols and abbreviations

Symbol	Unit	Meaning
v_p		stoichiometric coefficient product
ρ	kg m^{-3}	density
ΣIR	V	sum of IR drop
T		tortuosity
Φ		pressure ratio
ω	m	width of the flow channel
ω	Hz s^{-1}	rotation rate
∇c_i	$\text{mol m}^{-3} \text{m}^{-1}$	concentration gradient
a		activity of a gas with the partial pressure p
a		Tafel equation constant a
A	m^2	surface area of the electrode
A_{active}	cm^2	active membrane and catalyst area
a_{CS}	$\text{m}^2 \text{m}^{-2}$	ratio of catalytic surface area
$a_{P,i}$		activity of the product i
$a_{R,i}$		activity of the reactant i
b		Tafel equation constant b
C	$\text{C} = \text{As}$	Coulomb, unit for charge Q
c	mg l^{-1}	concentration
c_f	mol cm^{-3}	concentration of the fixed sites in a membrane
c_{H^+}	mol cm^{-3}	concentration of H^+
c_i	mol cm^{-3}	concentration of component i
d	mm	distance between electrodes
D_{eff}	$\text{m}^2 \text{s}^{-1}$	effective diffusion coefficient
d_{GDE}	μm	thickness gas diffusion electrode
d_{hyd}	m	hydraulic diameter of the flow channel
D_i	$\text{m}^2 \text{s}^{-1}$	diffusion coefficient of component i
d_M	μm	membrane thickness
d_{por}	μm	pore size
d_w	m	wall thickness
E_A	V	anodic electrode potential
E_A^0	V	anodic standard potential
E_C	V	cathodic electrode potential
E_C^0	V	cathodic standard potential
E_{eq}	V	equilibrium potential
$E_{\text{eq},A}$	V	anodic equilibrium potential
$E_{\text{eq},C}$	V	cathodic equilibrium potential
F	C mol^{-1}	Faraday constant, 96485 C mol ⁻¹
f		fugacity coefficient
g	m s^{-2}	acceleration due to gravity
$H_{i,P}$	kJ mol^{-1}	specific enthalpy of the products diffusing back from the GDE into the flow channel
$H_{i,R}$	kJ mol^{-1}	specific enthalpy of the reactants diffusing from the flow channel into the GDE

Symbol	Unit	Meaning
$H_{M,A}$	kJ mol^{-1}	specific enthalpy of the molar flow in the flow channel
I	A	current
j	A cm^{-2}	current density
j_0	A cm^{-2}	exchange current density
$j_{0,A}$	A cm^{-2}	anodic exchange current density
$j_{0,C}$	A cm^{-2}	cathodic exchange current density
k	$\text{W (m}^2\text{K)}^{-1}$	heat transfer coefficient
k_B	J K^{-1}	Boltzmann constant
k_{fw}	$\text{W (m}^2\text{K)}^{-1}$	heat transfer coefficient for the heat transfer between the fluid at the anode or cathode and the inside of the reactor wall
k_{se}	$\text{W (m}^2\text{K)}^{-1}$	heat transfer coefficient Nusselt Number
k_w	$\text{W (m}^2\text{K)}^{-1}$	heat transfer coefficient for the heat transfer through the reactor wall
k_{we}	$\text{W (m}^2\text{K)}^{-1}$	heat transfer coefficient for the heat transfer between the outside of the reactor wall and the ambient air
Kn		Knudsen Number
l	m	length flow channel
l_{se}	m	characteristic length Nusselt Number
m	kg	mass
M	mol g^{-1}	molar mass
M_p	mol g^{-1}	molar mass product
Nu		Nusselt Number
$\dot{n}_{A,i}$	mol s^{-1}	molar flow of the bulk fluid in the anodic flow channel
$\dot{n}_{C,i}$	mol s^{-1}	molar flow of the bulk fluid in the cathodic flow channel
$\dot{n}_{A/C,i}''$	$\text{mol m}^{-2} \text{s}^{-1}$	anodic or cathodic molar flux of component i per geometric surface area A
$\dot{n}_{A/C,\alpha,i}$	mol min^{-1}	molar flow rate of the reactant i at the inlet of the reactor
$\dot{n}_{A/C,\omega,t}$	mol min^{-1}	molar flow rate of the reactant i at the outlet of the reactor
$\dot{n}_{P,A/C,i}''$	$\text{mol m}^{-2} \text{s}^{-1}$	anodic or cathodic flux of the product per electrode surface area A
$\dot{n}_{R,A/C,i}''$	$\text{mol m}^{-2} \text{s}^{-1}$	anodic or cathodic flux of the reactant consumed per electrode surface area A
\dot{n}_{tot}''	$\text{mol m}^{-2} \text{s}^{-1}$	total molar flux per geometric surface area A
P	W	power
p	atm	reactor pressure
p^0	mbar	partial pressure
p_F	bar	vapor pressure
$p_{F,i}$	mbar	feed pressure
p_i	mbar	partial pressure of component i in the feed
$p_{P,i}$	mbar	partial pressure reactants or products
Pr		partial pressure of component i in the permeate
Q	$C = As$	Prandtl Number
		charge

Symbols and abbreviations

Symbol	Unit	Meaning
q	nm^{-1}	scattering vector
Q		ratio of the activities of the reactants and products
$\dot{q}_{\text{EE,A/C}}$	kW m^{-2}	heat flow transferred per area due to the conversion of electrical energy
$\dot{q}_{\text{HL,A/C}}$	kW m^{-2}	heat flow transferred per area to the ambient air
\dot{Q}_c	W	cooling duty
r	eV^{-1}	slope for volcano plot relations
R	$\text{kJ mol}^{-1} \text{K}^{-1}$	ideal gas constant
Ra		Rayleigh Number
Re		Reynolds Number
Sc		Schmidt Number
Sh		Sherwood Number
t	s	time
T	K	temperature
T^0	$^{\circ}\text{C}$	reactor temperature
T_0	K	ambient temperature
T_w	K	surface temperature of the wall
$T_{x,\text{A/C}}$	K	temperature in the anodic or cathodic flow channel
u	m s^{-1}	flow velocity
U_{cell}	V	cell potential
$U_{\text{cell,min}}$	V	minimum cell potential
U_D	V	portion of the cell voltage
U_{EP}	V	equilibrium potential
U_{th}	V	thermoneutral voltage
$U_{\Omega, E}$	V	ohmic voltage drop
V	I	volume
\dot{V}_A	ml min^{-1}	anodic feed flow rate
\dot{V}_C	ml min^{-1}	cathodic feed flow rate
x_i	mol mol^{-1}	mole fraction
$y_{A,i}$		anodic mole fraction reactant i
$y_{C,i}$		cathodic mole fraction reactant i
z		charge number of an (metal) ion
Z_f		charge of the fixed sites in a membranes
Z_{H^+}		charge of H^+
Z_i		charge of component i

Contents

Danksagung	iii
Abstract	vii
Zusammenfassung.....	ix
Graphical abstract	xi
Symbols and abbreviations	xiii
1. Introduction.....	1
1.1. The Haber process for large-scale NH ₃ synthesis	4
1.2. The role of electrochemistry for future chemical industry	5
1.3. Importance of NH ₃ for today's world	7
1.4. Alternative synthesis routes for NH ₃	9
1.5. Literature review about electrochemical NH ₃ synthesis.....	10
1.5.1. Liquid electrolytes	11
1.5.2. Molten salts	12
1.5.3. Composite electrolytes.....	13
1.5.4. Solid electrolytes	14
2. Electrocatalysts and their galvanic deposition.....	17
2.1. Introduction.....	19
2.2. Choice of catalyst	19
2.3. Electroplating and parameters	20
2.4. Electroplating of Rhodium and Ruthenium	23
2.4.1. Rhodium	23
2.4.2. Ruthenium	24
2.5. Materials & Methods.....	25
2.5.1. Chemicals & Materials	25
2.5.2. Pretreatment	25
2.5.3. BET surface measurements	25
2.5.4. Electroplating: Setup and conducted experiments	26
2.5.5. Analysis of coatings	26
2.5.6. Linear sweep voltammetry: Setup and conducted experiments.....	27
2.5.7. Analysis with the Berthelot reaction	28

Contents

2.6.	Results.....	30
2.6.1.	Pretreatment of randomly structured Ti felts.....	30
2.6.2.	Polarization curves for Rh and Ru	30
2.6.3.	Current efficiency, deposited masses, SEM and EDX analysis of Rh	33
2.6.4.	Current efficiency, deposited masses, SEM and EDX analysis of Ru	37
2.6.5.	XRD measurements of coated felts	41
2.6.6.	Linear Sweep Voltammetry measurements for Rh and Ru	42
2.6.7.	Economical estimation	44
2.7.	Conclusion.....	44
3.	Electrochemical NH₃ synthesis in liquid phase	47
3.1.	Introduction.....	49
3.2.	Electrochemical cells applied	50
3.2.1.	The one-compartment cell	50
3.2.2.	The two-compartment cell.....	51
3.3.	Materials & methods.....	52
3.3.1.	Pretreatment and activation	53
3.3.2.	Cyclic voltammetry	54
3.3.3.	Chronoamperometry	54
3.3.4.	Analysis	55
3.4.	Results.....	55
3.4.1.	Cyclic voltammetry	55
3.4.2.	Chronoamperometry	56
3.4.3.	Comparison of the one- and the two-compartment cell.....	60
3.5.	Conclusion.....	61
4.	The electrochemical membrane reactor - Materials & methods	63
4.1.	Introduction.....	65
4.2.	The electrochemical setup for NH ₃ synthesis	66
4.3.	Requirements for electrochemical cells	67
4.4.	The electrochemical membrane reactor - ecMR.....	68
4.5.	The membrane electrode assembly - MEA.....	69
4.5.1.	The anode - Iridium mixed metal oxide IrMMO	70
4.5.2.	The polymer cation exchange membrane - Fumapem F-14100	70
4.5.3.	The cathode - Titanium	72
4.6.	Fabrication of a membrane electrode assembly	72
4.7.	Electrochemical thoughts about NH ₃ synthesis	74
4.8.	Activity testing of IrMMO	75
4.8.1.	Results	76
4.9.	Water management in PEMFC and ecMR	78

5.	Electrochemical NH₃ synthesis in an ecMR	81
5.1.	Introduction.....	83
5.2.	Current voltage curves	83
5.3.	Production rates and current efficiency.....	85
5.3.1.	Influence of temperature and relative humidity.....	86
5.4.	Comparison of Ti, Fe and Ru as cathodic catalyst	89
5.5.	Conclusion.....	92
6.	Simulation and Modelling in Aspen Custom Modeler and Aspen+	95
6.1.	Introduction.....	97
6.2.	Proposed process	97
6.3.	Proposed ecMR.....	98
6.3.1.	Model structure of the ecMR.....	99
6.4.	Proposed catalyst.....	100
6.5.	Simulation results for the ecMR	102
6.5.1.	Reactor and process parameters	102
6.5.2.	Performance indicators	103
6.5.3.	System performance of the ecMR	104
6.5.4.	Process energetics.....	110
6.6.	Conclusion.....	112
6.7.	Appendix.....	113
6.7.1.	Basic laws and equations in electrochemistry	113
6.7.2.	Mass balance	116
6.7.3.	Mass transfer	117
6.7.4.	Energy balance	119
6.7.5.	Heat transfer	120
6.7.6.	Pressure loss	122
7.	Energetic optimization of the simulated ecMR	123
7.1.	Introduction.....	125
7.2.	Initial situation.....	125
7.3.	Product separation at the anode and cathode	126
7.3.1.	Gas separation by partial condensation and cryogenic distillation	126
7.3.2.	Gas separation by membranes.....	127
7.4.	Alternatives for the downstream separation.....	128
7.4.1.	Feed pre-treatment	128
7.4.2.	ecMR	129
7.4.3.	Anodic product separation	130
7.4.4.	Cathodic product separation	131
7.5.	Results.....	135
7.5.1.	Specific energy consumption of the entire process	135
7.5.2.	Economic evaluation.....	138

Contents

7.6.	Conclusion.....	139
7.7.	Appendix.....	140
7.7.1.	Theoretical background gas separation by membranes.....	140
8.	Conclusions & Outlook.....	141
8.1.	Summary and conclusions	142
8.2.	Outlook and future perspectives	145
References		147
Curriculum vitae		165

1. Introduction

1 Introduction

The global key challenge for today's industry and population is the climate change and the inevitable energy transition. The atmospheric CO₂ concentration, the demand for fossil resources and the global energy demand are steadily increasing. Within 10 years there was an increase of around 28% for the primary energy consumption from 9944 million tonnes of oil equivalent (toe) in 2003 to 12730 million toe in 2013. Today, primary energy comprises fossil fuels such as oil, natural gas and coal, nuclear and hydro power, and modern renewables for electricity generation. However, 85 to 90% of the total energy demand is covered by fossil fuels, from which oil is still the most important one. [1] Today, only 10% of the produced oil are used in the chemical industry, while 50% are used to produce fuels, 20% as raw material for heating oil and 20% for diverse applications [2]. Inevitably, CO₂ is emitted when fossil fuels are used for energy production. Consequently, it has been a global goal to reduce the worldwide CO₂ emissions, which has been a catalytic factor for the Kyoto Protocol in December 1997. The replacement of fossil fuels by renewable energy sources, efficiency improvements and lower energy demand in the energy sector and the chemical industry are mandatory to develop a sustainable energy scenario for the future and to reduce CO₂ emissions.

Along with the energy demand the worldwide population is also continuously growing and the supply with food is only possible as huge amounts of fertilizers are produced by the Haber process [3]. With a worldwide production capacity of about 140 million tonnes in 2013 [4], NH₃ quantitatively is the second largest heterogeneously catalyzed chemical after H₂SO₄. At ambient conditions NH₃ is a colorless, noxious gas with a characteristic pungent odor [5]. As scientists realized as early as 1840 that N₂ is an essential element for plant growth, N₂-based fertilizers have been developed. Nowadays around 80% of the produced NH₃ is used as the main active ingredient in fertilizers such as urea or ammonium phosphate. However, NH₃ may also become an important intermediate chemical for energy and indirect H₂ storage. [6,7] In fact, Lan and Tao used (NH₄)₂CO₃ in fuel cell applications [8]. Water electrolysis in a proton exchange membrane (PEM) electrolyzer is a well-developed process for sustainable H₂ production [9]. However, the transportation and storage of gaseous H₂ is more challenging than for liquid NH₃ [10]. Ammonia is also used for flue gas treatment to remove H₂SO₄. Furthermore NO_x emissions of ships and stationary facilities could be averted by reacting NH₃ with NO or NO₂ [11].

Only recently, the direct NH₃ synthesis from its elements N₂ and H₂ has been considered one of the most significant scientific achievements of the 20th century [3]. The significance of NH₃ is self-evident: with 20% of the global energy consumption in the chemical industry, corresponding to 1.4% of the worldwide energy demand, the NH₃ synthesis is one of the largest energy users. [12,13] The H₂ production, the N₂ purification and the energy intensive process condition for an acceptable conversion rate contribute significantly to the energy demand. At temperatures of 400 to 500°C and pressures of 150 to 200 bars, N₂ and H₂ gas react at a Fe₃O₄ based catalyst to form NH₃. [12] The required H₂ is produced by the reformation of CH₄ or coal with H₂O. It would be highly desirable to omit the use of carbon sources for H₂ production. Additionally, for each ton of NH₃ produced, approximately two tons of CO₂ are emitted. [14]

Bearing in mind that the worldwide resources of inorganic and organic material will get limited during the 21st century, a main goal for research must be to lower the energy and resource demand used for chemical synthesis. Therefore, the development of new technologies and the optimization of existing plants are of worldwide interest. Particularly, the consumption of oil, natural gas, and their secondary products must be decreased. A small-scale NH₃ synthesis

process at ambient conditions is desirable to overcome the mentioned disadvantages related to the Haber process and to narrow down the demand of valuable resources. To use all potential advantages of NH₃ as chemical for the future, an environmental friendly and sustainable alternative method for NH₃ synthesis is desired. Ideally, it should be CO₂-free, meaning no carbon resources should be consumed and CO₂ emissions have to be avoided. Furthermore an abundant and easily accessible H₂ source has to be considered. Finally renewable energy sources have to be applied to drive such a new NH₃ process. A new process fulfilling all criteria for a sustainable NH₃ synthesis is the reduction of N₂ in an electrochemical membrane reactor (ecMR) as schematically shown in Figure 1.1 [15].

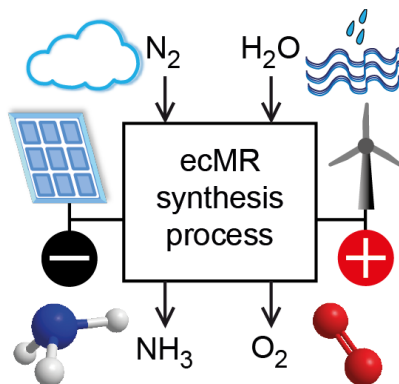


Figure 1.1: Schematic presentation of an environmentally friendly and sustainable NH₃ synthesis process starting from N₂ and abundant H₂O as H₂ source. The process is driven by renewable energy sources such as solar or wind power. [15]

The ecMR basically consists of two metal electrodes, the anode and the cathode, which are separated by a polymer membrane. The new ecMR synthesis process starts from N₂ produced by cryogenic air separation and abundant H₂O as H₂ source. The use of cheap pre-heated process steam is an environmentally friendly and economic viable possibility to increase the feasibility of the new NH₃ synthesis process. By driving the process with renewable energy sources such as solar or wind power, CO₂ emissions are avoided and the carbon footprint of NH₃ synthesis is reduced. Furthermore the energy intensive and polluting H₂ production via reformation of CH₄ or coal is redundant. Poisoning of the catalyst by sulfur compounds or CO present in the so produced H₂ is eliminated. [10] To increase the economic feasibility of the synthesis process, the valuable byproduct O₂ can be sold. Next to NH₃ also H₂ can be formed at the cathode. Hydrogen gas can be sold as additional valuable product or it can be recycled to the anodic reactant stream to be oxidized to H⁺.

The aim of the present thesis is the electrochemical reduction of N₂ for NH₃ synthesis. The importance of NH₃ for the today's world is exposed and the most important works reported in literature are summarized. The choice of proper catalysts for the electrochemical N₂ reduction is

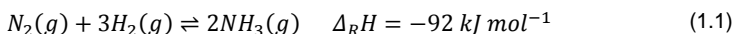
1 Introduction

discussed and a novel galvanic coating process for Rh and Ru on randomly structured Ti felts is introduced. Next to the gas phase NH₃ synthesis using an electrochemical membrane reactor, also the liquid phase synthesis is considered and investigated. The applied methods and procedures are documented and the used electrochemical cells are described in detail. To evaluate the complete electrochemical membrane based synthesis process for NH₃ production, a model of the ecMR was developed in Aspen Custom Modeler and integrated into a flow chart using Aspen+. The energy demand of the complete synthesis process is compared with the Haber process. A further optimization of the downstream separation process is conducted to decrease the overall energy demand.

1.1. The Haber process for large-scale NH₃ synthesis

Large-scale manufacturing of NH₃ is conventionally carried out by the Haber process, which was developed by Fritz Haber and Carl Bosch in the early 1900's. On 13 October 1908 Fritz Haber filed his patent for the synthesis of NH₃ from its elements N₂ and H₂ [16]. The first laboratory synthesis of NH₃ was conducted by Haber on 2 July 1909 at the Technische Hochschule Karlsruhe. This important occasion is documented by a letter of Haber sent to the directors of Badische Anilin- & Soda-Fabrik (BASF) on 3 July 1909 [3]. Subsequently, further laboratory experiments were carried out by Haber under atmospheric pressure and high temperature in the range of 1,000°C using an Fe-based catalyst to determine the thermodynamic equilibrium [17]. Later on, Haber suggested optimized pressure values of 150 to 200 bars and a temperature of around 500°C. The high technical requirements resulting from these extreme reaction conditions were solved by Bosch. On 9 September 1913, just about four years after the first laboratory NH₃ synthesis, the commercial production of NH₃ began, and the Haber process has been the first high-pressure industrial process [3]. In 1918 Fritz Haber was awarded the Nobel Prize in Chemistry for his invention of the NH₃ synthesis process. For his development of the Haber process to industrial scale, Carl Bosch was also awarded the Nobel Prize in Chemistry in 1931 [16].

Ammonia is synthesized in a heterogeneous gas-phase reaction, whereby N₂ and H₂ gas flow over an Fe-based catalyst promoted with K₂O, CaO and Al₂O₃ [5]. As this reaction is exothermic, the equilibrium conversion increases with decreasing temperature, see Equation (1.1).



However, due to the low activity of the applied catalyst at lower temperatures, the reaction temperature must be high enough to achieve reasonable reaction rates. On the other hand, NH₃ decomposition takes place as well. During NH₃ synthesis the gas volume decreases, and therefore high pressures have to be applied to shift the equilibrium towards the right side of Equation (1.1) according to the Le Chatelier principle [18]. The choice of the process parameters is driven by a compromise between the thermal stability of NH₃, the activity of the catalyst and the reaction rate. The industrial process is operated between 400 and 500°C and at 150 to 200 bars, which leads to a conversion, at equilibrium, of about 15%. The H₂ gas needed for NH₃ synthesis is mainly produced by steam reforming of natural gas at about 800°C. At

400°C the emitted CO is converted to CO₂, known as the water gas shift reaction. Hydrogen is produced as a by-product as well. All mentioned reactions are energy intensive. In total, the energy consumption of modern NH₃ plants in Western Europe is about 8 MWh/t_{NH₃}. Compared to NH₃ plants for instance in China, the energy demand is around 40% less. This decrease in energy demand is related to the application of energy efficient technologies such as the auto-thermal reforming process, which combines partial oxidation and steam reforming technology for the production of H₂. Using this technology, the overall process efficiency is as high as 60%. [13] Disadvantageously, CO₂ is emitted as well, which is considered to considerably influence global warming [19]. Detailed information about NH₃ synthesis, different process designs and general remarks about NH₃ can be found elsewhere [12,14,20]. In summary, the Haber process has serious disadvantages, such as high energy consumption, environmental pollution, and the thermodynamic limitation of the reaction. From an environmental point of view, an NH₃ synthesis process avoiding CO₂ - emissions is desirable. Additionally the direct N₂ fixation at temperatures below 100°C and ambient pressure could reduce the energy demand compared to the conventional Haber process.

1.2. The role of electrochemistry for future chemical industry

Nowadays the chemical industry is mainly based on thermally driven processes, e.g. the Haber process. The energy is primarily provided by fossil fuels, which inevitably result in CO₂ emissions. For reasonable reaction and conversion rates, selective catalysts are applied. These catalysts have no impact on the equilibrium of a chemical reaction. To shift the equilibrium towards the desired products, the reaction parameters such as temperature and pressure need to be matched to the energetic nature of the investigated reaction. In the case of NH₃ synthesis the reaction between N₂ and H₂ is exothermic and lower temperatures would shift the equilibrium towards NH₃, compare Equation (1.1). However, due to the low activity of the applied Fe catalyst, the reaction temperature needs to be increased for reasonable reaction rates. To shift the equilibrium finally towards the product side, high pressures are applied. Unfortunately, degradation of NH₃ takes place beginning at temperatures of 450 to 500°C [21], which is close to the optimal operation temperature of the Haber process. In general, conventional catalytic thermal processes suffer from high energy demand, possibly high CO₂ emissions and degradation of valuable products. Furthermore, expensive feed, e.g. CH₄ for H₂ production, are consumed. An environmentally friendly and sustainable alternative for NH₃ synthesis is the electrochemical reduction of N₂. The reactants N₂, H₂O and electrons are all inherently environmentally friendly and cheap [22]. The surrounding air contains 78 Vol.-% N₂, H₂O is abundant in most regions of the world and in terms of the energy transition the availability of cheap renewable energy is increasing. The advantages of electrochemical processes in general are (a) pollutant levels, e.g. that of CO₂, can be decreased, (b) possible overall higher energy efficiency compared to conventional thermal processes, (c) use of cheap reactant and feed streams, (d) less aggressive and challenging process conditions, e.g. ambient pressure and temperature, (e) due to lower temperature also lower degradation levels of valuable products, and (f) precise control of oxidation and reduction processes by the applied potential [22]. Electrochemical systems are compact, modular and can be designed in small scale. Due to the modularity, a scale-up for larger production capacities is easily achievable

1 Introduction

[23]. Furthermore electrochemical synthesis processes often show a high selectivity for the desired product. High product purities can be achieved even without cost intensive downstream separation steps [24].

Electrochemistry can play an important role in the future for the reduction, or avoidance, of CO₂ emissions. In general, there are four possibilities to reduce CO₂ emissions into the atmosphere: (a) application of carbon-free and possibly renewable energy sources such as wind, solar, hydro or nuclear power, (b) capture and geologic sequestration of CO₂ (CCS), (c) improvement of process efficiencies and reduction of the energy demand, and (d) utilization of CO₂ as feed for novel processes [23]. Due to fluctuations in the energy supply by renewable resources, direct application of renewable energy is difficult and an electrochemical conversion of renewable energy into chemical energy is necessary. The CCS technology is also problematic, since it is limited to certain regions with proper geologic formations. Furthermore CCS is cost intensive and the long-term impact on the environment is not yet fully clear. Higher process efficiencies either result in less amounts of feed required for a certain amount of product or more products can be produced with the same amount of feed. The emission rate, e.g. of CO₂ and the energy demand per unit of product are decreased. However, the optimization of existing plants is cost intensive and sometimes economically not feasible. The utilization of CO₂ as feed for further chemical conversion is an interesting and worthwhile alternative. Carbon dioxide nowadays is already used as feed for the synthesis of methanol CH₃OH [25]. However, an undesired side reaction is the formation of carbon monoxide CO, which forms CO₂ again in the water gas shift reaction [20]. The electrochemical conversion of CO₂ to hydrocarbons is an interesting, novel method to use CO₂ and renewable energy to produce valuable products. Parallel to the work on the electrochemical NH₃ synthesis, which is part of this thesis, the electrochemical reduction of CO₂ in a similar system using an ecMR was also investigated at the AVT.CVT by Stefanie Kriescher [26].

There are many other "up-to-date" industrial and novel, future processes, which use the advantages of electrochemical systems. The aluminum and chlor-alkali industry represent the two largest industrial processes which are based on the application of electrodes and electrical energy. Together they account for more than 90% of the electricity demand of electrolytic processes. [22] Organic electrosynthesis is an environmentally friendly and competitive methodology to synthesize organics. It is capable to replace toxic or dangerous oxidizing or reducing reagents, reduce the energy demand and unstable or hazardous reagents can be produced *in situ* directly during the electrochemical synthesis. [27] Two organics, which are mainly produced via electrosynthesis are p-aminophenol and anthraquinone [22]. Polymer electrolyte membrane (PEM) electrolysis is a feasible technique for H₂ production. Renewable energy sources such as wind or solar are coupled with abundant H₂O as H₂ source. The only waste stream produced is highly pure O₂ which can be further used or sold to enhance the overall efficiency. [9] A further novel electrochemical process is the electrochemical lignin cleavage. This process is widely investigated in the Cluster of Excellence "Tailor-Made Fuels from Biomass" (TMFB) at the RWTH Aachen University. [28] Electrochemical lignin cleavage is a sustainable and green process for the production of renewable chemicals such as vanillin and vanillic acid [29].

In summary, electrochemistry can play a vital role in the future of industrial chemistry. When fossil resources will get scarce in future, the aforementioned advantages will no doubt tip the balance in favor of electrochemical processes.

1.3. Importance of NH₃ for today's world

As basic chemical, NH₃ is used for the production of nitrogenous chemicals such as hydrazine N₂H₄, hydrogen cyanide HCN, nitric acid HNO₃, urea CO(NH₂)₂ or hydroxylamine H₃NO, see Figure 1.2. Around 80% of the produced NH₃ are used as fertilizer precursor to supply the world population with sufficient amounts of food [12]. Crops dunned with NH₃-based fertilizers feed around 50% of the world population [30].

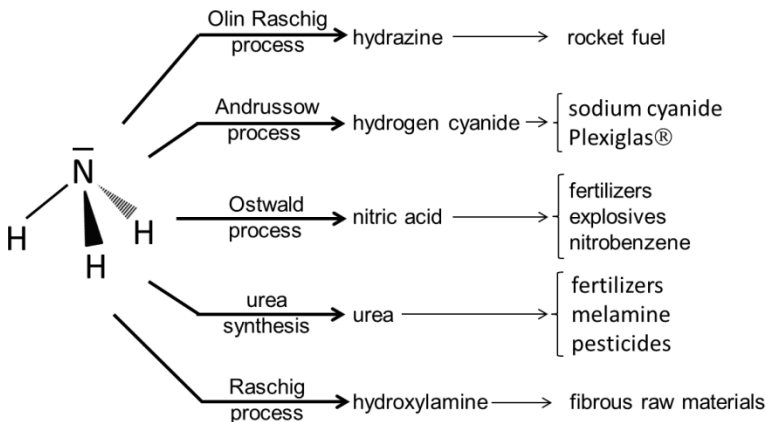


Figure 1.2: Applications of NH₃ to produce nitrogenous chemicals (adapted from [31,32])

Life on earth essentially depends on three cycles - the carbon, the nitrogen and the sulfur cycle. While carbon is the main building block of living cells, nitrogen is the key component of proteins and disulfide bridges necessary for three dimensional protein networks. Only these networks make enzymatic reactions possible. Furthermore proteins serve as signaling and structural compounds. [33] However, in its atmospheric form, N₂ is not usable for nature due to the strong triple bond between the two nitrogen atoms. Only reactive N₂ compounds such as NH₃ or urea CO(NH₂)₂ can be used by plants for growing. [34]

Next to the common applications as indicated by Figure 1.2, NH₃ attracts attention of the energy industry as a H₂ and energy carrier. The global energy demand is continuously increasing and at the same time the fossil resources get limited. In terms of the energy transition, the application of renewable energy sources is getting more important. From 2003 to 2013 the power supply by renewable energy increased by a factor of 4. Nevertheless, the share of renewable energy in the total primary energy demand is only ~2%. [1] Renewable energy sources such as solar or wind power suffer from severe disadvantages. The sun and wind

1 Introduction

cannot be turned on spontaneously and are not available 24/7. Due to this fluctuating and unpredictable power supply, coverage of peak loads and of the daily energy demand of industry is not possible [35]. To make the energy produced by renewable energy sources available when it is needed, an efficient and cost effective storage technology is needed. Furthermore this technology must be capable to storing large amounts of energy for a long period of time. Next to pumped storage hydro power stations, also batteries, such as Li-ion batteries are possible energy storage technologies. To evaluate the capability of a storage technology, the energy density is considered. Both, hydro power stations and batteries suffer from low energy densities of up to 0.2 kWh kg^{-1} [36]. Unfortunately, hydro power stations are limited to mountainous regions and conservationists often claim the protection of these areas. The battery technology is cost intensive due to its need for novel metal catalysts and up to now not applicable for the storage of large energy quantities. An interesting and promising technology is the conversion of electrical energy to chemical energy. With an energy density of 6.3 kWh kg^{-1} , which is close to the one of fossil fuels [37,38], NH_3 is an interesting chemical for energy storage purposes [36]. Nowadays NH_3 is mainly produced by the Haber process, which strongly depends on fossil resources. In future, when fossil resources will get scarce, the combination of renewable energy and an electrochemical synthesis of NH_3 can be a reasonable option to convert renewable energy to chemical energy. This conceptual idea is also the basis for the Juneau Project in Alaska. Excess wind power shall be used to synthesize NH_3 . When the wind is low the produced NH_3 can be burnt for energy production. [30] More recent developments use NH_3 as fuel for alkaline or high temperature fuel cells [8,39–41]. Ammonia can also be directly used as fuel in combustion engines, resulting in N_2 and H_2O as the only byproducts. Small traces of nitrogen oxides can be removed by a catalytic converter in the exhaust stream. [42]

The development of a H_2 economy is a feasible option to reduce the world's dependency on fossil fuels. However, the storage and transportation of H_2 is challenging. In liquid state H_2 is transported in cryogenic tanks at a temperature of -253°C and at ambient pressure. The liquefaction process is energy demanding and thermal insulation of the storage vessel needs further improvement to reduce losses due to boiling-off of H_2 . High pressure gas cylinders with a pressure of 200 bars are the most common storage systems. However, the volumetric density in $\text{kg H}_2 \text{ m}^{-3}$ system is low and can only be increased to the level of liquid H_2 of around $40 \text{ kg H}_2 \text{ m}^{-3}$ system by increasing the pressure to around 800 bars. Due to the high diffusion coefficient of H_2 in metals, hydrogen embrittlement is a typical issue when storing and transporting H_2 in metal containers. Alternative H_2 carriers are required, which fulfil certain criteria. An ideal H_2 carrier must be safe, fully recyclable and should not be more expensive than H_2 itself [43]. Ammonia is assumed to play an important role in a H_2 economy as H_2 storage and transportation medium [6,7,44,45]. The decomposition of NH_3 produces highly pure H_2 and N_2 . Ammonia contains 17.6 wt% H_2 and in the liquid state the energy content of NH_3 is around 50% higher compared to that of liquid H_2 [10]. Since NH_3 is carbon-free, the decomposition process has a zero CO_2 footprint. Furthermore, for easy storage and transportation, NH_3 can be liquefied at pressures of 9 to 10 bar at ambient temperature [46]. Instead of using NH_3 directly, also the use of chemically bound NH_3 is a versatile option. Recently, metal amine complexes, e.g. $\text{Mg}(\text{NH}_3)_6\text{Cl}_2$ have been suggested as possible H_2 storage and transportation materials [47,48]. The salt is formed by flowing NH_3 gas over anhydrous MgCl_2 at ambient temperature. Advantageously, the adsorption and desorption of

NH₃ is completely reversible. At temperatures of 200 to 350°C NH₃ desorbs from the saturated salt. The decomposition of NH₃ to N₂ and H₂ takes place at a specific decomposition catalyst starting at around 330°C. [47] For easy transportation and handling, the saturated salt is pressed into pellets and is stored together with an NH₃ decomposition catalyst in one container. This system offers an easy and safe way for NH₃ storage and H₂ supply at the same time. Similar to the electrochemical NH₃ synthesis, also the electrochemical decomposition of NH₃ or NH₃ electrolysis is of great research interest. Hydrogen of high purity can be produced and applied in fuel cell applications for instance. [49–53]

The various applications of NH₃, the use as basic material for many other products and the increasing interest of the energy industry in using NH₃ as fuel or energy storage medium will lead to an increase in NH₃ production capacities in the future. Nevertheless, the production of fertilizers will remain the main application of NH₃, since the world population and its need for food will further rise. Highly developed alternative synthesis processes for NH₃ are necessary to decrease the energy demand, to be more environmentally friendly and to be economically more viable.

1.4. Alternative synthesis routes for NH₃

There are several synthesis routes for converting N₂ to NH₃, which could surmount the aforementioned limitations of the catalytic large-scale Haber process. All routes aim to run the process either at ambient pressure or ambient temperature or a combination of both.

Mother Nature is able to reduce atmospheric N₂ to NH₃ at ambient conditions. The enzyme nitrogenase, which consists of the two proteins Fe-protein and MoFe-protein, acts as a kind of catalyst for this natural process [54]. The reactive center of nitrogenase is the metal-cluster MoFe₇S₈N called iron molybdenum cofactor, FeMoco [55]. Nonetheless, it is still not completely clear where and how N₂ is bound to FeMoco. Numerous efforts have been undertaken so far to create metal complexes with a similar activity for N₂ fixation as nitrogenase [54,56–59]. One of the most promising investigations is by Yandulov and Schrock [59]. This group developed a new molybdenum catalyst which contains tetradequate triamidoamine ligands, such as [HIPTN₃N]Mo(N₂). Slowly adding the proton source [{2,6-lutidinium}{BAr'₄} where Ar' is 3,5-(CF₃)₂C₆H₃] and the reductive decamethyl chromocene [CrCp*₂, Cp* = η⁵-C₅Me₅] was crucial to obtain an efficiency of about 66%. X-Ray measurements showed that the FeMoco cluster has a sterically protected, single molybdenum center, at which N₂ is reduced. During this reduction, molybdenum exists in different oxidation states from Mo(III) to Mo(VI). [59] For further details the interested reader is referred to the review of Svea Hinrichsen et al. on "Recent developments in synthetic nitrogen fixation" [60].

Technical alternatives are the application of photocatalytical [61–63] and electrochemical methods, which will be discussed in detail later. Schrauzer and Guth [61] investigated the photolysis of H₂O on wet TiO₂-powder at temperatures from 30 to 180°C and varying partial pressure of N₂. Prior to each experiment, a complex pretreatment of the used TiO₂-powder is necessary. In an Ar working atmosphere, H₂O is split to H₂ and O₂. By adding 0.2 wt% Fe₂O₃ to the TiO₂-powder, the yield of H₂ and O₂ was increased. However, the evolution of H₂ becomes limited when Ar is replaced by N₂, whereas this replacement has no effect on the yields of O₂. Instead of H₂, NH₃ and N₂H₄ are formed, which corresponds to the ability of TiO₂ to chemisorb

1 Introduction

H_2O and N_2 . After three hours reaction time, the achieved yield of NH_3 ranges from 0.01 μmol up to 7 μmol depending on the reaction temperature and the partial pressure of N_2 . [61] In 1980, Miyama et al. studied the heterogeneous photocatalytical synthesis of NH_3 from H_2O and N_2 using binary wafered catalysts [62]. The NH_3 production was increased by combining semiconductor powders, such as TiO_2 , SrTiO_3 , CdS or GaP and platinum black powder, bound together by the copolymer of ethylene and vinylalcohol. Using GaP resulted in the highest yield of NH_3 of about 7.5 μmol . However, the preparation of the binary wafered catalysts is complex and, similar to the results of Schrauzer and Guth [61], the achieved NH_3 yield is small. In general, photolysis of H_2O is not an appropriate process for commercial NH_3 synthesis.

1.5. Literature review about electrochemical NH_3 synthesis

Contrary to the "natural" pathway mimicking nitrogenase and the photocatalytical pathway, the electrochemical reduction of N_2 to NH_3 is attracting increasing interest of research. By applying an external potential between an anode and a cathode, electrical energy is used as the driving force for chemical reactions in small-scale electrochemical cells. Since the ecMR consumes electrical energy, it belongs to the class of electrolysis cells. The anode of the ecMR is the positive electrode and the cathode is the negative electrode. Contrary, in energy generating electrochemical cells such as fuel cells, the polarity of the electrodes is vice versa (compare also Section 4.9 and Figure 4.11). [64] The main difference to the conventional catalytic process is the way of applying H^+ for the reaction. In the Haber process, NH_3 is synthesized from its elements N_2 and H_2 according to a Langmuir-Hinshelwood reaction pathway. Hydrogen and N_2 get adsorbed on the catalysts surface and active intermediate species N-S and H-S are formed. In three consecutive steps NH_3 is formed by the reaction of these intermediate species with each other. In the fourth step the adsorbed NH_3 desorbs from the catalysts surface and empty sites on the surface are available again for further reaction. [65] Contrary, in the electrochemical pathway H^+ are supplied by an oxidation reaction at the anode of the electrochemical cell powered by the applied external potential. Most commonly gaseous H_2 or H_2O in gaseous and/or liquid state are used as H^+ source. In the case of H_2O additional to the H^+ production, O_2 is also delivered, hence the term oxygen evolution reaction (OER) for this reaction. Both, the oxidation of H_2 and H_2O also deliver electrons, which are transported from the anode to the cathode through an external circuit. Due to the electrical field between the anode and the cathode and due to the applied external potential, the H^+ are transported from the anode through an electrolyte, e.g. a polymer membrane as in the case of the ecMR, to the cathode [64]. At the cathode there are four different reaction mechanisms possible for the electrochemical reduction of N_2 to form NH_3 : both an associative and dissociative Tafel type and Heyrovsky type mechanism [66]. In an associative mechanism adsorbed N_2 adatoms are directly hydrogenated by H^+ at the catalysts surface, whilst in a dissociative mechanism, N_2 is first dissociated at the catalysts surface and then hydrogenated. In the Tafel type mechanism H^+ ions first adsorb at the catalysts surface and react with electrons to form molecular H_2 adatoms which then react with adsorbed N_2H_x or NH_x species [67]. In contrast, in the Heyrovsky mechanism the adsorbed N_2H_x or NH_x species are hydrogenated directly by the attachment of H^+ and electrons [68]. Since the activation barrier for the Tafel type mechanism is relatively high (in the range of 1 eV) for most transition metal catalysts applied in low temperature applications,

the reaction rate will be slow. The process will follow more likely either the associative or dissociative Heyrovsky type mechanism [66]. The detailed reaction equations can be found in the work of Skúlason et al. [66]. In conclusion, the dissociative Heyrovsky mechanism is more likely to occur for early transition metal flat surfaces such as Ti, Sc, Y or Zr. On late transition metal surfaces the dissociative mechanism is impossible. [66]

Basically there are four different electrochemical systems available for the electrochemical NH₃ synthesis. These systems are categorized by the electrolytes and temperatures applied, see Figure 1.3. [10].

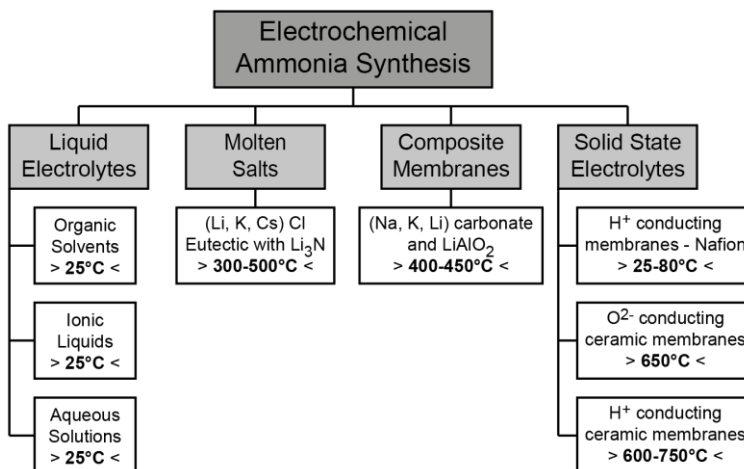


Figure 1.3: Electrochemical systems for the electrochemical NH₃ synthesis using varying electrolytes depending on the applied temperatures (adapted from [10])

For evaluating the work documented in literature, two parameters are used: (a) the NH₃ production rate in mol NH₃ produced per s of experimental time and cm² of active catalyst area and (b) the current efficiency (CE), which gives the share of the total charge C transported that was used for NH₃ synthesis.

1.5.1. Liquid electrolytes

Liquid electrolytes can be operated near room temperature. Early works have been published already in the 1960's [56,69–71]. However, these works were not very detailed and there are no numbers available for neither the production rate nor the current efficiency. More detailed works were published by Gorodyskii et al. [72] and Sclafani et al. [73] at the end of the 1970's and the beginning of the 1980's, respectively. Gorodyskii et al. could synthesize NH₃ in an alkaline methanol solution catalyzed by Ti(OH)₃-Mo(III) at 20°C and a N₂ pressure of 30 bars. A reasonable NH₃ yield of 43% and a production rate of 8.6 × 10⁻⁹ mol s⁻¹ at a current density of 0.5 mA cm⁻² were achieved using a mercury cathode. [72] Sclafani et al. report the

1 Introduction

electrochemical N₂ reduction at atmospheric pressure and three different low temperatures of 25, 35 and 45°C in a 6 N aqueous KOH solution. At a cathode potential of -0.84 V vs. NHE a maximum production rate of 5.3×10^{-14} mol s⁻¹ cm⁻² and a current efficiency of ~1% were achieved at 45°C using a Fe cathode. [73] Furuya and Yoshioka published three papers on the electroreduction of N₂ on different gas-diffusion electrodes [74–76]. The influence of different metal phthalocyanine cathodes and different potassium salt solutions applied as electrolyte were investigated. The best results were achieved using a Fe-phthalocyanine cathode in a 1 M aqueous KOH solution at 25°C. The corresponding production rate was 2.0×10^{-10} mol s⁻¹ cm⁻² at a current efficiency of 0.12% [74]. Both numbers were significantly increased to 6.4×10^{-9} mol s⁻¹ cm⁻² and 1.3%, respectively, when using a ZnSe-phthalocyanine electrode [76]. Tsuneto et al. [77,78] investigated the synthesis of NH₃ in an organic solvent. A mixture of 0.2 M LiClO₄ and 0.18 M ethanol as H₂ source in tetrahydrofuran THF was used as electrolyte. The electrolysis was conducted at a current density of 2 mA cm⁻² applying different metal cathodes, amongst others Al, Ti, Mo, Fe, Co, Ni, Cu and Ag. A current efficiency of 8.4% and a maximum production rate of 5.8×10^{-10} mol s⁻¹ cm⁻² were achieved with a Ag working electrode at a N₂ pressure of 1 bar. [77] The influence of an increased N₂ pressure of 50 bars was investigated with a Fe working electrode. The current efficiency was enhanced to 58% and the production rate increased to 4.0×10^{-9} mol s⁻¹ cm⁻² [78]. Pappenfus et al. [79] followed a similar approach as Tsuneto et al.. Again, LiClO₄ and ethanol were used as additives, but the organic solvent was replaced by ionic liquids. At a Ni working electrode a maximum current efficiency of 5.1% was achieved. Since no experimental time is given, the corresponding production rate could not be directly compared. [79] Köleli et al. [80,81] also used lithium salts as additives, but this time an aqueous electrolyte consisting of methanol and H₂SO₄ was applied. In a conventional three-electrode setup NH₃ was synthesized using Pt working electrodes coated with polyaniline (PAn) or polypyrrole (PPy). After one hour electrolysis time a maximum current efficiency of 16% was achieved with a PAn working electrode at a N₂ pressure of 50 bars. Contrary, the maximum production rate of 3.7×10^{-10} mol s⁻¹ cm⁻² was achieved with a PPy working electrode of 0.73 µm thickness at a N₂ pressure of 60 bars after five hours electrolysis time [81].

In summary, from the 1960s until today current efficiencies of up to 58% and production rates of up to 6.4×10^{-9} mol s⁻¹ cm⁻² have been achieved in liquid electrolytes. However, complex metal phthalocyanine cathodes [74–76], organic solvents mediated by LiClO₄ [77,78] or Pt electrodes coated with PAn or PPy at high N₂ pressures of up to 60 bars [80,81] were applied. All systems described above vary a lot with respect to the kind of electrodes and kind of setup applied. To increase the solubility of N₂ in the electrolyte high pressure is necessary. For a meaningful comparison, experiments in one particular electrolyte at varying reaction conditions and with different working electrodes are desired.

1.5.2. Molten salts

At temperatures of 300 to 500°C molten salt electrolytes can be applied. In 1997, Ito and Goto were the first to electrochemically reduce N₂ to nitride ions N³⁻ in an eutectic melt of LiCl and KCl using Ni and Ti working electrodes. The formed N³⁻ can react with H₂O vapor to produce NH₃. However, no numbers for the achieved current efficiencies or production rates were

reported. [82] Murakami et al. intensively studied the application of molten salts as electrolytes consisting of an eutectic mixture of the alkali-metal halides LiCl, KCl and CsCl [83–87]. Lithium nitride Li₃N was added as N³⁻ source. Nitrogen gas is reduced to N³⁻ at a porous Ni cathode and migrates through the molten salt electrolyte to the anode. Several hydrogen sources such as H₂ gas, CH₄ or H₂O vapor were tested. When using H₂ gas, NH₃ is synthesized at the anode by the reaction of H₂ and N³⁻. At 400°C a maximum current efficiency of 72% and a production rate of 3.3×10^{-9} mol s⁻¹ cm⁻² were achieved. [83] The replacement of H₂ by H₂O vapor at 300°C resulted in a six times higher production rate, but the current efficiency dropped to 23%. [85] Disadvantageously, the molten salts need to be prepared and kept under inert atmosphere, which makes their use in industrial applications more difficult. Just recently, Licht et al. synthesized NH₃ by N₂ and steam electrolysis using a molten hydroxide suspension of nanoscale Fe₂O₃ [88]. At a current density of 2 mA cm⁻² and an applied electrolysis voltage of 1.2 V, a current efficiency of 35% was achieved at a moderate temperature of 200°C compared to the previous works reported in literature.

In summary, the synthesis of NH₃ using molten salt electrolytes is feasible. However, high temperatures in the range of 300 to 500°C are necessary for the salt melt, which results in higher energy demand and more challenging material requirements than for liquid electrolytes.

1.5.3. Composite electrolytes

The application of composite electrolytes at temperatures of 400 to 450°C moves in the focus of research more recently. Composite electrolytes in general consist of several different ion conductive phases. For the purpose of electrochemical NH₃ synthesis, a solid oxide composite material is added to a carbonate or phosphate melt [10]. By adding the oxides, the electrical, thermal or mechanical properties of the resulting electrolyte can be modified. Wang et al. were the first to synthesize NH₃ using a composite electrolyte [89]. Starting from N₂ and natural gas, a maximum production rate of 7.0×10^{-9} mol s⁻¹ cm⁻² was achieved with a yttrium doped ceria composite material YDC–Ca₃(PO₄)₂–K₃PO₄ and two Ag–Pd electrodes at ambient pressure and a temperature of 650°C. Amar et al. investigated several different oxide-carbonate composite materials to synthesize NH₃ electrochemically [90–93]. Applying a composite cathode of the structure La_{0.6}Sr_{0.4}Fe_{0.8}Cu_{0.2}O_{3-δ}–Ce_{0.8}Sm_{0.2}O_{2-δ}, a Ni–Ce_{0.8}Sm_{0.2}O_{2-d} anode and a Ce_{0.8}Sm_{0.2}O_{2-d}–(Li/Na/K)₂CO₃ electrolyte resulted in the highest NH₃ production rate of 5.4×10^{-9} mol s⁻¹ cm⁻² at a temperature of 450°C and an applied potential of 0.8 V [91]. The highest current efficiency of 0.17% was achieved using a Ce_{0.8}Gd_{0.18}Ca_{0.02}O_{2-δ} (CGDC)–ternary carbonate composite electrolyte, a CoFe₂O₄–Ce_{0.8}Gd_{0.18}Ca_{0.02}O_{2-δ} (CFO-CGDC) composite cathode and a Sm_{0.5}Sr_{0.5}CoO_{3-δ}–Ce_{0.8}Gd_{0.18}Ca_{0.02}O_{2-δ} (SSCo-CGDC) composite anode at a temperature of 400°C and an applied potential of 1.6 V [92]. Lan et al. investigated the electrochemical synthesis of NH₃ starting from wet air [94,95]. The highest production rate of 1.1×10^{-10} mol s⁻¹ cm⁻² was achieved at a temperature of 400°C and an applied potential of 1.4 V applying a Ce_{0.8}Gd_{0.2}O_{2-δ}–(Li,Na,K)₂CO₃ composite electrolyte and a perovskite oxide Pr_{0.6}Ba_{0.4}Fe_{0.8}Cu_{0.2}O_{3-δ} as catalyst for both electrodes. However, the corresponding current efficiency was less than 1%. [94]

In summary, there are some composite electrolytes available for electrochemical NH₃ synthesis at ambient pressure. However, high intermediate temperatures of 400 to 450°C are necessary.

1 Introduction

A further increase of temperature will lead to decreasing production rates due to increasing NH₃ decomposition. The achieved production rates for composite electrolytes are in the range of liquid and molten salt electrolytes, but the corresponding current efficiencies are at least one order of magnitude smaller.

1.5.4. Solid electrolytes

Solid electrolytes can be applied in a wide temperature range from room temperature to 800°C depending on the material structure of the used membrane. Solid electrolytes have several advantages over the other mentioned electrolytes. They are easy to handle, scalable and exhibit exceptional mechanical and chemical stability. In general solid electrolytes can be either ceramic or polymeric.

a) Ceramic solid electrolytes

There are three different types of ceramic oxides which are applied in electrochemical devices such as fuel cells or electrochemical synthesis systems: perovskites, fluorites and pyrochlores. It is beyond the scope of the present thesis to discuss all different structures of these ceramics. Interested readers are referred elsewhere [10,96,97]. A general overview about solid-electrolyte membrane reactors is given by Stoukides [98].

Ceramic solid electrolytes have been used for the first time for electrochemical NH₃ synthesis by Marnellos and Stoukides starting from N₂ and H₂ [99]. At 570°C and atmospheric pressure a maximum NH₃ production rate of 3.1×10^{-9} mol s⁻¹ cm⁻² was achieved using a strontia-ceria-ytterbia SCY perovskite of the form SrCe_{0.95}Yb_{0.05}O₃ and two porous Pd electrodes. The current efficiency was as high as 78%. However, the net efficiency dropped to around 50% due to decomposition of the formed NH₃. In a different approach Skodra and Stoukides could synthesize NH₃ electrochemically from N₂ and steam instead of H₂ under atmospheric pressure using the same electrolyte. The Pd catalyst at the cathode was replaced by an industrial Ru/MgO catalyst. However, the achieved production rate dropped remarkably to 4.0×10^{-13} mol s⁻¹ cm⁻² at a temperature of 650°C. [100] Intensive studies have been carried out about the application of ceramic electrolytes for the electrochemical NH₃ synthesis by Wang et al. [101–106]. In their studies perovskites, fluorites and pyrochlores were applied as electrolytes. In all experiments NH₃ was synthesized starting from N₂ and H₂ at atmospheric pressure using Ag-Pd electrodes at an applied potential of 0.6 V. The maximum production rate of 8.2×10^{-9} mol s⁻¹ cm⁻² was achieved with a fluorite electrolyte of the structure Ce_{0.8}Sm_{0.2}O_{2-δ} at a temperature of 650°C [105]. Ouzounidou et al. [107] used a similar setup to the one of Marnellos and Stoukides [99]. Interestingly, an industrial Fe catalyst was used at the cathode, while Ag was used as the anodic catalyst. The solid electrolyte was a strontia-zirconia-yttria SZY perovskite of the form SrZr_{0.95}Y_{0.05}O_{3-α}. Starting from N₂ and H₂ a maximum NH₃ production rate of 0.7×10^{-11} mol s⁻¹ cm⁻² at a temperature of 450°C and an applied voltage of 2 V was achieved. Obviously, the catalytic activity of the industrial Fe catalyst is high for a thermally driven process such as the Haber process, but the electrochemical activity is poor compared to other catalysts used together with ceramic electrolytes. [107] The group of Guilin Ma [108,109] showed that a BaCe_{0.85}Y_{0.15}O_{3-α} ceramic electrolyte has a high H⁺ conductivity and gives

reasonable results for the electrochemical NH₃ synthesis. The maximum NH₃ production rate of 4.1×10^{-9} mol s⁻¹ cm⁻² was obtained at a temperature of 530°C at atmospheric pressure.

In summary several ceramic electrolytes have been proven to be applicable for electrochemical NH₃ synthesis. The maximum production rate achieved is in the same range as for liquid, molten salt and composite electrolyte systems. However, for high H⁺ conductivity of the ceramic electrolytes temperatures ranging from 450 to 650°C are necessary to provide sufficient H⁺ for the reduction of N₂. At these elevated temperatures, NH₃ decomposition is a severe issue and NH₃ synthesis is kinetically hindered due to the exothermic heat of the reaction. Furthermore, the preparation of ceramic electrolytes by sintering of raw powders at temperatures of 800 to 1500°C for several hours is energy demanding.

b) Polymer solid electrolytes

Beside perfluorosulfonic acid membranes such as Nafion from Dupont, there are also polyether ether ketone PEEK and polybenzimidazole PBI membranes available exhibiting high H⁺ conductivity. However, Nafion-like polymer membranes are the most popular ones being used in many industrial applications such as the chlor-alkali process or H₂ fuel cells. [10]

In 1988 Cook and Sammells reported the electrochemical N₂ reduction to NH₃ at ambient temperature and pressure for the first time using a polymer electrolyte interface [110]. Starting from N₂ and H₂ a maximum production rate of 4.9×10^{-11} mol s⁻¹ cm⁻² was achieved using a Ru cathode and a Pt anode. The two electrodes were separated by a Nafion 417 membrane and the corresponding current efficiency was as low as 0.002%. Kordali et al. synthesized NH₃ at atmospheric pressure and a temperature of 90°C using H₂O as H⁺ source [111]. Similar to Cook and Sammells [110], Ru and Pt were used as cathodic and anodic catalyst separated by a Nafion membrane. The anodic electrolyte was an aqueous KOH solution and an Ag/AgCl electrode was applied as reference. At a cathodic potential of -1.02 V vs. Ag/AgCl a maximum production rate of 2.1×10^{-11} mol s⁻¹ cm⁻² and a low current efficiency of 0.24% were achieved. Xu et al. intensively studied the electrochemical synthesis of NH₃ using a polymer Nafion membrane and ceramic catalysts [112–114]. On the anode side of the cell a Ni doped ceramic catalyst in the form of Ni-Ce_{0.8}Sm_{0.2}O_{2-δ} (Ni-SDC) was applied. On the cathode side a Sm_{1.5}Sr_{0.5}NiO₄ (SSN) [112] or SmFe_{0.7}Cu_{0.1}Ni_{0.2}O₃ (SFCN) [113] ceramic catalyst was used. Both catalysts showed an equally high activity for the electrochemical NH₃ synthesis. The highest production rate documented so far in literature of 1.1×10^{-8} mol s⁻¹ cm⁻² was achieved using the SFCN ceramic catalyst at a temperature of 80°C and an applied cell potential of 2 V. The corresponding current efficiency was as high as 90.4%. [113] In a further study, Liu et al. compared the standard Nafion membrane with a sulfonated polysulfone membrane (SPSF) prepared in their laboratory [114]. The cathodic catalyst was again the SSN ceramic catalyst used before [112]. The achieved production rate at a temperature of 80°C and an applied cell potential of 2.5 V was in the same range as compared to the same experiments conducted with the standard Nafion membrane. Zhang et al. also investigated the application of a ceramic cathode catalyst in combination with a Nafion membrane [115]. Using the same cell design as Liu et al. [114] a maximum production rate of 0.9×10^{-8} mol s⁻¹ cm⁻² was achieved at a temperature of 80°C and an applied cell potential of 2.5 V. The used ceramic catalyst was of the structure SmBaCuNiO_{5+δ}. Lan and Tao again used H₂O instead of H₂ as H⁺ source [116,117]. In

1 Introduction

their first approach a membrane electrode assembly consisting of two Pt electrodes and a Nafion 211 membrane was applied. To avoid losses of produced NH₃ due to dissolution of NH₃ in the moistened membrane, the Nafion membrane was transferred from the H⁺-form to the NH₄⁺-form before starting the experiment. The membrane conversion is carried out by storing the membrane in a 35 wt% aqueous NH₃ solution for one day. Afterwards, the membrane was rinsed with de-ionized H₂O to flush away residual NH₃. The maximum production rate achieved was 1.1×10^{-9} mol s⁻¹ cm⁻² at room temperature and ambient pressure at an applied cell potential of 1.6 V. The current efficiency achieved was less than 0.5%. [116] Replacing the Nafion 211 membrane in H⁺ form by a H⁺/Li⁺/NH₄⁺ mixed conducting membrane had no positive impact on the achieved production rate [117]. At a temperature of 80°C and an applied cell potential of 1.2 V the production rate dropped to 9.4×10^{-10} mol s⁻¹ cm⁻². However, the current efficiency was slightly increased to 0.8%.

In summary the application of solid electrolytes is possible in a wide temperature range from room temperature up to 100°C for polymer electrolytes and from 450 to 650°C for ceramic materials. The highest production rate and current efficiency reported so far were achieved with a combination of ceramic catalysts and a polymer electrolyte [113].

In comparison to the conventional Haber process, all electrochemical systems described before suffer from too low production rates. So far the achieved production rates are in the range of 10^{-13} to 10^{-8} mol s⁻¹ cm⁻². An increase in temperature could lead to an increase in reaction rate and thus to an increase of the production rate. However, at higher temperatures the rate of NH₃ decomposition is also increasing. Unfortunately, the main parallel reaction is still the evolution of H₂ out of H⁺ called hydrogen evolution reaction (HER). Due to the strong triple bond of N₂ the recombination of two H⁺ to H₂ is much more likely for most systems compared to the synthesis of NH₃. For future systems, separation of H₂ from N₂ and NH₃ at the cathode side is a feasible option to produce two valuable products, H₂ and NH₃, at the same time. For a commercial application of electrochemical NH₃ synthesis systems, significant improvements in catalyst and electrolyte materials are desired.

2. Electrocatalysts and their galvanic deposition

Parts of this chapter have been published in: Physical Chemistry Chemical Physics

Title: *Galvanic deposition of Rh and Ru on randomly structured Ti felts for the electrochemical NH₃ synthesis*

DOI: 10.1039/c4cp05501b

Abstract

Nowadays NH_3 is exclusively synthesized by the Haber process. Unfortunately, the energy demand and the CO_2 emissions due to H_2 production are high. Hydrogen production utilizes precious carbon sources such as coal and natural gas. An alternative process concept applies a membrane electrode assembly in an electrochemical membrane reactor (ecMR). At the anode H_2O is oxidized at an IrMMO catalyst to form protons. By applying an external potential to the ecMR N_2 is reduced to NH_3 at the cathode. Just recently Rh and Ru were identified as possible cathodic electrocatalysts by DFT calculations. Here, an easy and highly efficient method for galvanic coatings of Rh and Ru on randomly structured Ti felts to be used in a membrane electrode assembly is presented. Linear sweep voltammetry measurements give a slightly higher activity of Ru for the liquid phase electrochemical NH_3 synthesis. The reached NH_4^+ concentration is 8 times higher for Ru than for Rh. From an economical point of view, Ru is also more feasible for an electrochemical NH_3 synthesis process. Such electrodes can now be evaluated in an ecMR in comparison to recently demonstrated Ti-based electrodes.

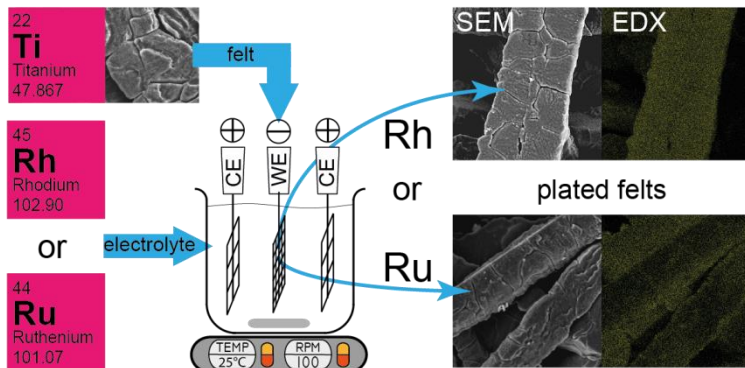


Figure 2.1: Graphical abstract of Chapter 2: Rhodium and ruthenium are each electroplated with current efficiencies above 90% on titanium support felts to be used as electrodes for the electrochemical ammonia synthesis in liquid phase.

2.1. Introduction

To overcome the disadvantages of the Haber process (compare Section 1.1) a more sustainable and potentially cost saving alternative for NH₃ synthesis is desirable. One potential alternative is the application of an electrochemical membrane reactor (ecMR) at ambient conditions (see Chapter 4). The core of this reactor is a membrane electrode assembly (MEA), which consists of a polymer proton exchange membrane (PEM) and two metal electrodes pressed into the PEM from both sides. Electrical energy, e.g. from renewable energy sources such as wind or solar power, is used as driving force for the chemical reactions taking place at the MEA. For an efficient synthesis of NH₃ in the ecMR, a high catalytic surface area at the anode and the cathode is required. Randomly structured metal felts with certain porosity and high specific surface area are used as electrodes in the ecMR [26]. These metal felts are either directly prepared out of the catalytic material, e.g. Fe, or a thin coating in the range of 1 µm of a desired metal, e.g. Rh or Ru has to be applied on a proper support material. The support material has to withstand severe conditions, such as corrosion based on the applied direct current or formed anodic O₂, acidic conditions due to the applied H⁺ modified PEM and temperatures up to 120°C [118]. A suitable support material is Ti. In air, a thin around 10 nm thick corrosion resistant TiO₂ layer is formed. Unfortunately TiO₂ has a lower conductivity compared to pure Ti and the surface is quite smooth. For a successful coating the TiO₂ layer has to be removed prior to the coating process by etching with hot concentrated HCl. [119] In this chapter an easy and highly efficient method for galvanic coatings of Rh and Ru on randomly structured Ti felts is introduced. Based on polarization curves, the influence of the applied charge, i.e. the applied current and plating time, on the deposition process is investigated. First activity measurements with the coated electrodes are presented and an economical estimation is given, whether Rh or Ru is more feasible for an electrochemical NH₃ synthesis process using an ecMR.

2.2. Choice of catalyst

Large-scale NH₃ synthesis via the Haber process mainly uses a promoted Fe₃O₄ catalyst. A Ru based catalyst would be more favorable due to its higher catalytic activity. However, the raw material price is too high for a large-scale application and Ru is poisoned by H₂. [120,121] Just recently, Skúlason et al. evaluated theoretically possible transition metals as catalysts for the electrochemical NH₃ synthesis [66]. Using the density functional theory (DFT), they calculated the Gibbs free energy profile for the reduction of N₂. By assuming that the activation energy scales with the free energy difference in each elementary step, the catalytic activity has been investigated. The potential was calculated at which -ΔG for each reaction step is smaller than or equal to zero to achieve significant reaction rates [66]. The resulting Volcano plot is given in Figure 2.2.

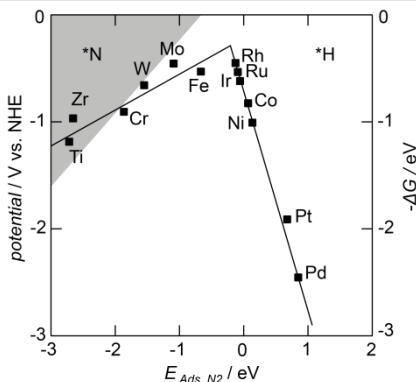


Figure 2.2: Volcano curve for the N_2 reduction (redrawn after [66]).

According to Figure 2.2 Fe, Rh and Ru show the highest activity. However, the metal surface will mainly be covered by $*H$ as indicated by the white background and H_2 formation will be a competing reaction. In comparison Ti or Zr will mainly be covered by $*N$ as indicated by the grey background and NH_3 will rather be synthesized than H_2 . Hence, early transition metals should be applied as electrocatalysts for the electrochemical NH_3 synthesis preferably. In Chapter 5 the application of Ti electrodes in an ecMR will be discussed. However, Rh, Ru and Fe catalysts should be considered as well due to their high activity. Furthermore, Ru and Fe based catalysts are already applied in the large scale Haber process. While Fe is easily accessible in different modifications such as solid plates, powders or felts, Rh and Ru are too expensive to use bulk materials for the manufacturing of electrodes.

2.3. Electroplating and parameters

In a wide variety of industrial processes such as electronics or the automotive industry electroplating is a key method for preparing thin metal layers. Even though there are many alternatives such as chemical vapor deposition, electroless deposition and atomic layer deposition, electroplating is used nevertheless due to its easy handling and economic aspects. [122] Electroplating on flat Ti surfaces such as discs [123] or foils [124] is a known technique for preparing thin catalyst layers on a corrosion resistant support material. Allen et al. even deposited Pt-based electrocatalysts on regular structured Ti expanded metal meshes by electroplating [125]. However, no research has been reported so far on electroplating on randomly structured Ti felts.

During electroplating of metals solid deposits are formed based on chemical reactions occurring at the surface of conductive materials. The electron charge transfer takes place between the cathode and a metal ion dissolved in an electrolyte. [126] Depending on the use of a soluble or passive anode the concentration of the dissolved metal ions stays constant or decreases in time. For the coating of Rh or Ru a passive anode, e.g. a platinized Ti electrode is used and the electrolyte has to be replaced or refreshed from time to time for constant plating conditions.

Since no oxidation of the anode material occurs, dissolved components of the electrolyte, e.g. SO_4^{2-} ions have to be oxidized.

The main objective of electroplating is to form regular deposits of the desired metal on the support material. Several parameters such as agitation of the electrolyte, temperature, concentration, pH and composition of the electrolyte and the applied current density influence the coating quality and properties. [122] Agitation of the plating bath prevents concentration polarization and gradients in the electrolyte. Depletion of metal ions and formation of pin holes close to the cathode surface are avoided. The morphological structure of deposits is influenced as well. To some extent coarser deposits can be formed and impurities can get embedded. [127,128] Controlling the temperature is crucial for high quality electroplating. In a temperature interval of 5°C around the optimum plating temperature high quality coatings are achieved and sufficient plating rates are accessible. In general a higher temperature leads to a higher plating rate. [128] The composition of the electrolyte affects the appearance of the coating as well. For Cu coatings it is well known that the addition of Cl^- ions leads to a smoother surface with smaller grain size [129] and the coating patterns are spherical [130]. Sulfuric acid is often used as basic solvent for plating baths due to its good conductivity. The coating properties are more affected by the concentration of H_2SO_4 than by the metal ion concentration. Rh coatings can tend to build micro-cracks if the acid concentration is too high [131]. During electroplating sulfate ions undergo a cyclic process. In diluted H_2SO_4 the sulfate ions SO_4^{2-} get oxidized at the anode to SO_4^- . These SO_4^- ions react with H_2O to HSO_4^- and O_2 . The HSO_4^- ions dissociate again to SO_4^{2-} and H^+ . Finally, these H^+ react at the cathode to form H_2 . In total, one H_2O molecule is oxidized, while two SO_4^{2-} ions act as catalyst for the cyclic electrolysis process. Finally, the applied current density has to be matched to the applied temperature and to the electrolyte composition by measuring polarization curves. A low current density will result in a low coating rate and defects in the support material will eventually not be coated at all. Furthermore the deposits contain more impurities and residual stress and changing material properties are the consequences. At high current densities rough deposits are formed. However, with increasing coating thickness the surface gets smoother. Additionally a high current density does not automatically increase the plating rate, but burned coatings can be formed. At high current densities not only the desired metal ions are reduced, but also H_2 is formed. The formed H_2 can creep underneath a coating layer causing delamination. [122,127] Not only the magnitude of the applied current density is important, but also the current distribution on the electrode surface. Metal ions will not deposit evenly over a large surface, but rather will emerge at preferential domains. The surface of planar support materials develops a certain roughness. There are spots which are closer to the counter electrode, resulting in a localized higher current density. Both, the preferred spots and the localized higher current density, lead to a heterogeneous distribution of the coating on the plating target. A homogeneous electric field parallel to the plating target can support an equal current distribution. [128] Controlling the current density and the current distribution on the electrode surface is crucial for high quality plating results. Considering the nature of randomly structured support materials like the meshes used in the present study, obviously the distribution of the coating will be influenced by the heterogeneous distribution of the current.

2 Electrocatalysts and their galvanic deposition

The mentioned parameters influence the shape and position of the polarization curve measured for a particular electrolyte. A typical polarization curve can be divided in four parts depending on varying rate limiting factors [132,133], see Figure 2.3.

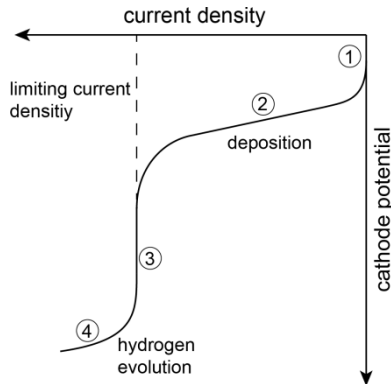


Figure 2.3: Schematic presentation of a polarization curve (adapted from [133])

(1) The first part corresponds to the activation or transfer polarization. The applied potential leads to dissociation and ionization of the desired metal. With increasing potential the resulting current density stays close to zero and the process is determined by the kinetics of the electrode reactions. The rate limiting step is the transfer of metal ions through the electrode electrolyte interface.

(2) The second part corresponds to the concentration polarization domain. The applied potential mainly leads to the deposition of metal ions. The number of discharged and deposited ions is rising and the current density and the diffusion rate are increasing as well. The rate limiting step is the depletion of metal ions close to the cathode surface. However, diffusion limitation increasingly hampers the supply of ions out of the bulk of the solution through the Nernst layer towards the electrode surface.

(3) The third part corresponds to the domain of the limiting current. The current density stays constant at the value of the limiting current density and the ion concentration at the surface has reached a value close to zero. The rate limiting step is the diffusion of metal ions.

(4) The fourth part corresponds to the post limiting region. An additional reaction such as co-deposition or H₂ evolution takes place to further increase the current density. The pH increases at the cathode and metal hydroxides can be incorporated into the metal deposit [128]. The current efficiency decreases and the plating appearance will be rough [133].

By choosing current densities which lie within the second part of the polarization curve, the best plating results should be achieved.

2.4. Electroplating of Rhodium and Ruthenium

Electroplating of platinum group metals such as Rh and Ru is relevant for high temperature corrosion protection, low resistance contacts and for preparing thin catalyst layers. Rh and Ru catalysts are particular interesting for electrochemical processes such as the electrochemical NH₃ synthesis or the oxidation of H₂O to produce H₂. However, the raw material prices are high and thin electrodeposited catalyst layers are desirable.

2.4.1. Rhodium

Rhodium is an ideal metal for electrical applications, finishes on scientific and surgical instruments and as contact material in radio frequency circuits since there is no oxide layer present on Rh at ambient conditions. [134] Furthermore deposits of Rh are hard, show low abrasion and are corrosion resistant. According to the volcano plot presented by Skúlason et al. [66] the catalytic activity of Rh and Ru for the electrochemical NH₃ synthesis is comparable. However, Rh is around 17 times more expensive than Ru (see also Table 2.6) [135].

As early as 1842, H.B. Leeson filed a patent, which announced the possibility of electroplating of Rh [136]. Only 50 years later, July and Leidiè and parallel to them E.F. Smith tried to electrodeposit Rh for the first time. July and Leidiè found that Rh can not only be deposited from RhCl₂ but also from Rh₂(SO₄)₃ electrolytes. In 1912 Marino filed a patent for a RhCl₂ based electrolyte. [137] However, for technical purposes Rh is usually electrodeposited from sulfate, phosphate or sulfate-phosphate electrolytes today [138].

For Rh coatings, the surface pretreatment is important, since the electrodeposited material shows poor adhesion to the substrate. Cracks in or spalling of the deposit may occur, which is more likely for thick coatings. With rising temperature the tendency for cracking is increasing as well. However, cracks in the deposit can be avoided by electroplating at room temperature [134]. Contrary, the current efficiency increases with temperature, but decreases with decreasing current density. [134,139] Typically Rh is electrodeposited from sulfate electrolytes at the following conditions listed in Table 2.1.

Table 2.1 Optimal parameters for the electrochemical deposition of Rh		
Parameter	Value	Reference
pH	< 1	[140]
Temperature [°C]	35 - 45	[141]
Rh concentration [g l ⁻¹]	< 4	[137]
Current density [A dm ⁻²]	1 - 11	[141]

Electrodeposition of Rh is widely applied on different substrate materials for several applications. Brylev and his co-workers intensively worked on the electrodeposition of Rh on pyrolytic graphite electrodes for the reduction of nitrate and nitrite [142–144]. Several works have been published on the electrodeposition of Rh on Pt electrodes and Pt and Au single-crystals to investigate its electrochemical and electrocatalytic properties, e.g. the adsorption

2 Electrocatalysts and their galvanic deposition

capacity for CO and NO [145–149]. Quite recently, Rh was electrodeposited from ionic liquids by Jayakumar et al. [150,151]. There are also some works on electrodeposition of Rh on Ti substrates [140,152,153], but to the best of our knowledge there are no reports available about electrodeposition of Rh on Ti felts.

2.4.2. Ruthenium

Being much cheaper than Rh, Ru is even more interesting for the electrochemical NH₃ synthesis. Electrodeposited Ru is hard, has a high wear and arc resistance and shows good electrical conductivity [154–157]. Even at ambient conditions Ru quite readily forms a protective RuO₂ layer. However, in contrast to TiO₂, this oxide layer has the same conductivity as pure Ru [156,158].

Electrodeposition of Ru is a well investigated cheaper method for the preparation of electrical contacts instead of using Au or Rh [157]. In 1936 a patent by Zimmermann and Zschiegner announced the electrochemical deposition of Ru for the first time using various nitrosyl ruthenium complexes [159]. Only 20 years later Volterra was able to electrodeposit Ru on Ag for electrical contacts. However, the formation of toxic RuO₄ at the anode was an undesired parallel reaction [158,160,161]. A detailed investigation of Ru electrolytes was carried out by Reid and Blake [161]. They used a ruthenium nitrosyl sulphamate plating solution which was derived from RuCl₃, HNO₃ and NaHCO₃ with a valency of Ru of +3. The plating solution was difficult to be prepared reproducible and the reached current efficiencies were less than 20%. With increasing Ru content the current efficiencies got even lower and large scale Ru plating was impossible. In 1969 Reddy and Taimsalu [162] presented a new plating electrolyte based on a well-defined Ru complex, referred to as RuNC. The core is a Ru-N-Ru bridge and the valency of Ru is +4. The reached current efficiencies strongly depend on the operation parameters and electrolyte properties. With increasing pH and temperature the current efficiency increases. Contrary with increasing Ru concentration and current density the current efficiency decreases. The best results were achieved at the following operation parameters, see Table 2.2.

Table 2.2 Optimal parameters for the electrochemical deposition of Ru [162]

Parameter	Value
pH	< 1
Temperature [°C]	35 - 45
Ru concentration [g l ⁻¹]	< 4
Current density [A dm ⁻²]	1 - 11

Parallel to the work of Reddy and Taimsalu, Bradford, Cleare and Middleton [163] also performed experiments on Ru electroplating using the same Ru complex. Both groups found that the addition of NH₄⁺ to the electrolyte or the use of NH₄⁺ as counter ions of the Ru complex leads to the suppression of RuO₄ evolution at the anode.

Many studies have been carried out about electroplating of Ru on metal substrates with different goals to be achieved. Electrodeposited Ru or RuO₂ can be used for supercapacitors [164,165], corrosion protection of bipolar plates for polymer electrolyte membrane fuel cells [166] or for the production of electrical contacts [155,156].

Similar to Rh, also the electrochemical deposition of Ru from ionic liquids attracted more attention quite recently [151,167–169]. Due to its corrosion resistance Ti is particularly interesting as support material for Ru coatings. Several works have been published about electroplating of Ru on planar Ti substrates [170–173], but to the best of our knowledge similar to Rh there are no reports available about electrodeposition of Ru on Ti felts.

2.5. Materials & Methods

2.5.1. Chemicals & Materials

Commercial available Rh and Ru electrolytes (Wieland Edelmetalle GmbH) were used as received for the galvanic coating experiments. The Rh electrolyte consists of $\text{Rh}_2(\text{SO}_4)_3$ dissolved in H_2SO_4 with a Rh concentration of 2 g l⁻¹ and a pH < 1. The optimal coating temperature is 20 to 30°C. The Ru electrolyte consists of a Ru complex of the form $(\text{NH}_4)_3[\{\text{RuCl}_4(\text{H}_2\text{O})_2\}(\mu\text{-N})]$ dissolved in H_2SO_4 with a Ru concentration of 5 g l⁻¹ and a pH of 1.2 to 1.8. The optimal coating temperature is 60 to 70°C. Randomly structured sintered Ti felts (ST Titanium 15/40, Bekaert Fibre Technologies) with an average fiber diameter of 15 µm, a thickness of 100 µm and a porosity of 40% were used as plating targets. To remove greasy production residues, the Ti felts were pre-cleaned in an ultrasonic bath using an alkaline cleaning bath (Puro S, Wieland Edelmetalle GmbH) according to the manufacturer's guidelines.

2.5.2. Pretreatment

The pre-cleaned Ti felts were etched in 20 wt% HCl (ACS reagent, Sigma Aldrich) at 90°C for 4 min. Afterwards the etched Ti felts were electrolytic degreased for 1 min using a cyanide free degreasing solution (WILAPLAT ZFM, Wieland Edelmetalle GmbH) and two stainless steel anodes parallel to the Ti felt. Hydrogen is formed at the surface, in defects and in re-entrant angels and remaining micro contaminations are blasted off. A rough, micro cleaned well wettable surface is achieved. Both the Rh and the Ru electrolytes are strongly acid and corrosion on top of the plating target will occur. Since the surface of the Ti felts was etched prior to each experiment anyway, no protective thin Au or Ni layer from non-corrosive plating baths [157] was electrodeposited prior to the actual coating experiments.

2.5.3. BET surface measurements

The used Ti felts are randomly structured, thus the specific surface area had to be determined to calculate the resulting current density for the coating experiments. The surface area was measured with a BET device (ASAP 2020, Micromeritics) using Kr as measuring gas. Prior to each measurement the Ti felts were pretreated at 80°C for 60 min under vacuum to desorb adsorbed molecules from the surface. The surface area was calculated using the BET-isotherm. Three samples of each 7 x 7 cm² were measured resulting in an average mass related surface area of 717 cm² g⁻¹ with a maximum relative deviation of 0.42%. The average specific surface

2 Electrocatalysts and their galvanic deposition

area is $19 \text{ m}^2 \text{ m}^{-2}$. The Ti felts were not etched prior to the BET measurements. For the calculation of current densities the surface area of the pre-cleaned Ti felts was used.

2.5.4. Electroplating: Setup and conducted experiments

The coating experiments were conducted in a glass beaker filled with 100 ml electrolyte. The Ru electrolyte was kept at constant temperature of 65°C , while the Rh electrolyte was used at 25°C . Both electrolytes were magnetic stirred at 100 rpm (RCT classic IKAMAG). A potentiostat / galvanostat (PGSTAT302N, Metrohm Autolab) was used as direct current supply. The square plating target, connected to the working electrode of the potentiostat, had a size of $1.5 \times 1.5 \text{ cm}^2$. At the anode platinized Ti expanded metal electrodes (Wieland Edelmetalle GmbH) were used as insoluble counter electrodes. To achieve homogeneous coating results, two counter electrodes were positioned parallel to the plating target. For polarization measurements an Ag/AgCl reference electrode (Metrohm Autolab) was applied. The duration of each experiment was dependent on the applied current density and the desired charge. To be comparable and for stable operation conditions the plating electrolytes were refreshed regularly. First both for Rh and Ru polarization curves were measured to identify proper current density regions for successful coatings. For four different chosen current densities varying plating times were calculated based on fixed charge numbers (see Table 2.4 and Table 2.5). Several sets of experiments were conducted to investigate the influence of the applied charge and plating time on the resulting coatings. The plating bath temperature, composition and pH value were not varied.

The mass of the coating layer is proportional to the plating time. At constant current the transferred charge Q increases with increasing plating time. According to Faraday's law the mass m of a deposited metal can be calculated with Equation (2.1) where M is the molar mass of the desired metal, F is the Faraday constant equal to 96485 C mol^{-1} and z the charge number of the metal ion. [174]

$$m = \frac{M * Q}{z * F} = \frac{M * I * t}{z * F} \quad (2.1)$$

2.5.5. Analysis of coatings

After etching, the Ti samples were dried at 90°C for 20 min. Following to the coating step the samples were dried again at the same conditions to determine the mass increase. The mass increase was determined using an analytical balance (CPA225D, Sartorius) with an accuracy of 0.01 mg. The morphology and homogeneity of the resulting coatings were analyzed using a scanning electron microscope (S-3000N, Hitachi and DSM 982 Gemini with Field Emission Gun, Zeiss) with an energy-dispersive spectrometer (Oxford Link ISIS with HPGe detector). To visualize the distribution and to analyze the elemental composition of the coatings on the surface, energy-dispersive X-ray spectroscopy (EDX) measurements were conducted. Furthermore XRD measurements were performed to determine the phase and crystal structure of the deposits. The measurements were done in a PANalytical Empyrean diffractometer at

40 kV and 40 mA. A Cu x-ray tube with a line source of $12 \times 0.04 \text{ mm}^2$ provided CuK_α radiation with $\lambda = 0.1542 \text{ nm}$. The K_β line was removed by a Ni filter. Source and detector moved in the vertical direction around a fixed horizontal sample. After passing a divergence slit of $1/8^\circ$ and an anti-scatter slit of $1/4^\circ$, the beam reached the sample at the center of a phi-chi-z stage. In the Bragg-Bretano geometry used, the beam was refocused at a secondary divergence slit of $1/4^\circ$. Finally, the signal was recorded by a pixel detector with 256×256 pixels of $55 \mu\text{m}$ as a function of the scattering angle 2Θ . Subsequently, the peak positions were calculated with Equation (2.2) in which \mathbf{q} is the scattering vector.

$$\mathbf{q} = \frac{4\pi}{\lambda} \sin\theta \quad (2.2)$$

The detector was used in a scanning geometry that allowed all rows to be used simultaneously. To reduce the background, the divergent beam perpendicular to the scattering plane was controlled by a mask of 4 mm restricting the width of the beam at the sample position to about 10 mm. In addition, the perpendicular divergence was restricted by Soller slits to angles $\leq 2.3^\circ$. The scanning was conducted in a range of $2\theta = 30 - 90^\circ$ with a step size of 0.006° . The diffraction patterns were recorded at room temperature. The analysis of the recorded XRD spectra was conducted with the PANalytical software HighScore Software, Version 3.0e.

2.5.6. Linear sweep voltammetry: Setup and conducted experiments

Linear sweep voltammograms were recorded to determine the activity of the Rh and Ru coatings for the electrochemical NH_3 synthesis. The experiments were conducted in a three-electrode configuration in a closed single-compartment cell at 30°C , see Figure 2.4.

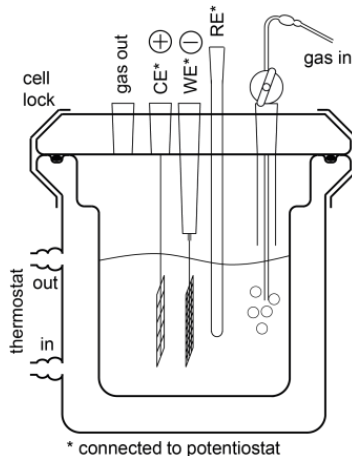


Figure 2.4: Scheme of the electrochemical cell for linear sweep voltammogram measurements.

2 Electrocatalysts and their galvanic deposition

The cell was filled with 190 ml of 0.5 M H₂SO₄ (AVS Titrinorm, VWR) as electrolyte. A potentiostat / galvanostat (PGSTAT302N, Metrohm Autolab) was used as direct current supply. The coated felts with a size of 1.5 x 1.5 cm² were connected to the working electrode (WE). At the anode a platinized Ti expanded metal electrode (Wieland Edelmetalle GmbH) was used as counter electrode (CE) and an Ag/AgCl electrode (Metrohm Autolab) was applied as reference electrode (RE). Prior to each experiment the electrolyte was purged with an Ar/H₂ mixture (5 Vol% H₂) to remove dissolved gases. During this purging the working electrode was activated with several cyclic voltammetry runs at a scan rate of 50 mV s⁻¹. First three cycles starting at the open circuit potential (OCP) to -0.56 V vs. NHE were measured. Secondly three cycles from -0.56 to -1.36 V vs. NHE were performed. Thirdly ten cycles from -1.36 V vs. NHE to the OCP were measured. Finally a chronoamperometry at -0.26 V vs. NHE for 15 min was conducted to polarize the electrode. For the activity measurements for NH₃ synthesis, the electrolyte was purged with a N₂/H₂ mixture (5 Vol% H₂) for 20 min. The linear sweep voltammograms were performed from the OCP to -1.81 V vs. NHE with a sweep rate of 5 mV s⁻¹. After the measurement a sample of the electrolyte was taken and the NH₄⁺ concentration was determined based on a variation of the Berthelot reaction published by Willis et al. [175].

2.5.7. Analysis with the Berthelot reaction

During the Berthelot reaction an indophenol dye is formed and its concentration is determined photometrically. The Berthelot reaction takes place in alkaline media, meaning NH₃ is present instead of NH₄⁺ ions. Therefore 4 M sodium hydroxide NaOH solution is added to the sample. When adding sodium hypochlorite to the alkaline sample, monochloramine is formed. In the next reaction step, monochloramine reacts with sodium salicylate catalyzed by sodium nitroprusside. The resulting intermediate reacts with another sodium salicylate molecule to form the indophenol dye. The needed reagents are listed in Table 2.3.

Table 2.3 Composition of Berthelot reaction reagents

Solution	Amount	Reagent
Sodium hydroxide	16 g	sodium hydroxide
	100 ml	distilled water
Salicylate	32 g	sodium salicylate
	40 g	trisodium phosphate dodecahydrate
	0.5 g	sodium nitroprusside
	1000 ml	distilled water
Hypochlorite	50 ml	sodium hypochlorite (available chlorine 4.00 - 4.99%)
	1000 ml	distilled water

Samples of 5 ml are taken out of the electrochemical cell. A threefold analysis is performed with subsamples of 1 ml. To increase the pH to a level of 13, 0.25 ml of 4 M NaOH solution is added. In the next step 1 ml salicylate solution is added as phenol source, followed by adding 0.25 ml of the hypochlorite solution. Subsequently the samples are mixed using a vortex mixer to start the reaction. For a complete reaction, the samples are stored for 30 min. In the final step, the NH₄⁺ concentration is determined using a UV/VIS device at a wavelength of 685 nm.

To convert the UV/VIS signals into NH_4^+ concentrations, a calibration curve is recorded for samples of known concentration. 250 ml of a primary stock solution containing 1000 mg l⁻¹ nitrogen are prepared out of dried ammonium sulfate and the applied electrolyte (0.5 M H₂SO₄). The mass of ammonium sulfate is calculated with Equation (2.3).

$$\begin{aligned} m_{\text{ammonium sulfate}} &= c_{\text{nitrogen}} \times V \times \frac{M_{\text{ammonium sulfate}}}{2 \times M_{\text{nitrogen}}} \\ &= 1000 \text{ mg l}^{-1} \times 0.25 \text{ l} \times \frac{132.14 \text{ g mol}^{-1}}{2 \times 14.007 \text{ g mol}^{-1}} \\ &= 1.179 \text{ g} \end{aligned} \quad (2.3)$$

By diluting 10 ml of the primary stock solution with the electrolyte, 200 ml of a secondary stock solution are prepared containing 50 mg l⁻¹ nitrogen. From the secondary stock solution standard samples of known concentration in the range of 0 to 1 mg l⁻¹ nitrogen are prepared. The absorption value of the blank sample containing 0 mg l⁻¹ nitrogen is used to remove the influence of the color reagent on the measured signals. The higher the intensity of the green color, the more NH_4^+ the sample contains, see Figure 2.5.



Figure 2.5: Color change of samples containing NH_4^+ after adding all reagents for the Berthelot reaction. The higher the intensity of the green color, the more NH_4^+ the sample contains.

An exemplary calibration curve is shown in Figure 2.6. With the linear equation for the trend line of the calibration curve, nitrogen concentrations can be calculated from the measured UV/VIS signals. To receive NH_4^+ concentrations, the measured nitrogen concentrations are multiplied with the factor 1.288, meaning the ratio of M_{ammonium} to M_{nitrogen}. For every new analysis batch, the calibration was repeated to take small variations into account that will occur during the preparation of the needed reagents.

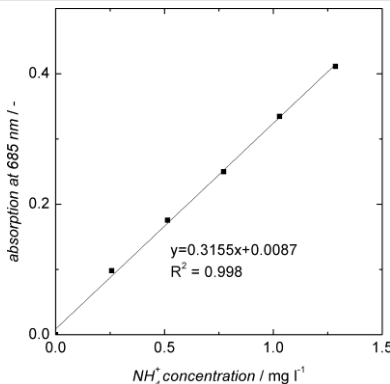


Figure 2.6: Exemplary calibration curve for a nitrogen concentration of 0 to 1.0 mg l⁻¹, corresponding to 0 to 1.288 mg l⁻¹ NH₄⁺ concentration.

2.6. Results

2.6.1. Pretreatment of randomly structured Ti felts

For successful coatings a rough surface with many re-entrant angles is necessary. Therefore the Ti felts were etched in 20 wt% HCl at 90°C for one to five minutes after the pre-cleaning step, see Figure 2.7. With increasing etching time, more TiO₂ gets removed and the surface gets more structured. The grain boundaries and the intergranular material are more affected by the acid than the grain's surface itself. In the first three minutes mainly intergranular material is removed, whereas in the fourth and fifth minute additionally the grain surface is etched as well. After five minutes the single grains are visible, but the surface roughness has not increased significantly compared to the four minute sample. However, due to the deep intergranular gaps, the mechanical stability of the five minute sample is reduced noticeably. The etching for four minutes is a compromise between the achieved surface roughness and the mechanical stability of the etched Ti felts.

2.6.2. Polarization curves for Rh and Ru

Polarization curves for the electroplating of Rh and Ru onto the Ti felts were measured in a three-electrode setup. The working electrode potential was increased by 5 mV for Rh and by 50 mV for Ru every 45 seconds and the resulting current was measured. Figure 2.8 shows the polarization curves for Rh at 25°C and Ru at 65°C. For Rh the open circuit potential (OCP) is -39 mV and the resulting current density is -4 mA dm⁻². Beginning at the offset potential of -165 mV the current density is steadily increasing. The resistance of the electrode electrolyte interface was overcome and Rh ions are deposited.

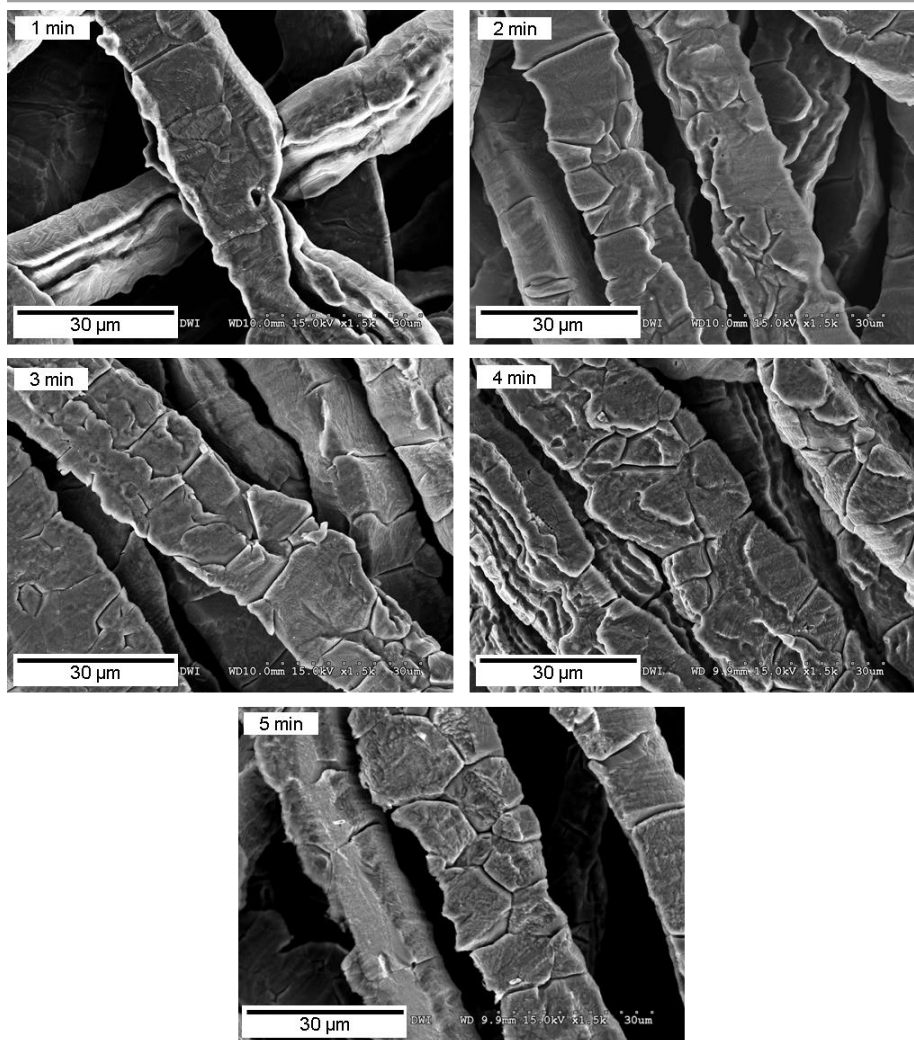


Figure 2.7: Etched Ti felts in 20 wt% HCl at 90°C for 1 to 5 min.

At -245 mV the limiting current density of -40 mA dm^{-2} is reached. However, the limiting current region for Rh is little developed only. At -250 mV and a current density of -45 mA dm^{-2} the post limiting region begins and H_2 evolution is a possible undesired parallel reaction. Based on the measured polarization curve, four interesting current densities for the plating experiments were chosen and the corresponding plating times for charges between 3 and 30 C were calculated, see Table 2.4.

2 Electrocatalysts and their galvanic deposition

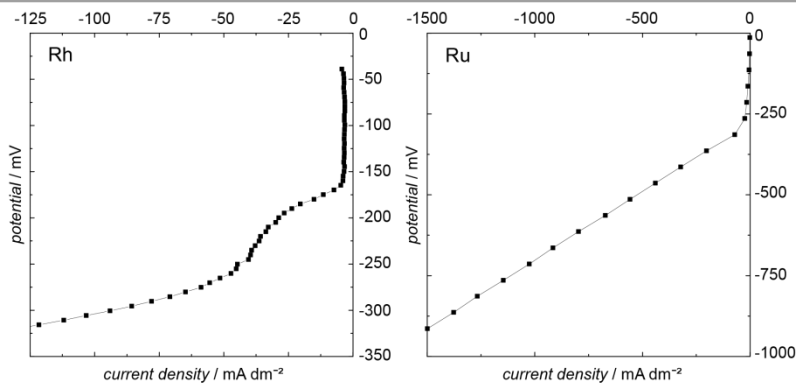


Figure 2.8: Polarization curves for Rh at 25°C and Ru at 65°C

Table 2.4 Corresponding plating times in seconds for four chosen current densities and fixed charge numbers (each absolute values) for Rh

Charge [C]	Current density [mA dm^{-2}]			
	12	24	48	96
3	600	300	150	75
6	1200	600	300	150
15	3000	1500	750	375
30	6000	3000	1500	750

The lower two current densities lie in the concentration polarization region of the polarization curve and optimal coating results should be achievable. The third current density is close to the starting point of the post limiting region and the fourth current density lies fully in the H_2 evolution region, meaning the coating quality should be reduced noticeable. In literature optimal current densities of 1 to 4 A dm^{-2} were announced for simple geometries such as plates and wires [134,140,152]. However, the measured polarization curve clearly gives the optimal plating range at current densities below 0.1 A dm^{-2} . The lower current densities can be caused by the three dimensional structure of the Ti felts. The felts are quite dense and inner parts may not be coated by Rh at all, resulting in lower currents measured.

Contrary to Rh, for Ru the OCP is +36 mV and the resulting current density is slightly positive being 0.03 mA dm^{-2} . At the offset potential of -314 mV the current density increases linearly. A limiting current density was not detectable in the investigated potential range. To make sure that the limiting current region was not overseen, measurements with potential changes of 5 mV and 0.5 mV every 45 seconds respectively were conducted as well. There were no differences in the polarization curves visible. Similar to Rh, also for Ru four current densities were chosen and the resulting plating times were calculated for charge values between 15 and 105 C, see Table 2.5.

Charge [C]	Current density [mA dm^{-2}]			
	115	230	345	460
15	300	150	100	75
45	900	450	300	225
75	1500	750	500	375
105	2100	1050	700	525

All chosen current densities lie within the upper third of the concentration polarization region starting close to the offset current density of around -70 mA dm^{-2} . Contrary to Rh, the measured current densities for Ru are in agreement with literature. Park et al. applied current densities of 300 to 900 mA dm^{-2} to deposit Ru on Ti [170]. Here the felt geometry seems to have no or only little influence on the current densities necessary for plating of Ru.

2.6.3. Current efficiency, deposited masses, SEM and EDX analysis of Rh

The current necessary to deposit a particular mass m of a desired metal with a current efficiency of 100% can be calculated with the Faraday's law according to Equation (2.1). To calculate the current efficiency of a plating process, this theoretical current is divided by the applied current and multiplied by 100%. The etched Ti samples were dried and weight before and after the plating experiments. The mass difference was used to calculate the theoretically necessary current.

Figure 2.9 shows the achieved current efficiencies for the plating of Rh as a function of the applied current density for four different charge values between 3 and 30 C. For the two lower current densities the current efficiency increases logarithmic with increasing charge. The larger the charge, the longer is the plating time and the more Rh molecules are deposited. More precipitation spots are available for following ions to be deposited and the current efficiency is increasing logarithmic. The large difference in current efficiencies for 3 and 6 C shows clearly, that a certain amount of charge is necessary to achieve a high plating efficiency. At smaller current densities the strength of the electric field between anode and cathode is lower and the diffusion of ions from the bulk to the electrode surface gets limited. Higher charges result in higher current efficiencies. Furthermore for a current density of 24 mA dm^{-2} the current efficiency is also higher than for 12 mA dm^{-2} , which is in agreement with literature [134]. At 12 mA dm^{-2} the resistance of the electrode electrolyte interface was not completely overcome, resulting in lower current efficiencies. At 24 mA dm^{-2} the diffusion of the ions is the only limiting factor and with increasing plating time the current efficiency is rising.

Contrary, for the two higher current densities the current efficiency decreases exponentially with increasing charge. Additionally to the deposition of Rh, H_2 evolution is a competing reaction and is lowering the current efficiency and disturbing the deposition process significantly. The longer the plating time, the more predominant the H_2 evolution becomes at the cathode. The more H_2 bubbles are formed, the more cathode surface is blocked and the less Rh can get deposited on the electrode surface.

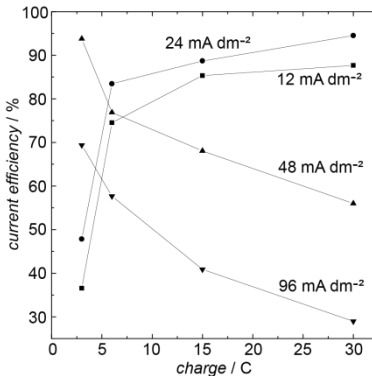


Figure 2.9: Achieved current efficiencies for the plating of Rh for applied current densities between 12 and 96 mA dm⁻² and charges between 3 and 30 C (absolute values each)

Also at low charge values the negative influence of the H₂ evolution is obvious. The decrease in current efficiency is more regularly than the increase for lower current densities.

The two highest current densities achieved are 94.5% at 24 mA dm⁻², 30 C and 93.8% at 48 mA dm⁻², 3C. In literature current efficiencies of around 75% are reported [157]. However, Pletcher et al. also achieved current efficiencies of around 90% [176]. The huge variances in the obtained current efficiencies can be related to the structural features as observed by SEM images, see Figure 2.10. In the top line of Figure 2.10 the SEM images for the two highest current efficiencies are shown. Although the two efficiencies are almost equal, the grain structures are completely different. The 48 mA dm⁻² sample shows a fine micro granular pattern with smaller cracks. However, these cracks reflect only the cracked sub-structure of the Ti substrate after four minutes etching (compare Figure 2.7). Contrary, the 24 mA dm⁻² sample shows a highly cracked surface. The single islands of the coating are quite smooth and do not show a granular structure at all. The cracks are deep and go from the surface of the coating down to the Ti substrate. Similar to the 48 mA dm⁻² sample the 12 and 96 mA dm⁻² samples also show a granular structure. Furthermore, the structure of the 96 mA dm⁻² sample shows a lot of defects and columnar structures. With increasing current density the average grain diameter is increasing as well and the surface gets rougher. According to literature, the surface gets smoother with increasing coating thickness, while at higher current densities a rough surface is formed [127].

Pushpavanan reports that cracking mainly occurs for thick Rh coatings [134]. When looking at the deposited masses for the different current densities, this suggestion is confirmed (see Figure 2.11). At 48 mA dm⁻², 3C 1.0 mg Rh was deposited. Contrary at 24 mA dm⁻², 30C 10.1 mg Rh were deposited. When assuming that all samples have the same average surface area, the thickness of the coating is increasing with increasing deposited mass. The 24 mA dm⁻² sample shows the highest mass increase and is also the crack-richest one. As described before, material deposited at lower current densities can obtain impurities which increase residual stress. Cracks in the coating can be the consequence.

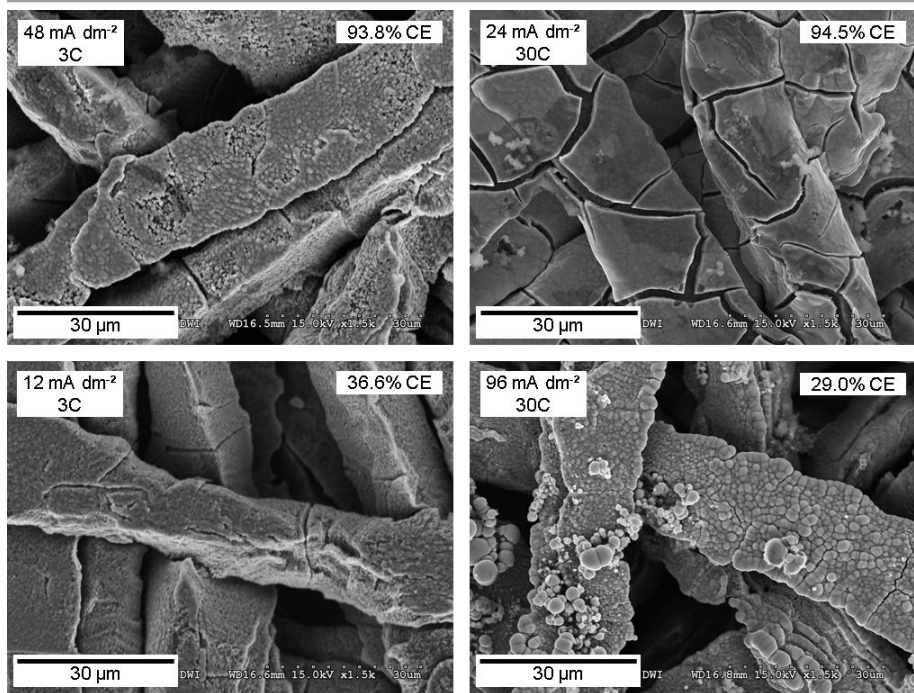


Figure 2.10: SEM images for Rh coatings at different current densities and charge values. The top line represents the two samples with the highest current efficiencies (CE) and the bottom line the two samples with the lowest current efficiencies.

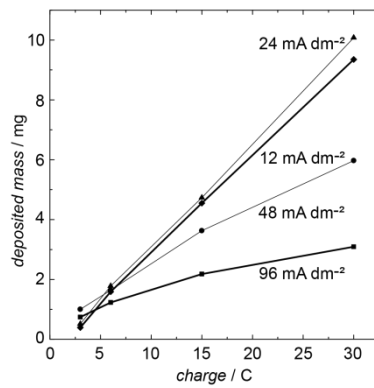


Figure 2.11: Deposited masses of Rh for different current densities and charge values.

2 Electrocatalysts and their galvanic deposition

Here, the sample coated at the lowest current density shows only minor cracks. However, only 0.4 mg Rh was deposited, resulting in a quite thin coating layer. Thus the structure of the support material is still present.

Figure 2.12 shows the results for EDX measurements for the 48 mA dm^{-2} , 3C sample with a current efficiency of 93.8%.

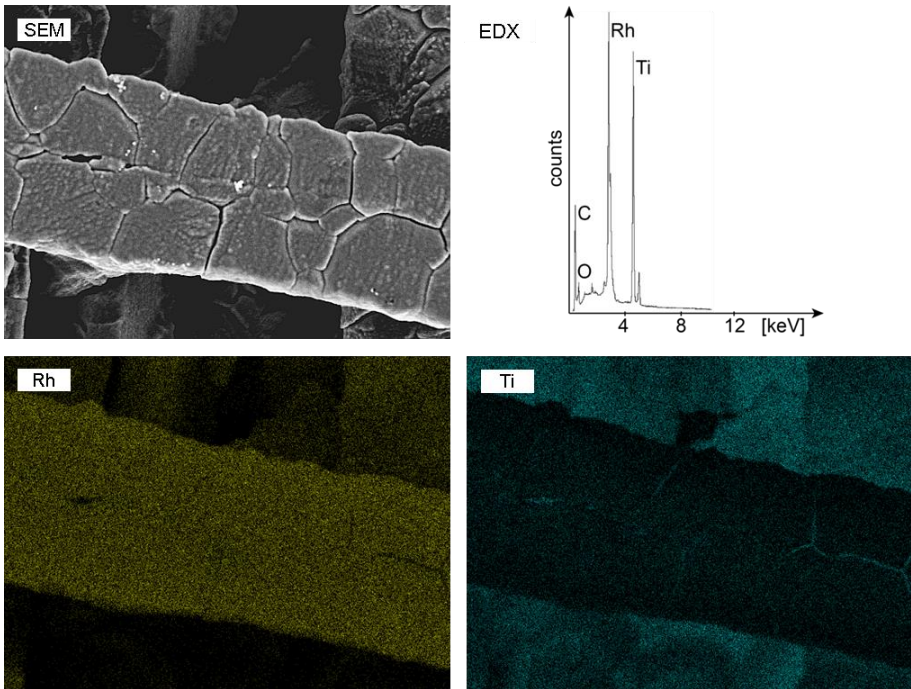


Figure 2.12: EDX results for a Rh coating at 48 mA dm^{-2} and 3C. Top left shows the SEM image, top right the corresponding EDX spectrum, bottom left EDX mapping for Rh and bottom right EDX mapping for Ti. Yellow and blue represent the element of interest in each case.

At the top right of Figure 2.12 the resulting EDX spectrum is shown. Peaks for C, O, Rh and Ti are visible. The C peak occurs due to the carbon adhesive tape used to fix the samples on the sample holders. Only a small peak for O appears, thus no Rh-O compounds were formed. Since the thickness of the Rh coating is low compared to the diameter of the Ti fibers, a relatively large Ti peak is visible as well. However, the Rh peak is the largest one, which is also confirmed by the EDX mappings shown in the bottom line of Figure 6. On the left the mapping for Rh and on the right the mapping for Ti is shown. Yellow and blue represent the element of interest in each case. The left mapping shows an almost completely closed layer of Rh on top of the support fiber, only minor cracks are visible. On the right the mapping for Ti only shows the corresponding cracks in blue color.

2.6.4. Current efficiency, deposited masses, SEM and EDX analysis of Ru

Figure 2.13 shows the achieved current efficiencies for the plating of Ru at four different current densities and resulting charge values between 15 and 105 C.

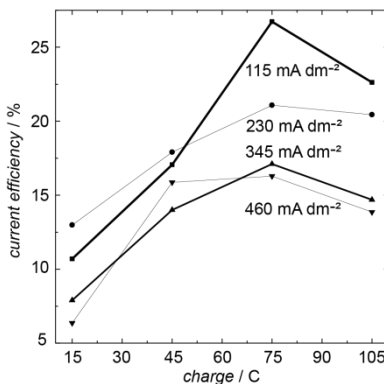
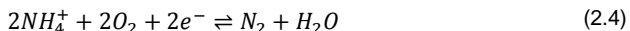


Figure 2.13: Achieved current efficiencies for the plating of Ru for applied current densities between 115 and 460 mA dm⁻² and charges between 15 and 105 C (absolute values each)

For all current densities the current efficiency is rising with rising charge until 75 C. The longer the plating time, the more Ru molecules can get deposited. However, a further increase in charge beyond 75 C leads to a decrease in current efficiency. At 75 C the current efficiency also decreases with increasing current density. This result is in agreement with the polarization curve for Ru (compare Figure 2.8). The four chosen current densities all lie within the optimal plating range close to the offset current density. For all current densities the electrical field is strong enough for the deposition of Ru and the resistance of the electrode electrolyte interface was completely overcome. In agreement with literature [162] an increase in current density only leads to undesired side reactions, which decreases the current efficiency.

Contrary to Rh the highest achieved current efficiency for the plating of Ru is only 26.7%. However, Reddy and Taimsalu [162] report current efficiencies of around 90% at a pH of ~ 2. To explain the reduced current efficiency, one has to consider the structure of the Ru complex RuNC being present in the electrolyte. The Ru complex consists of two RuCl₄ units bridged by one N atom. For charge neutrality 3 NH₄⁺ ions are necessary. Contrary to the Rh electrolyte, which only consists of Rh₂(SO₄)₃ dissolved in H₂SO₄, in the Ru electrolyte NH₄⁺ ions can react at the cathode as well. Lan and Tao [8] just recently suggested a possible reaction of NH₄⁺ at the cathode, see Equation (2.4).



2 Electrocatalysts and their galvanic deposition

Here O₂ is reduced to H₂O in the presence of NH₄⁺, which is oxidized to N₂. This reaction can take place during the electroplating of Ru as well. In each RuNC 2 Ru⁴⁺ and 3 NH₄⁺ ions are present, resulting in a factor of 2/3 for the probability for the reduction of a Ru⁴⁺ ion.

The deviation of four electrons needed for the reduction of Ru⁴⁺ and only one electron needed for the reaction of one NH₄⁺ ion at the cathode is considered when calculating the theoretical deposited mass of Ru with the Faraday law, see Equation (2.1). The electronegativity (Allred-Rochow) of O is 3.50, while it is only 1.42 for Ru. This leads to a factor of 142/350 for the affinity of electrons to react with a Ru⁴⁺ ion. When now multiplying a theoretical efficiency of 100% with these two factors, one gets a maximum efficiency of 27.05%, see Equation (2.5).

$$100\% * \frac{2}{3} * \frac{142}{350} = 27.05\% \quad (2.5)$$

Considering this value, the reached efficiency of 26.7% corresponds to a relative efficiency of 98.7%, which is even higher than the current efficiencies reported in literature [162]. To proof the reaction of NH₄⁺ at the cathode, the concentration of NH₄⁺ ions in the electrolyte before and after a coating step was analyzed using the Berthelot reaction. A strong decrease in NH₄⁺ concentration was observed. This observation is in agreement with the notice made by Reddy and Taimsalu [162]. They report that the used Ru electrolyte becomes more acidic during the plating process and that the addition of dilute NH₄OH solution is necessary to keep the pH constant.

Figure 2.14 shows SEM images for Ru coatings at 75 °C for the four chosen current densities between 115 and 460 mA dm⁻². As expected from the current efficiency curves (see Figure 2.13), the structure of the deposited material gets rougher with increasing current density. The coating gets more irregular and defects get more prevalent. The 115 mA dm⁻² sample reached the highest current efficiency and also shows the best coating result. The surface is quite smooth and the coating is regular. Compared to the Rh coatings, the structures are finer and the average grain diameter is smaller. According to literature low temperature electrodeposition leads to fine grain structures [157]. Although the Ru electrolyte was operated at 65°C compared to 25°C for the Rh electrolyte, the Ru coating structure is finer than the Rh one. The Rh electrolyte only consists of Rh³⁺ and SO₄²⁻ ions, while the Ru electrolyte also contains Cl⁻ ions. The phenomenon of smaller coating grains for Ru is similar to the coating of Cu. According to Yao et al. [129] the addition of Cl⁻ ions leads to a smoother surface with smaller grain size. In agreement with literature the coatings are crack free [162]. The visible gaps in the coating represent the original structure of the Ti substrate after the pretreatment. When looking at the deposited masses for the Ru coating (see Figure 2.15) this suggestion is confirmed. At 115 mA dm⁻² and 75 °C a mass increase of 5.25 mg was observed. Even when assuming that only 10% of the total available area of the Ti substrate was coated, an average coating thickness of ~1 µm is achieved. With increasing current density the deposited masses get less, thus the average coating thickness is decreasing as well and defects in the coating can be formed. Reddy and Taimsalu give a critical coating thickness of 1.5 µm to obtain crack free coatings [162].

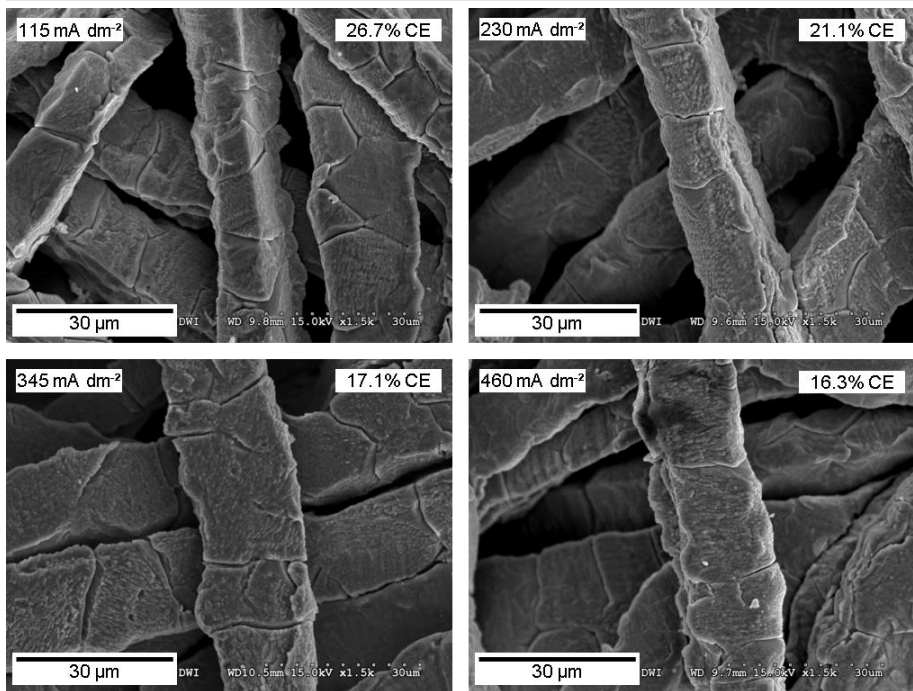


Figure 2.14: SEM images for Ru coatings at different current densities and a charge of 75 C. For all current densities the highest current efficiency (CE) was reached at 75 C.

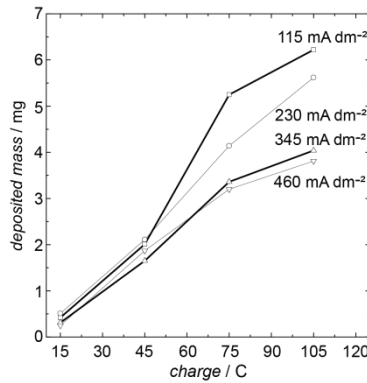


Figure 2.15: Deposited masses of Ru for different current densities and charge values.

2 Electrocatalysts and their galvanic deposition

Figure 2.16 shows the results for EDX measurements for the 115 mA dm^{-2} , 75 C sample with the highest current efficiency of 26.7%.

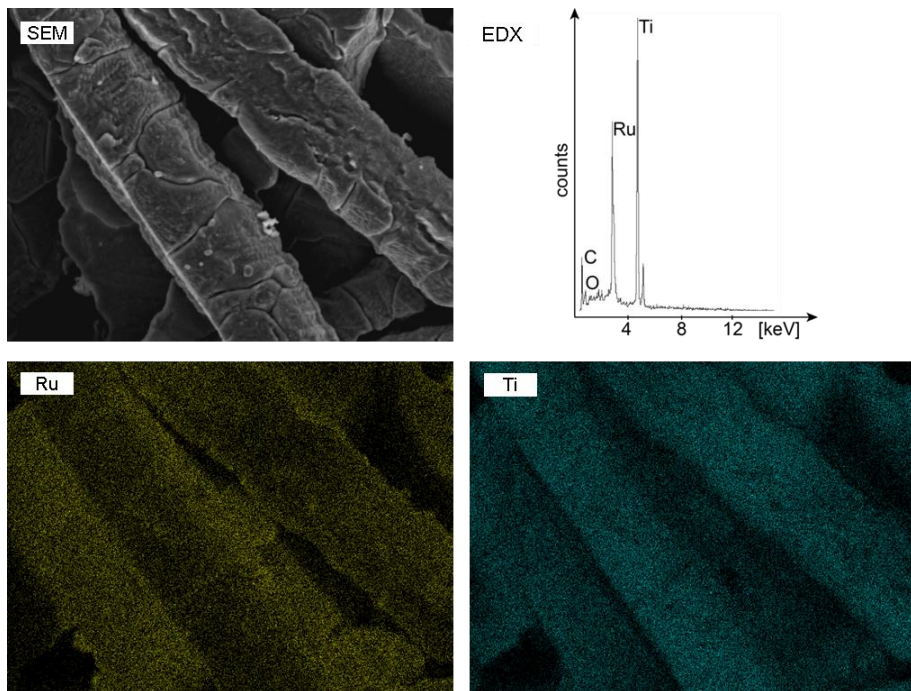


Figure 2.16: EDX results for a Ru coating at 115 mA dm^{-2} and 3 C . Top left shows the SEM image, top right the corresponding EDX spectrum, bottom left EDX mapping for Ru and bottom right EDX mapping for Ti. Yellow and blue represent the element of interest in each case.

At the top right of Figure 2.16 the resulting EDX spectrum is shown. Similar to the EDX spectrum for Rh peaks for C, O, Ru and Ti are visible. The C peak occurs due to the carbon adhesive tape used to fix the samples on the sample holders. Although Ru quite readily forms RuO_2 at ambient conditions [156,158] only a small peak for O appears, i.e. no Ru-O compounds were formed. Since the thickness of the Ru coating is lower than for the Rh one, the Ti peak is more dominant. This observation is also confirmed by the EDX mappings shown in the bottom line of Figure 2.16. On the left the mapping for Ru and on the right the mapping for Ti is shown. Yellow and blue represent the element of interest in each case. The left mapping shows a regular coating of Ru. However, contrary to Rh the coating is quite thin and the background signal of Ti is also visible. The mapping for Ti proves this statement.

2.6.5. XRD measurements of coated felts

Figure 2.17 and Figure 2.18 show the XRD patterns for an uncoated Ti felt and for felts coated with Rh and Ru.

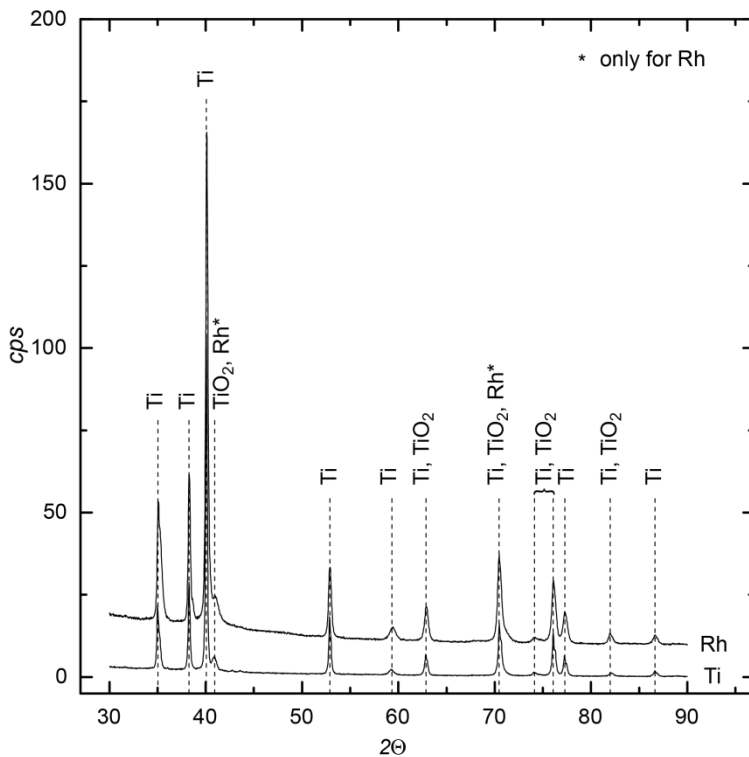


Figure 2.17: XRD pattern for a Rh coating on Ti at 48 mA dm^{-2} and 3 C. The pattern for Rh is shifted up for visual reason.

The peak identification was carried out by calculating the peak positions with d-spacings for the corresponding primitive cell of the element of interest. The Ti felt was etched for 4 min directly prior to the XRD measurement. The Ti pattern shows primarily peaks for Ti and only few peaks for TiO_2 . The patterns for Rh and Ru are quite similar to the Ti pattern. The XRD pattern for Rh does not show a specific peak for Rh. However, there are also no peaks apparent for RhO_2 , as expected from the EDX results (compare Figure 2.12). In the Ru pattern there is a single peak for Ru visible at $2\theta = 43.56^\circ$. As expected from literature, there are also a few peaks for RuO_2 .

[158]. However the corresponding EDX spectrum (see Figure 2.16) does not show a dominant O - peak. Most of the Ru, RuO₂ and Rh peaks are overlapping with more dominant Ti peaks. Since the Ru and Rh coatings only have a thickness of around 1 μm , the intensity of the Ti peaks is much stronger. Both the EDX and XRD results prove that Ru and Rh were successfully deposited on the Ti felt.

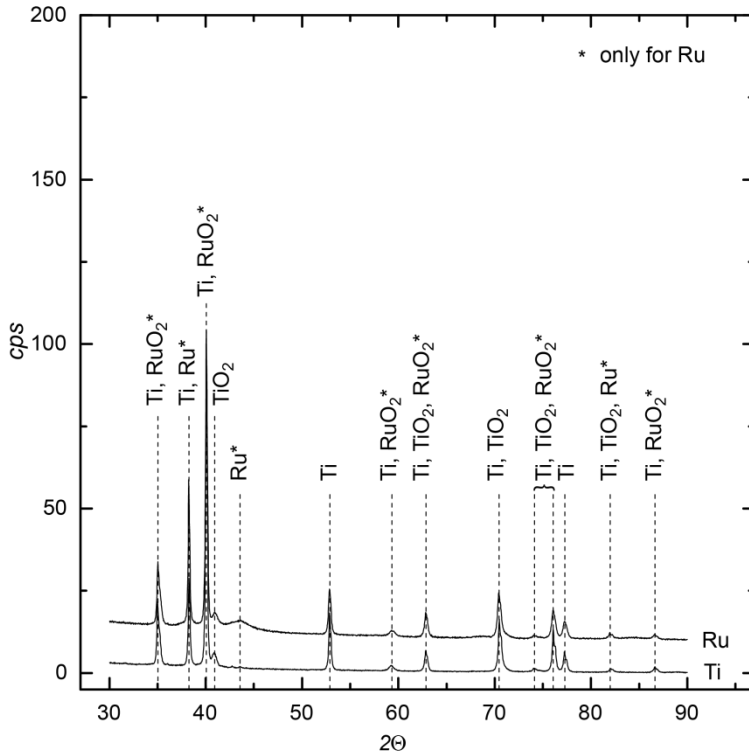


Figure 2.18: XRD pattern for a Ru coating on Ti at 115 mA dm^{-2} and 75 C. The pattern for Ru is shifted up for visual reason.

2.6.6. Linear Sweep Voltammetry measurements for Rh and Ru

Linear sweep voltammetry was conducted with Rh and Ru samples coated at the optimal plating conditions (Rh 48 mA dm^{-2} and 3 C, Ru 115 mA dm^{-2} and 75 C). Figure 2.19a) shows the linear sweep voltammogram for Rh and Ru electroplated on Ti felts for the electrochemical NH₃ synthesis in liquid phase. For all potentials recorded, the resulting current density is higher for Ru than for Rh.

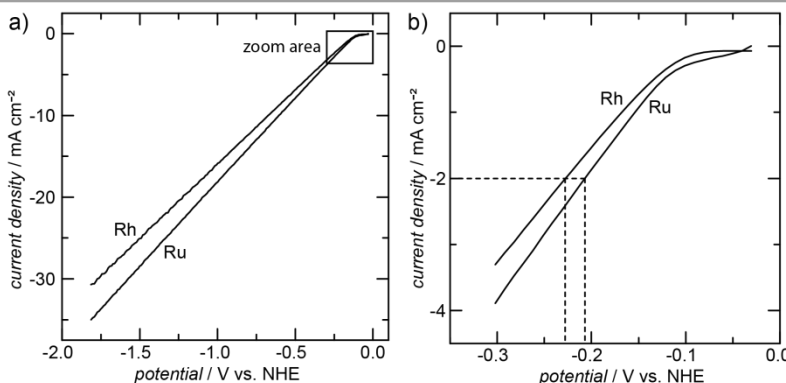


Figure 2.19: a) Linear sweep voltammogram for Rh and Ru coated Ti felts b) Zoom in to determine the overpotentials of Rh and Ru at a current density of 2 mA cm⁻² for the electrochemical NH₃ synthesis

The exact surface area of the coated Rh and Ru felt could not be measured due to lack of material. Therefore the specific surface area of the bare Ti support felt was used to calculate the corresponding current densities for Rh and Ru. The surface area of the Ti felt is assumed to represent the geometric area for the Rh and Ru coatings. In the analyzed potential range no limiting current density was observed.

A parameter for the activity of a catalyst for a desired reaction is the overpotential η at a particular current density. Miles et al. defined a current density of 2 mA cm⁻² as reasonable [177]. The lower the overpotential is the higher is the activity of the catalyst for the investigated reaction. Figure 2.19b) shows a zoom in for the potential range of 0.0 to -0.3 V vs. NHE to determine the overpotentials for Rh and Ru for the electrochemical NH₃ synthesis. The overpotential is defined as the difference between the measured potential and the standard potential of the desired reaction. The standard potential of the electrochemical NH₃ synthesis is $E_{NH_3}^0 = -0.057V$ vs. NHE [178]. For the applied reaction conditions Rh has a slightly higher overpotential than Ru. The values are $\eta_{Rh} = 171$ mV and $\eta_{Ru} = 150$ mV. The activity of the Ru coating should be higher than the one of the Rh coating. This assumption is confirmed by analysis of the samples taken after the measurement.

The NH₄⁺ concentration in the electrolyte was 0.07 mg l⁻¹ for Rh and 0.58 mg l⁻¹ for Ru corresponding to production rates of 1.5×10^{-11} mol s⁻¹ cm⁻² for Rh and 1.2×10^{-10} mol s⁻¹ cm⁻² for Ru. The values for the standard deviation for the NH₄⁺ concentration are 3.9% for Rh and 0.3% for Ru. Contrary to the predictions of Skúlason et al. [66], the activity of Rh should be slightly higher than the one of Ru. There are a few works reported in literature on the electrochemical synthesis of NH₃ in liquid phase by Furuya and Hoshiba [74–76], Tsuneto et al. [77,78] and Köleli and Röpke [80,81]. Production rates between 6.3×10^{-12} [81] and 6.4×10^{-9} mol s⁻¹ cm⁻² [76] were achieved. However, complex metal phthalocyanine cathodes [74–76], organic solvents mediated by LiClO₄ [77,78] or Pt electrodes coated with polyaniline or polypyrrole at high N₂ pressures of up to 50 bars [80,81] were used. Apparently, comparable

2 Electrocatalysts and their galvanic deposition

production rates were achieved but the electrochemical cell used here comprises an ordinary three electrode configuration and an aqueous electrolyte.

2.6.7. Economical estimation

To answer the question whether Rh or Ru as potential cathodic catalyst in an ecMR is more feasible, several aspects have to be considered. The first aspect relates to the costs for an efficient plating of Rh and Ru. Table 2.6 gives an overview about cost relevant numbers.

Parameter	Rh	Ru
Deposited mass [mg]	1.0	5.25
Price [€ g^{-1}] [135]	35.5	2.15
Plating time [s]	150	1500
Consumed power [10^{-6} kWh]	0.2	6.9
Factor material costs Rh/Ru		3.2

At the two highest current efficiencies of 93.8% for Rh and 26.7% for Ru, 1.0 mg of Rh and 5.25 mg of Ru were deposited. However, as mentioned before, Rh is much more expensive than Ru. The plating time for Rh is ten times shorter than for Ru. When considering the necessary current and the resulting potential values, plating of Rh consumes ~35 times less power than plating of Ru. However, the costs for electricity are significantly lower than the raw material costs for Rh and Ru. The material costs for a Rh coating at the given parameters are around three times the costs for a Ru coating. Since the material densities for Rh and Ru are almost equal being 12.38 and 12.37 g cm^{-3} [157], the costs for a deposited layer with a particular thickness are much cheaper for Ru. Considering the higher activity of Ru and the higher concentration of NH_4^+ reached during the linear sweep voltammetry measurements, Ru is superior to Rh for the electrochemical NH_3 synthesis. This analysis is based on the assumption that liquid phase catalysis proceeds following the same principles as a gas phase catalysis using the proposed membrane electrode assembly in an electrochemical membrane reactor. This needs to be analyzed and verified through systematic electrochemical characterization.

2.7. Conclusion

In this chapter an easy and highly efficient method for galvanic coatings of Rh and Ru on randomly structured Ti felts was presented. Due to the random structure of the Ti felts, the pretreatment with 20 wt% HCl was optimized. Based on polarization curves, proper plating conditions were identified. The current necessary for a successful and high quality coating of Ru is much higher than for Rh. The optimal current density for Ru was 115 mA dm^{-2} , while for Rh 48 mA dm^{-2} was applied. The investigated current density values are in agreement with literature for Ru. However, for Rh much higher values of 1 to 4 A dm^{-2} are reported. The successful coatings were proved both for Rh and Ru by SEM/EDX and XRD measurements.

Both for Rh and for Ru high current efficiencies of 93.8% and 98.7% respectively were achieved. The activity of the Rh and Ru coatings for the electrochemical NH₃ synthesis was confirmed by linear sweep voltammetry measurements. The voltammograms give a slightly higher activity for Ru, which was confirmed by a higher NH₄⁺ concentration in the electrolyte after the measurement. From an economical point of view Ru is also more interesting for an electrochemical NH₃ synthesis process, since the total costs for a Ru coating are only around 1/3 of the costs related to Rh. For a future electrochemical NH₃ synthesis processes Ru can play an important role as catalyst material, since the presented plating method is highly efficient and cost-saving.

2

3. Electrochemical NH₃ synthesis in liquid phase

Comparison of one- and two-compartment cells

Abstract

In this chapter, the electrochemical reduction of N₂ was investigated in liquid phase using 0.5 M H₂SO₄ as electrolyte. Two different types of electrochemical cells were applied: an one- and a two-compartment cell. In the latter case, the cell was divided in two compartments by a NH₄⁺ modified PTFE membrane. Here, the counter electrode was spatially separated from the working and the reference electrode. In each cell, chronoamperometry measurements were conducted at 30, 50 and 70°C using a Ti electrode tip. The production rate and the current efficiency were determined at -0.26, -0.46 and at -0.66 V vs. NHE. The employed electrodes, their positions in the cells as well as the applied electrolyte were the same in both setups. Measurements in the two-compartment cell could help to answer the questions if there are undesired back-reactions of formed NH₃ at the counter electrode and if the production rate and the current efficiency can be enhanced by using a H⁺ conductive membrane. Indeed, the most promising values for the production rate and current efficiency were obtained with the two-compartment cell at 50°C and -0.46 V vs. NHE being 2.4×10^{-10} mol s⁻¹ cm⁻² and 59.4% after 1 hour experimental time.

3.1. Introduction

The electrochemical reduction of N_2 in an electrochemical membrane reactor (ecMR) is a feasible alternative to the state-of-the-art Haber process. However, an investigation only of the cathodic catalyst characteristics is not possible when applying a double-sided membrane electrode assembly, as it is the case in the ecMR, see Chapter 5. The anodic and the cathodic reactions are always coupled with each other and the applied potential is representing the sum of the anodic and the cathodic potential. For instance, to investigate the reaction behavior of the cathode, one has either to replace the anodic gaseous half-cell by a liquid compartment to be able to apply a reference electrode with a known standard potential, or one has to apply an anodic catalyst without any kinetic and thermodynamic limitations. However, in the latter case the applied potential is still equal to the cell potential and not representing a single electrode potential, in this case the potential of the cathode.

An easier and more accurate method to investigate the reaction behavior of catalysts for electrochemical systems is to apply liquid phase analysis systems. In these systems usually a three-electrode configuration consisting of a working electrode (WE), meaning the electrode of interest, a counter electrode (CE) to close the electrical circuit and a reference electrode (RE) as reference point for the applied potential at the WE are applied. The electrodes are immersed into an aqueous liquid electrolyte. To suppress mass transport limitations within the electrolyte usually a rotating disk electrode (RDE) is applied at the WE. The rotating electrode surface thereby acts as a pump, pushing the surrounding solution away from the surface, see Figure 3.1.

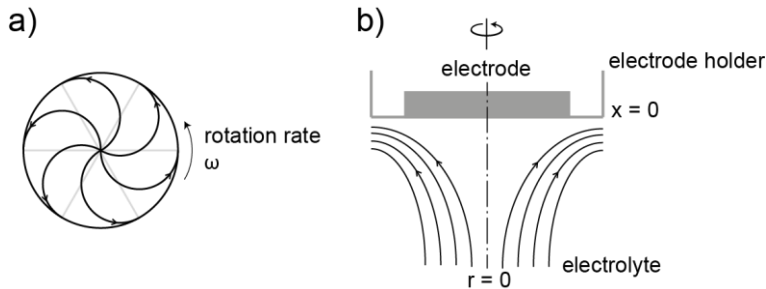


Figure 3.1: Schemes of the movement of a rotating disk electrode (RDE) and the liquid at its surface with a) the tangential liquid motion in the place of the RDE and b) the perpendicular liquid motion towards the RDE (adapted from [64])

This motion is tangential to the plane of the electrode, see Figure 3.1a). Subsequently, the removed solution is replaced by new solution moving in a perpendicular direction from the bulk to the surface, see Figure 3.1b).

The WE itself consists of a RDE and an exchangeable tip, shown in Figure 3.2, which is composed of several parts. The core of the tip is made from stainless steel with a thread to

mount it at the RDE. An insulation of PEEK ensures that only the actual surface of the catalytic material has an electrical connection to the electrolyte.

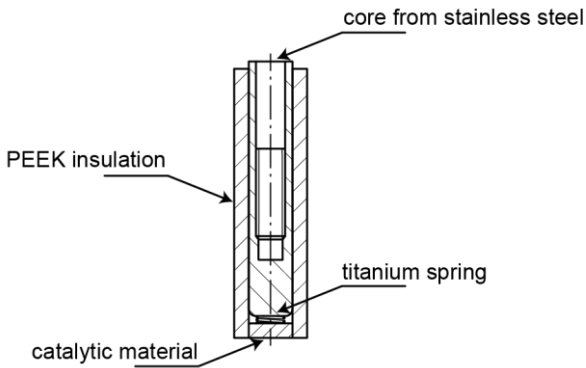


Figure 3.2: Design of the changeable working electrode tip which can be mounted at a rotating disk electrode (RDE)

To ensure the electrical connection between the catalytic material and the stainless steel core a titanium spring is used. A disk with 6 mm diameter of the catalytic material is water jet cut from a 2 mm thick plate and wrapped in PTFE tape to ensure tightness when pressed into the electrode tip. The resulting electrode tips can easily be exchanged and, hence, different catalysts can be investigated subsequently under the same conditions. The catalyst surface is polished flush with the insulator prior to each experiment, to yield an electrode where only the bottom end will be exposed to the electrolyte. To evaluate the reaction behavior of the investigated catalyst, two parameters are of interest: the production rate of NH₃ in mol s⁻¹ cm⁻² and the current efficiency. The latter indicates which part of the flown current was used for NH₃ production and which part was used for undesired side reactions. Two different types of electrochemical cells were applied: an one- and a two-compartment cell. In the latter case, the cell was divided in two compartments by a NH₄⁺ modified PTFE membrane (compare also Section 4.5.2). Measurements in the two-compartment cell can help to answer the questions if there are undesired back-reactions of formed NH₃ at the CE and if the production rate and the current efficiency can be enhanced by using an H⁺ conductive membrane.

3.2. Electrochemical cells applied

3.2.1. The one-compartment cell

A scheme of the one-compartment glass cell used in the present thesis is shown in Figure 3.3. A classical three-electrode arrangement was applied. The WE consisted of an electrode tip as shown in Figure 3.2, in which a Ti plate of 6 mm diameter and 2 mm thickness was pressed into.

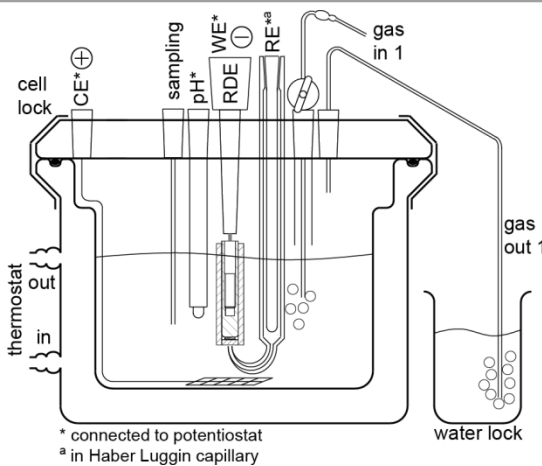


Figure 3.3: Scheme of the one-compartment cell for liquid phase analysis of the electrochemical NH_3 synthesis

The $\text{Hg}/\text{Hg}_2\text{SO}_4$ reference electrode was placed within a Haber-Luggin capillary filled with the same electrolyte as applied for the electrochemical measurements, in this case 0.5 M H_2SO_4 . The small tip of the Haber-Luggin capillary can be placed close to the surface of the WE at a distance $2d$, where d is the diameter of the capillary opening. The potential drop between the RE and the WE is thus reduced and precise measurements are possible. The utilized CE consisted of a platinized Ti expanded metal electrode (Wieland Edelmetalle GmbH) which was placed parallel to the surface of the WE. Additionally, a pH-electrode was applied to monitor pH changes within the electrolyte during the measurements. To ensure constant and controllable conditions, the cell was connected to a thermostat and the temperature was kept constant at 30, 50 or 70°C. The pressure was not varied; however, a slight overpressure was created within the cell to prevent air from entering the reaction system. A water lock was employed and either a N_2 or an Ar gas mixture comprising each 5 Vol% H_2 was constantly fed into the cell. The gas inlet stream could be switched between electrolyte aeration and surface aeration. A septum integrated into the lid of the cell allows for easy sampling with the help of a syringe.

3.2.2. The two-compartment cell

The two-compartment glass cell as applied in the present thesis was similarly designed as the one-compartment cell introduced before, see Figure 3.4. The utilized electrodes, their positions in the cell as well as the applied electrolyte were the same as for the one-compartment cell. However, the WE and RE were separated from the CE by a NH_4^+ modified PTFE membrane (compare also Section 4.5.2). Therefore, a second compartment was added, which is supplied with a second gas inlet stream and also has a connection to the before mentioned water lock.

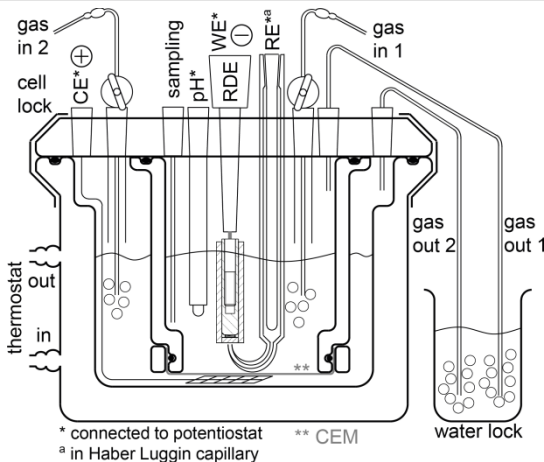


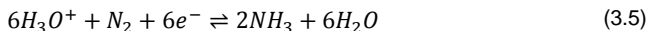
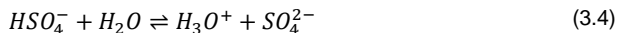
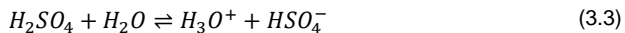
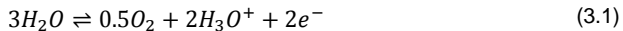
Figure 3.4: Scheme of the two-compartment cell for liquid phase analysis of the electrochemical NH₃ synthesis

The cation exchange membrane (CEM) is installed in a second cell, which is mounted at the lid of the glass cell, see Figure 3.4. The second cell is made from acrylic glass and the membrane can be changed. The CE is placed in the gap between the CEM and the bottom of the glass cell. The separation of the CE from the WE can help to avoid undesired back reactions, such as the oxidation of produced NH₃ to N₂ at the CE. The outer compartment was also filled with 0.5 M H₂SO₄. Sampling was analogous to the one-compartment cell conducted from the inner compartment. Contrary to the one-compartment cell, only the inner compartment was aerated with the N₂ or the Ar gas mixture, while solely Ar was fed to the outer compartment. To compare the experiments conducted in the two-compartment cell with those conducted in the one-compartment cell, all reaction conditions were kept constant.

3.3. Materials & methods

For the experiments conducted in the present thesis, five different electrochemical procedures were applied. The potentiostat (PGSTAT302N, Metrohm Autolab) used during all experiments was controlled through the Metrohm own software NOVA. The pretreatment and activation procedure (see Section 3.3.1) was carried out prior to each experiment. Cyclic voltammetry (CV) or chronoamperometry (CA) measurements were performed to characterize the investigated Ti catalyst. The applied N₂ and Ar gas mixtures contained each 5 Vol% H₂. The added H₂ should prevent the oxidation of H₂O at the CE. The standard potential for H₂ oxidation is defined as 0 V, and thus much lower than the standard potential of H₂O oxidation being 1.23 V vs. NHE. [178] When H₂O is oxidized besides H₃O⁺ and e⁻ also O₂ is formed, see Equation (3.1), which can disturb the performed experiments. By oxidizing the added H₂ only H₃O⁺ and e⁻ are formed, see Equation (3.2). Also the electrolyte itself can act as proton donor.

Here, 0.5 M H₂SO₄ is used as electrolyte, which is a double protonic acid, see Equations (3.3) and (3.4). The electrochemical NH₃ synthesis in liquid phase either uses H₃O⁺ derived from H₂ oxidation or from the dissociation of the H₂SO₄, see Equation (3.5). The formed NH₃ subsequently reacts with H₂O to form ammonium ions NH₄⁺, see Equation (3.6).



To prevent undesired side reactions, such as the reduction of O₂, the electrolyte is purged with Ar prior to each experiment, see Section 3.3.1, or with N₂ during the experiment.

3.3.1. Pretreatment and activation

Before starting the electrochemical pretreatment and activation of the WE, the electrode tip was polished with different grades of sandpaper starting with the coarsest and finishing with the finest one. After polishing, the electrode was rinsed with distilled H₂O. Subsequently, the WE was electrochemically cleaned prior to each experiment. The parameters for the different steps applied are given in Table 3.1.

Table 3.1 Parameters applied during the pretreatment and activation process prior to each experiment

Step	Attribute	Duration	Scan rate [mV s ⁻¹]	Potential vs. NHE [V]	Potential vs. Hg/Hg ₂ SO ₄ [V]
1	OCP value	≤ 120 s	-	-	-
2	Ar/H ₂	3 cycles	50	-0.56 → OCP	-1.2 → OCP
3	Ar/H ₂	3 cycles	50	-1.36 → -0.56	-2.0 → -1.2
4	Ar/H ₂	10 cycles	50	-1.36 → OCP	-2.0 → OCP
5	Ar/H ₂	900 s	-	-0.26	-0.9
6	OCP value	≤ 120 s	-	-	-

3 Electrochemical NH₃ synthesis in liquid phase

First CV measurements (steps 2 to 4) were carried out to clean the surface of the catalyst. However, it is noteworthy that catalysts often experience a decrease in activity during this cleaning step. Therefore, the activity was renewed by polarizing the electrode at a constant potential (step 5). During this process the electrolyte was constantly purged with the Ar/H₂ gas mixture to remove dissolved gases such as O₂ and to saturate the electrolyte with Ar. The pretreatment and activation was carried out at the temperature of the subsequent experiment, meaning either at 30, 50 or 70°C.

3.3.2. Cyclic voltammetry

Cyclic voltammetry measurements were only conducted for the one-compartment cell, since only the potentials were determined at which the following chronoamperometry measurements were carried out. For the reason of comparability between the one and the two-compartment cell, the same potentials were applied in the two-compartment cell. The applied parameters for the CV measurements shown in Table 3.2 can be divided into three parts, during which the electrolyte was purged either with the Ar gas mixture or the N₂ gas mixture.

Table 3.2 Parameters applied during cyclic voltammetry measurements

Step	Attribute	Duration	Scan rate [mV s ⁻¹]	Potential vs. NHE [V]	Potential vs. Hg/Hg ₂ SO ₄ [V]
1	OCP value	≤ 120 s	-	-	-
2	Ar/H ₂	2 cycles	5	-1.36 → OCP	-2.0 → OCP
3	OCP value	≤ 120 s	-	-	-
4	N ₂ /H ₂	1200 s	-	-	-
5	OCP value	≤ 120 s	-	-	-
6	N ₂ /H ₂	2 cycles	5	-1.36 → OCP	-2.0 → OCP
7	OCP value	≤ 120 s	-	-	-

After completing the mandatory pretreatment and activation process, a first CV measurement was carried out within the Ar saturated electrolyte (step 2). Then the gas feed was switched to N₂/H₂ and after 20 min the electrolyte was saturated with N₂ (step 4). Subsequently a CV curve was recorded within the N₂ saturated electrolyte (step 6). Similar to the pretreatment and activation, the CV measurements were also carried out at 30, 50 and 70°C.

3.3.3. Chronoamperometry

To determine how the reaction as well as the production rate changes over time, the catalyst was tested at constant potentials over prolonged times. The parameters applied are shown in Table 3.3. The actual procedure used had to be adjusted depending on the time and potential investigated. Again the mandatory pretreatment and activation procedure was carried out and the system was saturated with N₂ (step 1) prior to the actual measurement. Prior to the start of any measurement, a sample was always taken to assess the NH₃ concentration formed before

the actual measurement to avoid an adulterated production rate determination. A constant potential was then applied for either 6 or 15 hours (step 3).

Table 3.3 Parameters applied during chronoamperometry measurements

Step	Attribute	Duration [s]	Potential vs. NHE [V]	Potential vs. Hg/Hg ₂ SO ₄ [V]
1	N ₂ /H ₂	1200	-	-
2	OCP value	≤ 120	-	-
3	N ₂ /H ₂	21600 or 54000	-0.26 / -0.46 / -0.66	-0.9 / -1.1 / -1.3
4	OCP value	≤ 120	-	-

During the 6-hour long experiments samples were taken every hour to monitor the progress during the experiment. In contrast, only two samples were taken during the 15-hour long experiment, one at the beginning and one at the end, to analyze the long term behavior. All chronoamperometry experiments were conducted at 30, 50 and 70°C.

3.3.4. Analysis

The NH₃ concentration was determined through a method known as the Berthelot reaction. This method is based on the photometric concentration determination of an indophenol dye which is formed stoichiometrically during the reaction. Throughout the present thesis, a variation of the Berthelot reaction was used, based on the method published by Willis et al. [175]. Details about the analysis can be found in Section 2.5.7. As indicated before in Section 3.1, the two parameters production rate and current efficiency were applied to evaluate the achieved results.

3.4. Results

3.4.1. Cyclic voltammetry

An exemplary cyclic voltammogram recorded for Ti at 50°C within the one-compartment cell is shown in Figure 3.5a). Contrary to the expected appearance of a cyclic voltammogram, there was no redox-couple visible in the investigated potential range. Hence, it was not possible to determine the type of reaction occurring. However, it was clear that with increasing potential at the WE also the current density was increasing, thus the reactivity was enhanced. Figure 3.5b) shows the same cyclic voltammogram plotted as a function of time. The typical triangular changes of the applied potential and the resulting current density are visible. The changing pH value is a clear evidence for a reaction taking place at the WE. However, the pH value is also influenced by side reactions such as H₂O oxidation at the CE for instance. Thus, for further analysis, samples are taken from the electrolyte and the amount of NH₃ dissolved in the electrolyte is determined by the Berthelot reaction (compare Section 3.3.4). At higher applied potentials, beginning at around -1.0 V vs. NHE, gas evolution took place particularly at the CE. Since an aqueous electrolyte was applied, it can be assumed that O₂ was formed at the CE.

3 Electrochemical NH₃ synthesis in liquid phase

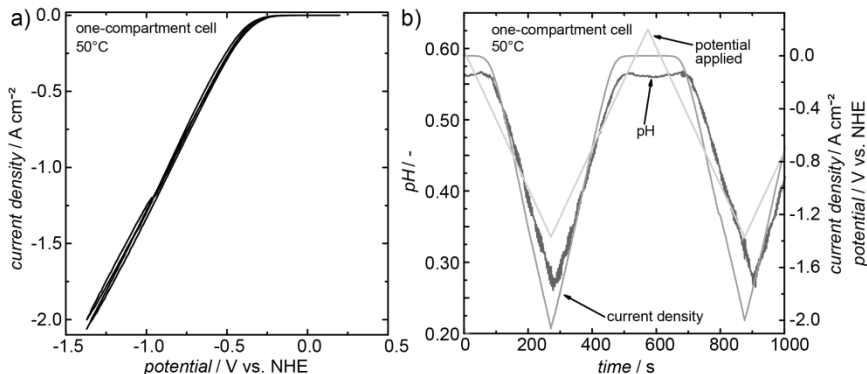


Figure 3.5: a) Cyclic voltammogram recorded for Ti at 50°C within the one-compartment cell
b) The same cyclic voltammogram plotted as a function of time. The pH value is plotted as well.

Parallel to O₂ evolution at the CE, also H₂ can be formed at the WE in an undesired parallel reaction. To avoid blocking of the WE surface by gas bubbles, three different potentials above -1.0 V vs. NHE were chosen for the following investigations by chronoamperometry experiments at a constant potential: -0.26, -0.46 and -0.66 V vs. NHE. At the lowest potential no or only a very small current density was detected in the cyclic voltammogram, meaning the reaction at the WE did not start yet. At -0.46 V vs. NHE the current density increased remarkable, indicating some kind of reaction is taking place at the WE. At the highest negative potential, also the highest current density was observed. However, undesired side reactions such as H₂ evolution or H₂O oxidation can also take place.

The CV experiments were not repeated in the two-compartment cell, since the electrode arrangement and the applied electrolyte were the same. For the following chronoamperometry measurements, the same potentials were applied as determined in the one-compartment cell.

3.4.2. Chronoamperometry

The influence of the reaction temperature was investigated for both the one-and the two-compartment cell. The two parameters of interest for the evaluation of the liquid phase synthesis were the production rate and the current efficiency (compare Section 3.3.4).

a) One-compartment cell

Table 3.4 gives the maximum achieved production rates for all chronoamperometry measurements conducted in the one-compartment cell. For the 6-hour experiments, the time interval after which the sample was taken is given in brackets behind the number for the production rate. For the 15-hour experiments, the maximum production rate is given for the 15-hour sample. In general, with increasing potential, also the production rate increased.

Table 3.4 Achieved production rates * in mol s⁻¹ cm⁻² for chronoamperometry measurements conducted at three different temperatures in the one-compartment cell.

Time [h]	Constant potential [V vs. NHE]	Production rate [10 ⁻¹³ mol s ⁻¹ cm ⁻²]		
		30°C	50°C	70°C
6	-0.26	180 (5 h)	1700 (1 h)	-1700 (3h)
	-0.46	450 (1 h)	2000 (1 h)	1500 (1 h)
	-0.66	-110 (4 h)	3800 (1 h)	1000 (1 h)
15	-0.26	5.7	-490	-4.5 x 10 ⁹
	-0.46	-210	7.3 x 10 ¹⁰	-2.4 x 10 ¹¹
	-0.66	160	3.6 x 10 ⁹	-1.7 x 10 ¹¹

* The number in brackets gives the time interval after which the sample was taken. For the 15-hour experiments the samples were taken at the end.

Since the applied potential is the driving force for the reactions taking place at the WE, such observation is reasonable. However, contrary to the Arrhenius equation, the production rate did not constantly rise with rising temperature. At 70°C the production rate was lower compared to the values at 50°C for all applied potentials. During the 6 hours experiments, the best production rates for the one-compartment cell were reached at 50°C after 1 hour experimental time. The reached production rates for the 15-hour experiments were not reliable for 50 and 70°C. In literature, production rates from 10⁻¹³ to 10⁻⁸ mol s⁻¹ cm⁻² are reported. The high production rates obtained during the 15-hour experiments could not be repeated. Since the system behaved unstable at longer experimental time, the values for the 15-hour experiment were not considered for further investigation. Negative production rates mean that there was less NH₃ dissolved in the particular sample than in the sample taken directly after the pretreatment and activation. The highest reliable production rate of 3.8 x 10⁻¹⁰ mol s⁻¹ cm⁻² was obtained at 50°C and -0.66 V vs. NHE after 1 hour experimental time.

Parallel to the production rate, also the current efficiency for the experiments conducted in the one-compartment cell in liquid phase was investigated. The best results for the current efficiency were also obtained at -0.66 V vs. NHE, but at 70°C instead of 50°C, see Figure 3.6. The highest realistic current efficiency of 64.1% was reached after 3 hours experimental time. Unfortunately, the current efficiency did not follow a trend, but increased and decreased irregularly with time. It is assumed that undesired parallel reactions such as NH₃ oxidation at the CE destabilized the system and thus lead to an unstable system response. In summary, a compromise between production rate and current efficiency has to be found. At 50°C the production rate was high, but the current efficiency was as little as 0.03%. Contrary, at 70°C the current efficiency was high, but the production rate of 4.8 x 10⁻¹¹ mol s⁻¹ cm⁻² was around one order of magnitude lower than the value reached at 50°C. Similar to the production rate, negative current efficiencies mean that NH₃ was decomposed instead of being synthesized. For that reason, in the next step the CE was separated from the WE by a cation exchange membrane, to avoid undesired parallel reactions and to stabilize the system.

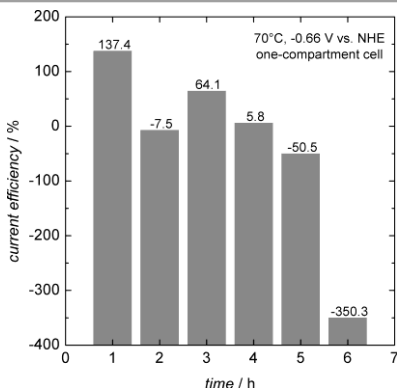


Figure 3.6: Development of the current efficiency reached for CA experiments conducted in the one-compartment cell at 70°C and an applied potential of -0.66 V vs. NHE

b) Two-compartment cell

To achieve more stable and reliable results, the conducted experiments were repeated in the two-compartment cell. Here the CE is separated from the WE by a H⁺ conductive membrane to stabilize the system and to avoid undesired parallel reactions, see Figure 3.4. Table 3.5 gives the maximum achieved production rates for all chronoamperometry measurements conducted in the two-compartment cell.

Table 3.5 Achieved production rates * in mol s⁻¹ cm⁻² for chronoamperometry measurements conducted at three different temperatures in the two-compartment cell.

Time [h]	Constant potential [V vs. NHE]	Production rate [10 ¹³ mol s ⁻¹ cm ⁻²]		
		30°C	50°C	70°C
6	-0.26	-260 (2 h)	2000 (1 h)	-1200 (1h)
	-0.46	930 (2 h)	2400 (1 h)	1900 (1 h)
	-0.66	-1400 (1 h)	4100 (1 h)	3300 (1 h)
15	-0.26	150	-450	-7.4 x 10 ¹⁰
	-0.46	250	-1.3 x 10 ¹¹	-4.0 x 10 ⁹
	-0.66	-6.8	-2.6 x 10 ¹⁰	-2.3 x 10 ¹⁰

* The number in brackets gives the time interval after which the sample was taken. For the 15-hour experiments the samples were taken at the end.

As before in Table 3.4, for the 6hour experiments the time interval after which the sample was taken is given in brackets behind the number for the production rate. For the 15-hour experiments, the maximum production rate is given for the 15-hour sample. Similar to the one-compartment cell, the production rate increased with increasing potential in the two-

compartment cell as well. An increase in temperature from 30 to 50°C significantly improved the production rate, while a further temperature increase to 70°C reduced it again. Just like in the one-compartment cell, the best production rates were achieved at 50°C after 1 hour experimental time. The highest production rate of $4.1 \times 10^{-10} \text{ mol s}^{-1} \text{ cm}^{-2}$ was obtained at an applied potential of -0.66 V vs. NHE at 50°C. In the two-compartment cell the maximum production rate was increased by approximately 10% compared to the one-compartment cell at the same reaction conditions. Only at 30°C and lower applied potentials, positive production rates were obtained during the 15-hour chronoamperometry experiments. Thus, the separation of the CE from the WE only had a positive impact on the system at shorter reaction times. The system still behaves unstable when running experiments of longer duration which needs to be investigated in future studies.

Also for the two-compartment cell, the current efficiency for the conducted experiments was investigated. Contrary to the one-compartment cell, the best results were obtained at the same temperature at which the best production rates were reached. However, in the two-compartment cell the maximum current efficiencies were reached at a lower potential than in the one-compartment cell. Thus the best effect of the separation of the CE from the WE was achieved at short experimental times and low potentials. Figure 3.7 shows the development of the current efficiency of chronoamperometry experiments conducted at 50°C and an applied potential of -0.26 V vs. NHE.

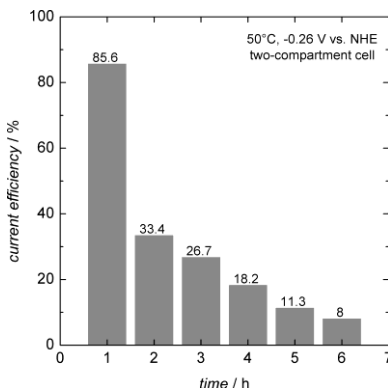
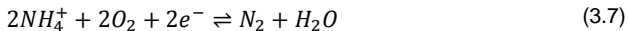


Figure 3.7: Development of the current efficiency reached for CA experiments conducted in the two-compartment cell at 50°C and an applied potential of -0.26 V vs. NHE

The highest current efficiency of 85.6% was reached after 1 hour experimental time. A continuous decrease of the current efficiency over time was obtained. Since N_2 was fed continuously to the electrolyte, a lack of reactant in the electrolyte can be excluded as possible explanation. Since the CE and the WE were separated from each other, undesired parallel reactions at the CE which reduce the amount of produced NH_3 were not possible. However, as indicated in Section 2.6.4, dissolved NH_3 can also further react at the cathode, meaning the WE, when O_2 is entering the system according to Equation (3.7).



Unfortunately, this reaction cannot be avoided by means of spatial separation of the WE from the CE. Since the electrolyte is purged with N₂ during the whole experiment, O₂ actually cannot enter the system. Further long term experiments are necessary to determine the reactions occurring in liquid phase at the WE and if O₂ is the reason for the reduced current efficiencies. In general, the selectivity of the catalyst for NH₃ synthesis needs to be enhanced to reach high current efficiencies also for longer experimental times.

3

The development of the achieved current efficiencies in the two-compartment cell is more stable than in the one-compartment cell and did not deviate as much as described before (compare Section 3.4.2 a)). In summary, the compromise between production rate and current efficiency is easier to achieve with the two-compartment cell, since both values are high compared to the one-compartment cell. For short experimental times, the separation of the CE from the WE is a promising mechanism to stabilize the system. However, for long term experiments further research is necessary. To find the most promising reaction conditions for the electrochemical NH₃ synthesis in liquid phase, the above results are compared in the following section.

3.4.3. Comparison of the one- and the two-compartment cell

Both in the one- and in the two-compartment cell the highest production rates were achieved at 50°C after 1 hour experimental time, see Figure 3.8.

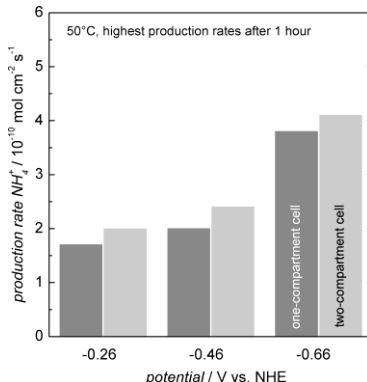


Figure 3.8: Comparison of the highest production rates achieved at 50°C and three different applied potentials after 1 hour experimental time in the one- (dark grey columns) and in the two-compartment cell (light grey columns).

For both setups an increase in potential leads to higher production rates. Furthermore, for all applied potentials higher production rates were achieved in the two-compartment cell. In Table

3.6 the achieved current efficiencies for the maximum production rates at 50°C in the one- and the two-compartment cell are given for three different potentials.

Table 3.6 Achieved current efficiencies for the maximum production rates at 50°C and three different potentials in the one- and the two-compartment cell		
Constant potential [V vs. NHE]	Current efficiency [%]	
	One-compartment cell	Two-compartment cell
-0.26	324.3	85.6
-0.46	0.8	59.4
-0.66	0.03	27.7

Contrary to the production rate, an increase in potential decreases the achieved current efficiency both for the one- and the two-compartment cell. The current efficiency of 324.3% at -0.26 V vs. NHE reached in the one-compartment cell is not realistic and was thus neglected. In general, higher current efficiencies were achieved in the two-compartment cell, which is in agreement with the observations about the production rate mentioned earlier. The corresponding current efficiency for the highest production rate at -0.66 V vs. NHE was 27.7%, and thus around only one third smaller of the maximum current efficiency of 85.6% reached at -0.26 V vs. NHE. The corresponding production rate at this potential was half the value of the maximum production rate of $4.1 \times 10^{-10} \text{ mol s}^{-1} \text{ cm}^{-2}$ reached at -0.66 V vs. NHE, see Figure 3.8. In summary, the results achieved in the two-compartment cell were improved compared to the one-compartment cell and the system behaved more stable. The positive impact of the separation of CE and WE from each other was more pronounced for the current efficiency than for the production rate. Apparently, most of the undesired side reactions at the CE were avoided by the spatial separation with the membrane. At this early stage of research high current efficiencies are more interesting, since the production rate can also be improved by scaling up the whole system. The best compromise between current efficiency and production rate was found at -0.46 V vs. NHE. The current efficiency was as high as 59.4% and the corresponding production rate was $2.4 \times 10^{-10} \text{ mol s}^{-1} \text{ cm}^{-2}$.

3.5. Conclusion

In this chapter the electrochemical synthesis of NH₃ in liquid phase was investigated in two different setups compromising a classical three electrode configuration. Titanium was used as catalyst at the WE and 0.5 M H₂SO₄ was applied as aqueous electrolyte. In the one-compartment cell all electrodes were immersed in the same electrolyte, while in the two-compartment cell the CE was separated from the WE by a H⁺ conductive membrane. In each setup cyclic voltammetry and chronoamperometry measurements were conducted. The CV experiments gave three interesting potentials, at which the following CA experiments were carried out: -0.26, -0.46 and -0.66 V vs. NHE. The following CA experiments were performed at three different temperatures of 30, 50 and 70°C. To evaluate the two systems, the two parameters production rate and current efficiency were chosen. The one-compartment cell behaved instable and no clear trend for the production rate and the current efficiency was

3 Electrochemical NH₃ synthesis in liquid phase

detectable. By the spatial separation of the CE from the WE in the two-compartment cell, the system was stabilized and more reliable results were obtained. Both for the production rate and the current efficiency the values reached in the two-compartment cell were higher compared to the one-compartment cell. The best compromise between both parameters was obtained at 50°C and an applied potential of -0.46 V vs. NHE. The reached production rate was 2.4×10^{-10} mol s⁻¹ cm⁻² and the corresponding current efficiency was as high as 59.4%. In future investigations, the selectivity of the catalysts needs to be improved to further increase the production rate and to reach current efficiencies close to 100%.

4. The electrochemical membrane reactor - Materials & methods

4

4.1. Introduction

The most significant chemical process invention of the 20th century is the Haber process for NH₃ production [3]. At 400 to 500°C and 150 to 200 bars, N₂ and H₂ react to form NH₃. The required H₂ is produced by the reformation of CH₄ or coal with H₂O. It would be highly desirable to omit the use of carbon sources for H₂ production. Additionally, for each ton of NH₃ produced, approximately two tons of CO₂ are emitted. [14]

A potentially more sustainable NH₃ synthesis method is the direct reduction of N₂ using an electrochemical membrane reactor (ecMR) [15]. The feasibility of the ecMR for the electrochemical reduction of CO₂ to synthesize hydrocarbons was proved [26]. An ecMR is similarly constructed as a PEM electrolyzer. The proposed ecMR process is carbon-independent and CO₂-free. In fact, H₂O is used as an abundant source of H₂ and renewable energy can drive the reaction. The core of the ecMR is the membrane electrode assembly (MEA), compare Section 4.5. The MEA combines (a) the oxygen evolution reaction (OER) at the anode, (b) the migration of H⁺ across the polymer cation exchange membrane (CEM) and (c) the reduction of N₂ to NH₃ at the cathode, see Figure 4.1.

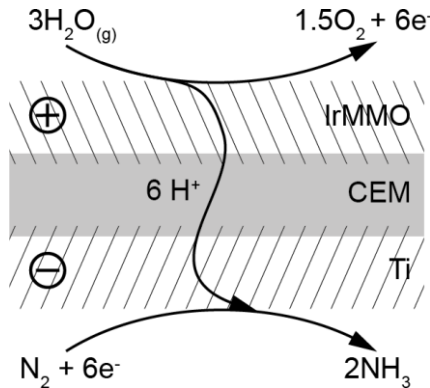


Figure 4.1: Reactions at the MEA: at the anode, H₂O is oxidized to form O₂ and e⁻, H⁺ migrate through the CEM to the cathode where N₂ is reduced to NH₃.

The corresponding reaction equations for the anodic and the cathodic reactions and their standard potentials are given in Section 4.7. The main parallel reaction at the cathode is the reduction of H⁺, i.e., a hydrogen evolution reaction (HER).

4.2. The electrochemical setup for NH₃ synthesis

All experiments for the gas phase electrochemical reduction of N₂ to NH₃ were performed in an ecMR. This reactor is the core of an electrochemical setup with gas and H₂O supply, an evaporation unit and analysis. The flowchart of the setup is shown in Figure 4.2.

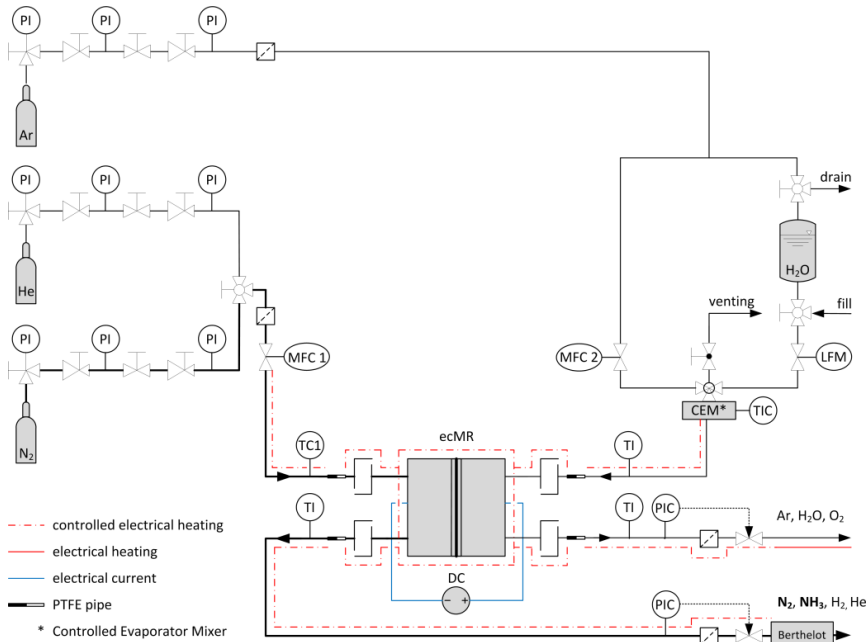


Figure 4.2: Flow chart of the electrochemical setup for NH₃ synthesis with the electrochemical membrane reactor (ecMR) as its core.

The setup consists of an anodic and cathodic compartment. The latter consists of a He and N₂ supply, the cathodic half-cell of the ecMR and the analysis, which is carried out by the Berthelot reaction, see Section 2.5.6. The anodic compartment consists of an Ar and H₂O supply, a Controlled Evaporator Mixer unit (CEM, Bronkhorst) and the anodic half-cell. The ecMR is heated with a tailor-made heating sleeve (Horst GmbH, 100 W) and the temperature of the tubing and the CEM unit is kept at 80°C (Horst GmbH, 50 W). Different reaction temperatures are realized by varying the ecMR temperature only.

All gases are taken from a central gas station at the research facility. The bottle pressure is reduced to the station pressure and then again reduced to the system pressure of 5 barg. To avoid contamination of the setup with small particles, 2 µm inlet filters (Swagelok) are installed in front of both MFC 1 and the tee connector for the splitting of Ar. Argon is used as carrier gas

for H₂O in the anodic compartment and for pressurizing the H₂O tank. All gas volume flows are controlled via digital mass flow controllers (MFC, Bronkhorst). The gas pressure of the ecMR is regulated by two back pressure controllers (WIKA) and pressure valves (Bürkert) installed behind the ecMR. Behind the two back pressure controllers 2 µm inlet filters are installed as well to prevent transportation of catalyst material to the analysis. To eliminate condensation of the products behind the back pressure controllers, the tubing before the analysis is heated with self-regulating heating cables (Horst GmbH) constantly to 120°C.

At the anode side of the ecMR a humidified Ar gas stream enters the reactor. Different relative humidity of the gas stream is achieved by varying the temperature of the ecMR or by varying the volume flow of H₂O entering the CEM unit. The H₂O tank is pressurized with Ar and the liquid flow meter (LFM) controls the water flux. In the CEM unit H₂O gets evaporated and is mixed with Ar. The minimum gas flow at the anode side is 50 ml n min⁻¹ since the CEM unit needs this gas flow for optimal operation. At the cathode side of the ecMR dry He or N₂ gas enters the reactor. The operating parameters of the setup are shown in Table 4.1:

Table 4.1 Operating parameters of the electrochemical setup	
Parameter	Value range
Pressure [barg]	0 - 2.5
Temperature [°C]	25 - 90*
Gas flow rate [mln min ⁻¹]	0 - 100
Liquid flow rate [g h ⁻¹]	0 - 1

* limited due to temperature stability of the pressure valve

The anodic gas stream is released to the atmosphere, while the cathodic gas stream is dissolved in two consecutive beakers filled with 0.5 M H₂SO₄. Samples are taken from each beaker for analysis with the Berthelot reaction (see Section 2.5.7).

The core of the setup is the electrochemical membrane reactor (ecMR). To electrically decouple the ecMR from other parts of the setup, PTFE tubes at the gas inlets and outlets are used. For easy and quick mounting of the ecMR into the setup, quick couplers (Swagelok) are installed. The power supply is carried out by a potentiostat (PGSTAT302N, Metrohm). The controlling of the electrochemical system is realized by a DASYLab user interface. The potentiostat is controlled by the Metrohm own software NOVA.

4.3. Requirements for electrochemical cells

The overall aim of the present thesis is to develop and to optimize an electrochemical membrane reactor (ecMR) for NH₃ synthesis. The ecMR belongs to the class of solid electrolyte systems (see Section 1.5.4), which basically consist of two porous electrodes, the anode and the cathode, and a dense solid electrolyte [179]. This electrolyte separates the anodic from the cathodic department and acts as a barrier for gas diffusion. Depending on the kind of electrolyte applied, either H⁺ or O²⁻ can permeate through it. Amar et al. summarize general requirements for the components of electrochemical cells for NH₃ synthesis. [96] The electrolyte should (a) have a high ionic conductivity in the range of 10⁻² S cm⁻¹ and a low electronic conductivity, (b) have mechanical and chemical stability in both oxidizing and reducing environments, and

4 The electrochemical membrane reactor - Materials & methods

(c) be highly dense to be gas-tight. The electrodes need to have a certain porosity and pore size to give a proper support layer for the catalyst material. Furthermore the electrodes must be stable at the operating temperature. The catalyst itself needs to be highly electronic conductive, and of course should have a high catalytic activity for the electrochemical NH₃ synthesis. Since the HER is the main competing reaction to NH₃ formation, the catalyst needs to have a high adsorption capacity for H⁺, but at the same time it should have a high selectivity towards NH₃ formation. The thermal expansion coefficients of all materials need to be matched to each other to avoid material failure while operating the system. [96] The costs for N₂, H₂O and renewable energy are fairly cheap. To benefit from these low costs for the reagents and energy used, further costs for materials such as the electrodes, catalyst and cell material need to be as low as possible. For instance costs for catalysts can be reduced by applying thin coatings of ~1 µm thickness on proper support materials such as carbon cloth or Ti felts, see also Chapter 2.

4.4. The electrochemical membrane reactor - ecMR

The electrochemical membrane reactor used for the present work is shown schematically in Figure 4.3: The ecMR basically consists of two Ti half-cells with an outer diameter of 90 mm and a thickness of 14 mm and the membrane electrode assembly (MEA) in the center. Each half-cell has two 1 mm boreholes with an ISO 1/8" thread on the outer side to fix the quick couplers for the gas in- and outlet stream. Centered on the outer face there is a M24 thread for mounting the setup fixture. The power supply is connected via 2 mm banana plugs. On the inner surfaces of the two half-cells there are serpentine flow fields milled in.

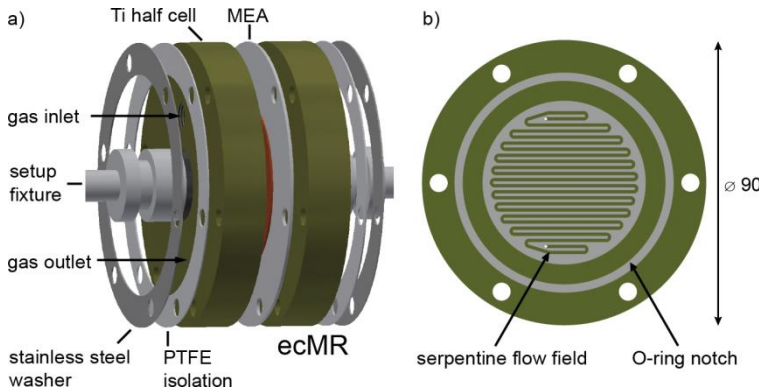


Figure 4.3: Schematic presentation of the electrochemical membrane reactor (ecMR) with an outer diameter of 90 mm. a) 3d model of the ecMR showing the membrane electrode assembly (MEA), two Ti half-cells, two PTFE isolation rings, two stainless steel washers and the setup fixture. Each half-cell has a gas inlet and outlet. b) Interior view of one Ti half-cell showing the serpentine flow field with gas inlet and outlet and the O-ring notch for sealing of the ecMR.

Each flow field is connected to the gas inlet and outlet. The serpentine shape of the flow field ensures a uniform gas distribution along the catalysts surface of the MEA and extends the residence time of reactants in the ecMR [180]. The two Ti half-cells act as current collector and distributor and as endplate of the ecMR. The specific parameters of the ecMR are given in Table 4.2:

Table 4.2 Specific parameters of the ecMR

Parameter	Symbol	Value
Channel length [mm]	l	913.8
Hydrodynamic channel diameter [mm]	d_{hyd}	1.0
Active membrane and catalyst area [cm^2]	A_{active}	19.6

The two half-cells are screwed together by six M5 screws with a torque of 1.8 Nm. Sealing of the ecMR is carried out by two alternated O-rings. Each O-ring seals one half-cell. The first O-ring is positioned close to the catalyst felt, while the second one is close to the boreholes for screwing together the half-cells. By this O-ring arrangement the separation of the anodic and cathodic compartment is assured. Furthermore the entering of foreign gases from the outside is avoided. The electrical isolation of the two half-cells is ensured by several arrangements. The membrane isolates the inner surfaces from each other. To prevent a short circuit caused by the screws, the six boreholes are outfitted with PTFE-tubes and PTFE isolation rings are placed between the screw heads, screw nuts and the half-cells. For a uniform power transmission from the screws to the two half-cells, two stainless steel washers are applied. By applying an external potential to the ecMR, the electrical energy is transferred from the two half-cells to the two electrodes of the MEA.



4.5. The membrane electrode assembly - MEA

The membrane electrode assembly (MEA) is the core of the ecMR. The MEA presented here consists of three elements: (a) an Iridium Mixed Metal Oxide (IrMMO) anode, (b) a polymer cation exchange membrane (CEM), and (c) a Ti cathode responsible for N_2 reduction. On top of Ti there is always a TiO_2 layer present when getting in contact with air. The formation of this layer cannot be avoided when working under oxidizing conditions. As will be shown in Chapter 6, a cryogenic air separation needs to be applied in an electrochemical large scale NH_3 synthesis process, to separate O_2 from N_2 and to produce highly pure N_2 . Further research has to be carried out to what extend the assumption of pure N_2 can be released and O_2 may be present in the feed gas.

The electrochemical reactions for the electrochemical reduction of N_2 to NH_3 take place at the triple phase boundary (TPB). At this boundary there is intensive contact between the gaseous reactant, the solid electrocatalyst and the solid electrolyte, i.e. the CEM [181]. By hot-pressing a MEA a TPB is created. The fabrication of a MEA will be explained in more detail in Section 4.6.

4 The electrochemical membrane reactor - Materials & methods

4.5.1. The anode - Iridium mixed metal oxide IrMMO

At the anode Iridium mixed metal oxide IrMMO is used as catalyst for the oxidation of H₂O, called oxygen evolution reaction (OER). The IrMMO catalyst was coated with Magneto Special Anodes B.V., BA Schiedam, The Netherlands, on Ti felts (compare Section 4.5.3) by the paint-thermal decomposition method. Iridium and tantalum salts were first dissolved in butanol. The prepared ink was paint-brushed on the Ti felts in layers of approximately 0.5 g metal m⁻². After 10 min drying, the coated felts were decomposed for 20 min at 500°C.

Next to IrO₂, also Ru and RuO₂ show a high activity for the OER [182]. However, catalysts containing only RuO₂ or a mixture of RuO₂ - TiO₂ show low corrosion resistance during the anodic O₂ evolution under acidic conditions. In contrast IrO₂ has a lower activity for the OER than RuO₂, but its stability is much higher. The mixture of RuO₂ and IrO₂ in the ratio 80/20 gives very good results both for the OER activity and the stability in acidic solutions. [183] Comninellis and Vercesi investigated nine binary coatings of IrO₂, RuO₂ and Pt as conductive component and TiO₂, ZrO₂ and Ta₂O₅ as inert metal oxide additives. The mixture of IrO₂ and Ta₂O₅ at a 70/30 ratio was found to be the most active and most stable composition. In the mixed metal oxide catalyst, IrO₂ is the active species for the OER, while Ta₂O₅ stabilizes the catalyst and retards the reduction of IrO₂ to the less active Ir. [184] Furthermore the thermal stability is improved. IrO₂ is decomposing between 380 to 400°C, while the mixture of IrO₂ and Ta₂O₅ can be exposed to temperatures of 450 to 500°C. [185]

4.5.2. The polymer cation exchange membrane - Fumapem F-14100

The membrane used here is a perfluorinated sulfonic acid polymer cation exchange membrane from FuMA-Tech, type fumapem F-14100. It shows high proton conductivity in wet condition, but it is electrical isolating. Technical data of the used membrane can be found in the technical data sheet [186]. The general structure of a perfluorinated sulfonic acid polymer membrane is shown in Figure 4.4. The backbone of such a membrane is composed of a hydrophobic polytetrafluoroethylene PTFE matrix to which negatively charged hydrophilic sulfonate ions SO₃⁻ are attached. Positive ions such as H⁺ or Na⁺ are necessary for charge neutrality. Due to the hydrophilic SO₃⁻ ions the membrane can be humidified with H₂O. The H₂O is stored in the porous structure and the membrane swells. This change in thickness causes material stress and needs to be avoided once a MEA has been fabricated. For a stable operation of a MEA, the relative humidity the MEA is operated at should be kept constant. For the present thesis the applied membranes were modified into a NH₄⁺-form to avoid the dissolution of NH₃ in the membrane, see also [116]. The membrane was pretreated in an aqueous 10 wt% HNO₃ solution for 3 hours at 80°C, followed by an 1 hour treatment in demineralized H₂O at 80°C. Subsequently, the membrane was stored in a 30 wt% NH₄OH solution for 18 hours at room temperature, followed by rinsing with demineralized H₂O for 6 days. By this modification, the H⁺ ions connected to SO₃⁻ get replaced by NH₄⁺ ions. However, a severe decrease in proton conductivity of up to 75 to 98% is the consequence [187,188]. Hongsirikarn et al. explain this finding with the increased size of the two different cations H⁺ and NH₄⁺. The radius of NH₄⁺ ions is four times larger compared to H⁺ ions. The ion transport mechanism can be shifted towards the slower vehicle mechanism, see also the next paragraph.

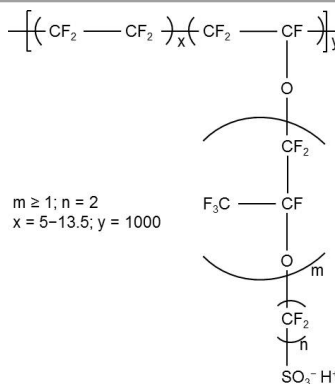


Figure 4.4: General chemical formula of a perfluorinated sulfonic acid polymer membrane (adapted from [189]).

Hongsirikarn et al. also observed a strong dependency of this effect on the relative humidity (RH). At 30% RH the proton conductivity of a NH_4^+ modified membrane was 55 times lower than for a membrane in H^+ form. However, at 100% RH the proton conductivity was only three times lower [188].

After fabrication of a MEA with a modified membrane, the MEA was flushed with an inert gas for 2 hours prior to the actual experiment to ensure that only produced NH_3 was analyzed.

Transport mechanism for H^+ through the membrane

The H^+ formed at the IrMMO anode migrate through the CEM, see Figure 4.1. The conductivity of the polymer membranes ranges from 0.01 to 0.1 S cm⁻¹ and depends mainly on the temperature and the relative humidity at which the membrane is operated [190]. Protons carry H_2O molecules through electro-osmosis: such H_2O transport needs to be balanced well as developed for water management strategies in H_2 fuel cells [191], see also Sections 4.9 and 5.3. There are two ways how H^+ can migrate through the membrane: The Grotthuss (hopping) mechanism and the vehicle (diffusion) mechanism [189,190], see Figure 4.5. In the Grotthuss mechanism, H^+ are transferred from hydronium ions H_3O^+ to H_2O molecules. Hereby the H_2O molecule becomes H_3O^+ and passes on the H^+ to the next H_2O molecule as shown in Figure 4.5a). Protons are hopping from one H_2O molecule to the next. The Grotthuss mechanism is predominating at high H_2O content of the membrane. With decreasing water content, also the H^+ conductivity of the membrane is decreased [192].

Diffusion is the main contributor to the vehicle mechanism. Protons connect with H_2O molecules to form H_3O^+ ions which diffuse through the membrane. The H_2O molecules act as vehicles for H^+ . At temperatures above 85°C diffusion and hereby the vehicle mechanism is predominant.

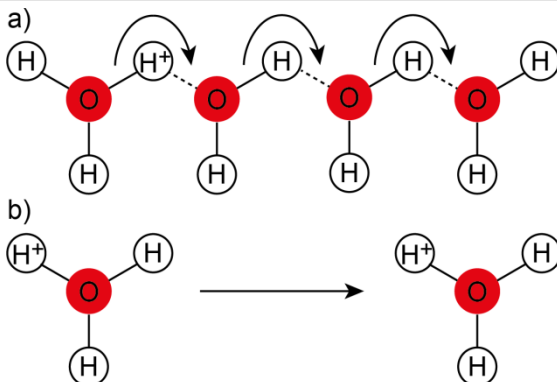


Figure 4.5: Schematic presentation of H^+ transport mechanism. a) Grothuss (hopping) mechanism and b) vehicle (diffusion) mechanism (adapted from [10])

4

4.5.3. The cathode - Titanium

The catalyst used for the N_2 reduction is the most critical component of the MEA. Skúlason et al. investigated the ability of transition metals, such as Ti, for the electrochemical synthesis of NH_3 by density functional theory (DFT) calculations. Titanium mainly adsorbs ${}^*\text{N}$ instead of ${}^*\text{H}$. The formation of NH_3 should be the predominant cathodic reaction [66], particularly because the overpotential for the HER on Ti is high [193], see also Section 2.2 and Section 6.4. Here a randomly structured sintered Ti felt (ST Titanium 15/40, Bekaert Fibre Technologies) with an average fiber diameter of 15 μm and a porosity of 40% is used as cathodic catalyst. For future investigations and modifications of the MEA, Ti is also available as flat plates and powders.

4.6. Fabrication of a membrane electrode assembly

The MEA is prepared via a hot-pressing process using a PE 30 hot press (Agila). The three parts of the MEA are piled according to Figure 4.6. Both catalyst felts have a diameter of 50 mm and a thickness of 100 μm . The membrane has a thickness of 100 μm in the dry state and 130 μm when swollen. The PTFE layers protect the catalysts from getting contaminated by rust or dirt on top of the heating plates. The spacers around the catalyst felts prevent the catalysts from being pressed too deep into the membrane. The MEA is fabricated at a pressure of 7.5 kN cm^{-2} corresponding to 111 bars and a temperature of 90°C for 20 min, followed by cooling at the same pressure for 1 min. Afterwards the MEA is tested for electric short-circuits.

Figure 4.7 shows the cross section of a typical MEA consisting of two catalytic metal felts and a proton conductive membrane in the middle. The top layer shows the IrMMO felt, followed by the cation exchange membrane and the Ti felt at the bottom. The metal felts are pressed into the membrane and a TPB is created.

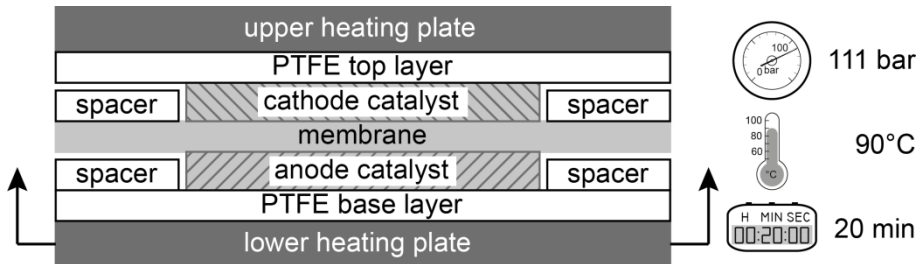


Figure 4.6: Arrangement of the different parts of a membrane electrode assembly (MEA) during the hot pressing process at 111 bar and 90°C for 20 min.

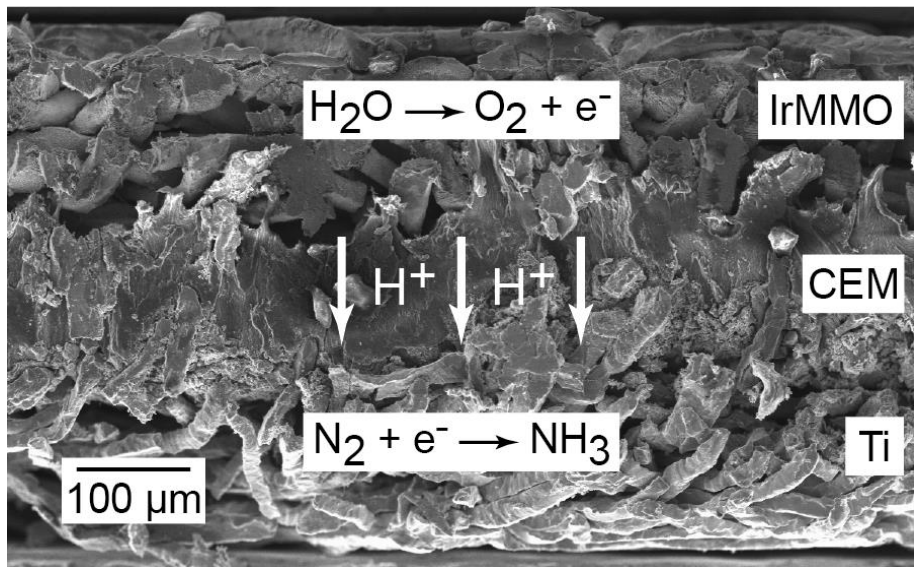


Figure 4.7: SEM image of the MEA consisting of an IrMMO anode, the CEM and a Ti cathode

Since spacers were used during the hot-pressing process, there is no electrical contact between the opposite metal felts. When measuring the resistance of the MEA after hot-pressing, values in the order of several mega ohms were detected. The total theoretical thickness of the MEA is 430 μm. The measured thickness is around 370 μm, i.e. both metal felts were pressed 30 μm into the membrane.

4.7. Electrochemical thoughts about NH₃ synthesis

The electrochemical NH₃ synthesis is a non-spontaneous process, which requires an external driving force, such as an applied electrical potential. When measuring polarization curves in the before described setup (compare Section 4.2), it is important to know in which potential range the reactions of interest take place.

For electrolysis cells energy supply is necessary, meaning the Gibbs free energy is positive, see Equation (4.1). Thus the difference in cathodic and anodic standard potentials ΔE^0 has to be negative, see Equation (4.2). The cell potential U_{cell} is the difference of ΔE^0 , the anodic and cathodic overpotentials η_A and η_C and the IR drop $\sum IR$, see Equation (4.3). The IR drop stands for loses due to the resistance of the electrical connections, the electrolyte and the cell. The anodic and cathodic overpotentials $\eta_{A/C}$ are defined as the difference of the anodic and cathodic electrode potential $E_{A/C}$ and the standard potential $E_{A/C}^0$, see Equation (4.4). [194]

$$\Delta G = -zF\Delta E^0 \quad (4.1)$$

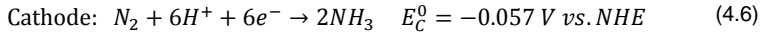
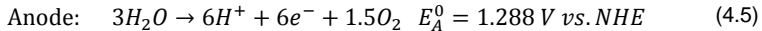
$$\Delta E^0 = E_C^0 - E_A^0 \quad (4.2)$$

$$U_{cell} = \Delta E^0 - |\eta_A| - |\eta_C| - \left| \sum IR \right| \quad (4.3)$$

$$\eta_{A/C} = E_{A/C} - E_{A/C}^0 \quad (4.4)$$

Equation (4.4) is only valid at standard conditions, meaning a temperature of 25°C, an electrolyte concentration of 1 mol and a pressure of 1 atm. At different reaction conditions $E_{A/C}^0$ is replaced by the equilibrium potential E_{eq} , which can be calculated by the Nernst equation.

In the case of electrochemical NH₃ synthesis the two key reactions are the oxidation of H₂O at the anode and the reduction of N₂ to NH₃ at the cathode. The standard potentials of each reaction are given in Equation (4.5) and (4.6) vs. the normal hydrogen electrode (NHE) [178]:



Under ideal reaction conditions, meaning there are no overpotentials and no ohmic losses, the minimum cell voltage $U_{cell,min}$ is equal to $\Delta E^0 = E_C^0 - E_A^0 = -0.057V - 1.228V = -1.285V$. However, both reactions at the anode and at the cathode underlie thermodynamic limitations and certain additional overpotentials $\eta_{A/C}$ have to be brought up. The IR drop further increases the cell potential.

4.8. Activity testing of IrMMO

As mentioned in Section 4.5.1 IrMMO is used as catalyst at the anode. To determine the overpotential of this catalyst for the OER several experiments have been conducted in a closed single-compartment cell. First a circular Ti substrate coated with IrMMO with a diameter of 6 mm was investigated using a rotating disk electrode (RDE) (Metrohm Autolab) at a rotation of 3600 rpm, see Figure 4.8.

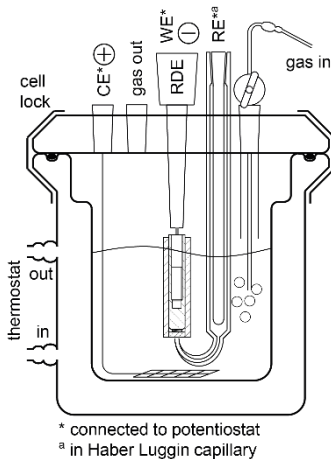


Figure 4.8: Scheme of the electrochemical cell for the activity testing of IrMMO with an electrode tip using a rotating disk electrode (RDE)

Second a Ti felt with a size of $2 \times 2 \text{ cm}^2$ coated with IrMMO (compare Section 4.5.1) was investigated in a three electrode setup (compare Figure 2.4).

Both cells were filled with 75 ml of 0.5 M H_2SO_4 (AVS Titrinorm, VWR) as electrolyte. In both experiments an $\text{Hg}/\text{Hg}_2\text{SO}_4$ reference electrode (RE) filled with 0.5 M H_2SO_4 (Sensortechnik Meinsberg GmbH) was used. For the RDE experiment the RE was mounted in a Haber-Luggin capillary, while it was only placed in the electrolyte close to the WE when measuring the IrMMO felt. For both experiments a platinized Ti expanded metal electrode (Wieland Edelmetalle GmbH) was applied as insoluble counter electrode (CE). All electrodes were connected to a potentiostat / galvanostat (PGSTAT302N, Metrohm Autolab). The activity testing was conducted at a cell temperature of 25°C, controlled by a thermostat (RE 2025, Lauda).

Prior to each activity testing by measuring linear sweep voltammograms, the electrolyte was purged with Ar for 45 min. During this purging the working electrode was activated with several cyclic voltammetry runs at a scan rate of 100 mV s^{-1} . First three cycles starting at the open circuit potential (OCP) to -0.22 V vs. NHE were measured. Secondly three cycles from the OCP to 2.18 V vs. NHE were performed. Thirdly ten cycles from the OCP to 2.18 V as upper vertex potential and back to -0.22 V vs. NHE as lower vertex potential were measured. Finally a

4 The electrochemical membrane reactor - Materials & methods

chronoamperometry at 1.28 V vs. NHE for 30 min was conducted to polarize the electrode. After the pretreatment the purging was switched from electrolyte purging to surface aeration during the activity measurements of IrMMO. The linear sweep voltammograms were performed from 1.13 to 2.00 V vs. NHE with a sweep rate of 5 mV s⁻¹. For the RDE measurements the resulting current was converted to the corresponding current density using the geometric surface area of the electrode tip.

4.8.1. Results

A parameter for the activity of a catalyst for the OER is the overpotential at a current density of 2 mA cm⁻² [177]. The lower the overpotential is the higher is the activity of the catalyst for the OER.

When measuring with the RDE, mass transport limitations are excluded. The resulting linear sweep voltammogram for the IrMMO tip applied as electrode at the RDE is shown in Figure 4.9.

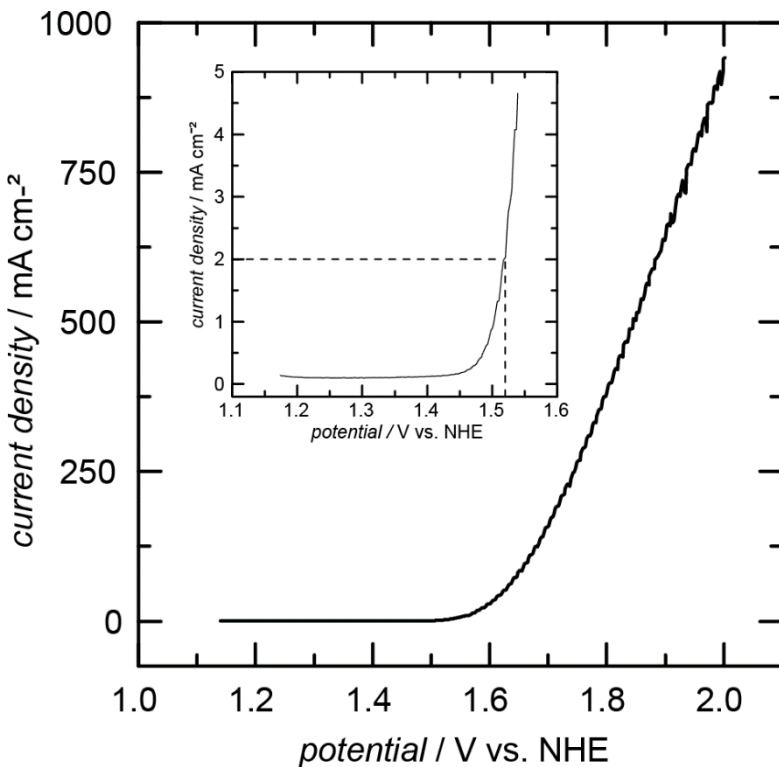


Figure 4.9: Linear sweep voltammogram of the IrMMO tip used as electrode at the RDE at 3600 rpm

Up to a potential of 1.45 V vs. NHE the current density is smaller than 0.2 mA cm^{-2} . Beyond this potential the current density increases steadily with increasing potential. In the analyzed potential range no limiting current density was observed. The onset potential for the OER was determined to 1.52 V vs. NHE at a current density of 2 mA cm^{-2} . The resulting overpotential of the investigated IrMMO tip according to Equation (4.4) is:

$$\eta_A = E_A - E_A^0 = 1.52V - 1.228V = 0.292V \quad (4.7)$$

The overpotential of the tested IrMMO catalyst of 292 mV for the OER is in the range of 160 to 300 mV mentioned in literature [182].

In the ecMR a Ti felt coated with IrMMO is used as anodic catalyst material. This IrMMO felt was tested under the same conditions as the IrMMO electrode tip. Contrary, the felt was not rotating during the measurement and the active catalyst area was different. The exact surface area of the IrMMO felt could not be determined due to lack of material. Only the surface area of the bare Ti support felt was determined with a BET device (ASAP 2020, Micromeritics) using Kr as measuring gas, compare Section 2.5.3. The average specific surface area is $19 \text{ m}^2 \text{ m}^{-2}$. Figure 4.10 shows the linear sweep voltammogram of the IrMMO felt.

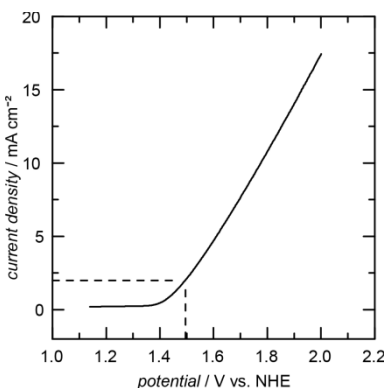


Figure 4.10: Linear sweep voltammogram of the IrMMO felt used as electrode

The current density was calculated with the specific surface area of an uncoated Ti felt, which is assumed to represent the geometric area for the IrMMO coating. The shape of the curve is similar to the voltammogram of the IrMMO tip, see Figure 4.9. However, the resulting current density is much lower, since the surface area of the felt is around 270 times higher than the one of the IrMMO tip. Contrary to the IrMMO tip, the current density values begin to increase at much lower potentials for the IrMMO felt. Similar to the IrMMO tip no limiting current density was observed. At 2 mA cm^{-2} the onset potential for the OER is 1.49 V vs. NHE and thus in the same range of the IrMMO tip. The resulting overpotential of the IrMMO felt according to Equation (4.4) is:

$$\eta_A = E_A - E_A^0 = 1.49V - 1.228V = 0.262V \quad (4.8)$$

The applied reaction conditions for the activity measurements are close to standard conditions. Thus in Equation (4.7) and (4.8) the standard potential for the OER of 1.228V vs. NHE is considered.

Similar to the IrMMO tip, the resulting overpotential of 262 mV is in the expected range of 160 to 300 mV reported in literature [182]. Both IrMMO modifications show a similar behavior and almost identical over potentials. However, the overpotential of the IrMMO felt is 30 mV lower than the one of the IrMMO tip. The felt geometry should have a positive impact on the activity, particularly when considering that the exact surface area of the IrMMO felt was not determined and mass transport limitations could not be excluded during the measurement.

4.9. Water management in PEMFC and ecMR

Polymer electrolyte membrane fuel cells (PEMFC) are an environmentally friendly and CO₂-free option for the generation of green energy. However, the large-scale application and the spread at the end-user site are still limited due to the high material costs for the required noble metal catalysts and the polymer membranes and due to the lower reliability and durability of PEMFCs. [195] For high performance and durability of a PEMFC, the relative humidity of the membrane material is a crucial factor. The proton transfer rate across the membrane mainly depends on the relative humidity of the membrane (see Section 4.5.2). With increasing relative humidity, PEMFCs often show an unstable behavior during operation, meaning the current response to the applied potential is irregular. The current response of a typical chronoamperometry is constant after reaching the equilibrium state. Instead, an unstable behavior of a PEMFC leads to sudden current increases, resulting in peaks in the current plot.

Protons connect with H₂O molecules to form hydronium ions H₃O⁺, meaning H₂O is transported across the membrane along with H⁺. Since an electric field is required for this transport phenomenon, it is called electroosmotic drag (ED) [192,196,197], see Figure 4.11a). Hereby, a concentration gradient for H₂O is established between anode and cathode. By back diffusion (BD) of H₂O molecules from the cathode to the anode, this gradient is equalized. At low current densities, back diffusion is predominant over the electroosmotic drag and vice versa at high current densities. Even if the relative humidity at the cathode is high, the anode can dry out due to a high electroosmotic drag. [198] As explained before, a certain relative humidity is required for high H⁺ conductivity. However, excessive H₂O can block the flow channel of the PEMFC and/or the pores of the gas diffusion electrode and of the catalyst layer, known as flooding. The activity of the catalyst is reduced due to the reduced amount of available active sites. Additionally, the accumulation of excessive H₂O increases the mass transport resistance [199]. In general, the issue of flooding mainly occurs at high current densities, since more H₂O is produced at the cathode than can be removed from it. Advantageously, most of the consequences related to short-term flooding are reversible and steady state conditions can be observed after a certain delay, depending on the operation conditions.

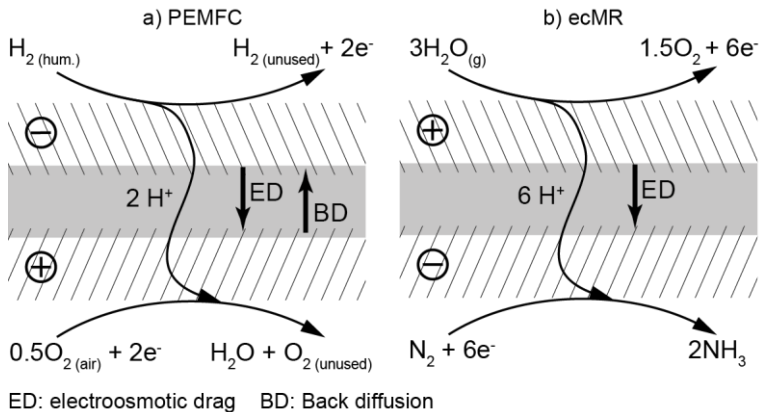


Figure 4.11: Water transport mechanism inside a) a polymer electrolyte membrane fuel cell (PEMFC) and b) an electrochemical membrane reactor (ecMR).

4

On the other hand, long-term flooding will cause mechanical deterioration of the MEA and thus loss of performance and durability. [200] In summary, a compromise between relative humidity, operation stability and performance is necessary for a PEMFC.

In the electrochemical membrane reactor (ecMR) applied for the present thesis, only the phenomenon of electroosmotic drag is expected to occur. At the cathode dry N_2 gas is fed to the ecMR, thus the H_2O concentration will always be higher at the anode. Depending on the relative humidity of the anodic feed stream, the concentration gradient is more or less pronounced. The phenomenon of back diffusion of H_2O from the cathode to the anode is not expected to occur, see Figure 4.11b). Dehydration of the membrane can occur either due to a low relative humidity at the anode or due to a high electroosmotic force when applying a high potential. As shown in Section 4.8.1 the activity of the applied IrMNO catalyst at the anode is high for the oxidation of H_2O . If the relative humidity at the anode is high, also the formation rate for H^+ is assumed to be high. However, excessive H_2O can also block active sites of the IrMNO catalyst and can limit the formation rate of H^+ . Depending on the applied potential more, or less, H_2O is transported from the anode to the cathode. Consequently, also active sites of the cathodic catalyst can be blocked and thus reducing the activity. Since H_2O is not a reactant at the cathode, here only H^+ and N_2 are assumed to react, H_2O needs to be removed from the cathodic department. Thus, a reasonable N_2 gas flow is necessary, considering a compromise between H_2O removal rate and residence time of N_2 in the ecMR. To support the H_2O removal, a certain porosity of the gas diffusion electrode (GDE) is necessary. In the present thesis, the applied Ti felt at the cathode acts as GDE and catalyst at the same time. For that reason, the porosity of the felt was chosen to 40%, giving both a high active surface area and enough open space to remove H_2O properly. In summary, the H_2O management both at the anode and at the cathode has crucial impact on the performance of the ecMR, see Section 5.3. By optimizing the operation parameters temperature and relative humidity, the H_2O transport across the membrane can be balanced.

4

5. Electrochemical NH₃ synthesis in an ecMR

5

Abstract

The direct electrochemical synthesis of NH₃ from N₂ and H₂O vapor without the use of a fossil carbon source is highly desired. This synthesis is a viable option to store energy and produce fertilizer precursors. Here a membrane electrode assembly (MEA) demonstrating the feasibility of co-generating NH₃ and H₂ directly from N₂ and H₂O vapor at ambient conditions is presented. The MEA comprises the O₂ evolution catalyst IrMMO producing O₂ and H⁺. Protons are transported under the influence of an electrical field through a polymeric proton exchange membrane to the cathode where they react with N₂ to form NH₃. As a parallel reaction, H₂ gas is evolved and an NH₃-specific current efficiency of up to 27.5% is achieved with Ti as cathodic catalyst. The co-generation of H₂ can be tuned by the balance of process parameters, such as the relative humidity and electrochemical reaction variables. Besides Ti, also Fe and Ru catalysts were tested.

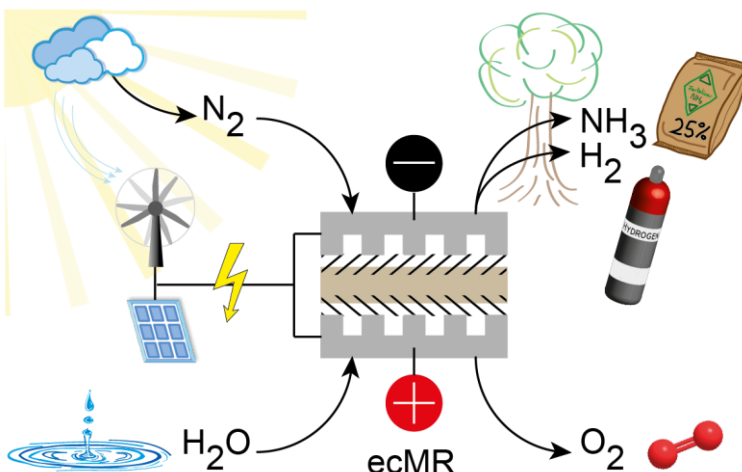


Figure 5.1: Graphical abstract of Chapter 5: Ammonia and H₂ are directly co-generated from N₂ and H₂O in an electrochemical membrane reactor (ecMR). Fossil feed stock is not used and renewable energy such as solar or wind power could drive the process.

5.1. Introduction

The electrochemical synthesis of NH₃ has attracted increased research interest [10]. Lan et al. reported the synthesis of NH₃ from air and liquid H₂O at ambient conditions using a MEA with two Pt/C electrodes and a Nafion 211 membrane. The viable production rates were approximately 1.1×10^{-9} mol s⁻¹ cm⁻² after 1 hour of experiment. However, the current efficiency was only approximately 0.5%. [116] A distinctive and novel difference of the ecMR was the control of the H₂O activity on the anode side. While Lan et al. used liquid H₂O, wherein the chemical potential could only be varied by temperature, we used gaseous H₂O, wherein we could change the chemical potential by varying the degree of saturation. The works published by Skodra et al. [100] and Licht et al. [88] also varied the partial pressure of H₂O used as abundant H₂ source. However, in both publications high temperatures in the range of 200 to 700°C and more complex electrolyte systems such as a strontia–ceria–ytterbia perovskite disk of the form SrCe_{0.95}Yb_{0.05}O_{3- δ} (SCY) [100] or a molten hydroxide suspension with a molar ratio of 0.5 NaOH/0.5 KOH were applied [88].

As described in the following sections, this control of the H₂O activity was an essential element of the ecMR. Using this new and versatile process, the influences of the temperature, the relative humidity (RH) of the anode feed stream and the applied cell potential on the NH₃ production rate and the current efficiency can systematically be studied. These parameters are also crucial for the stability of the reactor system with respect to the H₂O management as indicated for the operation of fuel cell systems [195].

5.2. Current voltage curves

The ecMR was operated with an Ar feed to the anode with varying amounts of H₂O vapor. Helium or N₂ was fed as the cathodic reactant and current voltage curves were recorded. Helium was used as a reference and to quantify the degree of H₂ production from H⁺. Nitrogen as the cathode feed led to NH₃ production as quantified in the Berthelot analysis of the reactor off-gas (compare Section 2.5.6). As indicated in Figure 4.1 Ti was used as catalyst at the cathode side. As explained beforehand, the electrochemical synthesis of NH₃ comprises two half-cell reactions. At the anode H₂O is oxidized, while at the cathode N₂ is reduced, compare reaction equations in Section 4.7. Under ideal reaction conditions, the minimum cell voltage for the electrochemical synthesis of NH₃ was equal to $U_{cell,min} = E_C^0 - E_A^0 = -0.057V - 1.228V = -1.285V$ [178]. Since the calculated value for $U_{cell,min}$ is only a lower boundary, the minor influence of the pH value and of the temperature on the standard potentials were not considered. The anodic and cathodic reactions were kinetically limited and additional overpotentials were observed. No significant current values were observed at potentials below -1.7 V, which was consistent with the high overpotential of Ti for the HER. In fact, this high overpotential for the HER may tailor the ratio of NH₃ and H₂ production rates.

Current voltage curves were recorded at 30, 50 and 70°C with varying relative Ar humidity of 25, 50 and 95% at 1 barg, see Figure 5.2. The corresponding H₂O flow rates in mg_{H2O} hour⁻¹ and the values for the corresponding partial pressure of H₂O in kPa are given in Table 5.1.

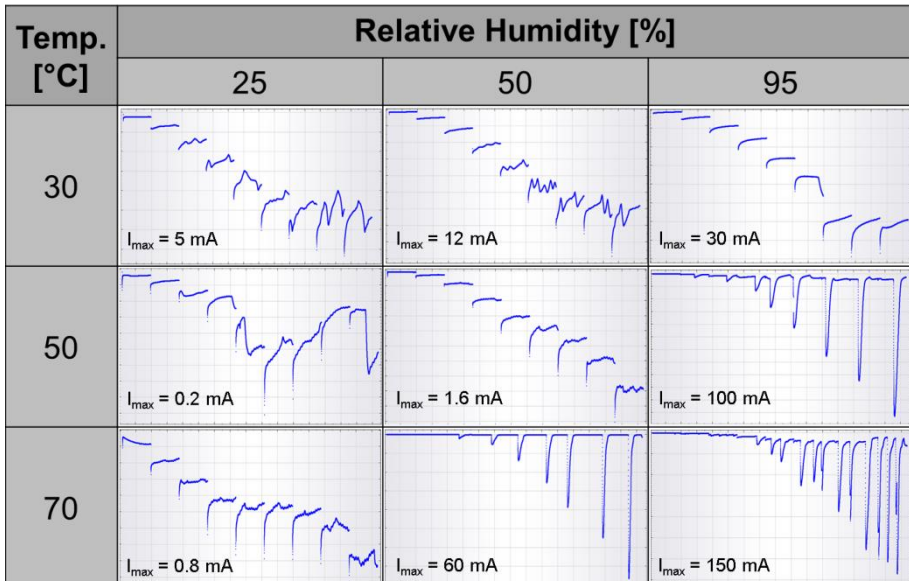


Figure 5.2: Current voltage curves recorded at 30, 50 and 70°C at a relative humidity of 25, 50 and 95% with N₂ as reactant gas. For better comparability, the maximum current is given for each curve.

Table 5.1 Investigated relative humidity values in %, mg_{H2O} per hour and the corresponding values of the partial pressure of H₂O in kPa

T [°C]	Relative humidity [%]					
	25		50		95	
	H ₂ O flow [mg hour ⁻¹]	Partial H ₂ O [kPa]	H ₂ O flow [mg hour ⁻¹]	Partial H ₂ O [kPa]	H ₂ O flow [mg hour ⁻¹]	Partial H ₂ O [kPa]
30	13	1.06	26	2.12	50	4.04
50	38	3.09	77	6.17	150	11.72
70	98	7.80	204	15.59	419	29.62

The flow rate of all gases applied was 50 ml min⁻¹ constantly. The cell potential ranged from -1.7 to -2.5 V with a potential sweep rate of 0.1 V h⁻¹. All experiments were conducted with the same MEA. The obtained current voltage curves at high temperatures (70°C at 50 and 95% RH; and 50°C 95% RH) showed severe current instabilities at higher potentials that were likely due to unstable H₂O management at the anode side similar to those observed in H₂ fuel cells [191]. Due to this unstable system behavior, only the results for 30°C (all RH) and 50°C (25 and 50% RH) are further discussed.

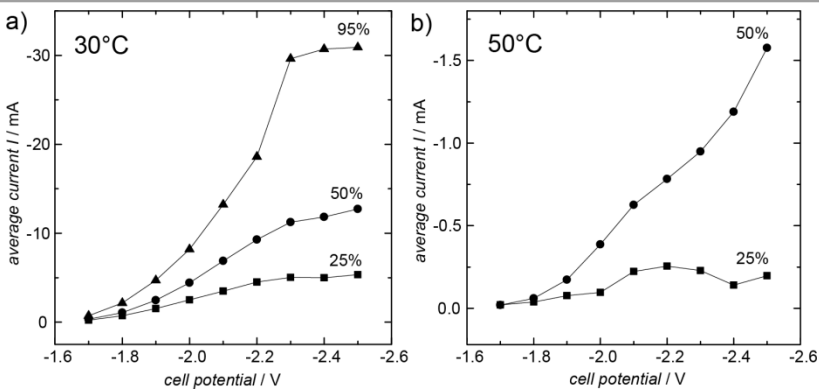


Figure 5.3: a) Current voltage curves for 25, 50 and 95% RH at 30°C and b) for 25 and 50% RH at 50°C. Currents were averaged for each potential step applied.

Figure 5.3a) and b) show the averaged currents measured for a N₂ feed. The current increased with the RH and the applied potential. At 30°C and -2.3 V, a leveling off was observed and the current increase was less pronounced. This intermediate limiting current was established above -2.5 V, but at even higher current values, the HER was predominant and the current increased (data not shown). For 50°C, the measured current was one magnitude smaller than that for 30°C. This was unexpected and cannot be explained at present. Higher current values were expected due to the increased conductivity for H⁺ and higher reaction rates at the cathode and anode. More H₂O was also supplied when compared to the same RH at 30°C.

5.3. Production rates and current efficiency

Two parameters were of interest to evaluate the results obtained here: (a) the NH₃ production rate in mol NH₃ produced per s of experimental time and cm² catalyst area perpendicular to the ionic flux and (b) the NH₃ specific current efficiency CE_{NH₃}, which gives the share of the total charge C transported compared with the amount of NH₃ synthesized, see Equation (5.1). In Table 5.2 numbers for the production rate and the CE_{NH₃} are given.

$$CE_{NH_3} = \frac{m_{NH_3} zF}{M_{NH_3} C_{corr.}} = \frac{m_{NH_3} zF}{M_{NH_3} (C_{N2} - C_{He})} \quad (5.1)$$

Here, z is the number of e⁻ needed to form one molecule of NH₃ (z = 3), F is Faraday's constant equal to 96485 C mol⁻¹ and m_{NH₃} and M_{NH₃} are the mass and the molar mass of NH₃, respectively. The charge C_{N2/He} is the measured average current multiplied by the experimental time.

Table 5.2 provides the maximum currents I_{max} and the achieved NH₃ production rates for the recorded current voltage curves. The phenomenon of decreased current at 50°C compared to the measurements at 30°C was also observed when measuring with He instead of N₂.

Table 5.2 Maximum average current, integral NH₃ production rates, average power density and integral NH₃ specific current efficiencies (CE) determined over whole polarization curves.

T [°C]	RH [%]	I _{max} [mA]	Production rate [10 ⁻¹² mol s ⁻¹ cm ⁻²]	Average power density [mW cm ⁻²]	NH ₃ specific CE [%]
30	25	5.0	0.7	0.40	0.1
30	50	12.0	2.7	0.80	0.2
30	95	30.0	53.0	1.80	2.1
50	25	0.2	2.5	0.02	9.0
50	50	1.6	4.1	0.08	2.3

The total charge passed during a current voltage curve recorded from -1.7 V to -2.5 V at a relative humidity of 25% was 5 times smaller for 50°C compared to 30°C. At 50% relative humidity the current at 50°C was even 22 times smaller compared to 30°C. The kinetics of the hydrogen evolution reaction usually gives higher H₂ evolution rates with increasing temperature. Due to the complex structure of the MEA, every component - anodic catalyst, membrane and cathodic catalyst - needs to be characterized by its own to further analyze the temperature and relative humidity dependency of the achieved current voltage characteristics. Electrochemical impedance spectroscopy (EIS) measurements can help to further evaluate the reaction behavior of the applied reactor and MEA system. However, it is beyond the scope of this work to focus on EIS measurements. The production rates increased with the RH and temperature. However, higher currents did not necessarily result in higher NH₃ production rates, but may have favored the co-generation of H₂. The highest NH₃ production rate of 53 × 10⁻¹² mol s⁻¹ cm⁻² was achieved at 30°C, 95% RH and a power density of 1.8 mW cm⁻². The power density was similar to the values observed in conventional industrial PEM and alkaline electrolyzer. Unlike fuel cells, ecMRs minimize the power densities by achieving maximum gas production rates. This maximizes the NH₃-specific current efficiency CE_{NH₃}.

To calculate an NH₃-specific CE (see Table 5.2), reference measurements with He were conducted resulting in H₂ production. Measurements with N₂ resulted in NH₃ production (m_{NH₃}), as measured and quantified by the Berthelot reaction. Figure 5.4 shows two polarization curve progressions recorded for N₂ and He at the same reaction conditions of 50°C and 50% RH. Clearly, the use of N₂ resulted in higher currents compared with the use of He. The produced NH₃ can be quantitatively analyzed in the off-gas. By subtracting the charge C_{He} measured for He, i.e., for the HER, from the charge C_{N₂} measured for N₂, i.e., for the formation of NH₃, a corrected current efficiency CE_{corr} specific for NH₃ synthesis was determined using Equation (5.1). For the integral current efficiency, the NH₃ produced was quantified by the Berthelot reaction after a complete polarization curve was measured over 9 hours. A maximum value of 9% was observed at 50°C and 25% RH.

5.3.1. Influence of temperature and relative humidity

Additional current voltage curves were recorded at 25% RH with varying temperature from 30°C to 70°C. The production rates increased with temperature up to 60°C.

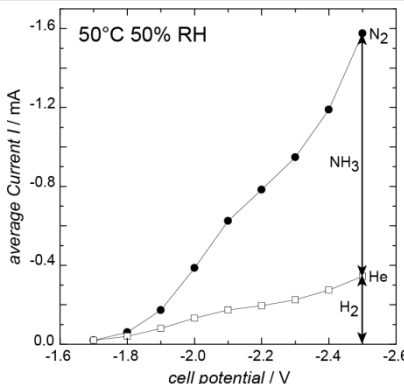


Figure 5.4: Determination of a corrected charge C_{corr} to calculate a NH_3 specific current efficiency.

However, the difference in the production rates between 50 and 60°C was negligible, but the CE_{NH_3} was approximately 3.5 times higher at 50°C. To prove the highest catalyst activity for NH_3 synthesis at 50°C, also reference measurements with He were conducted at 25% relative humidity. In the temperature range from 30 to 70°C, the measured current of a complete current voltage curve was decreasing with increasing temperature up to 50°C. Beyond 50°C, the current increased again. It is assumed that the adsorption of hydrogen atoms on the cathodic catalyst surface is limited in the applied reactor and MEA system at 50°C and a relative humidity below 50%. As indicated by Skúlason et al. the surface of the applied Ti catalyst will rather be covered with nitrogen atoms than hydrogen atoms. According to the achieved results, the adsorption of nitrogen atoms is even more preferred at 50°C and a relative humidity below 50%. Thus the corresponding production rates and current efficiencies are increased.

The following experiments were conducted at 50°C. To precisely quantify the NH_3 -specific production rates, hour-long chronoamperometry (CA) measurements were conducted at a constant reactor temperature of 50°C and 7.5, 15 and 25% RH. For potentials of -1.8 to -2.3 V, the achieved production rates are shown in Figure 5.5. At low voltages and high humidity, the current reactor system and the MEA architecture caused instabilities in the process behavior and required optimization, as has been observed in fuel cell systems for the past twenty years.

For 7.5 and 15% RH, approximately constant production rates were observed between cell potentials of -1.9 and -2.2 V. However, at 15% RH, the values were approximately 10 times higher at an average of $11.5 \times 10^{-12} \text{ mol s}^{-1} \text{ cm}^{-2}$. At 7.5% RH, the system was at its lower operating limit. At these operating conditions, membrane dry-out and fluctuations in the H_2O supply of the liquid flow meter could occur. At 25% RH, the system was unstable, and in the optimal potential range of -1.9 to -2.2 V, no constant production rates were obtained. The achieved CE_{NH_3} for the potential range at -1.8 to -2.3 V confirmed this observation, see Table 5.3. The most stable and highest CE_{NH_3} were achieved for a RH of 15% and cell potentials of -1.9 to -2.2 V. The CE_{NH_3} for 15% RH were very stable in the potential range from -1.9 to -2.2 V, and the same production rate of $12 \times 10^{-12} \text{ mol s}^{-1} \text{ cm}^{-2}$ was achieved.

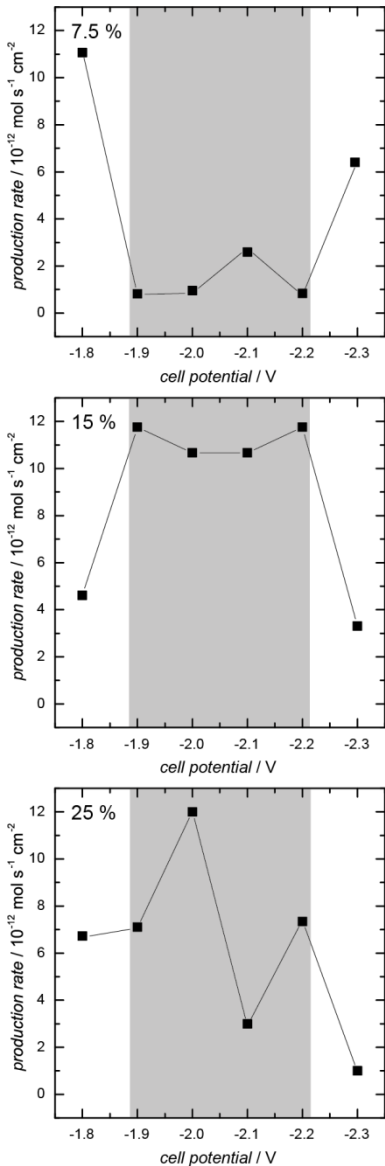


Figure 5.5: Production rates determined from Berthelot reactions after 1 hour chronoamperometry at 7.5, 15 and 25% RH at 50°C

Table 5.3 NH ₃ specific current efficiencies in % and the ratio for the measured C _{N2} and C _{He} after 1 hour chronoamperometry at 7.5, 15 and 25% RH at 50°C						
Potential [V]	Relative humidity [%]					
	CE _{NH₃}	7.5 C _{N2} /C _{He}	15 C _{N2} /C _{He}	25 C _{N2} /C _{He}	CE _{NH₃}	C _{N2} /C _{He}
-1.9	6.4	2.2	20.5	4.1	5.9	4.9
-2.0	8.5	1.8	16.3	2.9	7.9	3.4
-2.1	18.3	2.0	17.5	2.7	3.0	2.3
-2.2	8.8	1.5	27.5	2.1	18.3	1.5
-2.3	34.0	2.1	9.8	1.9	0.6	2.9

The CE_{NH₃} at -2.2 V was the highest at 27.5% for a power density of 0.05 mW cm⁻². The ratio of the integral charges C_{N2} to C_{He} was greater than 1, which indicated that more NH₃ was produced than H₂. Overall, the optimal process conditions were at 50°C and 15% RH at an applied potential range of -1.9 to -2.2 V. The highest production rate and the CE_{NH₃} were observed in this potential range during CA measurements. However, membrane dry-out at a RH below 25% has to be considered for future long-term stability tests.

5.4. Comparison of Ti, Fe and Ru as cathodic catalyst

Additionally to the experiments conducted with Ti, also Fe und Ru were investigated as cathodic catalysts in the ecMR. The measurement methods and procedures applied were the same as discussed in Section 5.2.

The Fe felt is similar to the Ti felt commercially available from the company Bekaert. The specifications are equally to those of the Ti felt, see Sections 4.5.3 and 4.6.

Since Ru is expensive, no bulk material was used as electrode material. Instead galvanic coatings of Ru were applied on particularly prepared Ti felts, compare Chapter 2. First the coating process was up-scaled from 1.5 x 1.5 cm² samples to samples with a diameter of 50 mm to be used in the ecMR. The ratio of the two geometric surface areas is 0.1145 and the ratio of the average mass increase for both samples is 0.1147. For the smaller samples the standard deviation was 5.8% with respect to the mass increase, while it was 7.1% for the samples with 50 mm diameter. Based on these numbers one can assume a successful plating also of larger electrodes.

The membrane electrode assemblies comprising Fe and Ru as cathodic catalyst were prepared in the same way as MEAs comprising Ti, see Section 4.6. When Ru was used as cathodic catalyst, the pressure for the hot pressing of the MEA was reduced to 6.1 kN cm⁻². Due to the etching of the Ti felt before the plating process of Ru, the fiber diameter and thus the thickness of the whole felt was reduced. To prevent a shortcut after pressing, the pressure was reduced. The anodic catalyst was an IrMMO felt in all cases.

For the comparison of Ti, Fe and Ru based MEAs, first the maximum current values measured in current voltage curves and then the achieved production rates and current efficiencies are

considered. Table 5.4 gives the maximum current values in mA measured at 30, 50 and 70°C at three different relative humidities of 25, 50 and 95%.

Temp [°C]	RH [%]	Maximum current I [mA]			Ratio maximum currents [-]		
		Ti	Fe	Ru	Ti / Fe	Ti / Ru	Fe / Ru
30	25	-5.0	-0.9	-3.0	5.6	1.7	0.3
	50	-12.0	-2.1	-21.3	5.7	0.6	0.1
	95	-30.0	-3.9	-8.6	7.7	3.5	0.5
50	25	-0.2	-0.02	-1.1	10.0	0.2	0.02
	50	-1.6	-0.2	-0.2	8.0	8.0	1.0
	95	-100.0	-22.0	-153.9	4.5	0.7	0.1
70	25	-0.8	-0.02	-40.9	40.0	0.02	0.0005
	50	-60.0	-12.0	-89.0	5.0	0.7	0.1
	95	-150.0	-43.0	-233.9	3.5	0.6	0.2

Similar to the results obtained for Ti, the current values for Fe and Ru also increased with increasing relative humidity. The currents measured for Ti and Ru are in the same order of magnitude of up to -233.9 mA, while the current values measured for Fe are around one order of magnitude smaller. The measured current is a benchmark for the performance of the whole system. Out of 9 cases, for Ru the highest currents were measured six times and for Ti three times. Consequently, Ru should also show the best numbers for the production rate and the current efficiency. However, high current values do not necessarily mean high production rates and current efficiencies for NH₃ as well.

For Ti lower current values were measured at 50°C and 25 and 50% RH compared to 30°C at the same relative humidity values. Interestingly, this phenomenon was also observed for Fe and Ru. A possible explanation could be a reduced activity of the applied IrMMO catalyst at these reaction conditions. However, there are still enough H⁺ ions produced at the anode for a sufficient NH₃ synthesis at the cathode. All catalysts showed instabilities at higher temperature and higher relative humidity. Thus temperatures above 50°C are not favorable for the current MEA and reactor system, independently from the applied cathodic catalyst. Furthermore, for all cathodic catalysts, instabilities occurred at 50°C and 95% RH.

Table 5.5 shows the achieved production rates for Ti, Fe and Ru at the investigated process conditions. As assumed before, Ru shows the best results for the production rates achieved in the ecMR. Only at 50°C and 50% RH, Ti shows an around 14 times higher production rate than Ru. At 30°C and 95% RH the production rate of Ti is 6 times higher, but high RH can cause instabilities in the system. The production rates for Fe are much smaller compared to Ti and Ru. At 30°C and higher relative humidity even negative production rates were measured. For Ti the production rate is increasing with increasing RH both for 30 and 50°C. Interestingly, at 50°C the production rate is smaller at 50% RH compared to 25% RH for Ru. Up to now, Ti and Ru are both promising catalysts for the electrochemical NH₃ in an ecMR.

Table 5.5 Achieved production rates for Ti, Fe and Ru at the investigated process conditions

Temp [°C]	RH [%]	Production rate [10 ⁻¹² mol s ⁻¹ cm ⁻²]		
		Ti	Fe	Ru
30	25	0.7	0.3	3.9
	50	2.7	-0.03	5.0
	95	53.0	-0.2	8.0
50	25	2.5	0.3	3.6
	50	4.1	2.2	0.3

To further narrow down the optimal catalyst and process conditions, the third parameter current efficiency is considered. Table 5.6 shows the achieved current efficiencies for the investigated catalysts.

Table 5.6 Achieved current efficiencies for Ti, Fe and Ru at the investigated process conditions

Temp [°C]	RH [%]	NH ₃ specific CE [%]		
		Ti	Fe	Ru
30	25	0.1	0.1	0.5
	50	0.2	-	0.2
	95	2.1	-	0.6
50	25	9.0	218	0.6
	50	2.3	1.6	5.0

Contrary to the achieved production rates, Ti shows better results for the achieved current efficiencies. However, at 30°C and 25% RH the current efficiency for Ru is three to four times higher than for Ti and Fe. With increasing RH, the achieved current efficiencies for Ti increased, while they decreased or just slightly increased for Ru. At 30°C Ru seems to be the better catalyst with respect to the current efficiency. At 50°C the results obtained for Ti are much better than for Ru. At 25% RH the achieved current efficiency for Ti is 15 times higher than for Ru. At 50°C and 50% RH Ru shows double the current efficiency of Ti. The results obtained for Fe were either small compared to Ti and Ru or no current efficiency was determined, since the production rates were negative. At 50°C and 25% RH an unrealistic current efficiency of 218% was determined. The current measured for these parameters was small (compare Table 5.4). Since the production rate was small as well (compare Table 5.5), the high current efficiency was the result of two measurement errors linked to each other.

At this early stage of research, high current efficiencies are more favorable than high production rates. For all investigated catalysts, 50°C is thus the temperature of choice. Similar to the experiments described in Section 5.3.1, further chronoamperometry experiments at 50°C and different relative humidity values were performed for Fe and Ru as well to find the best process

5 Electrochemical NH₃ synthesis in an ecMR

conditions. Table 5.7 summarizes the optimal process parameters and the achieved results for 1 hour experiments.

Catalyst	Temp	RH	Potential	Average current	Production rate	NH ₃ specific CE
	[°C]	[%]	[V]	[mA]	[10 ⁻¹¹ mol s ⁻¹ cm ⁻²]	[%]
Ti	50	15	-2.2	-0.46	1.2	27.5
Fe	50	30	-2.5	-0.006	1.1	432.0
Ru	50	50	-2.2	-0.57	2.2	50.3

As assumed beforehand, Ru showed the best results both for production rate and for current efficiency. For all catalysts a relative humidity of 50% or less was preferred. Interestingly, the optimal applied potential for Ru and Ti was the same and for Fe at least in the same range. Apparently, the Ti support material for the Ru coated felts had a pronounced impact on the results achieved for Ru. Only considering the average current values would lead to the conclusion that Fe is a poor catalyst. However, the achieved production rate was more or less the same compared to Ti. Due to the low current measured for Fe, the unrealistic high current efficiency of 432% was caused by measurement errors.

In summary, Ti is the best catalyst tested so far for low relative humidity conditions and Ru is the catalyst of choice for high relative humidity conditions. However, low relative humidity can cause dry out of the membrane and thus performance losses of the whole system during long term tests. From an economic point of view it has to be considered, that the application of Ru is more expensive and that an additional processing step is necessary to prepare the Ru cathode. For future experiments, the influence of the amount of Ru electroplated on Ti needs to be investigated. A mixed metal catalyst comprising both Ti and Ru can be favorable, since Ti favors the adsorption of nitrogen atoms, while Ru supports the adsorption of hydrogen atoms (compare Section 2.2). Finding the optimal ratio between Ti and Ru for an optimized cathodic catalyst can help to further increase the current efficiency and to achieve higher production rates for NH₃.

5.5. Conclusion

The presented results describe a successful electrochemical N₂ reduction to NH₃ in an ecMR. Titanium and Ru were shown as potential cathodic catalysts for a high NH₃-specific CE. However, the HER remains the dominant parallel reaction. This work encourages further research on catalysts for the electrochemical synthesis of NH₃ to make the process more efficient and effective with long-term stability. Points of interest for a performance improvement could be to increase the specific surface area of the catalyst, to further narrow down the optimal process parameters or to use an alternative membrane such as polybenzimidazole (PBI) membranes, which show H⁺ conductivity without the need of H₂O for the transport mechanism. When using PBI membranes, the reactor design needs to be changed, since the reactor material Ti is not corrosion resistant towards phosphoric acid required for the pretreatment of such membranes. Furthermore the catalyst material itself can be optimized or different

morphologies of the applied Ti and Ru catalysts or even a mixed metal catalyst have to be tested to increase the triple phase boundary between catalyst, membrane and the gaseous reactants. A research direction toward new N₂ reduction catalysts could result in the development of a technically viable ecMR based on this work.

5

6. Simulation and Modelling in Aspen Custom Modeler and Aspen+

Parts of this chapter have been published in: Physical Chemistry Chemical Physics

Title: *Towards a carbon independent and CO₂-free electrochemical membrane process for NH₃ synthesis*

DOI: 10.1039/c4cp00173g

Abstract

Ammonia is exclusively synthesized by the Haber process starting from precious carbon resources such as coal or CH₄. With H₂O, H₂ is produced and with N₂, NH₃ can be synthesized at high pressures and temperatures. Regrettably, the carbon is not incorporated into NH₃ but emitted as CO₂. Valuable carbon sources are consumed which could be used otherwise when carbon sources become scarce. An alternative process concept using an electrochemical membrane reactor (ecMR) is suggested. A complete synthesis process with N₂ production and downstream product separation is presented and evaluated in a multi-scale model to quantify its energy consumption. A new micro-scale ecMR model integrates mass, species, heat and energy balances with electrochemical conversions allowing further integration into a macro-scale process flow sheet. For the anodic oxidation reaction H₂O was chosen as an ubiquitous H₂ source. Nitrogen was obtained by air separation which combines with H⁺ from H₂O to NH₃ using a hypothetical catalyst recently suggested from DFT calculations. The energy demand of the complete electrochemical process is up to 20% lower than the Haber process using coal as H₂ source. For the case of natural gas, the ecMR process is not competitive under today's energy and resource conditions. In future however, the electrochemical NH₃ synthesis might be the technology-of-choice when coal is easily accessible over natural gas or limited carbon sources have to be used otherwise but for the synthesis of the carbon free product NH₃.

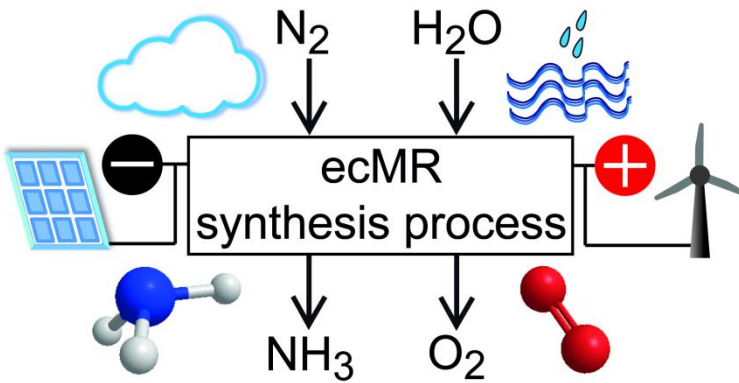


Figure 6.1: Graphical abstract of Chapter 6: A new NH₃ synthesis process using an electrochemical membrane reactor (ecMR) including N₂ production and product separation is modelled in Aspen+.

6.1. Introduction

The significance of NH₃ is self-evident: with 1 to 3% of the global energy consumption the NH₃ synthesis is one of the largest energy users in industry [12]. This is related to the energy intensive H₂ production, N₂ purification and the energy intensive process conditions to reach an acceptable conversion rate. The electrochemical NH₃ synthesis is an environmentally friendly alternative to the state-of-the-art Haber process for NH₃ synthesis. Here, a multi-scale simulation model approach comprising two scales: (1) a microscopic model represents the ecMR modeled using Aspen Custom Modeler (ACM) is presented. Mass and heat transport, species balances including chemical reactions and energy balances are solved. This complex ACM model can be integrated into (2) an overall macroscopic model using Aspen+ where all other unit operations are combined. A complete synthesis process with N₂ production and product separation downstream to the ecMR is then investigated. The present work aims to quantify whether such an electrochemical membrane based process is energetically favorable or competitive as compared to the Haber process. The approach as well as the results serve as a role model to investigate future chemical process scenarios that go beyond a fossil based society.

6.2. Proposed process

The entire synthesis process as shown in Figure 6.2 was investigated using the process simulation program Aspen+.

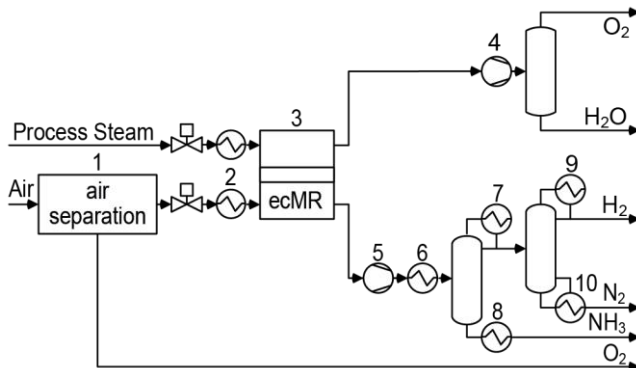


Figure 6.2: Flow diagram of the complete process modelled with Aspen Custom Modeler (ACM) including N₂ production by cryogenic air separation and product separation downstream to the ecMR.

The ecMR is a new user block modeled separately in ACM. Details of the complete set of energy and mass balances are described in Section 6.7. The process model can be divided into

three sections, namely feed pre-treatment, ecMR, and the anodic and cathodic product separation.

The first section is the feed pre-treatment. At the cathodic side this includes a cryogenic air separation which is not further optimized. The specific energy consumption is taken from literature [46]. The air separation is necessary to remove O₂ which otherwise would react with H⁺ to H₂O and hence reduce the current efficiency. The rate determining step of the overall reaction in the ecMR is most likely one of the cathodic reaction steps. Commonly N₂ leaves the cryogenic air separation unit at a pressure of 1.3 to 1.5 bar. At the cathode the amount of gas molecules increases during the reaction. Thus the N₂ pressure is reduced to atmospheric pressure before entering the reactor. To save costs the anodic feed is assumed to be conventional process steam. Depending on the steam available a pressure regulator has to be used and the steam has to be cooled. The ecMR of the process will be operated at 105°C, also compare Table 6.2.

The second section is the ecMR with the MEA as its core. The membrane acts as a gas diffusion and electron barrier to separate the anodic and cathodic half-cell. In each half-cell a serpentine flow channel is assumed to distribute the reactants on the catalyst layer of the MEA. An external power source delivers electrical current to the ecMR.

The third section is the product separation from unconverted feed gas to achieve a purity of 99.5% for each product. Oxygen, which is produced at the anode, is a by-product and can be sold to enhance the cost efficiency. Preliminary investigations have shown that simple condensation of H₂O in the anodic product stream is sufficient to obtain these purities. The cathodic product stream consists of NH₃, unconverted N₂ and H₂, which might be formed as side product at the cathode, depending on the current efficiency of the ecMR. In the Haber process NH₃ is liquefied in a multi-stage condenser system. Since the product stream leaves the reactor at high pressure, H₂O can be used to liquefy NH₃ at room temperature. In general no further purification of NH₃ is necessary [12]. However, the ecMR is operated at lower pressure. Thus the product stream has to be pressurized and cooled in the separation unit. As a reference case two distillation columns are implemented in Aspen+ for the separation of the cathodic product stream. In the first column NH₃ is separated from H₂ and N₂. Subsequently N₂ and H₂ are separated in the second column. Although the energy demand of the product separation is significantly less compared to the ecMR, downstream processes and energy integration can be anticipated to reduce the overall energy demand, compare Chapter 7. The results obtained here can serve as an upper estimate for the complete synthesis process and can give a first estimation of the energy consumption for a comparison with other processes.

6

6.3. Proposed ecMR

The modeled ecMR shown in Figure 6.3 comprises seven functional elements. The core is a polymeric membrane, which is laminated between the anodic and cathodic gas diffusion electrode (GDE). On top of these two electrodes the active catalyst layers (ACL) are located. Finally the two flow channels act as gas distributor and as electron distributor and collector at the cathode and the anode. Each half cell of the reactor can be exposed to different gases [201]. The electrocatalytic reactions take place at the triple phase boundary (TPB) between fluid, membrane and one of the electrodes.

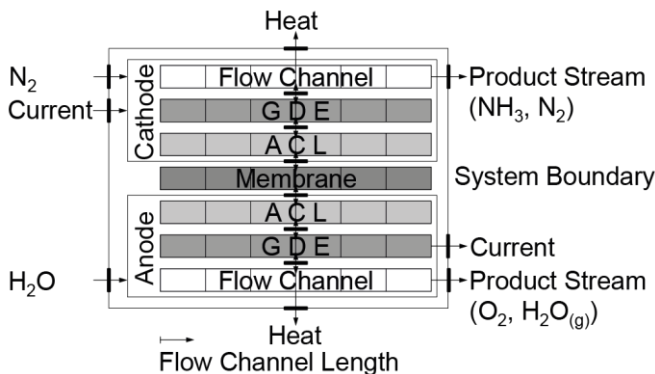


Figure 6.3: Main elements of the modeled ecMR and model discretization along the flow channel length in single elements (vertical dashed lines). Mass, heat and electron transfer to the surrounding.

A high catalytic surface area is required for an efficient process. The reactants are fed at the inlet of the reactor and flow through the flow channel where they get in contact with the GDE. The reactants diffuse through the electrodes to the ACL where the reactions take place. The products diffuse back to the flow channel and leave the reactor at the outlet.

6.3.1. Model structure of the ecMR

The model structure of the ecMR is illustrated in Figure 6.3 as well. Heat is transferred to the ambient air through the outer walls of the cell. The electrons are supplied to and removed from the GDE. The cathode and anode consist of the flow channel, the GDE and the ACL. The flow channel and the GDE are connected through a boundary layer. Finally, a TPB layer connects the membrane with the ACL.

The heat and mass balance are calculated one dimensional along the flow channels. The concentrations in orthogonal direction to the flow channel, i.e. within the GDE and the ACL are calculated by linear mass transport relations. For this model the only assumed anodic reaction is the oxidation of H_2O to O_2 and protons. The reduction of N_2 to NH_3 and the formation of H_2 are the only cathodic reactions considered. Water crossover was neglected to keep the model simple. The ratio γ of the H_2 and NH_3 formation rate is given by Equation (6.1).

$$\gamma = \frac{\dot{n}_{H_2}}{\dot{n}_{NH_3}} \quad (6.1)$$

For the H_2 formation two electrons are required, while the NH_3 synthesis consumes three electrons. Hence, the current efficiency β of the cathode can be calculated as:

$$\beta = \frac{1}{1 + \frac{2}{3}\gamma} \quad (6.2)$$

The model is implemented in ACM and consists of a set of parameters, variables and equations, which describe the physical and thermodynamically behavior. Therefore the flow channel is discretized along its length and is divided in incremental elements of the same length, as illustrated in Figure 6.3 by the vertical dashed lines. Sufficient discretization steps were applied to achieve independency from the discretization. For the numerical solution ACM calculates the variables for each element and the trend of each variable can then be examined along the domain. The proposed ecMR is modeled for a production capacity of $\sim 1500 \text{ t d}^{-1}$, i.e. $20.3 \text{ m}^2 \text{ t}_{\text{NH}_3}^{-1}$ of flown through MEA area are needed.

6.4. Proposed catalyst

The H^+ for the cathodic reaction are delivered by an oxygen evolution reaction (OER) at the anode, see also Sections 4.1 and 4.5.1. The catalysts with the highest activity and the lowest overpotential for the OER are RuO_2 and IrO_2 [202]. Many reaction mechanisms have been suggested and the electrochemical oxide path as well as the oxide path are widely accepted to occur for these catalysts [203]. For the N_2 reduction at the cathode four different reaction mechanisms are possible, namely both an associative and dissociative Tafel and Heyrovsky type mechanism [66], see also Section 1.5. Theoretical considerations showed that for most of the transition metals the dissociative mechanism occurs at lower voltages than the associative one. Furthermore, the activation barrier for the N_2 adsorption is relatively high for late transition metals [66].

The principle of Sabatier has widely been applied for the electrochemical H_2 production resulting in the so-called Volcano curve [204]. It allows estimating the activity of different catalysts [205]. Using Volcano plots Trasatti showed that the exchange current density j_0 of the hydrogen reaction on transition metals depends on the Gibbs free energy of adsorption of hydrogen atoms on the metal surface $\Delta G(\text{M}-\text{H})$ [206,207]:

$$\ln j_0 \sim \frac{\alpha \Delta G(\text{M} - \text{H})}{k_B T} \quad (6.3)$$

Recently, Skúlason et al. evaluated theoretically possible transition metals as catalysts for the electrochemical NH_3 synthesis [66]. Using the density functional theory (DFT), they calculated the Gibbs free energy profile for the reduction of N_2 . By assuming that the activation energy scales with the free energy difference in each elementary step, the catalytic activity has been investigated. The potential was calculated at which $-\Delta G$ for each reaction step is smaller than or equal to zero to achieve significant reaction rates [66]. The resulting Volcano plot is given in Figure 2.2. The metals Fe, Rh and Mo have the highest activity for the electrochemical NH_3 synthesis.

For the simulation Ti electrodes are considered because of their commercial availability and low price. Here an alternative synthesis process for NH₃ at mild reaction conditions, i.e. temperatures around 100°C and ambient pressure is investigated. Kordali et al. used a Ru cathode to synthesize NH₃ at ~90°C and 1 atm [111]. These reaction conditions are quite similar to the desired operating conditions of the proposed ecMR. The electrolytic cell of Kordali et al. is divided in two half-cells by placing a Nafion membrane between the anode and the cathode. Nitrogen was fed to the cathode, while an aqueous KOH solution was used as anodic electrolyte. At the anode an oxygen evolution reaction takes place. By applying a potential of -0.96 V a current density j of 1.2×10^{-6} A cm⁻² was obtained at an overpotential of 0.08 V. The conventional Butler-Volmer equation can be used to calculate the current exchange density j_0 of the Ru electrode. For the given conditions j_0 equals 5.5×10^{-10} A cm⁻².

The reaction mechanism for the N₂ reduction is assumed to be similar to the HER, namely a Heyrovsky- or Tafel-type reaction [66]. Thus, the dependencies for the hydrogen reaction, i.e. the Volcano curve and Equation (6.3) might also be valid for the N₂ reduction. According to the Volcano curve the following equation is valid:

$$\frac{\partial(\log j_0)}{\partial(G(M-H))} = r \quad (6.4)$$

Since the NH₃ synthesis follows the same reaction mechanism, the same slope r is assumed to be representative for the N₂ reduction. The dependency of j_0 on the adsorption energy and the results of Kordali et al. have been combined to estimate j_0 for Ti.

$$\log j_{0,Ti} = r\Delta(\Delta G(Ti - N) - \Delta G(Ru - N)) + \log j_{0,Ru} \quad (6.5)$$

The NH₃ reaction rate increases with the applied current. However, a maximum for the reaction rate exists [96]. A further increase of the applied current does not result in a higher NH₃ reaction rate [108]. The electrode material and its catalytic activity have a significant influence on the reaction rate. Since some catalysts rather form H₂ than NH₃ the current efficiency depends on the catalyst material as well [96]. Based on the positive results of the present study, we motivate more synthetic effort to tailor the catalysts to higher selectivity and productivity making the ecMR concept even more attractive. The cell potential has a similar impact on the NH₃ formation as the applied current. The reaction rate increases with the cell potential and a maximum exists above which the reaction rate is independent of the applied voltage [103]. For both low and high temperature applications the NH₃ reaction rate increases with temperature due to a higher protonic conductivity of the electrolytes [96]. However, an optimal temperature exists above which NH₃ decomposes and the process efficiency gets reduced. For low temperature processes using polymer electrolytes, the ideal temperature depends on the H₂O content of the electrolyte and thus on the protonic conductivity.

6.5. Simulation results for the ecMR

The electrochemical membrane reactor (ecMR) is an user block modeled in Aspen Custom Modeler (ACM). Details of the complete set of energy and mass balances are described in Section 6.7.

6.5.1. Reactor and process parameters

Important parameters such as the applied voltage or feed flow are changed within a specific range to find the optimal operating conditions of the ecMR. Reference values and the variation range are defined in Table 6.1.

Table 6.1 Reference parameters for the ecMR model				
Parameter	Symbol	Value	Band	Unit
Current density	j	11	2 - 18	kA m ⁻²
Cell potential	U_{cell}	2.2	2 - 2.325	V
Cathodic exchange current density	$j_{0,c}$	10^{-18}	$10^{-35} - 10^0$	A m ⁻²
Anodic feed flow rate	\dot{V}_A	180	120 - 240	ml min ⁻¹
Cathodic feed flow rate	\dot{V}_C	60	40 - 80	ml min ⁻¹
Current efficiency	β	1.0	0.8 - 1.0	-

The overpotential and thus the cell voltage U_{cell} are mainly influenced by the current density. Conventional PEM electrolyzer for H₂ production work at $j \approx 10 \text{ kA m}^{-2}$ [208]. A current density in this range is assumed to be optimal for the NH₃ synthesis as well, since the same electrolyte is used and the anodic reactions are equivalent. At the reference cell voltage of 2.2 V the current density is 11 kA m⁻². The lower bound for the cell voltage is 2 V since at lower values j is almost 0 kA m⁻² and a reasonable operation of the reactor is not possible. For the investigated ecMR almost all of the reactants are converted at a cell voltage of 2.325 V and a higher cell voltage would lower the energy efficiency of the process, also compare Figure 6.7.

The exchange current density for a Ti electrode has been estimated by combining theoretical calculations with experimental results for other electrodes. This theoretical consideration might not necessarily display the reality correctly. Accordingly, a wide band for j_0 has been examined to investigate its influence on the process performance.

The anodic and cathodic feed flow mainly influences the space-time-yield as well as the conversion rate. The conversion rate itself influences the energy demand for the separation units in the proposed process. The reference value for the anodic flow rate is three times higher than the cathodic one, since three times more H₂O than N₂ are converted to form NH₃.

At the chosen reference flow rates a conversion rate of ~50% is obtained. The upper bounds for the flow rates correlate to low conversion rates of ~35% for the given reference scenario. The lower bound for the flow rate corresponds to a conversion rate of ~80%. A further decrease of the flow rate would result in lower energy consumption for the separation units. The current efficiency β mainly influences the energy demand of the ecMR. For $\beta = 1$ no undesired parallel

reactions such as H₂ formation are considered. At $\beta = 0.8$ the total energy demand of the suggested process is higher than for a coal based Haber process. Thus in the variation range of 0.8 - 1.0 a comparison with the Haber process is possible. Further parameters and important constants of the reactor model are listed in Table 6.2:

Parameter	Symbol	Value	Unit
Anodic equilibrium potential ^a	E _{eq,A}	1.17	V
Anodic exchange current density ^b	j _{0,A}	10 ³	A m ⁻²
Anodic charge transfer coefficient ^b	α_A	0.5	-
Number of transferred electrons anode ^b	v _{e,A}	2	-
Cathodic equilibrium potential ^a	E _{eq,C}	-0.03	V
Cathodic charge transfer coefficient ^c	α_C	0.5	-
Number of transferred electrons cathode ^b	v _{e,C}	6	-
Membrane conductivity ^d	κ	17	A (Vm ²) ⁻¹
Membrane thickness ^d	d _M	100	μm
GDE thickness ^c	d _{GDE}	200	μm
Ratio of catalytic surface area ^a	a _{cs}	5.3	m ² m ⁻²
Length flow channel ^c	l	0.9	m
Reactor temperature ^c	T ⁰	105	°C
Reactor pressure ^c	p	1	atm

^a calculated, ^b taken from [209], ^c assumed, ^d taken from [210]

6.5.2. Performance indicators

For an energetic comparison of the ecMR with the Haber process three different performance indicators are applied.

The first indicator is the specific energy consumption, which gives the energy consumed per ton synthesized product:

$$E_{spec} = \frac{U_{cell} v_e F}{\beta M_p v_p} \quad (6.6)$$

where M_P is the molar mass and v_p the stoichiometric coefficient of the product.

The second indicator is the conversion rate of the reactants:

$$\zeta_{i,A/C} = \frac{\frac{\dot{n}_{A,C,i}}{\bar{C}_{A,i}} - \frac{\dot{n}_{A,C,\omega,i}}{\bar{C}_{A,i}}}{\frac{\dot{n}_{A,C,i}}{\bar{C}_{A,i}}} \quad (6.7)$$

where $\dot{n}_{A/C,i}$ is the molar flow rate of the reactant i at the inlet of the reactor and $\dot{n}_{A/C,\omega,i}$ at the outlet.

The third indicator is the energy efficiency, which is the ratio between the enthalpy of reaction and the consumed energy for the synthesis:

$$\eta = \frac{\Delta_R H}{U_{cell} v_e F} \quad (6.8)$$

6.5.3. System performance of the ecMR

Table 6.3 summarizes the simulation results for the performance indicators for the reference case.

Parameter	Symbol	Value	Unit
Current density	j	11.00	kA m ⁻²
Cell potential	U	2.20	V
Specific energy consumption	E _{spec}	11.41	MWh t ⁻¹
Energy efficiency	η	0.47	-
Conversion rate H ₂ O	ζ_{H_2O}	0.53	-
Conversion rate N ₂	ζ_{N_2}	0.53	-
Mole fraction H ₂ O in anodic product stream	y _{A,H₂O}	0.64	-
Mole fraction O ₂ in anodic product stream	y _{A,O₂}	0.36	-
Mole fraction N ₂ in cathodic product stream	y _{A,N₂}	0.69	-
Mole fraction NH ₃ in cathodic product stream	y _{A,NH₃}	0.31	-

The evolution of the current density along the flow channel for different cell voltages is given in Figure 6.4:

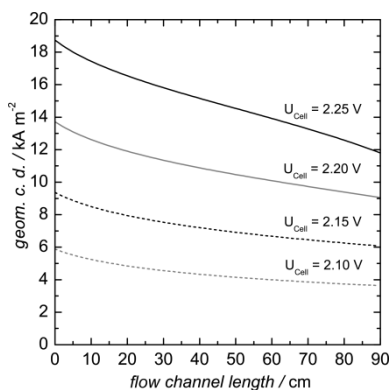


Figure 6.4: Evolution of the current density along the flow channel length for different cell voltages

The current density increases with increasing cell voltage. This is reasonable, as a higher cell voltage results in higher overpotentials for the electrochemical reactions. The current density decreases along the flow channel length, which can be explained considering the Gibbs free energy of the overall cell reaction $\Delta_R G$:

$$\Delta_R G = \Delta_R G^0 + RT \ln \left(\frac{\left(\frac{p_{O_2}}{p^0} \right)^{\frac{3}{2}} \left(\frac{p_{NH_3}}{p^0} \right)^2}{\left(\frac{p_{H_2O}}{p^0} \right)^3 \left(\frac{p_{N_2}}{p^0} \right)} \right) \quad (6.9)$$

The concentration and the partial pressure of the reactants decrease along the flow channel, whereas the partial pressure of the products increases. Consequently $\Delta_R G$ increases and therefore the equilibrium potential of the cell increases as well. Otherwise the overpotential for the charge transfer has to decrease if the equilibrium potential decreases. This results in a lower current density along the flow channel length. This effect is more severe if a high cell voltage is applied. As the reaction rate increases with the cell voltage the conversion rate rises as well. Thus higher values for the second term on the right side of Equation (6.9) occur.

The conversion rate of the reactants for the investigated ecMR is shown in Figure 6.5.

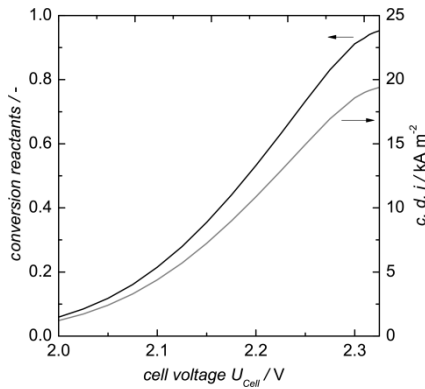


Figure 6.5: Influence of the cell voltage on the conversion rate and the average current density of the ecMR

At low cell voltages the conversion rate increases exponentially. The current density increases exponentially with the cell potential according to the Butler-Volmer equation. At higher cell voltages and thus higher current densities the effect of Equation (6.9) increases. Hence, j only increases linearly with the cell voltage. At very high cell voltages almost all of the reactants are converted and higher cell potentials cannot further increase the average current density and the conversion rate. Thus a minor dependency of the cell voltage on the average current density and conversion rate is observed at high cell potentials.

Figure 6.6 shows the evolution of the mole fractions along the flow channel.

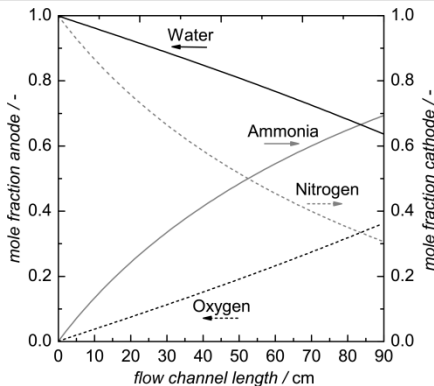


Figure 6.6: Evolution of the mole fraction in the anodic and cathodic flow channel

The slope of the mole fraction evolution decreases along the flow channel length due to the decreasing current density at the end of the reactor. Different mole fractions at the anode and at the cathode are obtained for the same conversion rates of H_2O vapor and N_2 . One reactant molecule forms two product molecules at the cathode, whereas two reactant molecules form only one product molecule at the anode.

The mole fractions at the outlets have main impact on the cost for the product separation. In Figure 6.7 the achieved mole fractions for different cell voltages are shown.

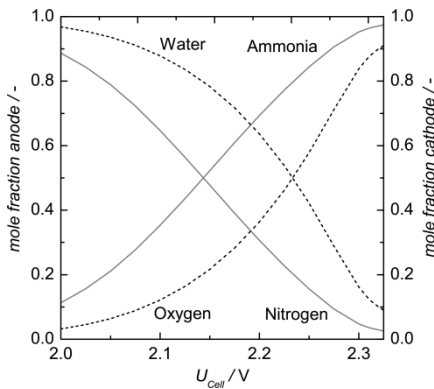


Figure 6.7: Mole fractions at the reactor outlets for different cell voltages

At the reference flow rates almost all of the reactants are converted at a cell voltage equal to or higher than 2.3 V.

The energy demand of the separation units are influenced by the volumetric feed flow rates at the anode and the cathode as well. At a fixed current density these parameters influence the

conversion rates and thus the mole fractions at the outlet of the reactor. Besides that, these parameters might influence the cell voltage which has to be applied to obtain the reference current density. To investigate this effect, one of the volumetric flow rates has been held constant whereas the other one has been varied. The results are given in Figure 6.8.

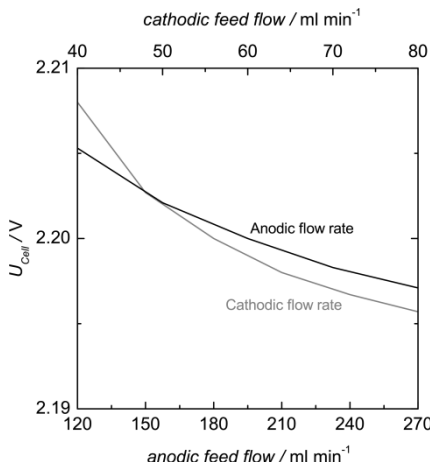


Figure 6.8: Cell potential which has to be applied to obtain the reference current density at different anodic and cathodic feed flow rates

The flow rate has only a minor influence on the cell voltage. Only at very low flow rates a higher cell voltage has to be applied since almost all of the reactants are converted. Thus the energy demand of the complete synthesis process can be reduced by decreasing the flow rate because at low flow rates very pure products are obtained. In Figure 6.4 it was shown that the current density decreases along the flow channel, although the influence of the feed flow rate and thus of the conversion rate on the cell voltage is minor, see also Figure 6.7. To explain this, the influence of the mole fraction is considered. The difference of the equilibrium potential between a situation where the partial pressure of the reactants is 99% of the total pressure and a situation where the partial pressure of the products is 99% of the total pressure is 0.16 V. Obviously the composition has only a small impact on the equilibrium potential. However, it can be deduced that the reduction of the overpotential for the charge transfer due to an increased equilibrium potential results in a higher decrease of the current density at higher overpotentials. Thus the decrease of the current density is higher at higher cell potentials, see also Figure 6.4. There are two possibilities to reduce the expenditure of the separation units: increase of the cell voltage or decrease of the flow rate. An increase of the cell voltage leads to higher operation costs whereas a lower flow rate decreases the space-time yield. A lower space-time yield generally increases the investment costs for the reactor. Hence, there will be a trade-off between the energy consumption for the separation units, the energy-consumption of the reactor and the investment costs.

The exchange current density has been estimated combining the theoretical calculations of Skúlason et al. and the experimental results of Kordali et al. for a Ru cathode [66,111]. However, the exchange current density obtained from this consideration might not be exact. The influence of this parameter on the process performance has been investigated as well, which is shown in Figure 6.9.

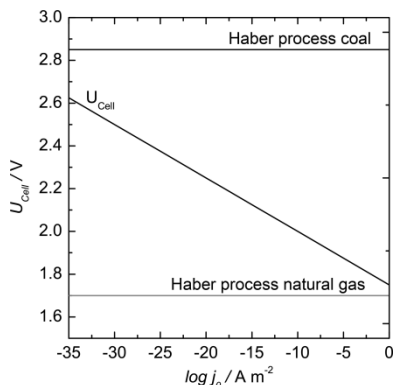


Figure 6.9: Cell voltage for different exchange current densities at a given current density. The horizontal lines represent the cell potential which can be applied so that the energy consumption of the ecMR equals different Haber processes

The cell voltage which has to be applied for a given current density of 11 kA m^{-2} is plotted against the logarithmic exchange current density of the cathodic reaction. A linear curve is obtained which is reasonable as the overpotential is a linear function of the logarithm of the exchange current density and of the logarithm of the current density, which has been held constant, as well. Equation (6.6) allows the calculation of the energy consumption for the ecMR. Based on this equation the cell voltage which can be applied to equal the energy consumption of the ecMR with the energy demand of conventional NH_3 synthesis plants can be determined. The cell voltages representing conventional Haber plants are given by two horizontal lines in Figure 6.9.

The upper one corresponds to the Haber process using coal as H_2 source, whereas the lower one belongs to the Haber process using natural gas. For this consideration neither the energy for the product separation nor for the feed pre-treatment are taken into account yet. However, even if the exchange current density for the cathodic reaction is very high, the electrochemical process cannot compete in terms of energy consumption with the natural gas based Haber process. But even at very low exchange current densities the energy consumption will be lower than for a Haber process using coal as feedstock for H_2 production.

To investigate potentials for the process improvement, the different potential drops within the reactor are plotted for different current densities in Figure 6.10.

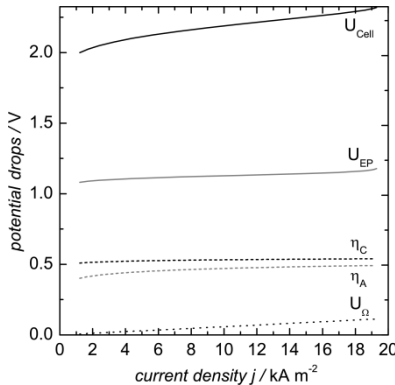


Figure 6.10: Cell voltage and overpotentials of the electrochemical membrane reactor for different current densities

The equilibrium potential is the main contributor to the cell voltage. This value cannot be changed as it is determined by thermodynamics. Further main contributors are the cathodic and anodic overpotentials to drive the charge transfers. The overpotential for the cathodic reaction is higher which relates to the low activity of the cathodic reaction and thus to the very low exchange current density. Hence, this gives the highest potential to improve the process performance. The overpotential at the anode is lower, but it is worthwhile to search for a better catalyst at the anode. The ohmic potential loss increases linear with the current densities. Thus for high current densities this contribution cannot be neglected.

At the cathode H₂ formation is a competing reaction for the NH₃ synthesis. So far a current efficiency of unity, which means that no H₂ is produced, was assumed because it is expected that on Ti electrodes mainly NH₃ is produced [66]. However, these assumptions are based on theoretical considerations taking the binding energy of N₂ and H₂ on the electrode surface into account. In this work the influence of the current efficiency on the specific energy consumption as well as on the composition of the product stream is investigated, see Figure 6.11.

The energy consumption per ton product in kWh t_{NH₃}⁻¹ can be calculated as following [64]:

$$E_{spec} = \frac{U_{cell} v_e}{3.6 \beta M_{NH_3} v_{NH_3}} \quad (6.10)$$

At a current efficiency of unity 10.4 MWh t_{NH₃}⁻¹ are consumed at the reference cell voltage. This value increases up to 13.0 MWh t_{NH₃}⁻¹ for a current efficiency of at least 80%. As mentioned before, there are no experimental results concerning the current efficiency available. However, it is expected that the current efficiency is relatively high because N₂ atoms bind more strongly than H₂ on the Ti surface. Hence, the electrode will mainly be covered by N₂ and NH₃ will be formed more probably [66]. Accordingly, a current efficiency of 80% seems to be reasonable.

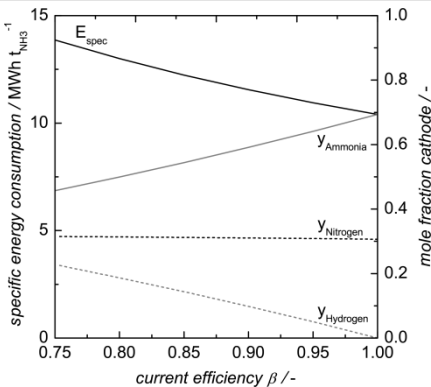


Figure 6.11: Influence of the current efficiency on the specific energy consumption and on the molar composition of the product stream at the cathode

A lower current efficiency does not only increase the specific energy consumption of the reactor, but also the separation is more complex and particularly the H₂/N₂ separation is energy intensive. For the investigated current efficiencies the molar H₂ fraction in the cathodic product stream varies between 0 and approximately 20%.

6.5.4. Process energetics

The multi-scale modeling presented above allows answering the question if the electrochemical membrane based process is energetically favorable or competitive as compared to the Haber process. To answer this question the discussed reference case and four different cases shown in Table 6.4 are considered.

Table 6.4 Five different case conditions to investigate the energy demand of the model process

Case	Explanation	U _{cell} [V]	Current efficiency [%]
1	reference case	2.20	1.0
2	high cell voltage	2.25	1.0
3	low cell voltage	2.15	1.0
4	medium current efficiency	2.20	0.9
5	low current efficiency	2.20	0.8

The influence of different parameters on the energy consumption of the model process is investigated. These cases have been chosen arbitrarily, however, they can indicate how different process parameters influence the energy consumption of the separation units. The energy consumption per ton produced NH₃ of the different process units as numbered in Figure 6.2 are listed in Table 6.5.

Process unit	Case 1	Case 2	Case 3	Case 4	Case 5
Cryogenic air separation (1)	0.08	0.08	0.08	0.08	0.08
Heat exchanger (2)	0.04	0.03	0.06	0.04	0.04
ecMR (3)	10.40	10.63	10.16	11.50	13.00
Compressor (4)	0.26	0.13	0.34	0.30	0.24
Compressor (5)	0.31	0.25	0.40	0.36	0.43
Heat exchanger (6)	0.07	0.06	0.11	0.09	0.11
Condenser (7)	0.14	0.06	0.36	0.26	0.35
Reboiler (8)	0.11	0.12	0.08	0.13	0.12
Condenser (9)	-	-	-	0.12	0.13
Reboiler (10)	-	-	-	0.03	0.03
Sum	11.41	11.36	12.60	12.93	14.55

With 11.36 MWh $t_{\text{NH}_3}^{-1}$ the lowest energy demand for the entire process is achieved in case 2. In comparison to cases 1 and 3 the total energy demand is lower, since the energy demand for the separation units is much lower. At lower cell voltages and fixed flow rates the conversion rate is lower and much more flow volume has to be separated per ton NH₃. Additionally, the ecMR has the by far highest contribution to the total energy demand for the process.

Table 6.6 compares the ecMR with the Haber process: the energy demand for the ecMR in case 2 is 3.46 MWh $t_{\text{NH}_3}^{-1}$ higher than for the Haber process using natural gas as H₂ source.

Table 6.6 Energy demand of different process alternatives in MWh $t_{\text{NH}_3}^{-1}$ *		
Haber natural gas	Haber coal	ecMR U _{cell} = 2.25V
7.92	13.47	11.36

* values for Haber are taken from [19]

However, if other H₂ sources such as coal are used the energy demand of the Haber process almost doubles [211] and the suggested ecMR scenario becomes energy-wise viable. A comparison between the energy demands for cases 4 and 5 and for the coal based Haber process leads to a minimum current efficiency for the ecMR of 87% to be competitive. Otherwise the ecMR process is even less efficient than the coal based Haber process.

Since the conceptual ecMR can be installed in decentralized small-scale plants, the electrical energy can be delivered from local renewable energy sources such as wind or hydro-power. Additionally the electrochemical synthesis has several other advantages, which are summarized in Table 6.7. The ecMR can be operated at lower temperatures and lower pressure and thus the investment costs might be lower. Besides that smaller and more flexible plants can be used. In comparison the conventional Haber plants just work efficiently at very high capacities. In addition, the Haber process uses valuable carbon-based feedstock such as natural gas, heavy hydrocarbons or coal, whereas the electrochemical process uses easily accessible process steam and air. Since H₂O is used as H⁺ source, no CO₂-emissions will occur due to H₂ production. The catalytic activity of the electrodes, which result in a higher j_0 and thus lower overpotential for the charge transfer, shows the highest potential for improvements.

Table 6.7 Advantages and disadvantages of Haber and electrochemical NH ₃ plants	
Haber process	ecMR
Advantages	
+ High energy efficiency if natural gas is used	+ Moderate operation conditions + Lower investment costs + Flexible plants + Cheap feed (air and process steam) + No CO ₂ emission from H ₂ production + High optimization potential
Disadvantages	
- Process intensive - High capacities required for high efficiency - Less potential for optimization - Expensive feed (hydrocarbons) - Low energy efficiency for other hydrocarbons than natural gas - Hydrocarbons reserves are limited	- Investment costs increase linearly - High energy demand

Additionally, the separation processes can be improved significantly, see also Chapter 7.

6.6. Conclusion

In this work an electrochemical membrane reactor (ecMR) for the electrochemical reduction of N₂ to NH₃ has been modelled in Aspen Custom Modeler. The model of the ecMR is a powerful tool for the investigation of the influence of different process parameters, such as the applied cell voltage, on the process performance. Furthermore, the model can be exported to Aspen+. This allows the simulation of an entire production process including feed pre-treatment and product separation.

To compare the energetics of this process with the conventional Haber process a possible complete synthesis plant has been investigated. Therefore the anodic and cathodic feed preparation and the product separation have been considered. The energy consumption of the ecMR is lower than the energy consumption of the Haber process which involves the use of valuable coal (with H₂O) to produce H₂. Besides that the ecMR has other advantages such as moderate reaction conditions. Thus, the ecMR is a promising alternative for the synthesis of NH₃.

Using current data from DFT simulations and applying a new microscopic reactor model integrated into a macroscopic process flow sheet we substantiate possible scenarios towards new process alternatives for the current Haber process. Most likely such processes will be of electrochemical nature; whether or not the electrochemical reactor proposed here will be the final choice is irrelevant. Essential is the proposed multi-scale approach of quantum chemical and molecular simulations with a microscopic reactor model integrated into an overall chemical process.

The activity of the electrodes has been estimated using theoretical considerations. The scope of future work will be to validate this estimation and the behavior of the reactor experimentally. In parallel, the separation processes will be optimized and an energy integration of the process will be conducted. Based on that, the operation and investment costs of the entire process can be narrowed down. This will allow an even more profound and optimized economical comparison between conventional Haber plants and the synthesis of NH₃ with an ecMR.

6.7. Appendix

In the following sections model equations describing the electrochemical membrane reactor are given and discussed.

6.7.1. Basic laws and equations in electrochemistry

Electrochemistry deals with the processes and factors, that affect the exchange of charge between chemical phases, e.g. between an electron donor (anode) or acceptor (cathode), and an ionic conductor. In an electrochemical reactor this charge transfer is realized by an applied cell voltage or current to drive an otherwise non-spontaneous chemical reaction [174].

The cell voltage U_{Cell} of any operating electrochemical reactor consists of nine contributions, which are depicted in Figure 6.11 [64]:

1. Equilibrium potential difference of the cell reaction: U_{EP} = E_A - E_C
2. Overpotential of the anode required to drive the charge transfer: η_A
3. Overpotential of the cathode required to drive the charge transfer: η_C
4. Ohmic voltage drop due to charge transfer between the anode and the cathode (electrolyte): ΔU_{Ω,E}
5. Anodic overpotential due to concentration polarization: ΔU_{CP,A}
6. Cathodic overpotential due to concentration polarization: ΔU_{CP,C}
7. Ohmic voltage drop within anode due to ohmic resistance of the anode: ΔU_{Ω,A}
8. Ohmic voltage drop within cathode due to ohmic resistance of the cathode: ΔU_{Ω,C}
9. Potential drop due to contact resistance: ΔU_{Contact}

In comparison to the electrochemical potential drops 1. to 6., the contributions of the potentials 7. to 9. are relatively small and can be neglected [64]. Accordingly, the following equation can be derived [208]:

$$U_{cell} = U_{EP} + \eta_A - \eta_C + \Delta U_{\Omega,E} + \Delta U_{CP,A} + \Delta U_{CP,C} \quad (6.11)$$

The equilibrium potential of an electrode reaction U_{EP} is determined by the Gibbs free enthalpy of the reaction ΔG [204]:

$$E_{A/C} = \frac{\Delta G}{v_e F} \quad (6.12)$$

where F is the Faraday constant which equals 96485 C mol⁻¹ and v_e the number of moles of electrons transferred in the half cell reaction, respectively.

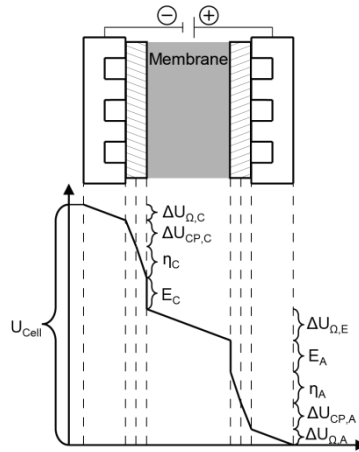


Figure 6.12: Main elements of the modelled ecMR and model discretization along the flow channel length in single elements (vertical dashed lines). Mass, heat and electron transfer to the surrounding.

In general, the Gibbs free energy depends on temperature and the concentration of the reactants and products:

$$\Delta_R G = \Delta_R G^0 + RT \ln Q \quad (6.13)$$

$$Q = \frac{\prod a_{P,i}^{v_i}}{\prod a_{R,i}^{v_i}} \quad (6.14)$$

where $\Delta_R G^0$ denotes the Gibbs free energy at standard conditions, R the ideal gas constant, T the temperature, $a_{P,i}$ and $a_{R,i}$ the activities of the products and reactants and v_i the stoichiometric coefficients. Thus the equilibrium potential is also dependent on the concentration and temperature and can be calculated by adding the equilibrium potentials of the two electrodes. This is given by the Nernst's equation [204]:

$$U_{EP} = E_A - E_C \quad (6.15)$$

$$U_{EP} = \left[E_A^0 + \frac{RT}{v_e F} \ln \left(\frac{\prod a_{ox,i}^{v_i}}{\prod a_{red,i}^{v_i}} \right) \right]_A - \left[E_C^0 + \frac{RT}{v_e F} \ln \left(\frac{\prod a_{ox,i}^{v_i}}{\prod a_{red,i}^{v_i}} \right) \right]_C \quad (6.16)$$

with E_A and E_C as the equilibrium potential of the anode and the cathode and E_A^0 as well E_C^0 as the standard equilibrium potential of the anode and the cathode, respectively.

The activity α of a gas with the partial pressure p is:

$$\alpha = \frac{f}{p^0} p \quad (6.17)$$

where f is the fugacity coefficient of the gas.

The Butler-Volmer expression correlates the current density, which is comparable with the reaction rate of a conventional chemical reaction, and the overpotential for the charge transfer [204]:

$$j = j_0 \left(\exp\left(\frac{\alpha_f v_e F \eta}{RT}\right) - \exp\left(\frac{-\alpha_b v_e F \eta}{RT}\right) \right) \quad (6.18)$$

where j_0 denotes the exchange current density which is the current density exchanged back and forth under equilibrium potential. The forward and backward charge transfer coefficients α_f and α_b correlate the change of the current densities due to a change in overpotential [204]. In general, it is assumed that α_f and α_b are 0.5 [209]. However, at high overpotential one of the two terms of Equation (6.18) outweighs the other and thus for engineering purposes the Butler-Volmer equation can be shorten to a single term [204]:

$$j = j_0 \exp\left(\frac{\alpha_f v_e F \eta}{RT}\right) \text{ if } \frac{\alpha_f v_e F \eta}{RT} \gg 1 \quad (6.19)$$

or

$$j = j_0 \exp\left(\frac{-\alpha_b v_e F \eta}{RT}\right) \text{ if } \frac{-\alpha_b v_e F \eta}{RT} \gg 1 \quad (6.20)$$

Under these conditions the Tafel equation can be derived:

$$\eta = a + b \ln|j| \quad (6.21)$$

where a equals $\frac{RT}{Fv_e\alpha} \ln j_0$ and b equals $\frac{RT}{Fv_e\alpha}$ with α either α_f or α_b .

The ohmic voltage drop $\Delta U_{\Omega,E}$ due to charge transfer between the anode and the cathode is determined by the current density j , the electrode distance d , and the conductivity κ of the electrolyte, i.e. of the membrane [64]:

$$\Delta U_{\Omega,E} = \frac{j d}{\kappa} \quad (6.22)$$

For an ecMR the electrode distance d is the thickness of the membrane minus the press-in depth of the GDE. The conductivity κ of the membrane is determined as following [212]:

$$\kappa = \frac{F^2}{RT} \sum_i z_i^2 D_i c_i \quad (6.23)$$

where i denotes the components permeating through the membrane, z_i their charges and D_i their diffusion coefficients within the membrane. Within the membrane electro neutrality has to be hold [212]:

$$z_f c_f + \sum_i z_i c_i = 0 \quad (6.24)$$

where z_i is the charge of the fixed sites within the membrane and c_f its concentration. In the case of the membrane reactor the only mobile ions are H^+ , thus Equation (6.24) becomes:

$$z_f c_f + z_{H^+} c_{H^+} = 0 \quad (6.25)$$

Hence, the H^+ concentration within the membrane is assumed to be constant. Accordingly the conductivity of the membrane can be calculated with Equation (6.26) [212]:

$$\kappa = \frac{F^2}{RT} D_{M,H^+} c_{M,H^+} \quad (6.26)$$

As mentioned above, an overpotential caused by concentration polarization due to limited mass transfer at the anode and the cathode may arise. The overpotential can be determined by a modified Nernst-Equation:

$$\Delta U_{CP,A/C} = \frac{RT}{v_e F} \ln \left[\frac{\prod a_{ox}^{v_i}}{\prod a_{red}^{v_i}} \right]^{x=0} - \frac{RT}{v_e F} \ln \left[\frac{\prod a_{ox}^{v_i}}{\prod a_{red}^{v_i}} \right]^{x=\infty} \quad (6.27)$$

where $a_i^{x=0}$ is the activity of the species i at the electrode surface, $a_i^{x=\infty}$ is the activity in the bulk fluid and v_i is the stoichiometric coefficient of the component i .

6.7.2. Mass balance

The Faraday's law correlates the current and the formed product or converted reactant, respectively:

$$I = \frac{v_e F d n_i}{v_i dt} \quad (6.28)$$

with I as the current, $d n_i$ as the amount of component i produced during the time dt and v_i as the stoichiometric coefficient for the component i in the half cell reaction. With $j = I/A$ it follows:

$$j = \frac{\nu_e F \dot{n}_{A,C,i}''}{\bar{c}_i} \quad (6.29)$$

where $\dot{n}_{A,C,i}''$ denotes the molar flux of component i per geometric surface area A of the electrode. Since the current density can be calculated with Equation (6.29) the mass balance for a differential element of the bulk fluid in the flow channel of the anode and cathode can be derived as shown in Figure 6.13.

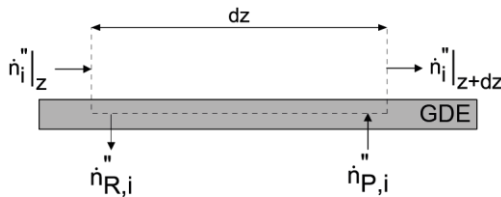


Figure 6.13: Mass balance of an incremental flow channel element

Thus the mass balance can be written as Equation (6.30) for the anode and Equation (6.31) for the cathode:

$$\frac{d}{dz} \dot{n}_{A,i} = \omega (\dot{n}_{P,A,i}'' - \dot{n}_{R,A,i}'') \quad (6.30)$$

$$\frac{d}{dz} \dot{n}_{C,i} = \omega (\dot{n}_{P,C,i}'' - \dot{n}_{R,C,i}'') \quad (6.31)$$

where $\dot{n}_{A,i}$ and $\dot{n}_{C,i}$ are the molar flows of the bulk fluid in the anodic and cathodic flow channel, $\dot{n}_{R,A/C,i}''$ the flux of the reactant consumed per electrode surface area A, $\dot{n}_{P,A/C,i}''$ the product flux per electrode surface area A and ω the width of the flow channel.

6.7.3. Mass transfer

Concentration polarization due to limited mass transfer at the electrodes causes an overpotential. The reactants as well as the products have to pass the boundary layer between the bulk fluid and the Gas Diffusion Electrode (GDE) as well as the GDE itself to reach the active catalyst layer. The concentration at the surface of the GDE can be calculated by balancing the molar flux with the mass transfer coefficient and the driving concentration difference:

$$\dot{n}_{\frac{R}{P}A,i}'' = \beta(c_{i,bulk} - c_{i,GDE}) \quad (6.32)$$

The mass transfer coefficient β is obtained from dimensionless correlations of the Schmidt-, Sherwood and Reynolds-Number:

$$Sh = 1.62 \left(Re Sc \frac{d_{hyd}}{l} \right)^{\frac{1}{3}} \quad (6.33)$$

$$Re = \frac{u \rho d}{\eta} \quad (6.34)$$

$$Sc = \frac{\eta}{\rho d} \quad (6.35)$$

$$Sh = \frac{\beta d}{D} \quad (6.36)$$

where u is the flow velocity, ρ the density of the fluid, η the fluid viscosity, d the hydraulic diameter of the flow channel and D the diffusion coefficient.

The mass transport of the fluid in the gas diffusion electrode is modeled as multicomponent diffusion in porous media. The Knudsen number determines whether statistical mechanics or continuum mechanics should be used to describe the mass transport. The Knudsen number is given by Equation (6.37):

$$Kn = \frac{\lambda}{d_{por}} \quad (6.37)$$

For this work the pore size d_{por} is assumed to be 50 μm and the mean free path of the gas molecules λ is about 68 nm [213]. Thus the Knudsen number is about 0.0014. Hence, the Knudsen number is smaller than 0.01 and the mass transport obeys continuum mechanics. Thus, the mass transport can be described by ordinary multicomponent diffusion [20]:

$$\dot{n}_i'' = x_i \dot{n}_{tot}'' - D_{eff} \nabla c_i \quad (6.38)$$

In case of diluted mixtures, the diffusion process can be considered as two component diffusion [20]:

$$\dot{n}_{tot}'' = \sum_i \dot{n}_i'' \quad (6.39)$$

The effective diffusion coefficient D_{eff} accounts the geometric constraints of the porous media, which reduce the diffusivity. Thus, the open space diffusivity D is modified by a correction factor [214]:

$$D_{eff} = D \varepsilon^\alpha \quad (6.40)$$

$$\alpha = \frac{\log_{10} \left(\frac{\varepsilon}{\tau} \right)}{\log_{10} \varepsilon} \quad (6.41)$$

Here, the porosity ε of the GDE used for the preparation of the membrane electrode assembly (MEA) is approximately 0.3 and for typical cases the tortuosity τ is three [214].

6.7.4. Energy balance

The energy balance for a differential element of the bulk fluid in the flow channel is shown in Figure 6.14.

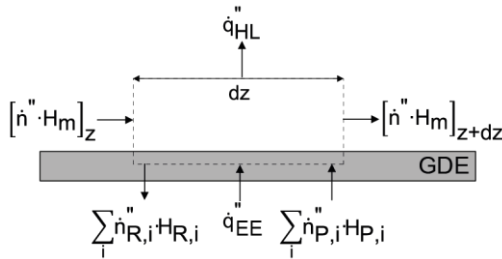


Figure 6.14: Energy balance of an incremental flow channel element

6

In the balance, the enthalpy flux due to mass flux, heat loss to the ambient air as well as heat generation due to consumption of electrical energy are considered. Accordingly, the energy balance for the anode and the cathode can be written as Equation (6.42) and (6.43):

$$\frac{d}{dz} (\dot{n}_A H_{M,A}) = \sum_{i,P} \dot{n}_{P,i} H_{P,i} \omega - \sum_{i,R} \dot{n}_{R,i} H_{R,i} \omega + \dot{q}_{EE,A} \omega - \dot{q}_{HL,A} \omega \quad (6.42)$$

$$\frac{d}{dz} (\dot{n}_C H_{M,C}) = \sum_{i,P} \dot{n}_{P,i} H_{P,i} \omega - \sum_{i,R} \dot{n}_{R,i} H_{R,i} \omega + \dot{q}_{EE,C} \omega - \dot{q}_{HL,C} \omega \quad (6.43)$$

with $H_{M,A}$ as the specific enthalpy of the molar flow in the flow channel, $H_{i,R}$ as the specific enthalpy of the reactants diffusing from the flow channel into the GDE and $H_{i,P}$ as the specific

enthalpy of the products diffusing back from the GDE into the flow channel, $\dot{q}_{HL,A/C}''$ as the heat flow transferred per area to the ambient air and $\dot{q}_{EE,A/C}''$ as the heat flow transferred per area due to the conversion of electrical energy.

The Gibbs free energy ΔG of any cell reaction is the minimal amount of electrical energy per mol converted substrate which is required to drive the electrochemical process. However, the total energy to be expended is the reaction enthalpy $\Delta_R H$ which is the sum of ΔG and the entropic term $T\Delta S$:

$$\Delta_R H = \Delta G + T\Delta S \quad (6.44)$$

Any electrochemical process with $\Delta G > 0$ and negative reaction entropy must transfer heat from the cell to the surroundings if the reaction is performed reversibly, but at constant temperature, as $\Delta_R H$ is smaller than ΔG . Therefore any process involving positive reaction entropy has to be supplied with thermal energy. If the electrochemical process is conducted under adiabatic conditions, the thermoneutral voltage U_{th} must be applied to balance the energy required for the cell reaction with the electrical energy [64]:

$$U_{th} = \frac{\Delta_R H}{z_e F} \quad (6.45)$$

If a portion U_D of the cell voltage U_{Cell} exceeds the thermoneutral voltage U_{th} , heat is generated [64]:

$$\dot{q}_{EE}'' = jU_D = j(U_{Cell} - U_{th}) \quad (6.46)$$

As mentioned before, a term describing the heat transfer from the membrane reactor to the ambient air has to be considered:

$$\dot{q}_{HL,A/C}'' = k(T_{x_{\overline{C}}} - T_0) \quad (6.47)$$

with $T_{x_{\overline{C}}}$ as the temperature in the anodic or cathodic flow channel, T_0 as the ambient temperature and k as the heat transfer coefficient.

6.7.5. Heat transfer

As described before, heat is transferred from the inside of the membrane reactor to the ambient air. The heat transfer from the fluid to the ambient air can be considered as heat transfer processes connected in series. Thus the heat transfer coefficients add inversely:

$$\frac{1}{k} = \frac{1}{k_{we}} + \frac{1}{k_w} + \frac{1}{k_{fw}} \quad (6.48)$$

with k_{we} as the heat transfer coefficient for the heat transfer between the outside of the reactor wall and the ambient air, k_w as the heat transfer coefficient through the reactor wall and k_{fw} as

the heat transfer coefficient for the heat transfer between the fluid at the anode or cathode and the inside of the reactor wall, respectively. The heat transfer coefficient through the reactor wall is given by:

$$k_w = \frac{\lambda}{d_w} \quad (6.49)$$

where λ is the thermal conductivity of the reactor wall and d_w its thickness. The heat transfer between the outside of the wall and the surrounding air can be considered as heat transfer due to free convection along a vertical surface. The Nusselt-Number is defined as the ratio of convective to conductive heat transfer across the boundary:

$$Nu = \frac{k_{se}l_{se}}{\lambda} \quad (6.50)$$

For this kind of heat transfer the Nusselt number can be calculated as follows:

$$Nu = \left(0.825 + 0.387(Ra f(Pr))^{\frac{1}{6}} \right)^2 \quad (6.51)$$

with Ra as Rayleigh number and the function $f(Pr)$ which takes the influence of the Prandtl number Pr into account:

$$Ra = \frac{g\beta}{\nu\alpha} (T_w - T_0) l^3 \quad (6.52)$$

$$f(Pr) = \left(1 + \left(\frac{0.492^{\frac{9}{16}}}{Pr} \right) \right)^{-\frac{16}{9}} \quad (6.53)$$

$$Pr = \frac{\nu}{\alpha} \quad (6.54)$$

with g as the acceleration due to gravity, β as the thermal expansion coefficient which is given by $\beta = 1/T_0$ for ideal gas, ν as the kinematic viscosity of the surrounding air, α as the thermal diffusivity, T_w as the surface temperature of the wall and T_0 as the temperature of the ambient air. Finally, the heat transfer between the fluid in the flow channel and the reactor wall has to be considered. The heat transfer is considered as forced convection in a fully developed laminar pipe flow with uniform surface temperature. In this case the Nusselt number is constant:

$$Nu = 3.66 \quad (6.55)$$

$$Nu = \frac{k_{fw}d_{hyd}}{\lambda_f} \quad (6.56)$$

with d_{hyd} as the hydraulic diameter of the flow channel and λ_f as the thermal conductivity of the fluid within the flow channel.

6.7.6. Pressure loss

The pressure in the reactor influences the concentration of the product and therefore the equilibrium potential of the half-cell reaction. The convective flow along the electrodes causes a pressure loss, which can be calculated by using the law of Hagen-Poiseulle for laminar flows:

$$\frac{dp}{dz} = \frac{32\rho u^2}{Re \times d} \quad (6.57)$$

7. Energetic optimization of the simulated ecMR

Abstract

Today NH₃ is mainly produced by the Haber process, which is very process intensive, energy consuming and polluting. The electrochemical synthesis of NH₃ in an electrochemical membrane reactor (ecMR) is a promising environmentally friendly alternative. Water and air are used as abundant reactants and the required electrical energy can be delivered by renewable energy sources. Based on a recently published model of the ecMR modelled in Aspen Custom Modeler (ACM), three different alternatives for the downstream process were developed. The most energy efficient alternative uses cryogenic distillation for the separation of NH₃ from the product stream and membranes for the separation of N₂ and H₂. Compared to preliminary results, the specific energy consumption of the downstream process has been reduced by 39.2%, resulting in a reduction of 3.9% for the entire process. Finally, a short economic evaluation has been conducted, which proves the potential of the ecMR for economic feasibility.

7.1. Introduction

Typically NH₃ is produced via the Haber process at 400 to 500°C and 150 to 200 bar in a quantity of 135 Mio tones per year. Due to the harsh process conditions the NH₃ synthesis contributes with 1 to 3% to the global energy consumption. [12] Around 2 tons CO₂ are emitted per ton produced NH₃ using natural gas for the production of H₂ [14]. Just recently we proposed the environmentally friendly and CO₂-free electrochemical NH₃ synthesis in a membrane based process using an electrochemical membrane reactor (ecMR) as an alternative synthesis route. The core of the ecMR is a membrane electrode assembly (MEA) consisting of a H⁺ exchange membrane and two embedded metal electrodes acting as anodic and cathodic catalyst. At the cathode N₂ is reduced to NH₃ and the required H⁺ are provided by the oxidation of H₂O to O₂ at the anode. The process operates at atmospheric pressure and temperatures of about 100°C. The driving force for the reaction is supplied by an external electrical potential. [15]

In a previous work a model for the ecMR implemented in Aspen Custom Modeler (ACM), see Chapter 6, was presented. Based on this model a complete synthesis process with N₂ production and product separation downstream to the ecMR was developed in Aspen+. The energy demand of the complete electrochemical synthesis process is up to 20% lower than the Haber process using coal as H₂ source. [15] However, the question arises if the total energy demand can be narrowed down by optimizing the downstream separation process.

This chapter aims to develop and to compare different alternatives for the downstream process of the electrochemical synthesis of NH₃. Finally, the complete synthesis process will be compared with the Haber process and an economical evaluation will be conducted.

7.2. Initial situation

Different factors have a major influence on the reactions taking place in the ecMR and thus on its performance. An increase of the applied current or the cell potential supports the formation of NH₃. However, for both values a maximum exists, after which no further increase in NH₃ production is observed. For the solid electrolyte and the catalyst suitable materials have to be selected. The catalyst determines the selectivity of the reactions and the current efficiency β . Another important parameter is the operating temperature. An increase favors the reaction rate due to a higher conductivity of the membrane, but the decomposition of NH₃ is more likely as well. However, polymer membranes begin to lose H₂O at certain temperatures and therefore the H⁺ conductivity is reduced. Thus, based on the chosen membrane an optimal operating temperature for the electrochemical synthesis of NH₃ in the ecMR exists. [96]

The ecMR model can be used to analyze the influence of different parameters on the reactor's performance. Furthermore an entire synthesis process was designed and different techniques for the separation of the gaseous product streams can be compared.

7.3. Product separation at the anode and cathode

The product streams at both electrodes of the ecMR contain valuable gaseous products and the gas mixtures have to be separated. The anodic outlet stream only consists of O₂ and H₂O. Depending on the current efficiency, the cathodic stream contains NH₃ and unconverted N₂ and H₂ as undesired byproducts. Furthermore, the cell potential U_{cell} and the applied current have influence on the compositions of the outlet streams.

For liquid separation, distillation is in most cases the technique of choice. However, for the separation of gases there is no preferred method such as distillation and different techniques have to be considered. [215] The major requirement for the separation technique is the capability to produce high purity products. For NH₃, a purity of at least 99.5 wt% is required [46]. For O₂ and N₂ purities of 99.5 mole-% and for H₂ a purity of 95.0 mole-% were desired. Ammonia impurities in the N₂ recycling stream would affect the equilibrium of the cathodic reaction and lower the NH₃ formation. The use of H₂ and O₂ as valuable byproducts is considered later for the economic evaluation. According to Seider et al. partial condensation, cryogenic distillation and membrane separation were chosen as the major separation techniques in this study [216]. Absorption is used in one of the process alternatives as an additional purification technique.

For the design of an optimal separation system, the sequencing of the multiple separation steps is of major importance. According to Barnicki and Fair corrosive and hazardous materials have to be removed first, followed by troublesome trace impurities. Components, which are desired products and are present in large quantities, should be separated secondly. [215] Additionally, split which separate the feed into equimolar streams are beneficial. At the anode, the gaseous mixture only consists of two components, which can be separated in one step. Contrary, the separation of the cathodic product stream is realized in two major steps. In the first split NH₃ is separated from N₂ and H₂, since it is the desired product, present in large quantities, and also corrosive. If considerable NH₃ concentrations are present in the N₂/H₂ stream, they are removed in an additional purification step. Finally N₂ and H₂ are separated.

7.3.1. Gas separation by partial condensation and cryogenic distillation

Both partial condensation and cryogenic distillation are thermal separation methods, which are based on the relative volatility of the components. Partial condensation is highly favorable for the separation of high-boiling components from non-condensable gases. It should be considered, if the difference between the boiling temperatures of the key components is larger than 40°C [215]. For the separation of H₂O from O₂ partial condensation is best suited due to the large difference in their boiling points. However, for the separation of the other components, partial condensation is inferior to cryogenic distillation. A more complex structure with multiple stages is required to fulfill the given product specifications and the specific energy demand is higher.

Cryogenic distillation is practicable for the sharp separation of gaseous mixtures when the relative volatility between the key components is larger than two [215]. At the cathode, the key

components of each suggested split have large differences in their boiling temperatures. High purities and high recovery rates are achievable by cryogenic distillation. However, large throughputs with more than 10 tons per day are highly recommended, since scaling effects have great influence on the specific energy consumption. Furthermore, the removal of components with high melting points is crucial, since freezing components may foul the equipment [215]. The melting point of NH₃ of -77.7°C [46] is high compared to the temperatures of below -200°C needed for a sharp split of N₂ and H₂.

When cryogenic distillation is used as separation technique, the condenser of the separation column is operated at temperatures below the cooling water temperature and refrigerants have to be used. The coefficient of performance (COP) describes the energy consumption of the cryogenic equipment. It is defined as the ratio of the cooling duty \dot{Q}_c to the required power consumption P. An increase in the column's operating pressure reduces the required condenser temperature. The COP of the cryogenic equipment increases and the energy consumption of the condenser decreases.

7.3.2. Gas separation by membranes

Alternatively, gaseous mixtures can be separated by using membranes. This technique is based on the varying permeability P of components through the membrane as a barrier. More permeable components are enriched in the permeate, whereas less permeable components are enriched in the retentate. This characteristic is represented by the selectivity α of a membrane material, which is given by the quotient of the pure gas permeability of the components i and j. For economic feasibility the selectivity of the membrane material should be 15 or larger [217]. In general, membrane materials with a high selectivity exhibit a lower permeability and vice versa [218]. Membranes with high permeability require a smaller membrane area. The permeance through the membrane is dependent on the permeability P and the thickness δ of the membrane's selective layer [219].

The product separation by membranes in this work is conducted in a two stage process. A single-stage membrane process cannot achieve high purity and recovery at the same time [219]. The operating pressure and the pressure ratio Φ of the partial pressures of feed and permeate are selected individually for the different process alternatives. The values were chosen with focus on the specific energy consumption. However, investment costs have not been considered. Membranes are considered for the separation of NH₃ from N₂ and H₂ and for the separation of N₂ from H₂. The separation of H₂O from O₂ could also be conducted by membranes. However, the major part of H₂O can be liquefied by use of cooling water coupled with very low costs.

Today the separation of NH₃ from N₂ and H₂ by membranes is not of significant industrial importance. The modeled ecMR is operated at atmospheric pressure and NH₃ liquefaction is coupled with high costs for refrigeration and/or compression. Therefore, separation by membranes is only considered as alternative separation technique. For the separation of NH₃ from N₂ and H₂ rubbery membranes have to be used. Owing to its molecule structure and the polarization of its bonds, NH₃ has a good solubility in many materials[46].

The separation of N₂ from H₂ was the first industrial application of membranes for gas separation done by Monsanto in 1980 [219]. Glassy membranes are used, which are

preferentially permeable for H₂ due to its small molecule size. Because of missing literature values for permeability values of NH₃, it is assumed to be equal to the permeability of N₂. However, the concentration of NH₃ in the feed stream of the membrane separation unit is reduced before to ppm-level and is not of significant influence on the compositions of the product streams.

7.4. Alternatives for the downstream separation

Figure 7.1 shows the general structure of the entire synthesis process.

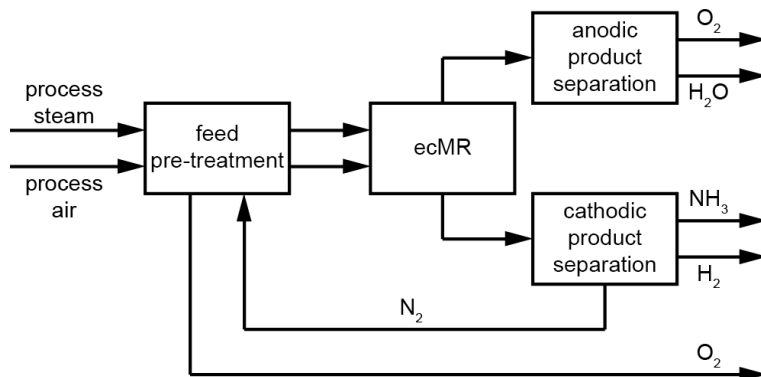


Figure 7.1: General block flow sheet of the entire synthesis process

It can be divided into four major process steps, namely the feed pre-treatment, the ecMR, and the anodic and cathodic product separation. The temperature of cooling water is assumed to be 30°C. For the design of all heat exchangers in this work a minimal driving temperature difference ΔT_{\min} of 5°C is assumed. The COP of the cryogenic equipment used for several heat exchangers and condensers, was calculated by using a suitable refrigerant. Due to the conducted energy integration, integrated heat exchangers are named EI. Heat exchangers, which make use of cooling water, are labelled with CW and heat exchangers with external heat or cooling sources are named HX. Other equipment is also labelled with a proper abbreviation. All components have an increasing number for reasons of clarity and comprehensibility.

7.4.1. Feed pre-treatment

Figure 7.2 shows the flow sheet of the feed pre-treatment. Process steam is used as anodic feed. Depending on its pressure level, the pressure has to be reduced by a valve and the steam has to be cooled down to the operating temperature of the ecMR. The cathodic reactant is N₂ derived by a cryogenic air separation unit, which is simulated as black box unit.

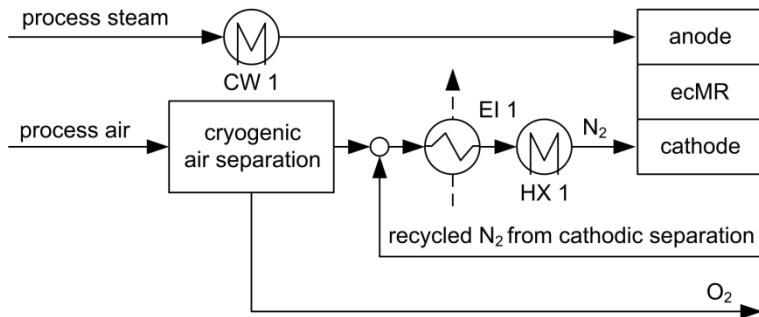


Figure 7.2: Flow sheet of the feed pre-treatment

The specific energy consumption is taken from literature [46]. Unconverted N₂ is recycled and the stream is heated up, before it is fed to the ecMR.

7.4.2. ecMR

The ecMR consists of a dense polymer membrane serving as solid H⁺ conductor, two porous metal electrodes acting as anode and cathode and an electron distributor at the cathode and an electron collector at the anode. The anodic and cathodic half-cell of the ecMR are separated by the MEA so that the anode and the cathode can be exposed to different gases [201]. Details about the ecMR can be found in Chapter 4.

The aim of this chapter is to evaluate different alternatives for the downstream process of the electrochemical NH₃ synthesis. The developed process alternatives are compared in terms of specific energy consumption on the basis of four different cases, see Table 7.1:

Table 7.1 Four different cases to investigate the energy demand of the downstream process

Case	Explanation	U _{cell} [V]	Current efficiency [%]
1	reference case	2.2	0.9
2	high conversion with lower feed flow rate of 2/3 $\dot{V}_{A,C}^{ref}$	2.2	0.9
3	low current efficiency	2.2	0.8
4	high current efficiency	2.2	1.0

For this work the reference case is set to a cell potential of 2.2 V and a current efficiency of 90%. The reference case of the previous work [15] is considered in this work as well as case 4. The reduced flow rate of case 2 results in a higher conversion rate and thus the separation task of the products should be less. The defined cases result in different compositions of both product streams, listed in Table 7.2:

Table 7.2 Molar compositions (in mole-%) of the ecMR product streams at the anode and the cathode for four defined cases					
Electrode	Component	Case 1	Case 2	Case 3	Case 4
Anode	O ₂	35.3	56.5	36.4	34.4
	H ₂ O	64.7	43.5	63.6	65.6
Cathode	NH ₃	58.1	69.9	49.1	68.1
	N ₂	32.3	18.4	32.5	31.9
	H ₂	9.7	11.7	18.4	-

Case 2 shows the highest conversion rate for O₂ at the anode and NH₃ at the cathode. However, a higher conversion rate does not automatically lead to a lower energy demand. For all cases the product streams consist of gaseous mixtures. For the anodic separation only one possibility is considered, whereas for the cathodic separation three different alternatives are considered.

7.4.3. Anodic product separation

Figure 7.3 shows the separation of the anodic product stream by partial condensation, described in Section 7.3.1.

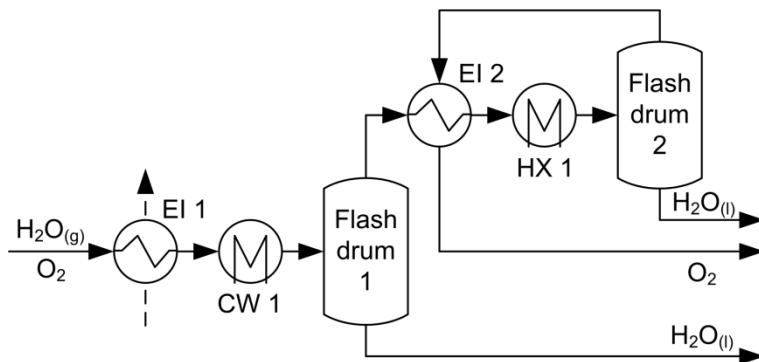


Figure 7.3: Anodic product separation by partial condensation

The separation is conducted in two steps. First the major part of H₂O is removed by cooling with cooling water at atmospheric pressure in flash drum 1, resulting in a pure H₂O stream and an enriched O₂ stream. Before it enters flash drum 2, the O₂ rich stream is cooled further down and remaining H₂O is liquefied at 2°C and atmospheric pressure. These operating conditions result in the lowest specific energy consumption, as can be seen in Figure 7.4. For the second split cooling cannot be achieved with cooling water. It either has to be done by heat integration with a colder process stream or with cryogenic equipment.

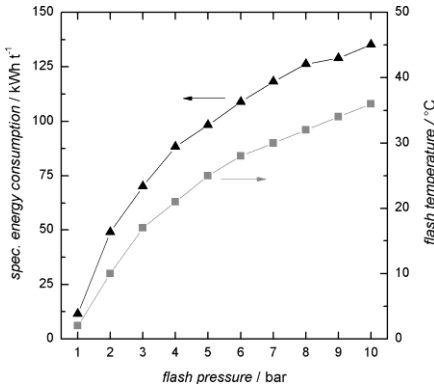


Figure 7.4: Specific energy consumption of the O₂ separating flash drum depending on the operating pressure

7.4.4. Cathodic product separation

For the cathodic product separation three alternatives have been developed:

- Process A: separation by cryogenic distillation with two columns
- Process B: separation by membranes in two consecutive separation steps
- Process C: separation of NH₃ by cryogenic distillation, purification by absorption with H₂O and N₂ - H₂ separation by membranes

Process A - Separation by cryogenic distillation

Figure 7.5 shows the separation of the cathodic product stream by cryogenic distillation. For a current efficiency β of unity, no H₂ is present in the cathodic product stream. The separation can then be simplified and flash drum 1 and column 2 including all peripheral devices are not necessary any more. The N₂ rich stream leaving column 1 is passing the condenser 1 and is then fed to turbine 1 before being released over the heat exchanger EI 3. In column 1 NH₃ is separated from N₂ and H₂. For the optimal design of the separation unit, different parameters have to be adjusted. First, the optimal operating pressure of column 1 is calculated. The specific energy consumption is chosen as the major criterion. Figure 7.6 shows the comparison of different pressure levels. At an operating pressure of 40 bar the specific energy demand of the NH₃ separating column is the lowest. Pressures of less than 20 bars are not feasible since the condenser temperature is below the melting point of NH₃. After removal of NH₃ the remaining NH₃ concentration of 0.5 mole-% is reduced to ppm-level by further cooling of the distillate below the melting point of NH₃. This may result in fouling of the flash drum. A discontinuous operation with two flash drums and regeneration may be needed. Before being fed to column 2, the stream is cooled further down by heat integration and use of a cryogenic turbine. However, for the condenser of column 2 further cooling by an external refrigeration cycle is necessary.

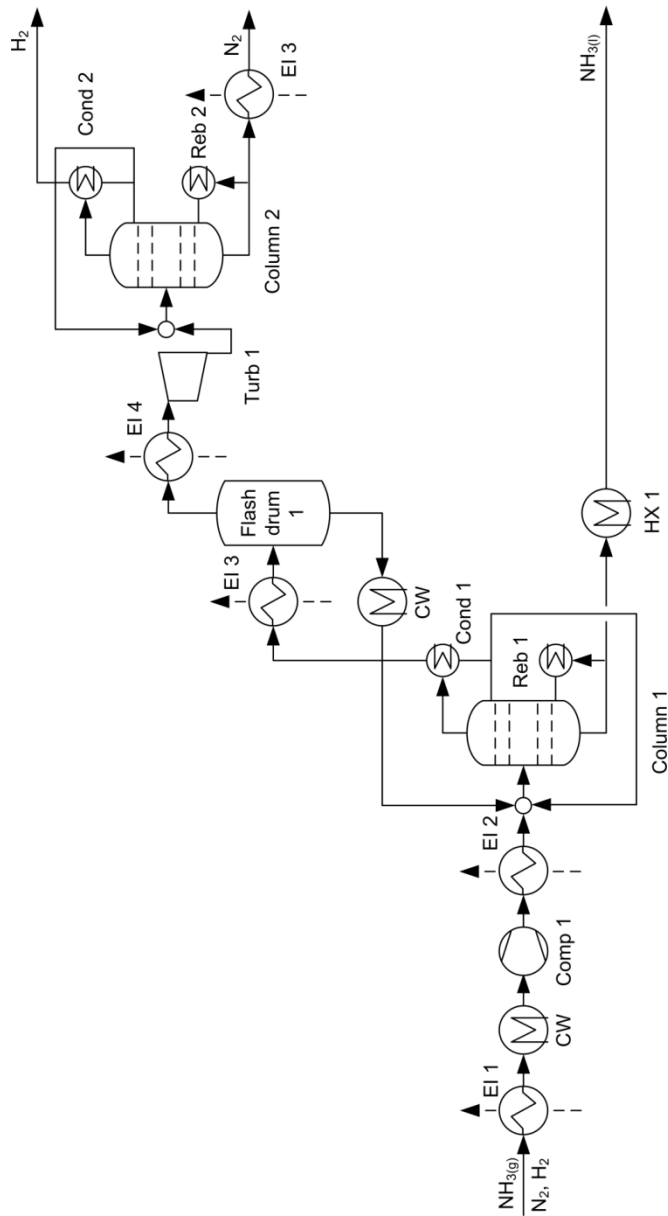


Figure 7.5: Process A - cathodic product separation by cryogenic distillation

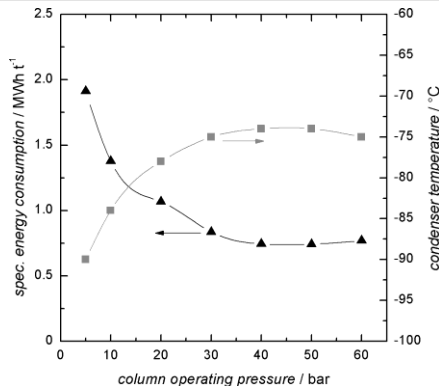


Figure 7.6: Specific energy consumption of the NH_3 separating column depending on the operating pressure

For the cryogenic separation of N_2 from H_2 very low temperatures below -200°C are necessary. The operating temperatures can be increased by increasing the operating pressure. However, a pressure increase from 1 to 20 bar increases the temperature only from -215°C to -200°C . At a pressure of 5 bar the condenser temperature is -207°C . A further pressure increase only leads to a minor temperature increase, but the specific condenser duty is rising significantly. In preliminary simulations cooling by expansion of the feed stream according to the Joule-Thomson effect combined with energy integration did not cover the overall cooling duty. The external cooling can be done by physical processes using the Joule-Thomson-Effect. Also a separate cooling cycle using He or Ne as refrigerant can be applied. For the simulations, a COP of 0.05 was assumed [220].

Process B - Separation by membranes

Figure 7.7 shows the designed process using membranes for the separation. Here for a current efficiency of unity, the second membrane stage for the N_2 - H_2 separation can be neglected. The N_2 stream leaving the NH_3 membrane 1 is only fed to Turbine 1 before it is released. For the NH_3 removal, a two-stage process has been developed, using a membrane with high permeability and sufficient selectivity in the first stage. For the second stage, a more selective membrane is chosen in order to achieve the high product specifications of NH_3 . The separation of N_2 from H_2 is also conducted in a two stage process. The process structure is identical to the separation of NH_3 from N_2 and H_2 . However, in both stages the same membranes with a high permeability and a sufficient selectivity are used. The specifications of all applied membranes are given in Table 7.3. A pressure ratio Θ of 10 is chosen for both separation steps. This results in the lowest specific energy consumption of the required compressors, as can be seen in Figure 7.8.

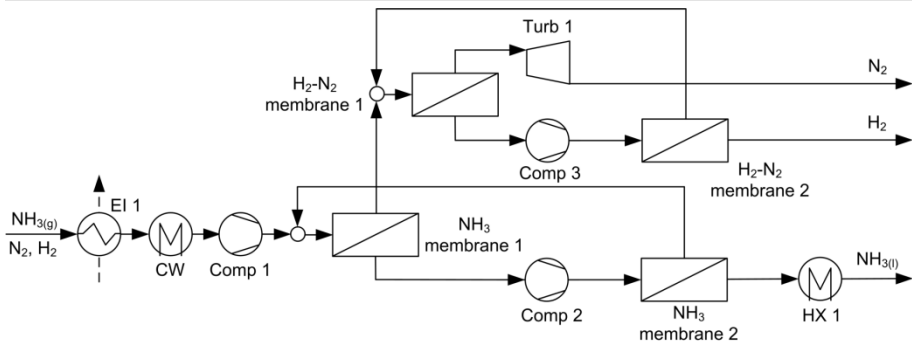


Figure 7.7: Process B - cathodic product separation in a two-stage membrane process

Table 7.3 Properties of the chosen membranes for the cathodic separation task

Separation	P_{NH_3}	P_{N_2}	P_{H_2}	α_{NH_3/N_2} or α_{H_2/NH_3}	α_{NH_3/H_2} or α_{H_2/N_2}	δ^*	Reference
NH ₃ from N ₂ /H ₂ Stage 1	5900	280	650	21.1	9.1	1**	[221]
N ₂ /H ₂ Stage 2	612.3	11.1	12.2	55	50.1	0.5**	[222]
N ₂ from H ₂ Stage 1/2	42**	42	860	20.5**	20.5	1**	[223]

P_i in barrer, * thickness of the selective layer in µm, ** assumed

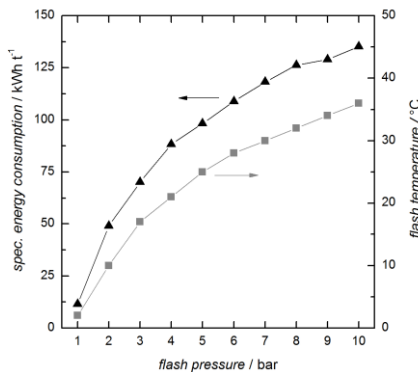


Figure 7.8: Specific energy consumption of the separation by membranes depending on the pressure ratio Θ

The feed pressure p_F is set to 10 bar. The selection of the optimal pressure ratio Θ is a tradeoff between operating costs and investment costs. Higher pressure ratios and therefore higher feed pressures result in a lower membrane area required. However, investment costs for compressors along with operating costs also increase with an increasing pressure ratio.

Process C - Separation by a combination of cryogenic distillation and membranes

Figure 7.9 shows the process flow sheet of the separation process as a combination of cryogenic distillation and membranes. In addition to these two separation methods, the purification of the distillate leaving column 1 is done by absorption with H_2O . The distillate of column 1 is present at high pressure and low temperatures, favoring the solubility of gases in liquids. The distillate is heated up to about $0^\circ C$ to avoid freezing of the washing water and fouling of the equipment. The contaminated washing water is purified in a second column and afterwards recycled. Compared to column 1, the throughput of column 2 is far smaller. The membrane separation of N_2 from H_2 is operated at a feed pressure p_F of 40 bar and a pressure ratio Θ of 40, since the feed stream already has this pressure.

7.5. Results

7.5.1. Specific energy consumption of the entire process

The specific energy consumption for the developed process alternatives has been calculated using Aspen+, see Table 7.4 to Table 7.6. Since the required electrical energy shall be delivered by renewable energy sources, losses of conventional power plants are not considered.

Table 7.4 Specific energy consumption of the entire NH_3 synthesis process A using cryogenic distillation in $MWh\ t_{NH_3}^{-1}$

Process A	Process Unit	Case 1	Case 2	Case 3	Case 4
Feed pre-treatment	Cryogenic ASU	0.039	0.062	0.036	0.042
	HX 1	0.003	0.002	0.003	0.002
ecMR	ecMR	11.56	11.56	13.00	10.40
Anodic separation	HX 1	0.011	0.011	0.013	EI*
Cathodic separation	Comp 1	0.391	0.322	0.468	0.331
	Cond 1	0.227	0.143	0.335	0.324
	HX 1	0.045	0.046	0.047	0.045
	Turb 1	- 0.007	- 0.005	- 0.014	- 0.019
	Cond 2	0.485	0.354	0.834	-
	Sum	12.75	12.49	14.72	11.12

* heat of HX 1 of the anodic separation is used for further heating of EI 3 of the cathodic separation

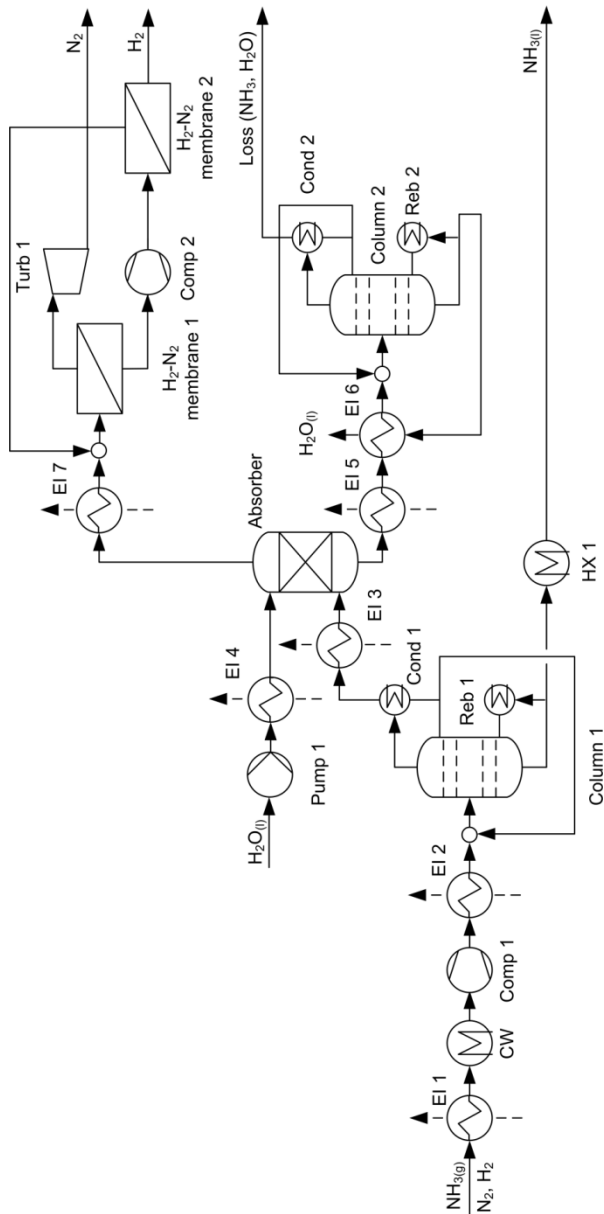


Figure 7.9: Process C - cathodic product separation by a combination of cryogenic distillation and membranes

Table 7.5 Specific energy consumption of the entire NH₃ synthesis process B using membranes in MWh t_{NH₃}⁻¹

Process B	Process Unit	Case 1	Case 2	Case 3	Case 4
Feed pre-treatment	Cryogenic ASU	0.039	0.062	0.036	0.042
	HX 1	0.003	0.002	0.003	0.002
ecMR	ecMR	11.56	11.56	13.00	10.40
Anodic separation	HX 1	0.011	0.011	0.013	0.010
Cathodic separation	Comp 1	0.244	0.201	0.289	0.207
	Comp 2	0.711	0.532	0.812	0.423
	HX 1	0.235	0.206	0.200	0.263
	Comp 3	0.102	0.056	0.146	-
	Turb 1	- 0.028	- 0.013	- 0.032	- 0.024
	Sum	12.87	12.61	14.46	11.32

Table 7.6 Specific energy consumption of the entire NH₃ synthesis process C using a combination of cryogenic distillation and membranes in MWh t_{NH₃}⁻¹

Process B	Process Unit	Case 1	Case 2	Case 3
Feed pre-treatment	Cryogenic ASU	0.039	0.062	0.036
	HX 1	0.003	0.002	0.003
ecMR	ecMR	11.56	11.56	13.00
Anodic separation	HX 1	0.012	0.012	0.013
Cathodic separation	Comp 1	0.393	0.323	0.470
	Cond 1	0.235	0.142	0.332
	HX 1	0.046	0.047	0.047
	Pump 1	< 0.001	< 0.001	< 0.001
	Reb 2	0.072	0.041	0.100
	Comp 2	0.106	0.072	0.164
	Turb 1	- 0.037	- 0.017	- 0.043
	Sum	12.43	12.24	14.12

For all processes the ecMR is the most energy consuming process unit and contributes to more than 90% of the overall energy consumption. The cathodic product separation is the second largest contributor, particularly due to the compression of the gaseous products and/or the cryogenic equipment used. The feed pre-treatment and the anodic product separation are less energy demanding. For the separation of NH₃ from N₂ and H₂ cryogenic distillation has the lowest energy consumption in all different cases. However, plants with capacities of at least 5 t_{NH₃} d⁻¹ are required. Contrary, a major disadvantage of the separation by membranes is the gaseous permeate state of NH₃ at atmospheric pressure. Since NH₃ is stored and shipped in liquid state, the energy costs for liquefaction increase when membranes are applied for the separation. The separation of H₂ from N₂ by membranes has a significant lower energy consumption than the use of cryogenic distillation. Since the temperatures required for the sharp

separation of these components are very low, expensive cryogenic equipment has to be used. By the use of Ne as refrigerant, the required temperatures can be achieved. However, the specific energy consumption is very high due to the small COP of the cryogenic equipment. Membranes are best suited for this separation step, particularly since N₂ will be recycled and liquefaction is not necessary. As expected, the reduced flow rate of case 2 results in a reduced energy demand for the separation task of the products for all processes. For all cases process C, i.e. the combination of cryogenic distillation for the separation of NH₃ from N₂ and H₂ and membranes for the separation of N₂ and H₂, has the lowest energy demand. For case 4, i.e. a current efficiency of 100%, no separation of N₂ and H₂ is necessary. Here only one stage separation process is applied and process A has the lowest energy demand. Compared to preliminary results (compare Section 6.5.4), the specific energy consumption was reduced by a significant amount, as can be seen in Table 7.7.

	Case 1	Case 3	Case 4*
Process C	12.43	14.12	11.12
Preliminary results	12.93	14.55	11.41
Reduction for the entire process [%]	- 3.9	- 3.0	- 2.5
Reduction excluding the ecMR [%]	- 39.2	- 27.7	- 28.7

* case 4 for process A, since no separation of N₂ and H₂ is necessary

The highest energy reduction was achieved for case 1. The total energy demand was decreased by 3.9%, corresponding to 39.2% when only considering the downstream process. However, case 4 is the most efficient one and has the lowest energy demand. Here the energy demand was decreased by 28.7%. The Haber process using natural gas as H₂ source has an energy consumption of 7.92 MWh t_{NH₃}⁻¹, whereas the energy demand is increasing to 13.47 MWh t_{NH₃}⁻¹ when using coal. [19] However, coal will gain in importance in future due to its long reserves [46]. The NH₃ synthesis in an ecMR has a lower specific energy consumption than the Haber process using coal and thus may be the technology-of-choice in future.

7.5.2. Economic evaluation

An economic evaluation of the electrochemical NH₃ synthesis is given for process C based on the reference case (compare Table 7.1) and the following assumptions:

- electricity costs of 0.035 € kWh⁻¹ [224]
- steam generation costs of 24.9 € t_{steam}⁻¹ with 3.38 t_{steam} needed per t_{NH₃}
- production of 2.1 t_{O₂} per t_{NH₃} and an O₂ price of 120 € t_{O₂}⁻¹
- NH₃ price of 700 € t_{NH₃}⁻¹ [225]

The assumed costs and the price for selling O₂ result in a minimal price for NH₃ of 268 € t_{NH₃}⁻¹ to outweigh the costs. Without selling O₂, the minimal price for NH₃ is 520 € t_{NH₃}⁻¹. On the other side the electricity costs can increase to about 0.07 € kWh⁻¹ with an average price for NH₃ of 700 € t_{NH₃}⁻¹. These calculations only consider the operating and reactant costs. Furthermore, the sale of H₂ has not been included because of its lower purity of 95 mole-% and its small amount

of 0.03 to 0.08 t_{H₂} per t_{NH₃} produced. Table 7.8 shows the costs and returns of the entire NH₃ synthesis process. For an average price for NH₃ of 700 € t_{NH₃}⁻¹ the gains are 432 € t_{NH₃}⁻¹. Consequently, the electrochemical NH₃ synthesis has potential for economic feasibility.

Table 7.8 Economic evaluation of the electrochemical NH ₃ synthesis in € t _{NH₃} ⁻¹		
Contributor	Costs	Returns
Electricity	436	-
Steam	84	-
O ₂	-	252
NH ₃	-	700
Sum	520	952
Gains		432

In addition to the conducted optimization of the downstream process, further possibilities exist to increase the economic efficiency of the entire synthesis process. One option is to integrate the electrochemical NH₃ synthesis in a broader process network. The major use of NH₃ is for the production of synthetic fertilizers such as HNO₃. In the Ostwald process HNO₃ is produced from NH₃ in several steps. First NH₃ reacts with O₂ to form NO and H₂O in an exothermic reaction. In the following exothermic reaction NO₂ is formed out of NO and O₂. Finally HNO₃ is formed by the reaction of NO₂ with O₂ and H₂O. By using the waste heat from the exothermic reactions low pressure steam can be produced and can serve as reactant for the ecMR. Furthermore, the additional production of high pressure steam can be used to drive the compressors required for the separation of the gaseous products of the ecMR. Therefore, the use of the ecMR in a Verbund site may result in a significant increase of the energy efficiency of the overall production process.

7.6. Conclusion

In this chapter, based on the ACM model of the ecMR introduced in Chapter 6, three different alternatives for the downstream process have been developed. Compared to the preliminary results, the specific energy consumption of the entire process has been reduced significantly. In the Haber process natural gas is the main contributor to the energy demand. The NH₃ production costs depend strongly on the feedstock costs. With depletion of natural gas reserves, the production costs of NH₃ will rise. Inevitable, other feedstock has to be used, resulting in a major increase in production costs. Contrary, the reactants of the ecMR are cheap and available in large quantities. However, the NH₃ production costs depend strongly on the price of electricity. Under economic aspects, the ecMR is inferior to the Haber process using natural gas by now. However, the NH₃ synthesis in an ecMR has lower specific energy consumption than the Haber process using coal and no CO₂ emissions occur. Due to the moderate operating conditions, the investment costs of the ecMR might be lower than the costs for a conventional plant for the Haber process. The economic evaluation proves that the electrochemical NH₃ synthesis in an ecMR has potential for economic feasibility. If natural gas reserves run short and

other feedstock, i.e. coal, have to be used, the ecMR has the potential to become the technology-of-choice in future.

7.7. Appendix

7.7.1. Theoretical background gas separation by membranes

The separation mechanism behind the selectivity of a membrane is based on the membrane material. Three different types of membrane material are known: porous membranes, micro-porous membranes, and dense membranes. For gas separation dense membranes are used, which are mostly polymeric. The selectivity of these membranes is based on the solution-diffusion-mechanism. Hereby, the permeability of a component in the membrane material is determined by its solubility and diffusion coefficient [226]:

$$P = S \times D \quad (7.1)$$

Transport through a dense polymeric membrane based on the solution-diffusion model can be described by Equation (7.2) The flux of a component i is dependent on the permeability P , the thickness of the membrane δ and the partial pressures of the components in feed and permeate [226].

$$n_i'' = \frac{P_i}{\delta} (p_{F,i} - p_{P,i}) \quad (7.2)$$

The properties of a polymer are set by its state - whether it is a glassy or a rubbery polymer. Glassy polymers are tough and rigid, whereas rubbery polymers are more flexible, because the polymer segments are capable of rotations around the polymer backbone's axis [219]. The state of a polymer influences the diffusion of gases and consequently the selectivity for different gases. For solution-diffusion based materials a modified selectivity can be defined:

$$\alpha_{i,j} = \frac{S_i}{S_j} \times \frac{D_i}{D_j} \quad (7.3)$$

In general, the diffusion coefficient D decreases with increasing molecule size, since the interactions between molecules and the membrane increase. The decrease in glassy polymers is significantly stronger than in rubbery ones. [226] The solubility of a component is strongly dependent on the interactions between the gas and the membrane. The solubility coefficient S increases with increasing critical temperature, which corresponds to increasing molecule size. Solubilities of glassy and rubbery polymers do not differ significantly. [226] Consequently, the selectivity of glassy membranes is based on the difference in diffusivity between components and favor permeance of small molecules over larger ones. In contrast, the selectivity of rubbery membranes depends on the different solubility of components and larger molecules permeate preferentially.

8. Conclusions & Outlook

∞

8.1. Summary and conclusions

In the present thesis the electrochemical NH₃ synthesis using an electrochemical membrane reactor (ecMR) was investigated. Figure 8.1 gives an overview about the main aspects which have been considered to synthesize NH₃ in an ecMR. An ecMR consists of two compartments, the anodic and the cathodic half-cell, which are separated by a cation exchange membrane (CEM). The core of the ecMR is the membrane electrode assembly (MEA) which consists of two electrodes pressed into the CEM.

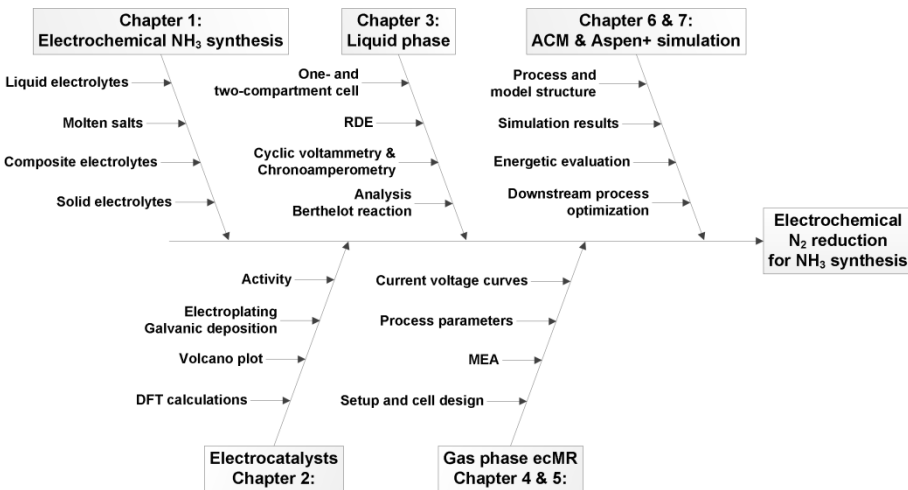


Figure 8.1: Fish bone diagram for the electrochemical NH₃ synthesis

In Chapter 1 the frame conditions are pointed out, why an electrochemical NH₃ synthesis is desirable at all. The state-of-the-art Haber process for large-scale NH₃ synthesis is introduced and its drawbacks are evaluated. The Haber process is one of the largest industrial energy consumers and from an environmental point of view not arguable any more. Therefore, alternative synthesis routes for NH₃ are briefly discussed. The focus is on the electrochemical NH₃ synthesis, where one can distinguish between systems applying liquid, molten salt, composite and solid electrolytes. The electrochemical NH₃ synthesis in an ecMR belongs to the group of solid electrolytes, since a polymer cation exchange membrane is applied in the MEA. In the present thesis an environmentally friendly alternative synthesis process for NH₃ starting from N₂ and H₂O as H⁺ source is proposed. Additionally, renewable energy sources such as wind or solar power can be used to drive the process.

In Chapter 2 the choice of proper electrocatalysts for the electrochemical NH₃ synthesis is discussed and a new galvanic coating process is introduced. Based on density functional theory (DFT) calculations and the resulting volcano plot recently published by Skúlason et al. [66], Ti,

Fe, Rh and Ru were chosen as potential electrocatalysts for the electrochemical NH₃ synthesis. While Ti and Fe were easily accessible in the form of metal plates and randomly structured felts, Rh and Ru catalysts had to be prepared in the laboratory. For that reason, the galvanic deposition of Rh and Ru on Ti felts was investigated and the results were evaluated both from an experimental and an economical point of view. For both metals current efficiencies for the plating process of 93.8% for Rh and 98.7% for Ru were achieved. Both, Rh and Ru showed a high activity for the electrochemical NH₃ synthesis in liquid phase as determined with first linear sweep voltammetry measurements in 0.5 M H₂SO₄ as electrolyte. However, the activity of Ru was around eight times higher compared to Rh and the total costs for a Ru coating were only around 30% of the total costs related to Rh. Therefore, Ru electrodes were further investigated in the ecMR, see Section 5.4.

In Chapter 3 the electrochemical reduction of N₂ was investigated applying a Ti catalyst in liquid phase using 0.5 M H₂SO₄ as electrolyte. Cyclic voltammetry and chronoamperometry measurements using a rotating disk electrode (RDE) were conducted at 30, 50 and 70°C. The results obtained were compared for two different types of electrochemical cells: an one- and a two-compartment cell. In the latter case, the cell was divided in two compartments by an NH₄⁺ modified PTFE membrane. The working and the reference electrode were spatially separated from the counter electrode to prevent undesired parallel reactions of produced NH₃ at the counter electrode. Better results for chronoamperometry measurements at -0.26, -0.46 and -0.66 V vs. NHE were achieved in the two-compartment cell. The analysis of the liquid samples aimed to determine the concentration of formed NH₃ and was performed with a method known as the Berthelot reaction [175]. To evaluate the experiments, the two parameters production rate of NH₃ in mol s⁻¹ cm⁻² and the achieved current efficiency for the electrochemical NH₃ synthesis were applied. The most promising results were obtained at 50°C and -0.46 V vs. NHE being 2.4 × 10⁻¹⁰ mol s⁻¹ cm⁻² and 59.4% after 1 hour experimental time in the two-compartment cell.

In Chapter 4 the materials and methods for the electrochemical NH₃ synthesis in an electrochemical membrane reactor (ecMR) are given. The reactions taking place at the membrane electrode assembly (MEA) are discussed. An electrical potential is applied to the ecMR as driving force. At the anode, IrMMO, a state-of-the-art catalyst for H₂O oxidation, is applied to oxidize H₂O to O₂, H⁺ and e⁻. Due to the applied potential, an electrical field is created. The formed H⁺ migrate through the cation exchange membrane to the cathode, where they react with N₂ to form NH₃. A flow chart of the whole electrochemical setup is presented and the individual parts of the setup are explained. The cell design of the ecMR is shown in detail and the preparation of the MEA as applied in the present thesis is introduced. One important aspect of the present thesis was to determine proper electrocatalysts which can be applied as cathode both in liquid phase and in gas phase in the ecMR. Since the anode and the cathode are coupled with each other by the membrane in the MEA of the ecMR, the applied anodic catalyst IrMMO was characterized separately in liquid phase as well. The overpotential, a parameter for the activity of a catalyst, of 292 mV determined for an IrMMO felt was in agreement with values reported in literature. To get a feeling for problems related to the use of H₂O in an ecMR, water management strategies as developed for polymer electrolyte membrane fuel cells, are briefly presented and discussed.

8 Conclusions & Outlook

In Chapter 5 the results of the electrochemical NH₃ synthesis in gas phase in an electrochemical membrane reactor (ecMR) using Ti as cathodic catalyst are presented. To determine the optimal process parameters, current voltage curves were recorded at three different temperatures of 30, 50 and 70°C at three different relative humidity values of 25, 50 and 95%. Similar to the experiments described earlier, the production rate for NH₃ and the achieved current efficiency were applied to evaluate the achieved results. However, for the ecMR a corrected NH₃ specific current efficiency was determined. Reference measurements with He were carried out at the same process parameters as used for the measurements with N₂. With these reference measurements a characteristic charge for the hydrogen evolution reaction (HER), the main parallel reaction in the ecMR, could be determined for each parameter combination of temperature and relative humidity. By subtracting this characteristic charge for the HER from the total charge measured, an NH₃ specific charge was calculated to determine the corrected NH₃ specific current efficiency. For Ti as cathodic catalyst, the best results were obtained at 50°C, a relative humidity of 15% and an applied potential of -2.2 V. The corresponding production rate was 1.2×10^{-11} mol s⁻¹ cm⁻² and the corrected NH₃ specific current efficiency was 27.5%. As indicated before, also Fe and Ru are potential electrocatalysts for the electrochemical NH₃ synthesis. For a comparison of Ti, Fe and Ru the same experiments as performed with Ti were repeated for Fe and Ru in the ecMR. All catalysts showed a high activity for the electrochemical NH₃ synthesis and the optimal temperature was 50°C for all catalysts. However, Ti showed the best results at a low relative humidity of 15%, Fe at an intermediate relative humidity of 30% and Ru at a high relative humidity of 50%. The calculated current efficiency for Fe was not reliable, since the currents measured for Fe were only in the range of single-digit μA. The overall best results were achieved with Ru at an applied potential of -2.5 V. The corresponding production rate was 2.2×10^{-11} mol s⁻¹ cm⁻² and the corrected NH₃ specific current efficiency was as high as 50.3%. However, one has to consider that the Ru electrode was prepared by an electroplating process on a Ti felt. Thus the combination of Ti and Ru could be a very promising composite catalyst material for future investigations.

In Chapter 6 a complete electrochemical NH₃ synthesis process including N₂ production by cryogenic air separation and gas separation downstream to the ecMR is proposed and modelled in Aspen+. A new model structure of the ecMR was developed in Aspen Custom Modeler and implemented in the complete synthesis process in Aspen+. The model allows taking molecular information from metal cluster and catalysis simulations and turning it into valuable information on the energetic feasibility on a process scale. The presented approach bridges length-scales and is therefore also a valuable tool to benchmark new achievements in catalyst developments. Initially, the downstream gas separation was performed with a 2-stage distillation process, which results in the valuable products NH₃, H₂ and O₂. The energy demand per ton NH₃ produced of the proposed electrochemical process is up to 20% lower than the Haber process using coal as H₂ source. In comparison to the Haber process starting from CH₄, the ecMR process is not yet competitive under today's energy and resource conditions. In the future however, when CH₄ resources will get scarce, the electrochemical NH₃ synthesis might be the technology-of-choice to produce NH₃ in a sustainable and environmentally friendly way.

In Chapter 7 three different alternatives for the downstream gas separation process introduced in Chapter 6 are developed and investigated in Aspen+. The three alternatives are (a) gas separation by cryogenic distillation, (b) gas separation by membranes and (c) gas separation by

a combination of both. The best results with respect to energy efficiency were achieved with alternative (c): cryogenic distillation was used for the separation of NH₃ from the product stream and membranes were applied for the separation of N₂ and H₂. Compared to the preliminary results presented in Chapter 6, the specific energy consumption of the downstream gas separation was reduced by 39.2%, which corresponds to a total decrease of the energy demand of 3.9% for the complete synthesis process. Based on the optimized numbers for the energy demand, an economical evaluation of the modelled process was conducted, which strongly demonstrates the potential of the ecMR for economic feasibility.

In summary, the present thesis demonstrates the proof of principle of the electrochemical NH₃ synthesis in an electrochemical membrane reactor. The presented approach using a membrane electrode assembly comprising IrMNO as anodic catalyst for the oxidation of H₂O, a H⁺ conductive polymer membrane and an active cathodic catalyst such as Ti or Ru for the reduction of N₂ to NH₃ encourages further research of the applied ecMR and MEA system.

8.2. Outlook and future perspectives

In the present thesis, the electrochemical NH₃ synthesis both in liquid and in gas phase was evaluated by the achieved values for the production rate of NH₃ and the reached current efficiency. However, at this early stage of research of the electrochemical NH₃ synthesis, the focus has to be on increasing the achieved current efficiency. For that reason it is mandatory to analyze the composition of the product stream leaving the ecMR in more detail. In the present thesis, the focus was on determining the concentration of formed NH₃ dissolved in H₂SO₄ with the Berthelot reaction. However, the amount of produced H₂ was not measured. The implementation of a gas chromatograph to analyze the gas stream leaving the ecMR is the most accurate possibility to determine the amount of produced H₂. Besides the analysis of the cathodic gas stream, also the anodic gas stream can be analyzed to determine the amount of produced O₂. In doing so, a closed mass balance can be established. The amount of H₂O supplied to the ecMR is known, thus the theoretical amount of produced O₂ and an anodic conversion rate can be calculated. For each mole of O₂ four moles H⁺ and four moles e⁻ are formed at the same time. Consequently, for each mol of O₂ two moles of H₂ can be formed at the maximum at the cathode. A cathodic conversion rate for H₂ and NH₃ can be determined as well. Besides the NH₃ specific current efficiency also the current efficiency for H₂ can be calculated. If the sum of both values is less than 100%, the electrical losses occurring in the complete ecMR and MEA system can be determined as well.

There are several ways to improve the achieved production rate and current efficiency of the ecMR. First of all the specific surface area of the applied catalysts need to be increased. For that reason particle synthesis of proper electrocatalysts need to be considered to replace the randomly structured metal felts applied in the present thesis by catalyst powders. The design and the preparation of the MEA need to be adjusted accordingly. Another advantage of applying catalyst particles instead of catalyst felts is, that the ratio of for instance two components of a binary catalyst can easily be changed and thus the properties of the investigated catalyst. In another approach the type and thus the properties of the applied membrane can be changed. One possibility is the use of polybenzimidazole (PBI) membranes instead of PTFE based cation exchange membranes. Since PBI membranes show H⁺ conductivity without H₂O needed for the

8 Conclusions & Outlook

transport mechanism, problems related to flooding of the cathodic compartment or blocking of active sites of the cathodic catalyst can be reduced. However, PBI membranes require pretreatment with phosphoric acid, to which Ti is not corrosion resistant. Thus, either the cell design or the cell material needs to be optimized. Finally, the cathodic catalyst can be further optimized or other catalysts can be tested. Studies in literature show high activity for instance of Ag or Pd catalysts. Nevertheless, the results obtained in the present thesis are very promising to encourage further investigation and optimization of the applied Ti and Ru catalysts.

From an experimental point of view, the optimal process parameters can further be narrowed down. Additionally, further aspects such as the application of higher pressure both at the anode and at the cathode and the pressure ratio between the anodic and the cathodic pressure can be considered as well. To find new electrocatalysts for the electrochemical NH₃ synthesis, experiments with a rotating disk electrode in liquid phase should be further investigated. Besides the catalysis research, also the electrochemical NH₃ synthesis itself in newly designed liquid phase setups is a versatile field of research. Finally, to get a better understanding of the complete synthesis process and of the reactions taking place in the ecMR, further simulation studies need to be conducted.

In summary, all the results obtained in the different fields of research - catalysis, liquid phase synthesis, gas phase synthesis in the ecMR and theoretical investigations using Aspen Custom Modeler and Aspen+ - presented in the present thesis encourage further research to make the electrochemical NH₃ synthesis the technology-of-choice in the future for the sustainable and environmentally friendly synthesis of NH₃.

References

- [1] BP, BP Statistical Review of World Energy, 2014.
- [2] Gesellschaft Deutscher Chemiker e.V. (GDCh), Gesellschaft für Chemische Technik und Biotechnologie e.V. (DECHEMA), Deutsche Wissenschaftliche Gesellschaft für Erdöl Erdgas und Kohle e.V. (DGMK), Verband der Chemischen Industrie e.V. (VCI), Positionspapier - Rohstoffbasis im Wandel, 2010.
- [3] V. Smil, Detonator of the population explosion, *Nature*. 400 (1999) 415.
- [4] U.S. Department of the Interior, U.S. Geological Survey, Mineral Commodity Summaries, 2014.
- [5] E. Riedel, Anorganische Chemie, 6th ed., Walter de Gruyter, Berlin, New York, 2004.
- [6] C. Zamfirescu, I. Dincer, Using ammonia as a sustainable fuel, *J. Power Sources*. 185 (2008) 459–465.
- [7] R. Lan, J.T.S. Irvine, S. Tao, Ammonia and related chemicals as potential indirect hydrogen storage materials, *Int. J. Hydrogen Energy*. 37 (2012) 1482–1494.
- [8] R. Lan, S. Tao, Ammonia Carbonate Fuel Cells Based on a Mixed NH₄⁺/H⁺ Ion Conducting Electrolyte, *ECS Electrochem. Lett.* 2 (2013) F37–F40.
- [9] M. Carmo, D.L. Fritz, J. Mergel, D. Stolten, A comprehensive review on PEM water electrolysis, *Int. J. Hydrogen Energy*. 38 (2013) 4901–4934.
- [10] S. Giddey, S.P.S. Badwal, A. Kulkarni, Review of electrochemical ammonia production technologies and materials, *Int. J. Hydrogen Energy*. 38 (2013) 14576–14594.
- [11] R.M. Heck, Catalytic abatement of nitrogen oxides—stationary applications, *Catal. Today*. 53 (1999) 519–523.

References

- [12] M. Appl, Ammonia, in: Ullmann's Encycl. Ind. Chem., Wiley-VCH Verlag GmbH & Co. KGaA, Weinheim, 2006.
- [13] IEA, Tracking Industrial Energy Efficiency and CO₂ Emissions, 2007.
- [14] I. Rafiqul, C. Weber, B. Lehmann, A. Voss, Energy efficiency improvements in ammonia production - perspectives and uncertainties, *Energy*. 30 (2005) 2487–2504.
- [15] K. Kugler, B. Ohs, M. Scholz, M. Wessling, Towards a carbon independent and CO₂-free electrochemical membrane process for NH₃ synthesis., *Phys. Chem. Chem. Phys.* 16 (2014) 6129–6138.
- [16] J.W. Erisman, M.A. Sutton, J. Galloway, Z. Klimont, W. Winiwarter, How a century of ammonia synthesis changed the world, *Nat. Geosci.* 1 (2008) 636–639.
- [17] F. Haber, G. van Oordt, Über die Bildung von Ammoniak aus den Elementen., *Z. Anorg. Chem.* 44 (1905).
- [18] H. Robel, G. Adolphi, S. Kattanek, H.-J. Kecke, K.-E. Militzer, M. Mittelstrass, et al., Lehrbuch der chemischen Verfahrenstechnik, 4th ed., VEB Deutscher Verlag für Grundstoffindustrie, 1967.
- [19] J. Hagen, Industrial Catalysis, Wiley-VCH Verlag GmbH & Co. KGaA, Weinheim, 2006.
- [20] M. Baerns, A. Behr, A. Brehm, J. Gmehling, H. Hofmann, U. Onken, et al., Technische Chemie, Wiley-VCH Verlag GmbH & Co. KGaA, Weinheim, 2006.
- [21] W. Ramsay, S. Young, XIV.-The Decomposition of Ammonia by Heat, *J. Chem. Soc., Trans.* 45 (1884) 88–93.
- [22] C.A.C. Sequeira, D.M.F. Santos, Electrochemical Routes for Industrial Synthesis, 20 (2009) 387–406.
- [23] A.S. Agarwal, Y. Zhai, D. Hill, N. Sridhar, The electrochemical reduction of carbon dioxide to formate/formic acid: engineering and economic feasibility., *ChemSusChem*. 4 (2011) 1301–1310.
- [24] C.H. Hamann, W. Vielstich, Elektrochemie, Wiley-VCH Verlag GmbH, Weinheim, 1998.
- [25] G.C. Chinchen, P.J. Denny, D.G. Parker, M.S. Spencer, D.A. Whan, Mechanism of Methanol Synthesis from CO₂/CO/H₂ Mixtures over Copper/Zinc Oxide/Alumina Catalysts: Use of ¹⁴C-Labelled Reactants, *Appl. Catal.* 30 (1987) 333–338.

- [26] S.M.A. Kriescher, K. Kugler, S.S. Hosseiny, Y. Gendel, M. Wessling, A membrane electrode assembly for the electrochemical synthesis of hydrocarbons from CO_{2(g)} and H₂O_(g), *Electrochim. Commun.* 50 (2015) 64–68.
- [27] B.A. Frontana-Uribe, R.D. Little, J.G. Ibanez, A. Palma, R. Vasquez-Medrano, Organic electrosynthesis: a promising green methodology in organic chemistry, *Green Chem.* 12 (2010) 2099–2119.
- [28] Tailor-Made Fuels from Biomass, (2007). www.fuelcenter.rwth-aachen.de (accessed January 22, 2015).
- [29] J. Zakzeski, P.C.A. Bruijnincx, A.L. Jongerius, B.M. Weckhuysen, The catalytic valorization of lignin for the production of renewable chemicals., *Chem. Rev.* 110 (2010) 3552–99.
- [30] H. Hodson, Out of thin air, *New Sci.* (2013) 22.
- [31] U. Onken, A. Behr, *Chemische Prozesskunde*, G. Thieme, 1996.
- [32] V. Hopp, *Grundlagen der chemischen Technologie*, Wiley-VCH Verlag GmbH, Weinheim, 2001.
- [33] V. Smil, Nitrogen cycle and world food production, *World Agric.* (2011) 9–13.
- [34] V. Smil, Global Population and the Nitrogen Cycle, *Sci. Am.* (1997).
- [35] P.A. Østergaard, Comparing electricity, heat and biogas storages' impacts on renewable energy integration, *Energy*. 37 (2012) 255–262.
- [36] A. Züttel, A. Remhof, A. Borgschulte, O. Friedrichs, Hydrogen: the future energy carrier., *Philos. Trans. A. Math. Phys. Eng. Sci.* 368 (2010) 3329–42.
doi:10.1098/rsta.2010.0113.
- [37] Deutscher Wasserstoff- und Brennstoffzellen-Verband e.V. (DWV), Energietabelle für die Umrechnung verschiedener Energieeinheiten und -äquivalente, (n.d.).
http://www.dwv-info.de/wissen/tabellen/wiss_enr.html (accessed January 20, 2015).
- [38] The Engineering ToolBox, Gross Combustion Value for some common Materials, (n.d.). http://www.engineeringtoolbox.com/combustion-values-d_411.html (accessed January 20, 2015).
- [39] T. Hejze, J.O. Besenhard, K. Kordes, M. Cifrain, R.R. Aronsson, Current status of combined systems using alkaline fuel cells and ammonia as a hydrogen carrier, *J. Power Sources*. 176 (2008) 490–493.

References

- [40] A. Fuerte, R.X. Valenzuela, M.J. Escudero, L. Daza, Ammonia as efficient fuel for SOFC, *J. Power Sources.* 192 (2009) 170–174.
- [41] L. Zhang, W. Yang, Direct ammonia solid oxide fuel cell based on thin proton-conducting electrolyte, *J. Power Sources.* 179 (2008) 92–95.
- [42] W.H. Avery, A Role for Ammonia in the Hydrogen Economy, *Int. J. Hydrog. Energy.* 13 (1988) 761–773.
- [43] C.H. Christensen, T. Johannessen, R.Z. Sørensen, J.K. Nørskov, Towards an ammonia-mediated hydrogen economy?, *Catal. Today.* 111 (2006) 140–144.
- [44] U.S. Department of Energy, Potential Roles of Ammonia in a Hydrogen Economy, 2006.
- [45] A. Klerke, C.H. Christensen, J.K. Nørskov, T. Vegge, Ammonia for hydrogen storage: challenges and opportunities, *J. Mater. Chem.* 18 (2008) 2304–2310.
- [46] M. Appl, Ammonia: Principles and Industrial Practice, Wiley-VCH Verlag GmbH, Weinheim, 1999.
- [47] C.H. Christensen, R.Z. Sørensen, T. Johannessen, U.J. Quaade, K. Honkala, T.D. Elmøe, et al., Metal ammine complexes for hydrogen storage, *J. Mater. Chem.* 15 (2005) 4106–4108.
- [48] T.D. Elmøe, R.Z. Sørensen, U. Quaade, C.H. Christensen, J.K. Nørskov, T. Johannessen, A high-density ammonia storage/delivery system based on $Mg(NH_3)_6Cl_2$ for SCR-DeNO_x in vehicles, *Chem. Eng. Sci.* 61 (2006) 2618–2625.
- [49] A. Skodra, M. Ouzounidou, M. Stoukides, NH₃ decomposition in a single-chamber proton conducting cell, *Solid State Ionics.* 177 (2006) 2217–2220.
- [50] S. Zisekas, G. Karagiannakis, G. Marnellos, M. Stoukides, Study of ammonia decomposition in a proton conducting solid electrolyte cell, *Ionics (Kiel).* 8 (2002) 118–122.
- [51] G.E. Pitselis, P.D. Petrolekas, C.G. Vayenas, Electrochemical promotion of ammonia decomposition over Fe catalyst films interfaced with K⁺- & H⁺- conductors, *Ionics (Kiel).* 3 (1997) 110–116.
- [52] F. Vitse, M. Cooper, G.G. Botte, On the use of ammonia electrolysis for hydrogen production, *J. Power Sources.* 142 (2005) 18–26.
- [53] G.G. Botte, M. Muthuvel, Electrochemical Energy Storage: Applications, Processes, and Trends, in: *Handb. Ind. Chem. Biotechnol.*, Springer Science+Business Media New York, 2012.

- [54] A.E. Shilov, Catalytic reduction of dinitrogen in protic media: chemical models of nitrogenase, *J. Mol. Catal.* 41 (1987) 221–234.
- [55] F. Tuczek, Synthetische vs . biologische Stickstoff-Fixierung, *Nachrichten Aus Der Chemie.* (2006) 1190–1194.
- [56] M.E. Vol'pin, V.B. Shur, Nitrogen Fixation by Transition Metal Complexes, *Nature.* 209 (1966) 1236.
- [57] E. Bayer, V. Schurig, Stickstoff-Fixierung und Reduktion zu Ammoniak mit metall-organischen Katalysatoren, 3390 (1969) 3378–3390.
- [58] C.J. Pickett, The Chatt cycle and the mechanism of enzymic reduction of molecular nitrogen, *J. Biol. Inorg. Chem.* 1 (1996) 601–606.
- [59] D.V. Yandulov, R.R. Schrock, Catalytic reduction of dinitrogen to ammonia at a single molybdenum center., *Science.* 301 (2003) 76–78.
- [60] S. Hinrichsen, H. Broda, C. Gradert, L. Söncksen, F. Tuczek, Recent developments in synthetic nitrogen fixation, *Annu. Rep. Prog. Chem., Sect. A Inorg. Chem.* 108 (2012) 17–47.
- [61] G.N. Schrauzer, T.D. Guth, Photolysis of Water and Photoreduction of Nitrogen on Titanium Dioxide, *J. Am. Chem. Soc.* 99 (1977) 7189–7193.
- [62] H. Miyama, N. Fujii, Y. Nagae, Heterogeneous Photocatalytic synthesis of ammonia from water and nitrogen, *Chem. Phys. Lett.* 74 (1980) 523–524.
- [63] K. Tennakone, C.A.N. Fernando, S. Wickramanayake, M.W.P. Damayanthi, L.H.K. Silva, W. Wijeratne, et al., Photocatalytic reduction of nitrogen to ammonia with coprecipitated Fe(III) and Ti(IV) hydrous oxides, *Sol. Energy Mater.* 17 (1988) 47–53.
- [64] V. Schmidt, *Elektrochemische Verfahrenstechnik*, Wiley-VCH Verlag GmbH & KGaA, Weinheim, 2003.
- [65] A. Hellman, K. Honkala, I.N. Remediakis, Á. Logadóttir, A. Carlsson, S. Dahl, et al., Ammonia synthesis and decomposition on a Ru-based catalyst modeled by first-principles, *Surf. Sci.* 603 (2009) 1731–1739.
- [66] E. Skúlason, T. Bligaard, S. Gudmundsdóttir, F. Studt, J. Rossmeisl, F. Abild-Pedersen, et al., A theoretical evaluation of possible transition metal electro-catalysts for N₂ reduction., *Phys. Chem. Chem. Phys.* 14 (2012) 1235–1245.
- [67] J. Tafel, Über die Polarisierung bei kathodischer Wasserstoffentwicklung, *Zeitschrift Für Phys. Chemie, Stöchiometrie Und Verwandschaftslehre.* 50 (1905) 641–712.

References

- [68] J. Heyrovsky, A Theory of Overpotential, *Recl. Des Trav. Chim. Des Pays-Bas.* 46 (1927) 582–585.
- [69] G.P. Haight, R. Scott, Molybdate- and Tungstate-Catalyzed Fixation of Nitrogen, *J. Am. Chem. Soc.* 86 (1964) 743–744.
- [70] E.E. van Tamelen, B. Akermark, Electrolytic reduction of molecular nitrogen, *J. Am. Chem. Soc.* 90 (1968) 4492–4493.
- [71] E.E. van Tamelen, D.A. Seeley, The Catalytic Fixation of Molecular Nitrogen by Electrolytic and Chemical Reduction, *J. Am. Chem. Soc.* 91 (1969) 5194.
- [72] A.V. Gorodyskii, V.V. Danilin, O.N. Efimov, N.E. Nechaeva, V.N. Tsarev, Electrocatalytic properties of the $\text{Ti}(\text{OH})_3\text{-Mo(III)}$ system in the reduction of molecular nitrogen, *React. Kinet. Catal. Lett.* 11 (1979) 337–342.
- [73] A. Sclafani, V. Augugliaro, M. Schiavello, Dinitrogen Electrochemical Reduction to Ammonia over Iron Cathode in Aqueous Medium, *J. Electrochem. Soc.* 130 (1983) 734–736.
- [74] N. Furuya, H. Yoshioka, Electroreduction of nitrogen to ammonia on gas-diffusion electrodes modified by Fe-phthalocyanine, *J. Electroanal. Chem. Interfacial Electrochem.* 263 (1989) 171–174.
- [75] N. Furuya, H. Yoshioka, Electroreduction of nitrogen to ammonia on gas-diffusion electrodes modified by metal phthalocyanines, *J. Electroanal. Chem. Interfacial Electrochem.* 272 (1989) 263–266.
- [76] N. Furuya, H. Yoshioka, Electroreduction of nitrogen to ammonia on gas-diffusion electrodes loaded with inorganic catalyst, *J. Electroanal. Chem. Interfacial Electrochem.* 291 (1990) 269–272.
- [77] A. Tsuneto, A. Kudo, T. Sakata, Efficient Electrochemical Reduction of N_2 to NH_3 catalyzed by Lithium, *Chem. Lett.* (1993) 851–854.
- [78] A. Tsuneto, A. Kudo, T. Sakata, Lithium-mediated electrochemical reduction of high pressure N_2 to NH_3 , *J. Electroanal. Chem.* 367 (1994) 183–188.
- [79] T.M. Pappenfus, K. Lee, L.M. Thoma, C.R. Dukart, Wind to Ammonia: Electrochemical Processes in Room Temperature Ionic Liquids, *ECS Trans.* 16 (2009) 89–93.
- [80] F. Köleli, T. Röpke, Electrochemical hydrogenation of dinitrogen to ammonia on a polyaniline electrode, *Appl. Catal. B Environ.* 62 (2006) 306–310.
- [81] F. Köleli, D.B. Kayan, Low overpotential reduction of dinitrogen to ammonia in aqueous media, *J. Electroanal. Chem.* 638 (2010) 119–122.

- [82] Y. Ito, T. Goto, The electrochemical reduction of N₂ Gas and its application to energy systems, in: Proc. 32nd Intersoc. Energy Convers. Eng. Conf., 1997: pp. 787–792.
- [83] T. Murakami, T. Nishikiori, T. Nohira, Y. Ito, Electrolytic synthesis of ammonia in molten salts under atmospheric pressure., J. Am. Chem. Soc. 125 (2003) 334–335.
- [84] T. Murakami, T. Nohira, Y.H. Ogata, Y. Ito, Electrochemical Synthesis of Ammonia and Coproduction of Metal Sulfides from Hydrogen Sulfide and Nitrogen under Atmospheric Pressure, J. Electrochem. Soc. 152 (2005) D109–D112.
- [85] T. Murakami, T. Nohira, T. Goto, Y.H. Ogata, Y. Ito, Electrolytic ammonia synthesis from water and nitrogen gas in molten salt under atmospheric pressure, Electrochim. Acta. 50 (2005) 5423–5426.
- [86] T. Murakami, T. Nohira, Y.H. Ogata, Y. Ito, Electrolytic Ammonia Synthesis in Molten Salts under Atmospheric Pressure Using Methane as a Hydrogen Source, Electrochem. Solid-State Lett. 8 (2005) D12–D14.
- [87] T. Murakami, T. Nohira, Y. Araki, T. Goto, R. Hagiwara, Y.H. Ogata, Electrolytic Synthesis of Ammonia from Water and Nitrogen under Atmospheric Pressure Using a Boron-Doped Diamond Electrode as a Nonconsumable Anode, Electrochim. Solid-State Lett. 10 (2007) E4–E6.
- [88] S. Licht, B. Cui, B. Wang, F.-F. Li, J. Lau, S. Liu, Ammonia synthesis by N₂ and steam electrolysis in molten hydroxide suspensions of nanoscale Fe₂O₃, Science. 345 (2014) 637–640.
- [89] B.H. Wang, J.D. Wang, R.Q. Liu, Y.H. Xie, Z.J. Li, Synthesis of ammonia from natural gas at atmospheric pressure with doped ceria–Ca₃(PO₄)₂–K₃PO₄ composite electrolyte and its proton conductivity at intermediate temperature, J. Solid State Electrochem. 11 (2005) 27–31.
- [90] I.A. Amar, R. Lan, C.T.G. Petit, V. Arrighi, S. Tao, Electrochemical synthesis of ammonia based on a carbonate-oxide composite electrolyte, Solid State Ionics. 182 (2011) 133–138.
- [91] I.A. Amar, C.T.G. Petit, L. Zhang, R. Lan, P.J. Skabara, S. Tao, Electrochemical synthesis of ammonia based on doped-ceria-carbonate composite electrolyte and perovskite cathode, Solid State Ionics. 201 (2011) 94–100.
- [92] I.A. Amar, C.T.G. Petit, G. Mann, R. Lan, P.J. Skabara, S. Tao, Electrochemical synthesis of ammonia from N₂ and H₂O based on (Li_xNa_yK_z)₂CO₃–Ce_{0.8}Gd_{0.18}Ca_{0.02}O_{2-δ} composite electrolyte and CoFe₂O₄ cathode, Int. J. Hydrogen Energy. 39 (2014) 4322–4330.

References

- [93] I.A. Amar, C.T.G. Petit, R. Lan, G. Mann, S. Tao, Electrochemical synthesis of ammonia from wet nitrogen using $\text{La}_{0.6}\text{Sr}_{0.4}\text{FeO}_{3-\delta}-\text{Ce}_{0.8}\text{Gd}_{0.18}\text{Ca}_{0.02}\text{O}_{2-\delta}$ composite cathode, *RSC Adv.* 4 (2014) 18749–18754.
- [94] R. Lan, K.A. Alkhazmi, I.A. Amar, S. Tao, Synthesis of ammonia directly from wet air at intermediate temperature, *Appl. Catal. B Environ.* 152–153 (2014) 212–217.
- [95] R. Lan, K.A. Alkhazmi, I.A. Amar, S. Tao, Synthesis of ammonia directly from wet air using new perovskite oxide $\text{La}_{0.8}\text{Cs}_{0.2}\text{Fe}_{0.8}\text{Ni}_{0.2}\text{O}_{3-\delta}$ as catalyst, *Electrochim. Acta* 123 (2014) 582–587.
- [96] I.A. Amar, R. Lan, C.T.G. Petit, S. Tao, Solid-state electrochemical synthesis of ammonia: a review, *J Solid State Electrochem.* 15 (2011) 1845–1860.
- [97] I. Garagounis, V. Kyriakou, A. Skodra, E. Vasileiou, M. Stoukides, Electrochemical Synthesis of Ammonia in Solid Electrolyte Cells, *Front. Energy Res.* 2 (2014) 1–10.
- [98] M. Stoukides, Solid-Electrolyte Membrane Reactors: Current Experience and Future Outlook, *Catal. Rev.* 42 (2000) 1–70.
- [99] G. Marnellos, M. Stoukides, Ammonia Synthesis at Atmospheric Pressure, *Science*. 282 (1998) 98–100.
- [100] A. Skodra, M. Stoukides, Electrocatalytic synthesis of ammonia from steam and nitrogen at atmospheric pressure, *Solid State Ionics*. 180 (2009) 1332–1336.
- [101] Y.-H. Xie, J.-D. Wang, R.-Q. Liu, X.-T. Su, Z.-P. Sun, Z.-J. Li, Preparation of $\text{La}_{1.9}\text{Ca}_{0.1}\text{Zr}_2\text{O}_{6.95}$ with pyrochlore structure and its application in synthesis of ammonia at atmospheric pressure, *Solid State Ionics*. 168 (2004) 117–121.
- [102] Z.-J. Li, R.-Q. Liu, Y.-H. Xie, S. Feng, J.-D. Wang, A novel method for preparation of doped $\text{Ba}_3(\text{Ca}_{1.18}\text{Nb}_{1.82})\text{O}_{9-\delta}$: Application to ammonia synthesis at atmospheric pressure, *Solid State Ionics*. 176 (2005) 1063–1066.
- [103] Z.-J. Li, R.-Q. Liu, J.-D. Wang, Y.-H. Xie, F. Yue, Preparation of $\text{BaCe}_{0.8}\text{Gd}_{0.2}\text{O}_{3-\delta}$ by the citrate method and its application in the synthesis of ammonia at atmospheric pressure.pdf, *J Solid State Electrochem.* 9 (2005) 201–204.
- [104] J.-D. Wang, Y.-H. Xie, Z.-F. Zhang, R.-Q. Liu, Z.-J. Li, Protonic conduction in Ca^{2+} -doped $\text{La}_2\text{M}_2\text{O}_7$ ($\text{M}=\text{Ce}, \text{Zr}$) with its application to ammonia synthesis electrochemically, *Mater. Res. Bull.* 40 (2005) 1294–1302.
- [105] R.-Q. Liu, Y.-H. Xie, J.-D. Wang, Z.-J. Li, B.-H. Wang, Synthesis of ammonia at atmospheric pressure with $\text{Ce}_{0.8}\text{M}_{0.2}\text{O}_{2-\delta}$ ($\text{M}=\text{La}, \text{Y}, \text{Gd}, \text{Sm}$) and their proton conduction at intermediate temperature, *Solid State Ionics*. 177 (2006) 73–76.

- [106] Z.-J. Li, R.-Q. Liu, J.-D. Wang, Z. Xu, Y.-H. Xie, B.-H. Wang, Preparation of double-doped BaCeO₃ and its application in the synthesis of ammonia at atmospheric pressure, *Sci. Technol. Adv. Mater.* 8 (2007) 566–570.
- [107] M. Ouzounidou, A. Skodra, C. Kokkofitis, M. Stoukides, Catalytic and electrocatalytic synthesis of NH₃ in a H⁺ conducting cell by using an industrial Fe catalyst, *Solid State Ionics*. 178 (2007) 153–159.
- [108] Y. Guo, B. Liu, Q. Yang, C. Chen, W. Wang, G. Ma, Preparation via microemulsion method and proton conduction at intermediate-temperature of BaCe_{1-x}Y_xO_{3-a}, *Electrochim Commun.* 11 (2009) 153–156.
- [109] W.B. Wang, X.B. Cao, W.J. Gao, F. Zhang, H.T. Wang, G.L. Ma, Ammonia synthesis at atmospheric pressure using a reactor with thin solid electrolyte BaCe_{0.85}Y_{0.15}O_{3-a} membrane, *J. Memb. Sci.* 360 (2010) 397–403.
- [110] R.L. Cook, A.F. Sammells, Ambient temperature gas phase electrochemical nitrogen reduction to ammonia at ruthenium / solid polymer electrolyte interface, *Catal. Letters*. 1 (1988) 345–349.
- [111] V. Kordali, G. Kyriacou, C. Lambrou, Electrochemical synthesis of ammonia at atmospheric pressure and low temperature in a solid polymer electrolyte cell, *Chem Commun.* (2000) 1673–1674.
- [112] G. Xu, R. Liu, Sm_{1.5}Sr_{0.5}MO₄ (M=Ni, Co, Fe) Cathode Catalysts for Ammonia Synthesis at Atmospheric Pressure and Low Temperature, *Chin. J. Chem.* 27 (2009) 677–680.
- [113] G. Xu, R. Liu, J. Wang, Electrochemical synthesis of ammonia using a cell with a Nafion membrane and SmFe_{0.7}Cu_{0.3-x}Ni_xO₃ (x = 0–0.3) cathode at atmospheric pressure and lower temperature, *Sci. China Ser. B Chem.* 52 (2009) 1171–1175.
- [114] R. Liu, G. Xu, Comparison of Electrochemical Synthesis of Ammonia by Using Sulfonated Polysulfone and Nafion Membrane with Sm_{1.5}Sr_{0.5}NiO₄, *Chin. J. Chem.* 28 (2010) 139–142.
- [115] Z. Zhang, Z. Zhong, R. Liu, Cathode catalysis performance of SmBaCuMO_{5+δ} (M=Fe, Co, Ni) in ammonia synthesis.pdf, *J. Rare Earths.* 28 (2010) 556–559.
- [116] R. Lan, J.T.S. Irvine, S. Tao, Synthesis of ammonia directly from air and water at ambient temperature and pressure, *Sci. Rep.* 3 (2013) 1–7.
- [117] R. Lan, S. Tao, Electrochemical synthesis of ammonia directly from air and water using a Li⁺/H⁺/NH₄⁺ mixed conducting electrolyte, *RSC Adv.* 3 (2013) 18016–18021.

References

- [118] E.M. Gabreab, G. Hinds, S. Fearn, D. Hodgson, J. Millichamp, P.R. Shearing, et al., An electrochemical treatment to improve corrosion and contact resistance of stainless steel bipolar plates used in polymer electrolyte fuel cells, *J. Power Sources.* 245 (2014) 1014–1026.
- [119] J. Matthew J. Donachie, *Titanium - A Technical Guide*, ASM International, 2000.
- [120] Huazhang Liu, *Ammonia Synthesis Catalysts - Innovation and Practice*, World Scientific Publishing Co. Pte. Ltd., 2013.
- [121] M. Kitano, Y. Inoue, Y. Yamazaki, F. Hayashi, S. Kanbara, S. Matsuishi, et al., Ammonia synthesis using a stable electride as an electron donor and reversible hydrogen store., *Nat. Chem.* 4 (2012) 934–940.
- [122] M. Schlesinger, M. Paunovic, eds., *Modern Electroplating*, John Wiley & Sons, Inc., Hoboken, New Jersey, USA, 2010.
- [123] T.M. Manhabosco, I.L. Muller, Electrodeposition of diamond-like carbon (DLC) films on Ti, *Appl. Surf. Sci.* 255 (2009) 4082–4086.
- [124] G.F. Ortiz, M.C. López, R. Alcántara, J.L. Tirado, Electrodeposition of copper–tin nanowires on Ti foils for rechargeable lithium micro-batteries with high energy density, *J. Alloys Compd.* 585 (2014) 331–336.
- [125] R.G. Allen, C. Lim, L.X. Yang, K. Scott, S. Roy, Novel anode structure for the direct methanol fuel cell, *J. Power Sources.* 143 (2005) 142–149.
- [126] A.A. Pasa, M.L. Munford, Electrodeposition, in: *Encycl. Chem. Process.*, Taylor & Francis Group, New York, USA, 2006.
- [127] T. Bergstresser, H. Merchant, Surface Morphology of Electrodeposits, in: H. Merchant (Ed.), *Defect Struct. Morphol. Prop. Depos.*, The Minerals, Metals & Materials Society, 1995.
- [128] M. Paunovic, M. Schlesinger, eds., *Metal Deposit and Current Distribution*, in: *Fundam. Electrochem. Depos.*, John Wiley & Sons, Inc., Hoboken, New Jersey, USA, 2006.
- [129] Y. Yao, Functions of Chloride in Copper-Refining Electrolyte, *Trans. Electrochem. Soc.* 86 (1944) 371–382.
- [130] S.C. Barnes, Cathode polarization and the growth habit of electrodeposited copper, *Electrochim. Acta.* 5 (1961) 79–86.
- [131] F.H. Reid, Electrodeposition of the Platinum-Group Metals, in: *Gmelin Handb. Inorg. Chem. Syst. Number 68. Pt, Platinum. Technol. Platinum-Gr. Met.*, Springer, 1986: pp. 66–91.

- [132] M. Paunovic, M. Schlesinger, Kinetics and Mechanism of Electrodeposition, in: M. Paunovic, M. Schlesinger (Eds.), Fundam. Electrochem. Depos., John Wiley & Sons, Inc., Hoboken, New Jersey, USA, 2006.
- [133] J.B. Mohler, Electroplating and Related Processes, Chemical Publishing Co., Inc. New York, 1969.
- [134] M. Pushpavanam, V. Raman, B.A. Shenoi, Rhodium - Electrodeposition and applications, *Surf. Technol.* 12 (1981) 351–360.
- [135] www.agosi.de, Price Raw Materials Rh and Ru, (2014), www.agosi.de, (accessed April 11, 2014).
- [136] P.D. Buchanan, Electroplating the Platinum Metals, *Platin. Met. Rev.* 25 (1981) 32–41.
- [137] E.R. Thews, Zur Galvanotechnik des Rhodium, *Metalloberfläche*. 10 (1956) 85–89.
- [138] F.H. Reid, Electrodeposition of the Platinum-Group Metals, *Metall. Rev.* 8 (1963) 167–211.
- [139] L. Serota, Science for Electroplaters - Rhodium Baths, *Met. Finish.* 64 (1966) 82–84.
- [140] A.M. Baraka, H.H. Shaarawy, H.A. Hamed, Electrodeposition of rhodium metal on titanium substrates, *Anti-Corrosion Methods Mater.* 49 (2002) 277–282.
- [141] K. Schumpelt, Electrodeposition of the Metals of the Platinum Group, *Trans. Electrochem. Soc.* 80 (1941) 489–498.
- [142] O. Brylev, L. Roué, D. Bélanger, Rhodium electrodeposition on pyrolytic graphite electrode: Analysis of chronoamperometric curves, *J. Electroanal. Chem.* 581 (2005) 22–30.
- [143] O. Brylev, M. Sarrazin, D. Bélanger, L. Roué, Rhodium deposits on pyrolytic graphite substrate: Physico-chemical properties and electrocatalytic activity towards nitrate reduction in neutral medium, *Appl. Catal. B Environ.* 64 (2006) 243–253.
- [144] O. Brylev, M. Sarrazin, L. Roué, D. Bélanger, Nitrate and nitrite electrocatalytic reduction on Rh-modified pyrolytic graphite electrodes, *Electrochim. Acta*. 52 (2007) 6237–6247.
- [145] R.T.S. Oliveira, M.C. Santos, L.O.S. Bulhões, E.C. Pereira, Rh electrodeposition on Pt in acidic medium: a study using cyclic voltammetry and an electrochemical quartz crystal microbalance, *J. Electroanal. Chem.* 569 (2004) 233–240.

References

- [146] J. Inukai, M. Ito, Electrodeposition processes of palladium and rhodium monolayers on Pt(111) and Pt(100) electrodes studied by IR reflection absorption spectroscopy, *J. Electroanal. Chem.* 358 (1993) 307–315.
- [147] F.J. Gutiérrez de Dios, R. Gómez, J.M. Feliu, Preparation and electrocatalytic activity of Rh adlayers on Pt(100) electrodes: reduction of nitrous oxide, *Electrochim. Commun.* 3 (2001) 659–664.
- [148] R. Gómez, J.M. Feliu, Rhodium adlayers on Pt(111) monocrystalline surfaces. Electrochemical behavior and electrocatalysis, *Electrochim. Acta* 44 (1998) 1191–1205.
- [149] M. Arbib, B. Zhang, V. Lazarov, D. Stoychev, A. Milchev, C. Buess-Herman, Electrochemical nucleation and growth of rhodium on gold substrates, *J. Electroanal. Chem.* 510 (2001) 67–77.
- [150] M. Jayakumar, K.A. Venkatesan, T.G. Srinivasan, Electrochemical behavior of rhodium(II) in 1-butyl-3-methylimidazolium chloride ionic liquid, *Electrochim. Acta* 53 (2008) 2794–2801.
- [151] M. Jayakumar, K.A. Venkatesan, R. Sudha, T.G. Srinivasan, P.R. Vasudeva Rao, Electrodeposition of ruthenium, rhodium and palladium from nitric acid and ionic liquid media: Recovery and surface morphology of the deposits, *Mater. Chem. Phys.* 128 (2011) 141–150.
- [152] M. Vukovic, Electrochemical investigation of an electrodeposited rhodium electrode in acid solutions, *J. Electroanal. Chem.* 242 (1988) 97–105.
- [153] M. Vukovic, D. Cukman, Enhanced oxygen evolution on an electrodeposited and activated rhodium electrode in alkaline solution, *J. Electroanal. Chem.* 333 (1992) 195–203.
- [154] T. Jones, Electroplating of Ruthenium, *Met. Finish.* 99 (2001) 121–128.
- [155] Anon., Supplier of Dry-Reed Relays Switches to Ruthenium, *Plat. Surf. Finish.* 73 (1984) 26–28.
- [156] T.A. Palumbo, Evaluation of an Improved Ruthenium Plating Process, *Plat. Surf. Finish.* 66 (1979) 42–44.
- [157] C.R.K. Rao, D.C. Trivedi, Chemical and electrochemical depositions of platinum group metals and their applications, *Coord. Chem. Rev.* 249 (2005) 613–631.
- [158] B.P.C. Hydes, Electrodeposited Ruthenium as an Electrical Contact Material, *Platin. Met. Rev.* (1980) 50–55.

- [159] F. Zimmermann, H. Emil, United States Patent Office 2,057,638, 1936.
- [160] R.U. Volterra, United States Patent Office 2,600,175, 1952.
- [161] F.H. Reid, J.C. Blake, Electrodeposition of Ruthenium, *Trans. Inst. Met. Finish.* 38 (1961) 45–51.
- [162] G.S. Reddy, P. Taimsalu, Electrodeposition of Ruthenium, *Trans. Inst. Met. Finish.* 47 (1969) 187–193.
- [163] C.W. Bradford, M.J. Cleare, H. Middleton, A New Ruthenium Plating Bath, *Platin. Met. Rev.* 13 (1969) 90–92.
- [164] V.D. Patake, C.D. Lokhande, O.S. Joo, Electrodeposited ruthenium oxide thin films for supercapacitor: Effect of surface treatments, *Appl. Surf. Sci.* 255 (2009) 4192–4196.
- [165] J.M. Sieben, E. Morallón, D. Cazorla-Amorós, Flexible ruthenium oxide-activated carbon cloth composites prepared by simple electrodeposition methods, *Energy.* 58 (2013) 519–526.
- [166] K.M. Kim, J.H. Kim, Y.Y. Lee, K.Y. Kim, Electrodeposition of ruthenium oxide on ferritic stainless steel bipolar plate for polymer electrolyte membrane fuel cells, *Int. J. Hydrogen Energy.* 37 (2012) 1653–1660.
- [167] O. Mann, W. Freyland, O. Raz, Y. Ein-Eli, Electrochemical deposition of ultrathin ruthenium films on Au(111) from an ionic liquid, *Chem. Phys. Lett.* 460 (2008) 178–181.
- [168] O. Raz, G. Cohn, W. Freyland, O. Mann, Y. Ein-Eli, Ruthenium electrodeposition on silicon from a room-temperature ionic liquid, *Electrochim. Acta.* 54 (2009) 6042–6045.
- [169] M. Jayakumar, K.A. Venkatesan, T.G. Srinivasan, P.R. Vasudeva Rao, Electrochemical behavior of ruthenium (III), rhodium (III) and palladium (II) in 1-butyl-3-methylimidazolium chloride ionic liquid, *Electrochim. Acta.* 54 (2009) 6747–6755.
- [170] B.-O. Park, C.D. Lokhande, H.-S. Park, K.-D. Jung, O.-S. Joo, Cathodic electrodeposition of RuO₂ thin films from Ru(III)Cl₃ solution, *Mater. Chem. Phys.* 87 (2004) 59–66.
- [171] Y.-Z. Zheng, H.-Y. Ding, M.-L. Zhang, Hydrous–ruthenium–oxide thin film electrodes prepared by cathodic electrodeposition for supercapacitors, *Thin Solid Films.* 516 (2008) 7381–7385.
- [172] J.-J. Jow, H.-J. Lee, H.-R. Chen, M.-S. Wu, T.-Y. Wei, Anodic, cathodic and cyclic voltammetric deposition of ruthenium oxides from aqueous RuCl₃ solutions, *Electrochim. Acta.* 52 (2007) 2625–2633.

References

- [173] Y.-S. Kim, H.-I. Kim, J.-H. Cho, H.-K. Seo, G.-S. Kim, S.G. Ansari, et al., Electrochemical deposition of copper and ruthenium on titanium, *Electrochim. Acta.* 51 (2006) 5445–5451.
- [174] A.J. Bard, L.R. Faulkner, *Electrochemical Methods - Fundamentals and Applications*, John Wiley & Sons, Inc., U.K., 2010.
- [175] R.B. Willis, M.E. Montgomery, P.R. Allen, Improved Method for Manual , Colorimetric Determination of Total Kjeldahl Nitrogen Using Salicylate, *J. Agric. Food Chem.* 44 (1996) 1804–1807.
- [176] D. Pletcher, R.I. Urbina, Electrodeposition of rhodium. Part 2. Sulfate solutions, *J. Electroanal. Chem.* 421 (1997) 145–151.
- [177] M.H. Miles, E.A. Klaus, B.P. Gunn, J.R. Locker, W.E. Serafin, The Oxygen Evolution Reaction On Platinum, Iridium, Ruthenium and their Alloys at 80°C in Acid Solutions, *Electrochim. Acta.* 23 (1978) 521–526.
- [178] M. Pourbaix, *Atlas of Electrochemical Equilibria in Aqueous Solutions*, Second Eng, NACE International Cebelcor, 1974.
- [179] L. Malavasi, C.A.J. Fisher, M.S. Islam, Oxide-ion and proton conducting electrolyte materials for clean energy applications: structural and mechanistic features., *Chem. Soc. Rev.* 39 (2010) 4370–4387.
- [180] K. Tüber, A. Oedegaard, M. Hermann, C. Hebling, Investigation of fractal flow-fields in portable proton exchange membrane and direct methanol fuel cells, *J. Power Sources.* 131 (2004) 175–181.
- [181] R. O'Hayre, D.M. Barnett, F.B. Prinz, The Triple Phase Boundary, *J. Electrochem. Soc.* 152 (2005) A439–A444.
- [182] S. Trasatti, Electrocatalysis in the anodic evolution of oxygen and chlorine, *Electrochim. Acta.* 29 (1984) 1503–1512.
- [183] R. Kötz and S. Stucki, Stabilization of RuO₂ by IrO₂ for anodic oxygen evolution in acid media, *Electrochim. Acta.* 31 (1986) 1311–1316.
- [184] Ch. Comninellis, G.P. Vercesi, Characterization of DSA-type oxygen evolving electrodes: choice of a coating, *J. Appl. Electrochem.* 21 (1991) 335–345.
- [185] P.C.S. Hayfield, Development of the Noble Metal/Oxide Coated Titanium Electrode Part III: Coated titanium anodes in widely ranging oxygen evolving situations, *Platin. Met. Rev.* 42 (1998) 116–122.
- [186] Fuma-Tech, Technical Data Sheet - fumapem F-14100, (n.d.).

- [187] K. Hongsirikarn, T. Napaprukchart, X. Mo, J.G. Goodwin, Effect of ammonium ion distribution on Nafion® conductivity, *J. Power Sources.* 196 (2011) 644–651.
- [188] K. Hongsirikarn, J.G. Goodwin, S. Greenway, S. Creager, Influence of ammonia on the conductivity of Nafion membranes, *J. Power Sources.* 195 (2010) 30–38.
- [189] M. Saito, K. Hayamizu, T. Okada, Temperature dependence of ion and water transport in perfluorinated ionomer membranes for fuel cells., *J. Phys. Chem. B.* 109 (2005) 3112–3119.
- [190] P. Choi, N.H. Jalani, R. Datta, Thermodynamics and Proton Transport in Nafion, *J. Electrochem. Soc.* 152 (2005) E123–E130.
- [191] T. V. Nguyen, R.E. White, A Water and Heat Management Model for Proton-Exchange-Membrane Fuel Cells, *J. Electrochem. Soc.* 140 (1993) 2178–2186.
- [192] T.A. Zawodzinski, C. Derouin, S. Radzinski, R.J. Sherman, V.T. Smith, T.E. Springer, et al., Water Uptake by and Transport Through Nafion 117 Membranes, *J. Electrochem. Soc.* 140 (1993) 1041–1047.
- [193] S. Trasatti, Work function, Electronegativity, and Electrochemical Behaviour of Metals III. Electrolytic Hydrogen Evolution in Acid Solutions, *J. Electroanal. Chem.* 39 (1972) 163–184.
- [194] D. Pletcher, *A First Course in Electrode Processes*, 2nd ed., RSC Publishing, 2009.
- [195] M. Ji, Z. Wei, A Review of Water Management in Polymer Electrolyte Membrane Fuel Cells, *Energies.* 2 (2009) 1057–1106.
- [196] T.A. Zawodzinski, T.E. Springer, J. Davey, R. Jestel, C. Lopez, J. Valerio, et al., A Comparative Study of Water Uptake By and Transport Through Ionomeric Fuel Cell Membranes, *J. Electrochem. Soc.* 140 (1993) 1981–1985.
- [197] T.A. Zawodzinski, J. Davey, J. Valerio, S. Gottesfeld, The Water Content Dependence Electro-Osmotic Drag in Proton-Conducting Polymer Electrolytes, *Electrochim. Acta.* 40 (1995) 297–302.
- [198] P. Sridhar, R. Perumal, N. Rajalakshmi, M. Raja, K.S. Dhathathreyan, Humidification studies on polymer electrolyte membrane fuel cell, *J. Power Sources.* 101 (2001) 72–78.
- [199] W. He, G. Lin, T. Van Nguyen, Diagnostic Tool to Detect Electrode Flooding in Proton-Exchange-Membrane Fuel Cells, *AIChE J.* 49 (2003) 3221–3228.

References

- [200] J. St-Pierre, D.P. Wilkinson, S. Knights, M. Bos, Relationships between water management , contamination and lifetime degradation in PEFC, *J. New Mater. Electrochem. Syst.* 3 (2000) 99–106.
- [201] G. Marnellos, M. Stoukides, Catalytic studies in electrochemical membrane reactors, *Solid State Ionics.* 175 (2004) 597–603.
- [202] K. Kinoshita, *Electrochemical Oxygen Technology*, John Wiley & Sons, Inc., 1992.
- [203] J.O. Bockris, Kinetics of Activation Controlled Consecutive Electrochemical Reactions: Anodic Evolution of Oxygen, *J. Chem. Phys.* 24 (1956) 817–827.
- [204] H. Wendt, G. Kreysa, *Electrochemical Engineering: Science and Technology in Chemical and Other Industries*, Springer-Verlag Berlin Heidelberg, 1999.
- [205] M.M. Jaksic, Volcano plots along the periodic table , their causes and consequences on electrocatalysis for hydrogen electrode reactions, *J New Mat Elect Syst.* 3 (2000) 167–182.
- [206] S. Trasatti, Development of the Work Function Approach to the Underpotential Deposition of Metals. Application to the Hydrogen Evolution Reaction, *Z Phys Chem Neue Fol.* 98 (1975) 75–94.
- [207] E. Santos, W. Schmickler, *Catalysis in Electrochemistry: From Fundamentals to Strategies for Fuel Cell Development*, John Wiley & Sons, Inc., 2011.
- [208] H. Wendt, H. Vogt, G. Kreysa, D.M. Kolb, G.E. Engelmann, J.C. Ziegler, et al., *Electrochemistry*, in: Ullmann's Encycl. Ind. Chem. Electrochem., Wiley-VCH Verlag GmbH & Co. KGaA, Weinheim, 2009.
- [209] P. Choi, D.G. Bessarabov, R. Datta, A simple model for solid polymer electrolyte (SPE) water electrolysis, *Solid State Ionics.* 175 (2004) 535–539.
- [210] S. Slade, S.A. Campbell, T.R. Ralph, F.C. Walsh, Ionic Conductivity of an Extruded Nafion 1100 EW Series of Membranes, *J. Electrochem. Soc.* 149 (2002) A1556–A1564.
- [211] M. Appl, The Haber-Bosch Heritage: The Ammonia Production Technology, in: 50th Anniv. IFA Tech. Conf. Sept. 25–26th 1997, Sevilla, Spain, 1997.
- [212] D.M. Bernardi, M.W. Verbrugge, Mathematical model of a gas diffusion electrode bonded to a polymer electrolyte, *AIChE J.* 37 (1991) 1151–1163.
- [213] S.G. Jennings, The mean free path in air, *J Aerosol Sci.* 19 (1988) 159–166.

- [214] B. Sundén, M. Faghri, *Transport Phenomena in Fuel Cells*, WIT Press, Southampton, 2005.
- [215] S.D. Barnicki, J.R. Fair, Separation System Synthesis : A Knowledge-Based Approach . 2. Gas/Vapor Mixtures, *Ind. Eng. Chem. Res.* 31 (1992) 1679–1694.
- [216] W. Seider, J. Seader, D. Lewin, S. Widagdo, *Product and Process Design Principles - Synthesis, Analysis and Evaluation*, John Wiley & Sons, Inc., 2010.
- [217] J.E. Hogsett, W.H. Mazur, Estimate membrane system area, *Hydrocarb. Process.* 62 (1983) 52–54.
- [218] L.M. Robeson, The upper bound revisited, *J. Memb. Sci.* 320 (2008) 390–400.
- [219] R.W. Baker, *Membrane Technology and its application*, John Wiley & Sons Ltd, England, 2004.
- [220] Stirling Cryogenics BV, Stirling Power Cooler LPC-RL Reliquefaction of boiling gases, 31 (n.d.). <http://www.stirlingcryogenics.com/~uploads/products/file/10800701-Power-Cooler-LPC-RL.pdf> (accessed June 17, 2014).
- [221] J.P. Montoya, Membrane Gas Exchange, MedArray Inc. (2010) 1–7.
http://www.permselect.com/files/Using_Membranes_for_Gas_Exchange.pdf (accessed June 18, 2014).
- [222] W.A. Phillip, E. Martono, L. Chen, M.A. Hillmyer, E.L. Cussler, Seeking an ammonia selective membrane based on nanostructured sulfonated block copolymers, *J. Memb. Sci.* 337 (2009) 39–46.
- [223] P.M. Budd, K.J. Msayib, C.E. Tattershall, B.S. Ghanem, K.J. Reynolds, N.B. McKeown, et al., Gas separation membranes from polymers of intrinsic microporosity, *J. Memb. Sci.* 251 (2005) 263–269.
- [224] Eurostat (european commission) - Energy price statistics, (n.d.).
http://epp.eurostat.ec.europa.eu/statistics_explained/index.php?Energy_price_statistic_s/de (accessed June 20, 2014).
- [225] ICIS, Indicative Chemical Prices A-Z, (n.d.). <http://www.icis.com/chemicals/channel-info-chemicals-a-z/> (accessed June 23, 2014).
- [226] T. Melin, R. Rautenbach, *Membranverfahren: Grundlagen der Modul- und Anlagenauslegung*, Springer-Verlag Berlin Heidelberg, 2007.

Curriculum vitae

Kurt Kugler

Born April 12th 1985 in Munich

1995 - 2004	Josef-Effner-Gymnasium, Dachau, Bavaria
2004 - 2010	Studies in Chemical Engineering at TU München Diploma thesis at the Chair of Chemical Engineering
2008	Trainee at Wacker Chemie AG, Burghausen, Bavaria
2008 - 2009	Research assistant at University of Auckland, New Zealand Department of Chemical and Materials Engineering
2011 - 2015	PhD student at the Chair for Chemical Process Engineering at RWTH Aachen

June 8th, 2015